Propositions

1. Neural networks have not been found to be as useful for discharge recognition as indicated in literature.

2. The changes in discharge patterns during ageing have implications for discharge recognition because patterns which occur at the beginning of a test differ from those at the end of the test. For periodic testing of electrical insulation a separate category can be created for each ageing stage.

3. Engineering is the art of using imperfect solutions in search of perfect ones.

4. A great scientist might coin one or two immortal propositions in a lifetime. The poor PhD student has to invent six of them within a period of few weeks.

5. With the language barriers and the nationalism throughout (Western) Europe, its ultimate unification is just a dream of hypocritical politicians.

6. The mind of a scientist must resemble that of jazz musician. He/she must not only master his/her instrument but must improvise as well.

7. The Czecho-Slovak Velvet revolution 1989 was a well-organized puppet theatre with a 15-million audience.

8. Recent action against Shell's dumping a platform in the ocean has proved that being 'green' has become a permanent market factor.

A. Krivda

Recognition of discharges

Discrimination and classification

Recognition of discharges

Discrimination and classification

PROEFSCHRIFT

ter verkrijging van de graad van doctor
aan de Technische Universiteit Delft,
op gezag van de Rector Magnificus, prof. ir. K.F. Wakker,
in het openbaar te verdedigen ten overstaan van een commissie,
door het College van Dekanen aangewezen,
op maandag 18 september 1995, te 10.30 uur

door

Andrej KRIVDA

inžinier, Vysoká Škola Technická v Košiciach

geboren te Humenné, Slowakije

Dit proefschrift is goedgekeurd door de promotor Prof. Dr. Ir. F. H. Kreuger

Samenstelling promotiecommisie:
Rector Magnificus, voorzitter
Prof. Dr. Ir. F. H. Kreuger, TU Delft, promotor
Prof. Dr. Ir. E. Backer, TU Delft
Prof. Ir. L. van der Sluis, TU Delft
Prof. Dr. W. R. Rutgers, TU Eindhoven
Dr. Ir. E. Gulski, TU Delft
Dr. Ir. E. F. Steennis, KEMA N.V., Arnhem

Published and distributed by:
Delft University Press
Stevinweg 1, 2628 CN Delft
Telephone: +31 15 783254
Fax: +31 15 781661

CIP-DATA KONINKLIJKE BIBLIOTHEEK, DEN HAAG

Krivda, A.
Recognition of discharges. Discrimination and classification/
A. Krivda - Delft: Delft University Press, - Ill.
Thesis Delft University of Technology. - With ref. - With summary in Dutch.
ISBN 90-407-1156-9
NUGI 832
Subject headings: high voltage, electrical insulation, partial discharge, discharge recognition

Printed in the Netherlands

Contents

Summary

Discharge detection and recognition have become important tools for the evaluation of insulating constructions. The core of this thesis is the application of pattern recognition techniques for the discrimination and classification of discharges.

The thesis is the continuation of previous work by Dr. E. Gulski on computer-aided discharge recognition which was also performed at the High Voltage Laboratory of Delft University of Technology. The aim of this study is to improve the tools developed for discharge recognition. Many methods have been tried out.

For discrimination of discharges, the group average method has been found to be useful, in particular when analysing discharge patterns during the ageing of insulation. The method can be helpful in data analysis for periodic testing of high voltage equipment. Also fractal descriptors of discharge patterns have shown a good discrimination potential.

For classification purposes, the centour score method has been found to be useful. The method has proved its potential in classifying discharges in high voltage equipment and has already been successfully implemented in a commercially available instrument. Neural networks did not prove to be a valuable tool for the classification of discharges.

In Chapter 1 a general introduction is given.

Chapter 2 describes discharge distributions used for recognition purposes. The information contained in the discharge distributions is quantified by statistical parameters, such as the skewness, the kurtosis, *etc.* of these distributions. A set of 29 statistical parameters is then used as a basic element for discharge recognition; this set is called a fingerprint of a discharge.

In Chapter 3 a detailed description of fingerprints of different discharge sources is given.

Chapter 4 discusses the use of mathematical methods for the discrimination and classification of discharge patterns. Mapping techniques, cluster analysis methods and fractals were employed to *discriminate* between discharge patterns. Of the methods studied, the group average technique is preferred. Fractals have also shown a good potential for the discrimination of discharge patterns.

To *classify* discharge patterns, neural networks and conventional classifiers were used. Neural networks did not prove to be a valuable tool for discharge recognition. Conventional classifiers, especially the centour score method, were successful in the discharge recognition.

Chapter 5 presents discharge patterns obtained during the ageing of simple models and industrial high voltage components. The patterns were analyzed using the above recognition techniques. The results indicate that these recognition tools (the group average method, the centour score method) have a good potential for industrial applications, such as the periodic testing of electrical insulation in high voltage components.

Chapter 6 summarizes the conclusions of this thesis and gives some suggestions for future work.

Chapter 1

Introduction

1.1 General aspects

Discharges which do not completely bridge the space between electrodes are called partial discharges. The occurrence of partial discharges in electrical equipment had been recognized as early as the beginning of the century [94]. As it became clear that partial discharges might substantially reduce the life of insulation [78,100], much effort was spent on investigating this phenomenon. New measurement methods were introduced [57], the physics and the chemistry of partial discharges were studied [17,81]. Discharge detection gradually evolved into an indispensable tool for the evaluation of modern insulating constructions [92].

A partial discharge is a complex physical process with stochastic properties [27,121]. It is accompanied by many phenomena, *e.g.*, charge displacement, acoustic waves, light, *etc.*, and these phenomena can be used for its detection. Detection of charge displacement is the most frequently chosen measurement method. The basic circuit employed for this type of discharge detection is shown in Figure 1.

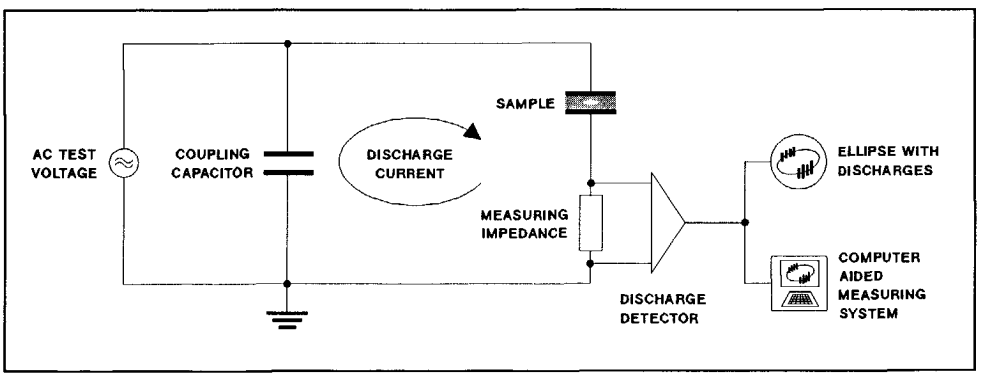

Figure 1. Discharge detection circuit.

The coupling capacitor provides a low impedance path for high-frequency discharge currents which cause voltage pulses over the measuring impedance. The pulses are then amplified and displayed, *e.g.*, on the power-frequency ellipse or stored in a computer for further processing.

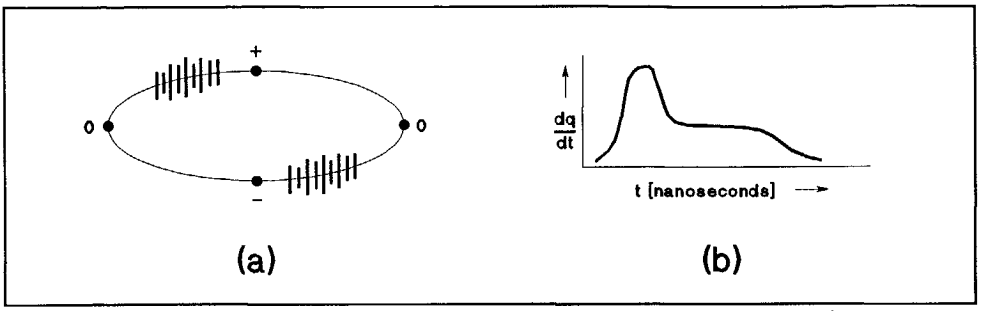

Figure 2. (a) Conventional discharge detection. (b) Time-resolved discharge detection.

There are basically two ways to perform discharge detection:

1. In a conventional detection system, discharge pulses are amplified with a detector having a bandwidth of several hundreds of kHz. The discharges are then displayed, *e.g.*, as short pulses on the power-frequency time base, see Figure 2.a. This type of discharge detection is used in this work.

2. In a time-resolved discharge detection, discharge pulses are amplified with a detector having a bandwidth of several hundreds of MHz. The true shape of the charge displacement in a defect, *e.g.*, in a cavity, is shown on a triggered time-base, see Figure 2.b.

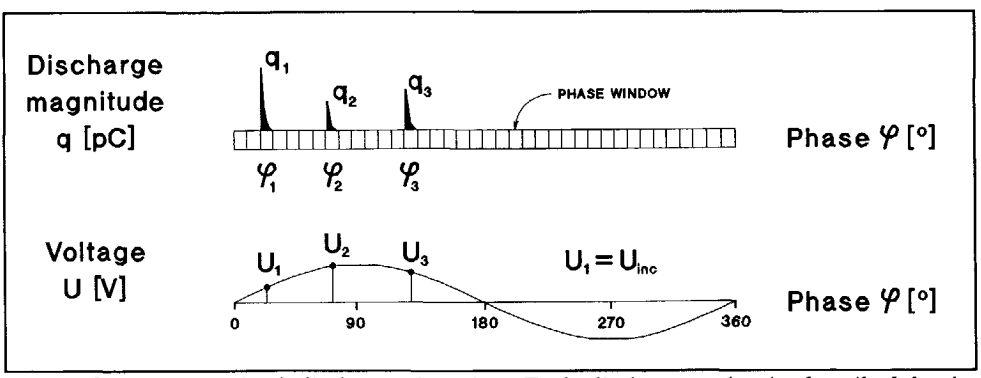

Figure 3. Phase resolved discharge detection. Each discharge pulse is described by its discharge magnitude q and the phase angle φ of the voltage cycle at which the discharge takes place. U_{inc} refers to the voltage at which a first discharge occurs.

Once discharges are detected they can be characterized by, see also Figure 3:

1. the apparent charge q of the discharge pulse. As has been shown before, the apparent charge is a reasonably good measure for the discharge energy at a discharge site which causes the deterioration of a dielectric. Furthermore, the

apparent charge can be directly related to the size of a defect [57].

2. the time of occurrence of the discharge pulse. At AC voltages discharge pulses are typically related to the phase angle of the power-frequency voltage.

These two characteristics have been combined into the well-known display of discharges on the power frequency ellipse, see Figure 4.

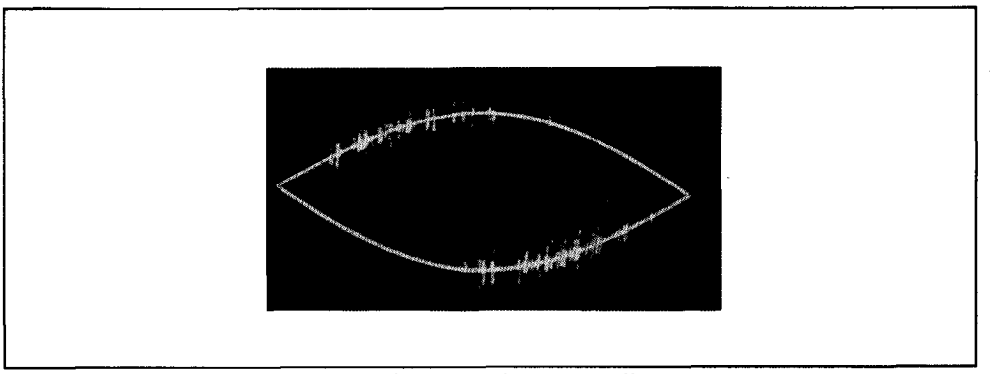

Figure 4. Display of discharges on the power-frequency ellipse.

The display has been found to be very useful tool to indicate the origin of discharges and is used even today. Besides such an analogue observation of discharges, also digital techniques for the processing, visualization and recognition of discharges have gained in popularity in the past two decades [123]. An example of various ways of discharge data visualization by computer-aided digital processing of discharge data is shown Figure 5.

Many attempts have been made to approach the problem of discharge recognition using such digitized data: expert systems [32,74,128], identification functions [56,64], neural networks [45,37,112], hidden Markov models [103], statistical operators [35,91], etc. The last one - the use of statistical operators - is a basic element for discharge recognition in this work. In this technique the power-frequency phase angle and the magnitude q of each discharge is recorded for a certain time, *e.g.*, some minutes. These recordings are then used to make statistical distributions, *e.g.*, the mean pulse height distribution $H_{qn}(\varphi)$, the pulse count distribution $H_n(\varphi)$ and others. The shapes of these distributions are described by statistical operators, such as the skewness, the kurtosis, etc. A simple algorithm called the recognition rate is then used to classify discharges. Thus is the visual recognition of discharges on the ellipse replaced by an automated, computer-aided classification system.

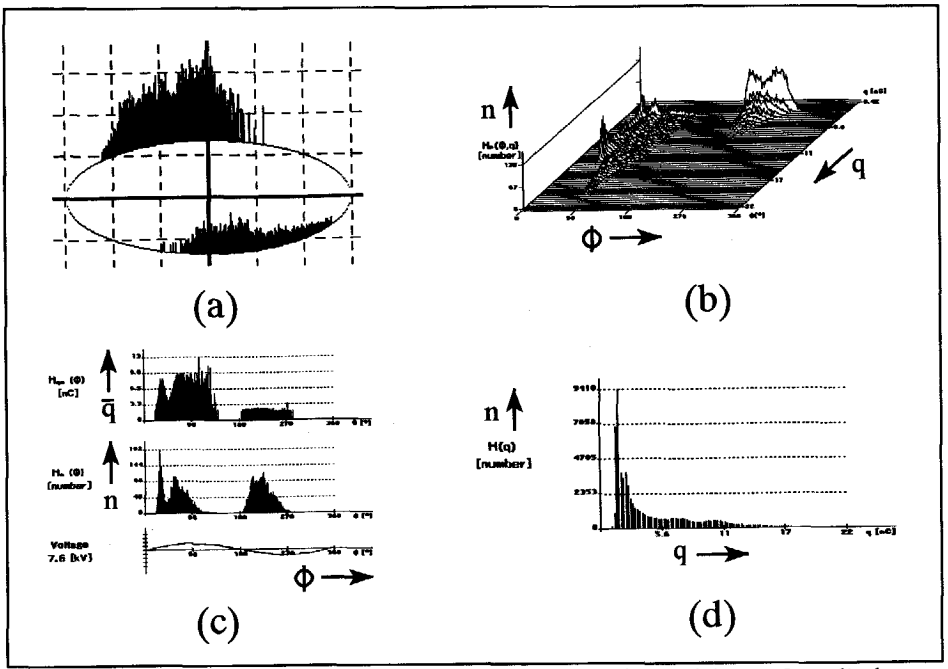

Figure 5. Various ways of displaying discharge data as obtained for surface discharges in air. Discharges were detected by a conventional discharge detector with a bandwidth of about 400 kHz and digitally processed by TEAS 570 discharge analyzer. (a) Partial discharges as seen on the power frequency ellipse. (b) The $H_n(\varphi, q)$ discharge distribution representing the relationship between the discharge count rate n and the discharge magnitude q as a function of the phase angle φ of the voltage cycle. (c) The mean pulse height discharge distribution $H_{qn}(\varphi)$, showing the average discharge magnitude at each phase angle of the applied voltage, and the pulse count discharge distribution $H_n(\varphi)$, showing the number of discharges at each phase angle. (d) The H(q) intensity spectrum, representing the number of discharges as a function of the discharge magnitude.

The aim of the thesis is to explore further possibilities of the statistical operators for discharge recognition, namely:

1. examination of **discrimination** methods. Here, methods suitable for the development of a data base for discharge recognition are studied. The methods should provide an answer as to whether patterns of various discharge sources can be discriminated from each other. This is important because only with this information can a separate category be formed for each discharge source in the data base.

2. improvement of **classification**. The recognition rate as developed by Gulski [35] was used as a temporary tool to test the efficiency of the statistical operators for discharge recognition. The relatively small classification power of the method left space for further systematic and detailed research. A new method should produce

much clearer results and be sufficiently versatile for the recognition of discharges not only in artificially prepared samples but also in industrial HV components.

1.2 State of the art

Efforts towards an automated discharge recognition are summarized in the following text.

Okamoto and Tanaka [91] were among the first to report an automated discharge recognition system. For recognition purposes, they used the skewness of the mean pulse height discharge distribution $H_{qn}(\varphi)$. This statistical parameter appeared to be a sensitive indicator of the shape of a void in which discharges occurred. It was also proposed to monitor electrical treeing degradation in this way.

Wootton [128] described an expert system where if-then rules were used to trace the origin of discharges. First, discharge patterns were visually observed on the power frequency ellipse on an oscilloscope screen; then the user had to answer a series of questions. By means of such a questionnaire, the classification of discharges was performed on the basis of the information published by CIGRE [97]. Clearly, results were still dependent on interpretation by the human user.

Gassaway *et al.* [32] developed an expert system which analyzed the mean pulse height discharge distribution $H_{qn}(\varphi)$ and the pulse count discharge distribution $H_n(\varphi)$. Various statistical parameters were then calculated and displayed, *e.g.*, the total discharge magnitude in the positive and negative half of the voltage cycle, phase centroids for the discharge magnitude, *etc.* Then, the user had to answer a series of questions which eventually led to the recognition of the discharge source. Good recognition was achieved for corona and surface discharges in air. As in the above case, the recognition performance of the expert system was limited.

Krump [56,64] described a system which employed identification functions and minimum distance classifiers for the discharge recognition. The identification functions were based on various parameters, *e.g.*, the discharge magnitude, the discharge energy, phase angles, *etc.* The author studied nine types of defects in a gas-insulated system with satisfactory results.

Hozumi *et al.* [45] and Suzuki and Endoh [112] applied neural networks to discharge recognition. The $H_n(\varphi,q)$ discharge distribution and the mean pulse height discharge distribution $H_{qn}(\varphi)$ were used to classify discharge patterns in a cavity before and after tree initiation. The achieved accuracy of the recognition was about 90%. Although only two types of defects were studied, the authors considered neural networks as a promising tool for discharge recognition. Recent results [37,61], however, have revealed several disadvantages of this approach. This subject is discussed further in Chapter 4 of this thesis.

Satish [103] classified discharge patterns by means of hidden Markov models. In this case, the input data consisted of a picture of the ellipse with superposed discharges, which was obtained by a CCD camera. The rejection of discharge patterns which do not belong to any of the known categories is, however, not considered in hidden Markov models. This can lead

to misclassification of such discharge patterns, which presents a limitation of this procedure.

Contin and Rabach [15] developed a method to indicate the presence of multiple discharge sources. The method is based on the evaluation of the cumulative distribution of the H(q) intensity spectrum using the Weibull graph. In the presence of multiple discharge phenomena, strong deviations from the Weibull distribution occur. Slot and surface discharges in addition to internal discharges in stator windings were identified in this way. The usefulness of this method was proved in the case of ageing of stator insulation.

Gulski's system for an automated classification of discharges has been briefly described above [35,36]. Further improvement of the system is the core of the thesis.

1.3 Object of the present study

Computer-aided measurement systems with pattern recognition algorithms have already positively contributed to the task of recognizing discharges. In this work, further aspects of automated discharge recognition using the statistical operators are discussed. The following is the aim of this study.

1. Introducing **discrimination** methods as an aid for the building of a data base for discharge recognition.

   Testing of the selected discrimination methods with data from laboratory samples and technical objects.

   These points are discussed in Chapter 4.

2. Improvement of the **classification** by applying more efficient mathematical methods than the recognition rate.

   Testing of the selected methods with artificial defects in laboratory samples and natural defects in technical objects.

   The subjects are also treated in Chapter 4.

3. The **ageing** of samples by discharges is a separate study. The effect of ageing on the discharge patterns is studied with the object of using the above techniques for the periodic testing of HV equipment in actual use.

   This is examined in Chapter 5.

Chapter 2

Acquisition and processing of discharge signals

2.1 Discharge detection

There are many ways to detect partial discharges, *e.g.*, electrically, acoustically, optically, *etc.* [7,57]. In this work the detection of the displacement of charge flowing in the leads of the sample with the circuit described in Figure 1 was used. A discharge detector according to IEC 270 with a bandwidth of 40 - 400 kHz was employed to detect the discharges. The discharge pulses were processed by a TEAS 570 analyzer (made by Haefely). This instrument is a commercial version of a partial discharge analyzer developed by Gulski in his work on automated discharge recognition [35]. Many new features have been added to this system since its first appearance, with the aim of improving the discharge recognition, *e.g.*, more discharge distributions were analyzed, more statistical parameters were used, *etc.* [38]. Only the basic essentials of the TEAS used for discharge recognition are described here.

2.2 Discharge distributions

By dividing the power frequency cycle of the test voltage into a number of phase windows, see Figure 3, the following phase discharge distributions are collected by the TEAS [35,38,91], see Figure 6.

1. The maximum pulse height distribution $H_{qmax}(\varphi)$, showing the maximum discharge magnitude in each window as a function of the phase angle φ.

2. The mean pulse height distribution $H_{qn}(\varphi)$, showing the average discharge magnitude in each window as a function of the phase angle φ.

3. The pulse count distribution $H_n(\varphi)$, showing the number of discharges in each window as a function of the phase angle φ.

The number of phase windows is typically 2000, *i.e.*, with a 50 Hz test voltage the pulse resolution is 10 μs.

Experience has shown that the distributions may be different in the positive and in the negative half of the voltage cycle, see Figure 6. Therefore, all distributions above are defined for both halves of the voltage cycle. Consequently, a total of six phase distributions is obtained: $H^{+}_{qmax}(\varphi)$, $H^{+}_{qn}(\varphi)$, $H^{+}_{n}(\varphi)$ and $H^{-}_{qmax}(\varphi)$, $H^{-}_{qn}(\varphi)$, $H^{-}_{n}(\varphi)$.

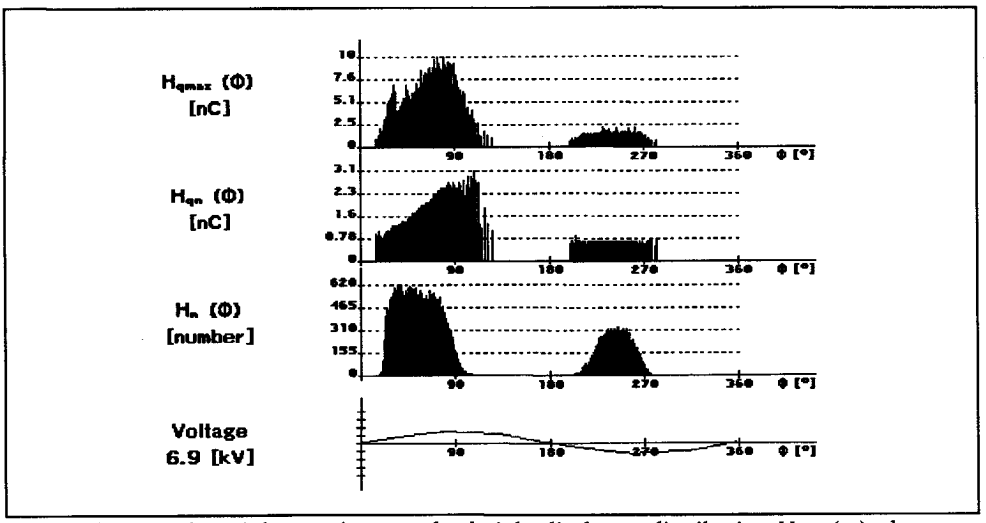

Figure 6. Examples of the maximum pulse height discharge distribution $H_{qmax}(\varphi)$, the mean pulse height distribution $H_{qn}(\varphi)$ and the pulse count distribution $H_{n}(\varphi)$. The discharge distributions describe surface discharges in air.

In addition, two intensity spectra are constructed [6,105], see Figure 7.

1. H(q) - the distribution of the number of discharges n as a function of the discharge magnitude q.

2. H(p) - the distribution of the number of discharges n as a function of the discharge energy p. The discharge energy p_i of i-th discharge is calculated by multiplying the apparent charge q_i by the instantaneous value of the test voltage U_i, see Figure 3.

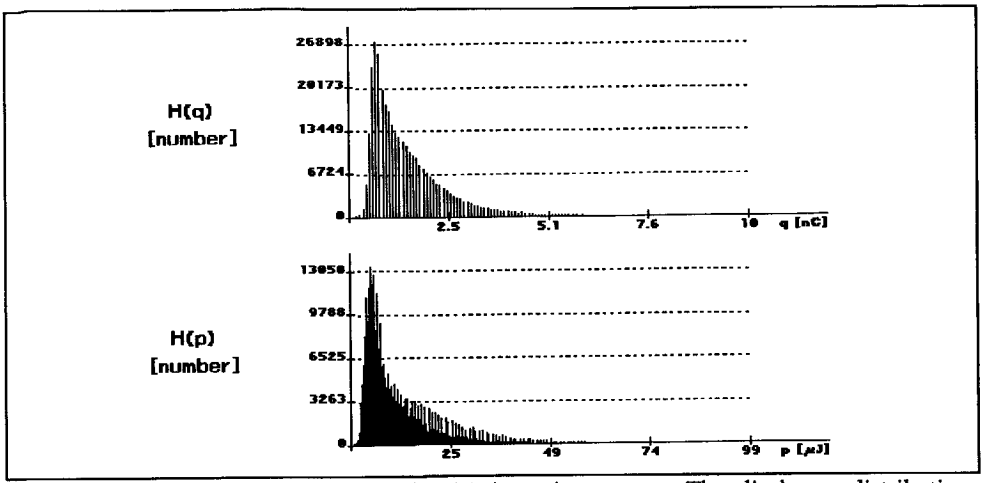

Figure 7. Examples of the H(q) and H(p) intensity spectra. The discharge distributions describe surface discharges in air.

It follows that a total of eight discharge distributions are used for discharge recognition, *i.e.*, six phase distributions and two intensity spectra.

In practice, also the three-dimensional representation of distribution $H_n(\varphi,q)$, see Figure 5.b, is used for discharge recognition. This discharge distribution may yield a better discrimination performance than the distributions above [27]. However, because of its complexity, a three-dimensional distribution is more difficult to analyze quantitatively. This is the main reason why two-dimensional representations of discharge distributions are used in this work.

2.3 Statistical operators

For pattern recognition purposes, the information contained in the discharge distributions is quantified. This is achieved by description of their shapes by various statistical parameters. To maintain consistency with previous work [35], these 'statistical parameters' will in this study be called 'statistical operators'. The following ones are used [35,91].

Skewness, *Sk*, describes the asymmetry of the distribution with respect to a normal distribution. It is defined as

$$Sk = \frac{\sum (x_i - \mu)^3 \cdot P_i}{\sigma^3} \qquad (1)$$

where x_i is the recorded value, P_i is the probability of appearance for that value x_i in the i-th phase window, μ is the mean value

$$\mu = \sum x_i \cdot P_i \qquad (2)$$

and σ is the variance

$$\sigma^2 = \sum (x_i \cdot \mu)^2 \cdot P_i \,. \tag{3}$$

For a symmetric distribution, Sk=0, if it is asymmetric to the left, Sk>0, and if it is asymmetric to the right, Sk<0, see Figure 8.

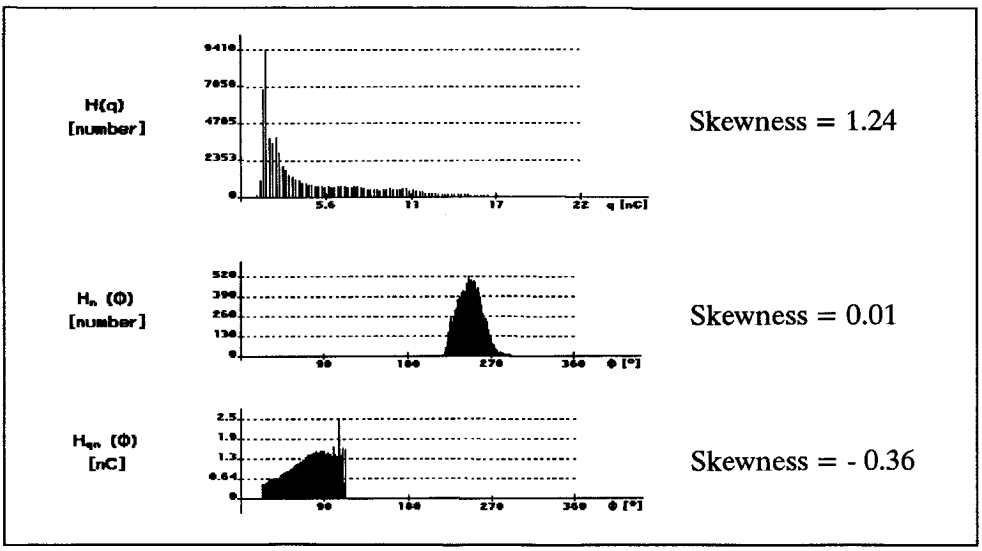

Figure 8. Examples of distributions and their resulting skewness.

Kurtosis, *Ku*, represents the sharpness of the distribution with respect to the normal distribution,

$$Ku = \frac{\sum (x_i - \mu)^4 \cdot P_i}{\sigma^4} - 3 \ . \tag{4}$$

If the distribution has the same sharpness as a normal distribution, $Ku=0$. If it is sharper than normal, $Ku>0$, and if it is flatter, $Ku<0$, see Figure 9.

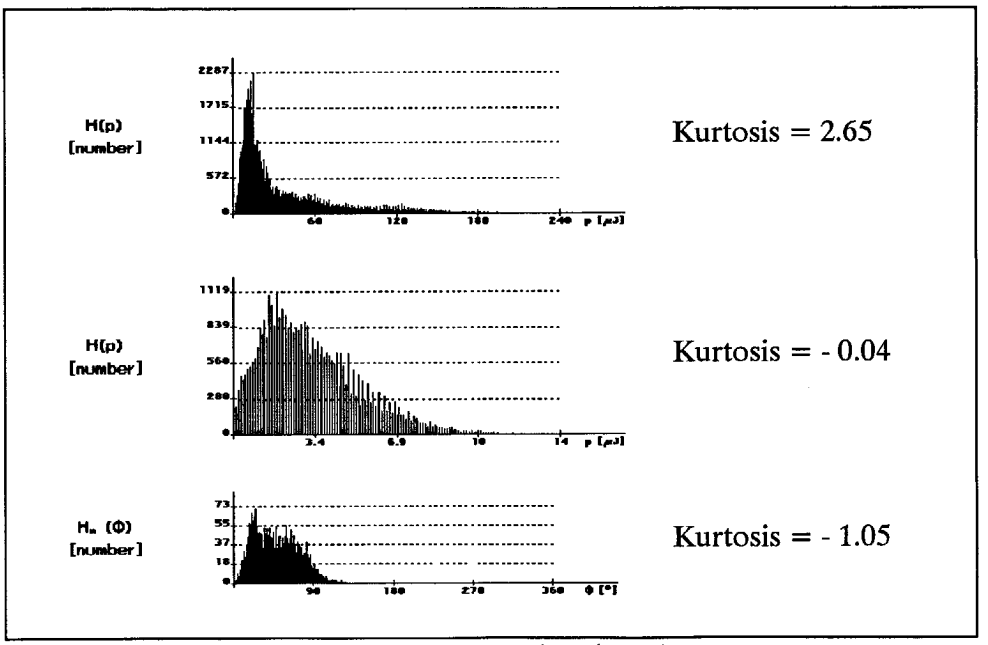

Figure 9. Examples of distributions and their resulting kurtosis.

Number of peaks, *Pe*, is used to distinguish between distributions with a single and those with several tops, see Figure 10. The top of a distribution is defined as

$$\frac{dy_{i-1}}{dx_{i-1}} > 0 \ , \qquad \frac{dy_{i+1}}{dx_{i+1}} < 0 \tag{5}$$

where $dy_{i\pm1}$ / $dx_{i\pm1}$ is the differential coefficient before and after the possible top of the distribution.

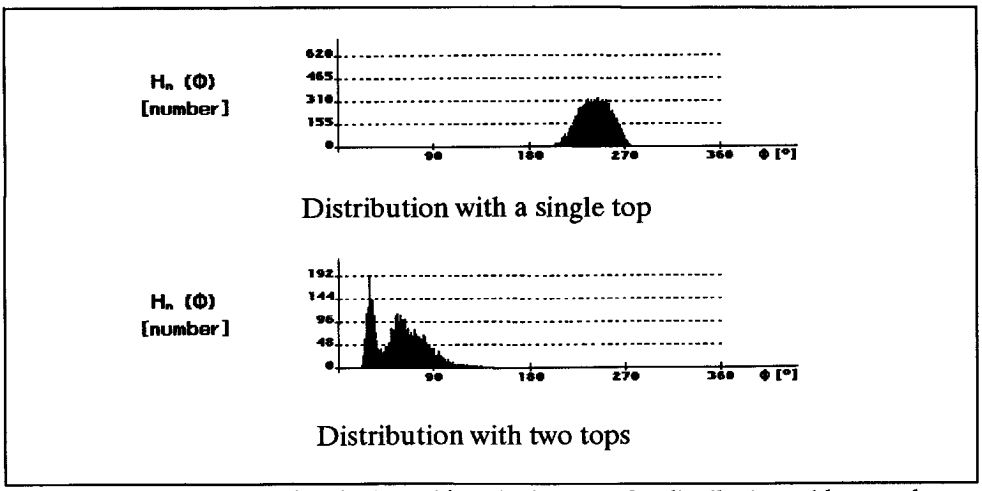

Figure 10. Examples of a distribution with a single top and a distribution with several tops.

Cross-correlation factor, *cc*, describes the difference in shape between $H^{+}_{qmax}(\varphi)$ and $H^{-}_{qmax}(\varphi)$, $H^{+}_{qn}(\varphi)$ and $H^{-}_{qn}(\varphi)$, and $H^{+}_{n}(\varphi)$ and $H^{-}_{n}(\varphi)$ distributions of the positive and the negative half of the voltage cycle. It is defined as

$$cc = \frac{\sum x_i y_i - \sum x_i \sum y_i / n}{\sqrt{[\sum x_i^2 - (\sum x_i)^2 / n][\sum y_i^2 - (\sum y_i)^2 / n]}} . \qquad (6)$$

In the case of the mean pulse height discharge distribution $H_{qn}(\varphi)$, the x_i is the average discharge magnitude in the i-th window of the positive half cycle and y_i the average discharge magnitude in the corresponding window in the negative half cycle; n is the number of phase windows per half cycle. In similar fashion, the cross-correlation factor can be calculated for the $H_{qmax}(\varphi)$ and the $H_n(\varphi)$ discharge distributions.

A value of cc=1 means 100% shape symmetry, cc=0 means total asymmetry, see Figure 11.

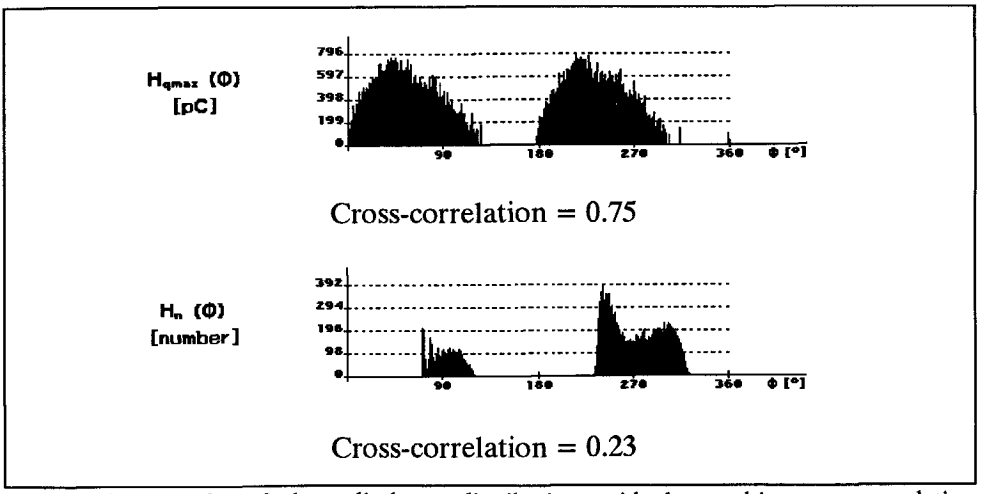

Figure 11. Examples of phase discharge distributions with the resulting cross-correlation factor.

Asymmetry is the quotient of the mean level in the negative and in the positive half of the voltage cycle of the $H_{qmax}(\varphi)$, $H_{qn}(\varphi)$ and $H_n(\varphi)$ distributions. In the case of the mean pulse height discharge distribution the asymmetry is calculated as:

$$asymmetry\ of\ H_{qn}(\varphi) = \frac{Q_s^- / N^-}{Q_s^+ / N^+} \tag{7}$$

where Q_s^+ and Q_s^- are the sum of discharges of the mean pulse height distribution in the positive and in the negative half of the voltage cycle; N^+ and N^- are the number of discharges of the mean pulse height distribution in the positive and in the negative half of the voltage cycle. In similar fashion, the asymmetry can be calculated for the $H_{qmax}(\varphi)$ and the $H_n(\varphi)$ discharge distributions.

The asymmetry can vary between −1 and 1. A value of 1 (−1) indicates that there is only a distribution in the negative (positive) half of the voltage cycle. A value of 0 shows that the distributions in the positive and the negative half of voltage cycle are of equal size, see Figure 12.

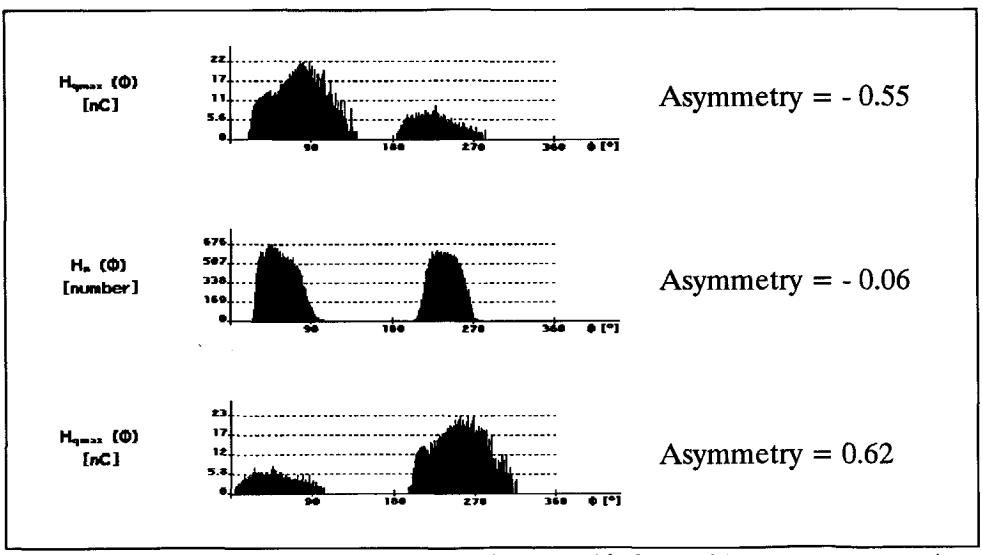

Figure 12. Examples of phase discharge distributions with the resulting asymmetry quotient.

Phase factor is used to study the difference in the inception voltage in the negative and in the positive half of the voltage cycle. It is defined as:

$$phase\ factor = \frac{\varphi^{-}_{inc}}{\varphi^{+}_{inc}} \qquad (8)$$

where $\varphi^{\pm}_{inc}$ is the inception phase in the positive or in the negative half of the voltage cycle.

In the original version of the discharge analyzer, also the **modified cross-correlation factor**, *mcc*, of the mean pulse height distribution $H_{qn}(\varphi)$ is used [35]. This operator is calculated by the multiplication of the asymmetry and cross-correlation factor of the $H_{qn}(\varphi)$ discharge distribution. The TEAS analyzer does not use the modified cross-correlation factor. Whenever data from the original version of the analyzer are examined, the use of the *mcc* is explicitly stated in text.

It can be seen that a total of six basic statistical operators are used by the TEAS for discharge recognition. These are:

1. skewness, *Sk*,
2. kurtosis, *Ku*,
3. number of peaks, *Pe*,
4. cross-correlation factor, *cc*,
5. asymmetry,
6. phase factor.

2.4 Fingerprint

It now follows that a total of six basic statistical operators were available for a description of the eight discharge distributions. Not all combinations 'operator-distribution' were possible and some of them were considered not useful. In the end, 29 resulting values of operators were chosen, see Figure 13.

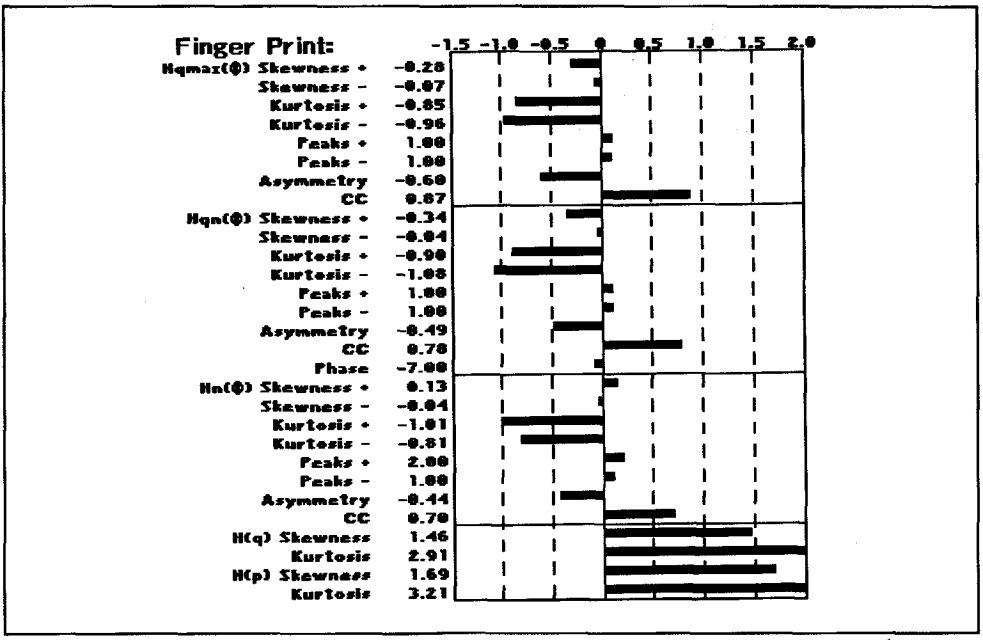

Figure 13. Example of 29 resulting values of statistical operators. Corresponding discharge distributions are shown in Figures 6 and 7. Thus a discharge is characterized by 29 numbers.

This set of 29 statistical operators is called here a fingerprint. This term was taken from police practice, where fingerprints are used to identify criminals. Similarly, discharge fingerprints are used to trace the origin of unknown discharge sources [35]. A fingerprint represents thus compressed information on a particular discharge source and it can be compared with the information of other sources [35,37,59]. The fingerprint is a basic element which is used for discharge recognition throughout this thesis.

Chapter 3

Discharge patterns of various insulation defects

In this chapter data of discharge measurements are presented, which are further used in Chapter 4 for the selection of a recognition method and development of a data base for discharge recognition. Some of these data have been measured by the author, other data have been obtained by Gulski [35]. This is indicated where appropriate.

3.1 Three categories of models

A methodology has been developed on physical discharge models that are needed when classifying discharges [59]. Three basic groups of models have been distinguished.

1. **Standard defects**. These are simple two-electrode models, representing the physical shape of possible defects in dielectrics. Examples are shown in Figure 14, where different types of artificial defects in dielectrics are represented. In Section 3.2 these defects are further studied.

2. **Industrial models**. In this case, artificial defects are introduced in actual high voltage constructions, *e.g.*, by inserting artificial particles in a gas insulated system, by drilling cavities in a cable, *etc.* These artificially created defects are designed to come as near to actual cases as they can be made. It has to be kept in mind, however, that actual defects in industrial objects may differ from artificial ones. For example, the surface of a drilled cavity in a plastic cable is far rougher than the surface of a cavity originating from the extrusion process of a cable production, *etc.* These defects are studied in Section 3.3.

3. **Industrial objects**. This group comprises naturally occurring defects in actual industrial objects. Recognition of this type of defects is the final aim and it can be done in two ways. First, fingerprints of industrial objects are compared with fingerprints of defects as discussed under 1 and 2. Second, fingerprints of industrial objects are mutually compared. For example, a manufacturer may reject its product due to high discharge levels. Data collected on the product can be compared to those of earlier cases of rejection. In the case of a match, a manufacturer may take appropriate action in accordance *with* the knowledge of this type of defect which has occurred earlier in the product. Defects in industrial objects are studied in Section 3.3.

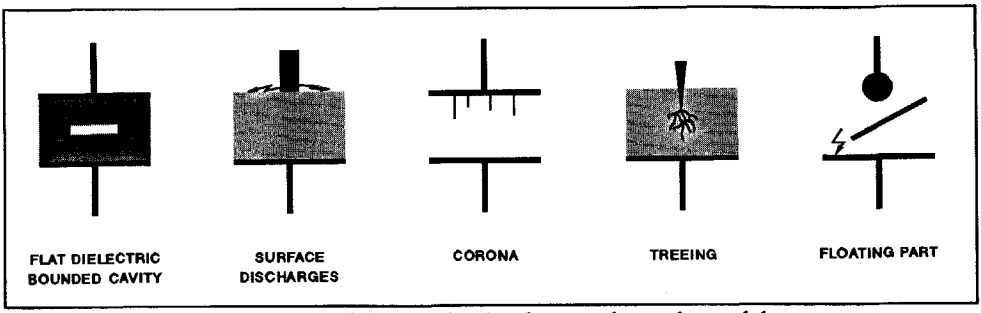

Figure 14. Examples of standard defects in simple two-electrode models.

A number of discharge data obtained from physical models were analyzed in this study. The models and corresponding fingerprints are briefly described in the following sections. To obtain statistically based data, six to twenty fingerprints per model were made.

Note that details about physical processes involved in the discharge phenomena are not required for discharge recognition. Although such information can be helpful in interpreting measured data, experience has shown that satisfactory recognition is obtained without it [35,59]. Fingerprints, as studied in this work, do not require this kind of knowledge.

3.2 Discharge patterns of standard defects

Discharge models with standard defects are simple two-electrode models as seen in Figure 14. The following defects were analyzed.

1. Discharges in gases:
   - corona in air,
   - surface discharges in air,
   - floating parts in air.

2. Discharges in liquids:
   - corona in oil,
   - surface discharges in oil.

3. Discharges in solids:
   - cavity discharges,
   - treeing initiated by a conductor.

3.2.1 Discharges in gases

Although not always fully realised, gaseous insulation, especially ambient air, is the most commonly used insulation in high voltage engineering. Common types of discharges in gases are corona discharges, surface discharges and discharges of floating parts. Fingerprints of

these three discharge types were analyzed in this study. All tests were carried out in ambient air at atmospheric pressure.

Corona in air

Corona discharges occur at sharp points at high voltage or ground potential [57]. Three test configurations were used to represent this discharge phenomena: single point-to-plane corona, multiple-point corona and wire-to-plane corona. The corona discharge data were measured by the author.

1. **Single point-to-plane corona** [1,16,35,68,118,121]. Needles with a point diameter between 40 and 100 μm, at a distance from the plane of 20 to 40 mm were employed in these experiments. The tests were carried out both with the point at high voltage and at ground potential, at test voltages 10 to 60% above the discharge inception. Typical corona patterns were observed on the ellipse. Discharges occurred in one half of the voltage cycle only. In the case of a needle at high voltage potential, the discharges were symmetrically distributed around the negative voltage peak. In the case of a needle at ground potential, the same took place around the positive voltage peak. The discharges were regularly spaced and had equal magnitude. Discharge data were collected for a period of 2 minutes. The test arrangements with corresponding fingerprints of the single point-to-plane corona are shown in Figure 15 (corresponding discharge distributions are shown in Appendix A). The fingerprints represent one typical measurement out of many. Both fingerprints were collected using the same test voltage, the same distance from the plane, and a needle with the same point diameter.

Note the values of the operators in both cases. In the case of a needle at high voltage potential, the asymmetry operator has a value of 1. This indicates that the discharges occurred in the negative half of the voltage cycle only, which was actually observed. In the case of a needle at ground potential, the asymmetry has a value of -1, which indicates that the discharges occurred in the positive half of the voltage cycle only. It can be seen that by multiplying the asymmetry by -1, it is possible to obtain a value of the asymmetry operator for corona of the opposite type.

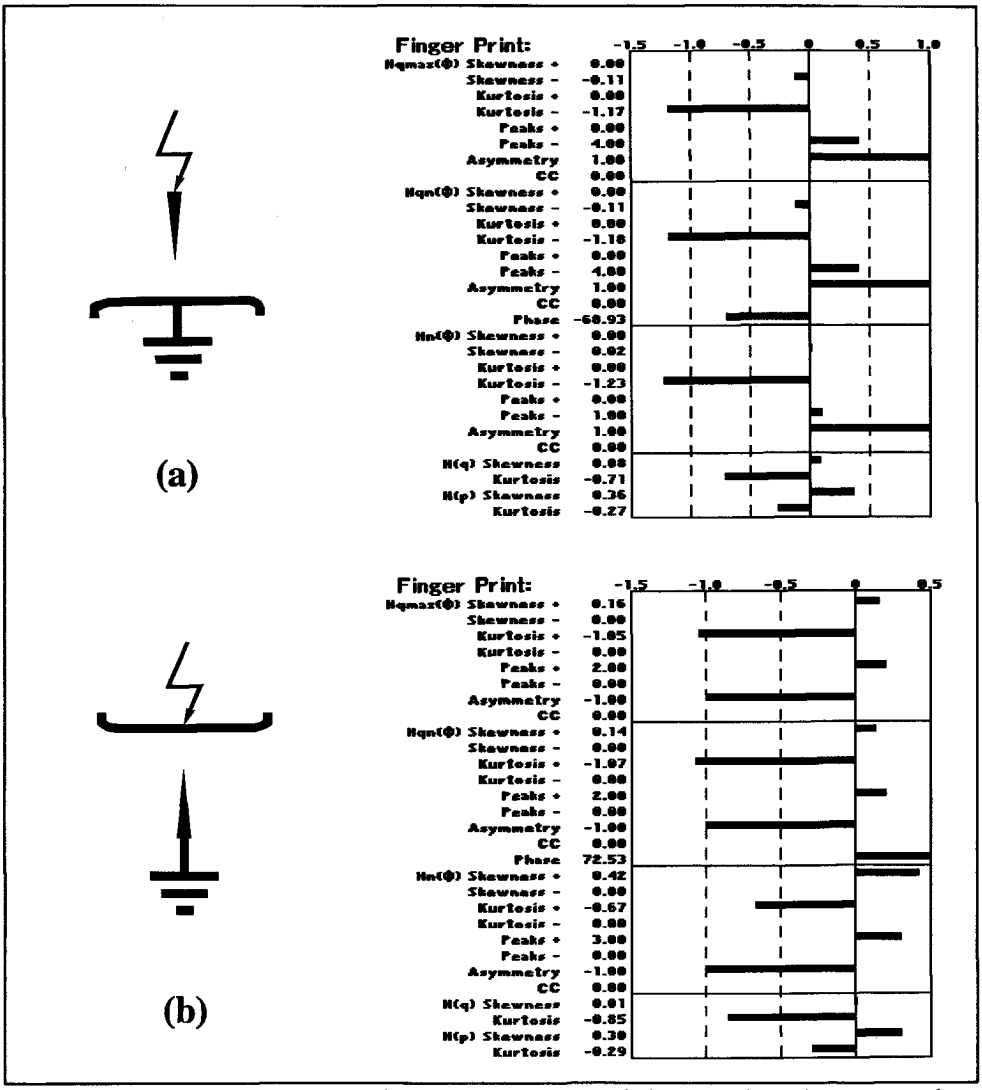

Figure 15. Typical fingerprints of the (a) high voltage and (b) ground single point-to-plane corona in air.

2. **Multiple point corona** [116]. Unraveled strands of a copper wire, with a distance from the plane of 20 mm, were used to produce discharges. The diameter of a single strand was 50 μm. Tests were carried out with points at high voltage and at ground potential, at voltages 50% above the discharge inception with a duration of 2 minutes. Visual observations of the discharge patterns on the ellipse revealed that the discharges occurred in *both half cycles* of the test voltage. They were symmetrically distributed around both voltage peaks with unequal discharge magnitudes in each cycle. In the case of points at the high voltage potential, larger discharges occurred in the positive half-cycle of the test voltage. Points at ground potential, showed the opposite. A fingerprint of multiple-point corona at the high voltage side can be seen in Figure 16.

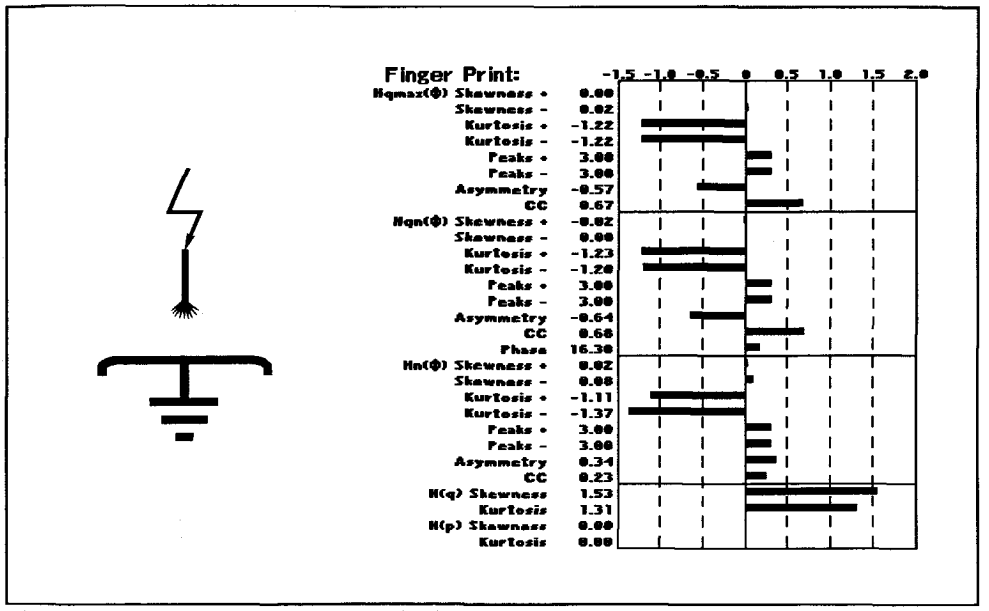

Figure 16. Typical fingerprint of multiple-point corona at the high voltage side in air.

Fingerprints of multiple point corona clearly differs from fingerprints of single point-to-plane corona. For example, the asymmetry operator is, in the case of multiple-point corona, not equal to 1 or -1, the cross-correlation is larger than zero, *etc.* Also, because discharges at multiple-point corona occur in both half-cycles of the test voltage, there are differences in values of operators in the positive and the negative half of the test voltage.

3. **Wire-to-plane corona**. In this case, a 80 mm-long copper wire with a diameter 50 μm was stretched above a plane electrode, see Figure 17. The distance from the plane was varied between 20 to 30 mm. At a voltage just above the discharge inception voltage, patterns on the ellipse resembled that of a single point-plane corona. However, fingerprints were obtained at a voltage of 50% over the inception voltage, throughout 2 minutes. For the wire at high voltage potential, the discharges were symmetrically distributed around the negative peak of the test voltage. In contrast to single point-to-plane corona, the discharges were not equally spaced and also their magnitude showed more variations. This can be explained by the fact that discharges can occur at different sites at the wire. The test configuration and the corresponding fingerprint is shown in Figure 17.

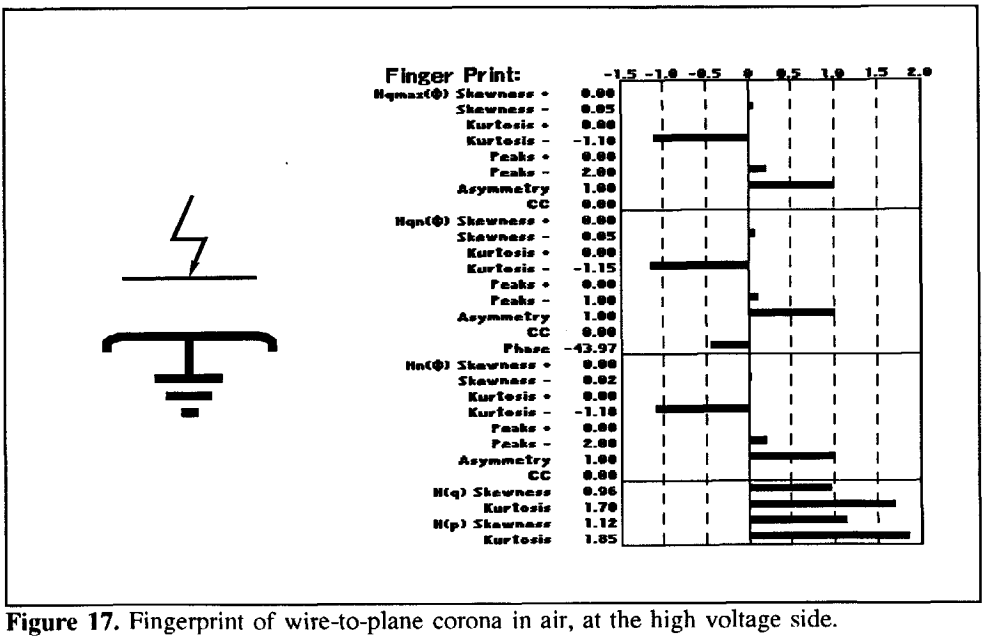

Figure 17. Fingerprint of wire-to-plane corona in air, at the high voltage side.

It can be seen that the fingerprint of wire-to-plane corona resembles, to some degree, that of single point-to-plane corona. Compare, e.g., the values of the asymmetry operator and cross-correlation factor in Figures 17 and 15.a which are the same in both cases..

Surface discharges in air

Surface discharges may occur along dielectric surfaces with a high tangential field stress. Typical examples of high-voltage components with frequent occurrence of surface discharges are bushings, ends of cables, the overhang of generator windings, *etc.* [57]. Due to the conductive nature of discharges they act as extensions of the electrode and can easily extend beyond the region where they originated [83,109].

A rod-plane configuration was used to model surface discharges. An aluminium, copper or stainless steel ring with a diameter of between 25 and 50 mm and with rounded edges was placed on top of a 10 mm-thick Perspex plate with a polyethylene sheet on it, see Figure 18. The thickness of the polyethylene sheet used in these experiments did not exceed 0.5 mm. The test voltage was chosen to be 50% above the discharge inception. Fingerprints were collected by the author for a period of 2 minutes, with the rod at high voltage and ground potential. After each test a new sheet was used. An example of a typical fingerprint of surface discharges in air, with the rod at high voltage potential can be seen in Figure 18.

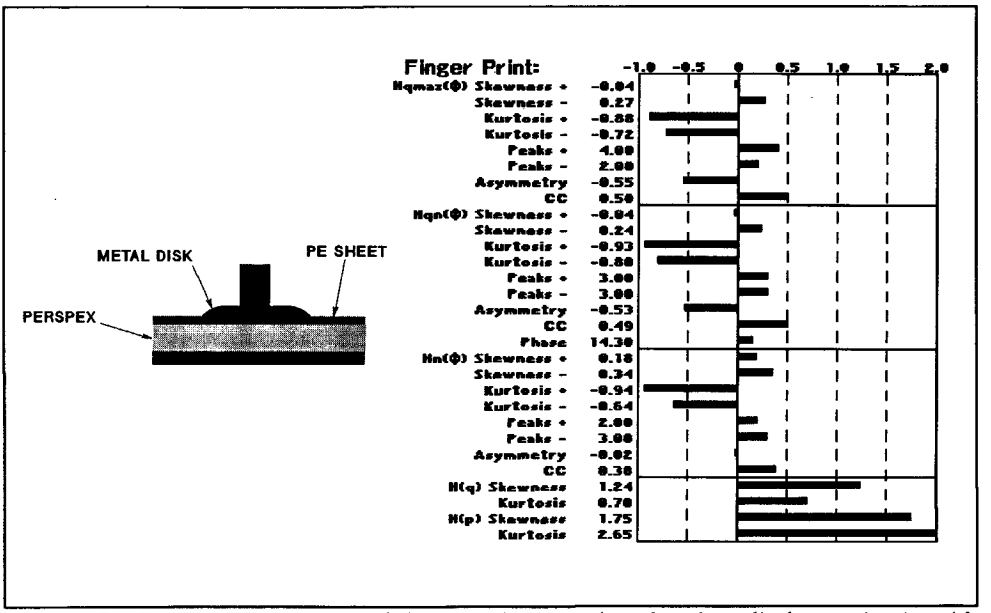

Figure 18. The test arrangement and the typical fingerprint of surface discharges in air, with the rod at the high voltage potential.

Floating parts in air

This type of discharge is usually caused by metallic parts left on the floor of a test area, or a loose connection of a ground screen inside a test object. These floating parts acquire voltage by electrostatic charging from the high-voltage test circuit and may produce typical discharges. Floating parts in air were modelled by an ungrounded metallic plate placed at 50 cm distance from a high-voltage terminal [35]. The air gap between the plate and the ground was varied between 1 to 2 mm. The discharge data were collected throughout 20 minutes at test voltages 20 to 60% above the discharge inception. The test arrangement and the typical fingerprint are shown in Figure 19.

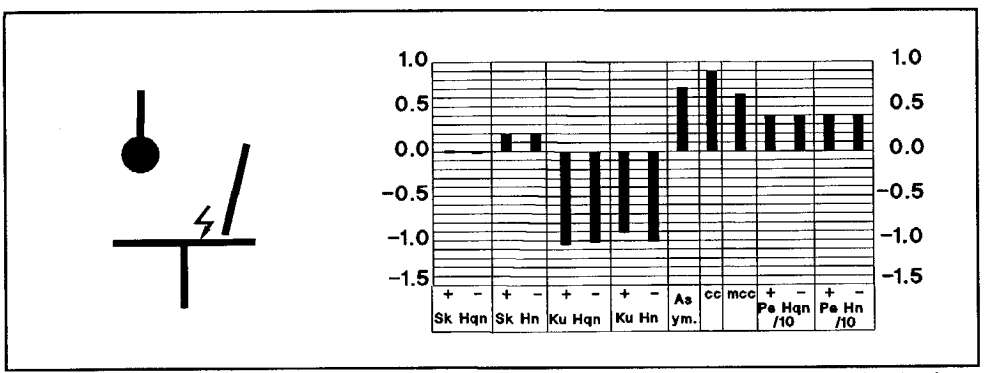

Figure 19. Discharge model of floating parts and corresponding fingerprint. Note that in these measurements the original version of the discharge analyzer was used, which at that time processed 15 statistical operators. Data after Gulski [35].

3.2.2 Discharges in liquids

Insulating liquids are used in a number of high-voltage components, such as cables, capacitors, bushings and transformers. Besides their use as an insulation, they can also serve as a cooling medium, *e.g.*, in transformers. Commonly used insulating liquids are mineral and synthetic oils. The initiation of discharges in liquids depends on many factors, *e.g.*, molecular structure of the liquid, water content, particle contamination, gas in solution, *etc.*, [12,24,71,124].

Fingerprints of two types of defects in dielectric liquids were analyzed by the author:

1. corona in oil,
2. surface discharges in oil.

A commercially available oil (Shell, Diala C) with a viscosity of about 20 cSt was used in experiments. No special precautions were taken to prevent water or particle contamination.

Corona in oil

This type of defect was modelled with a simple point-to-plane configuration, see Figure 20. A needle with a point diameter of 40 μm, with a distance from the plane of 40 mm, was used in the experiments. Fingerprints were collected for a period of two minutes at a test voltage of 50% above the discharge inception. With a needle at the high voltage potential, the discharges occurred in both half-cycles around the voltage peaks, with much larger discharges in the positive half-cycle, as has been observed before [97]. Rather erratic behaviour at a repetition rate of a few discharges per second was observed. The discharge model used and the typical fingerprint of the corona discharges in oil are shown in Figure 20.

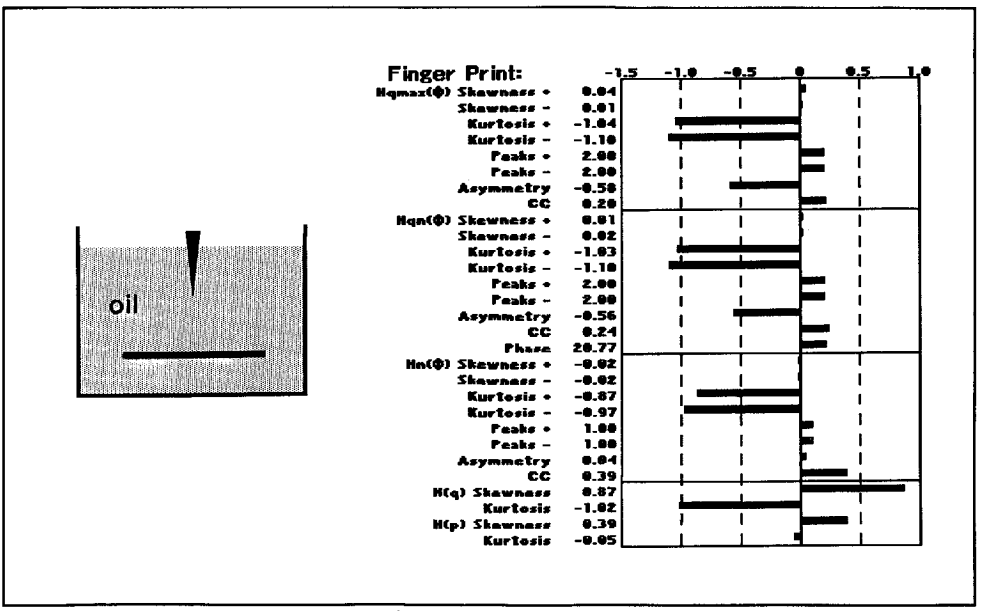

Figure 20. Typical fingerprint of single point-to-plane corona in oil, with the point at the high voltage side.

Discharges as observed on the ellipse were much larger in the positive half-cycle of the test voltage. This can be seen in the asymmetry of $H_{qmax}(\varphi)$ and $H_{qn}(\varphi)$ distributions which is less than -0.5. Relatively large variations were seen in the values of operators. This was caused by the low discharge repetition rate. Longer times are thus needed for data collection, so that more reliable data can be obtained.

Surface discharges in oil

Surface discharges in oil were modelled by a rod-plane arrangement similar to that of surface discharges in air, see Figure 18, but the test set-up was immersed in oil. A (1 mm- thick) copper ring with a diameter of 35 mm and with rounded edges was placed on top of a Perspex plate with a polyethylene sheet or with an oil-impregnated paper sheet on it. The thickness of the Perspex plate was varied between 3 to 10 mm. The thickness of the

polyethylene sheet or oil-impregnated paper sheet did not exceed 0.4 mm. Discharge data were collected throughout 2 minutes at test voltages of 50% above the discharge inception. After each test new samples were used. The discharges occurred in both half-cycles of the test voltage in advance of the voltage peaks, with approximately equal magnitudes in each half-cycle. This was reflected in the asymmetry operator which was approximately equal to zero. Large variations in discharge patterns were observed with each new sample. Furthermore, different fingerprints were obtained for different materials used in the tests, see Figure 21. Because the discharges patterns were not unique, the fingerprints represent just one of the many cases which occurred during the measurements.

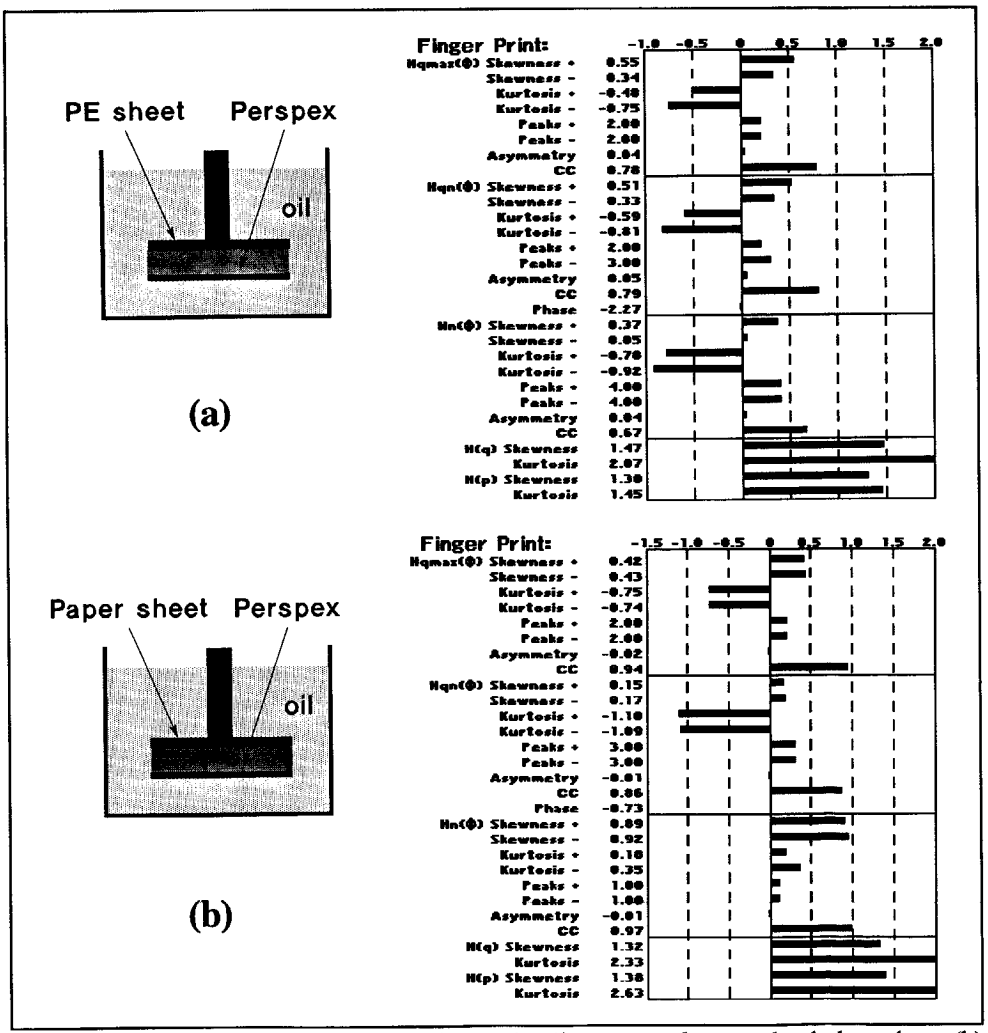

Figure 21. (a) Fingerprint of surface discharges in oil propagated on a polyethylene sheet. (b) Fingerprint of surface discharges in oil propagated on an oil-impregnated paper sheet.

3.2.3 Discharges in solids

Internal discharges in solids occur in inclusions of low dielectric strength [57]. These are, *e.g.*, cavities in cast resin components, extruded plastic cables, stator insulation, foreign particles such as dust or textile fibres embedded in insulation, *etc.* Discharges in these defects may develop to treeing discharges, which in the end cause the breakdown of the insulation. Therefore, detection and recognition of discharges is important from the practical and technological point of view. Fingerprints of the following artificially created defects were analyzed.

1. **Single cavity, dielectric bounded.** In this case flat, square and narrow dielectric bounded cavities were investigated.

2. **Single cavity, electrode bounded.** This cavity type was studied as the opposite case to a dielectric bounded cavity. Data from a flat cavity were examined only.

3. **Multiple cavities.**

4. **Treeing initiated by a conductor.**

Cavity discharges

Flat dielectric bounded cavity. A cavity was either drilled in PVC or Perspex or punched in a stack of polyethylene sheets [35]. The cavity dimensions were: 5 or 10 mm diameter, 1 mm height. An example of a fingerprint of this cavity type is shown in Figure 22. Typically, for fingerprints of a flat dielectric bounded cavity, the kurtosis of $H_{qn}(\varphi)$ distribution was negative, while all other operators were positive.

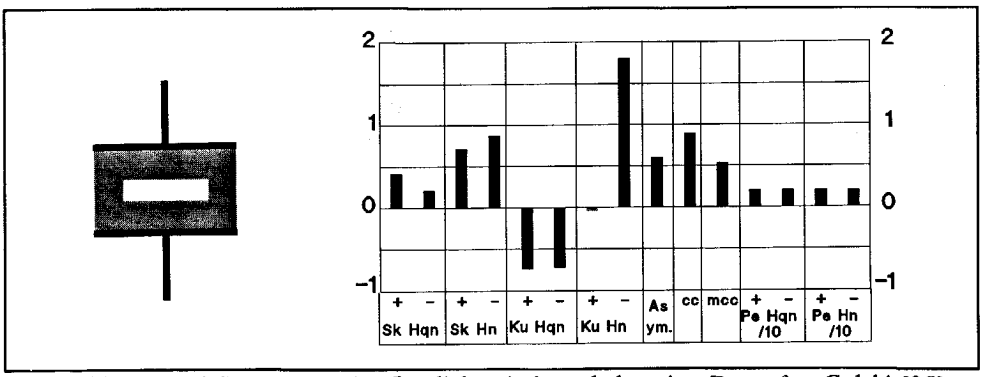

Figure 22. Typical fingerprint of a *flat* dielectric bounded cavity. Data after Gulski [35].

Square dielectric bounded cavity. A cavity was made in a way similar to the case above [35]. The dimensions of the cavity were: 1 mm diameter, 1 mm height. A fingerprint of this square, dielectric bounded cavity can be seen in Figure 23. The fingerprint resembles to some degree a fingerprint of a flat cavity, see Figure 22, although some fine differences can be found. For example, the kurtosis of $H^{-}_{n}(\varphi)$ distribution is much smaller in the case of a square cavity.

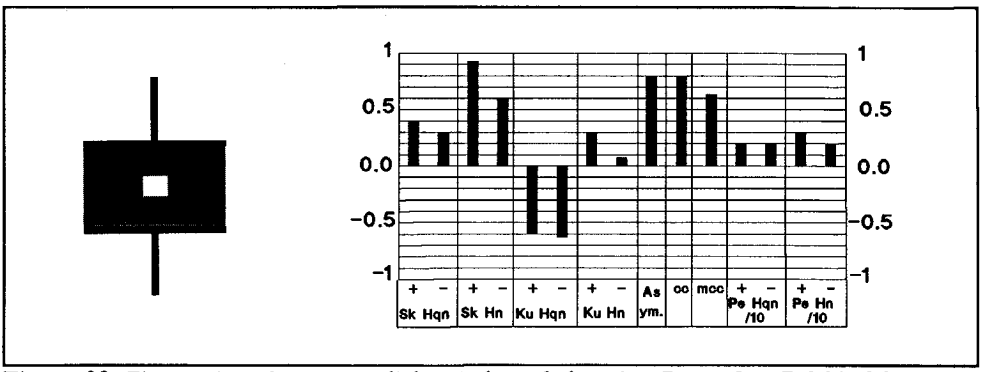

Figure 23. Fingerprint of a *square* dielectric bounded cavity. Data after Gulski [35].

Narrow dielectric bounded cavity. A cavity with a diameter of 1 mm and a height of 5 mm was drilled in PVC or Perspex [35]. A fingerprint of discharges in this cavity is shown in Figure 24. For a narrow cavity, the kurtosis of $H_{qn}(\varphi)$ and $H_{n}(\varphi)$ distributions and the skewness of $H_{qn}(\varphi)$ distribution were typically negative. Values of other operators tend to be positive.

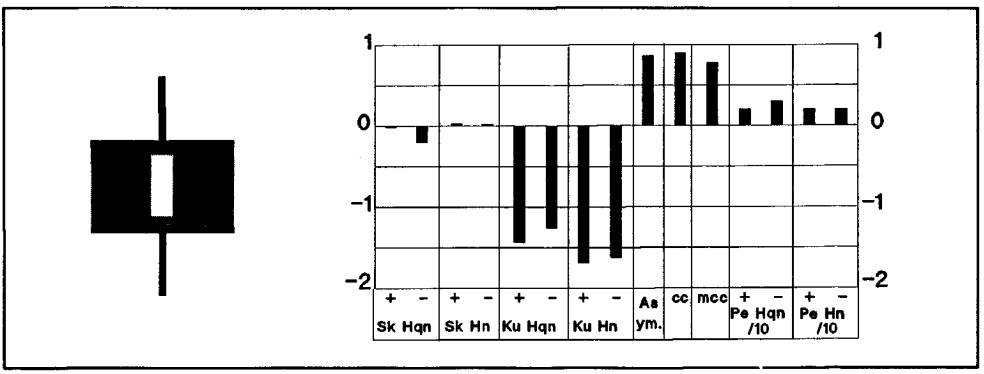

Figure 24. Typical fingerprint of a *narrow* dielectric bounded cavity. Data after Gulski [35].

Flat electrode bounded cavity. Discharges in this cavity type were studied with the aim of determining the position of a cavity in the dielectrics: an electrode as opposed to a dielectric bounded cavity. Data of a flat cavity with dimensions of 10 mm diameter and 1 mm height were examined only. A fingerprint of an electrode bounded cavity is shown in Figure 25. Typically, the kurtosis of $H_{qn}(\varphi)$ distribution was negative and values of other operators positive. The fingerprint seems to be similar to that of a square, dielectric bounded cavity, see Figure 23. Mathematical analysis is needed to recognize differences between these fingerprints.

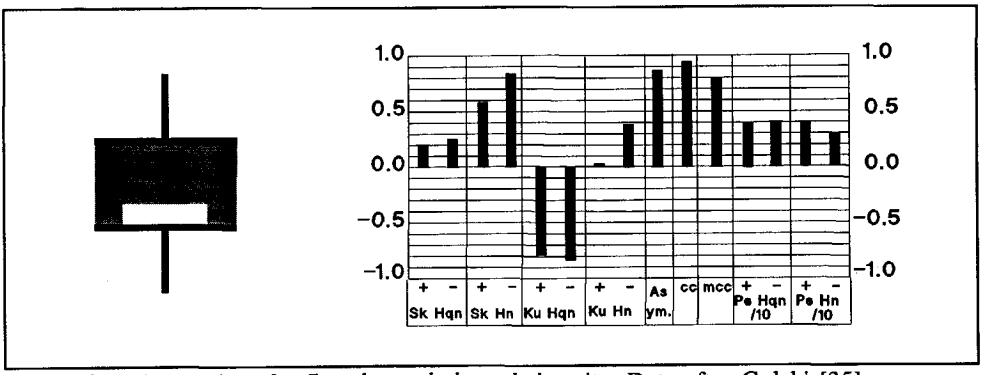

Figure 25. Fingerprint of a flat *electrode bounded* cavity. Data after Gulski [35].

Multiple cavities. During the extrusion of plastics or casting of epoxy resin, multiple cavities of various sizes may originate in the dielectrics. Therefore, from the technological point of view, it is important to recognize discharges in multiple cavities and discriminate them from single cavity discharges. Multiple cavities were modelled by a number of spherical cavities in a polyethylene slab [35]. The diameter of the cavities ranged from 0.5 to 4 mm. A typical finger-print of discharges in multiple cavities can be seen in Figure 26. At first sight, this fingerprint resembles that of a narrow cavity, see Figure 24. Closer inspection reveals differences between these fingerprints. In the case of multiple cavities, the kurtosis of $H_{qn}(\varphi)$ and $H_n(\varphi)$ distributions is larger than -1, while for a narrow cavity the kurtosis is smaller than -1.

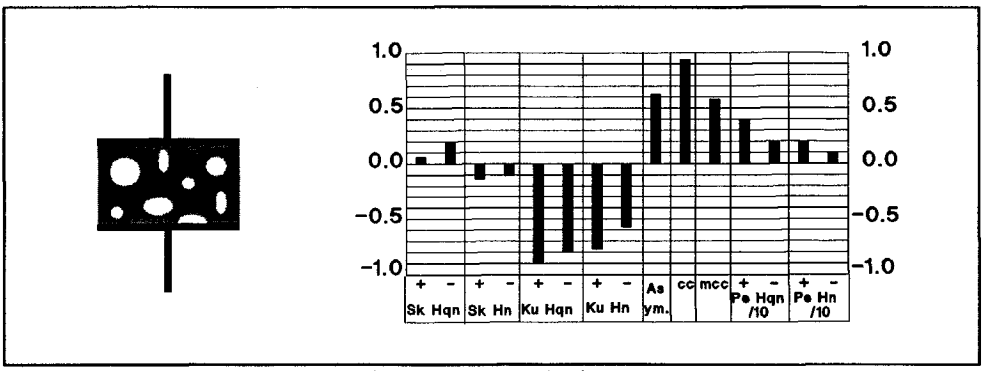

Figure 26. Typical fingerprint of discharges in multiple cavities. Data after Gulski [35].

Conclusion

It can be seen that the fingerprints of different cavities can be distinguished by visual comparison. However, the differences can in some cases be small, and, therefore, further mathematical analysis is needed to find the differences between the fingerprints.

Treeing initiated by a conductor

Treeing is one of the long-term mechanisms that are responsible for the breakdown of solid insulation. Electrical trees start from defects such as asperities, cavities, or foreign particles in the insulation [57]. They are composed of branched tubular channels with a diameter of several micrometers [13,19,25,115]. The propagation of trees is the result of gas discharges in the tubular structure. The incubation period is long and depends on the applied voltage. Sometimes years may pass before the first discharges are detected. Once trees are initiated, they grow rather quickly and may cause breakdown in an extremely short period of time, minutes or seconds.

Treeing discharges were initiated by a sharp needle inserted in Perspex [35]. The point diameter ranged from 40 to 100 μm, the point-to-plane distance was 40 mm. Discharge data were collected after an initiation period of about one hour for a period of 20 minutes at the

test voltage 50 kV. For fingerprints of treeing discharges, see Figure 27, the skewness of $H_{qn}(\varphi)$ distribution and the kurtosis of $H_{qn}(\varphi)$ and $H_n(\varphi)$ distributions were typically negative. Values of other operators were positive.

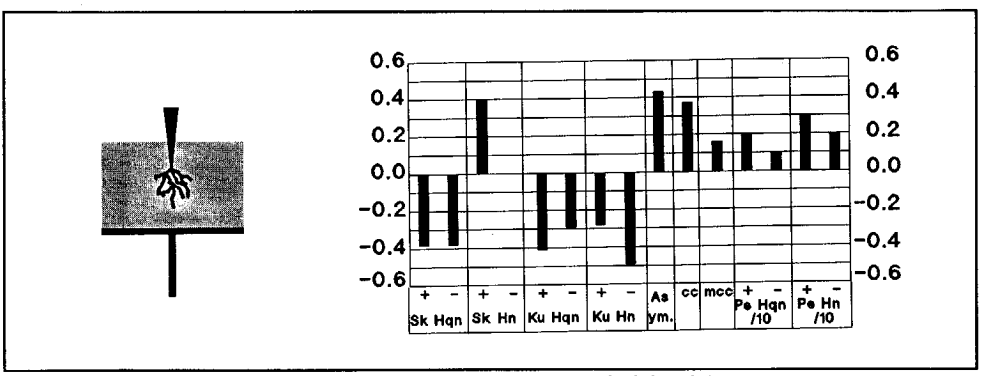

Figure 27. Fingerprint of treeing discharges. Data after Gulski [35].

3.3 Discharge patterns of industrial models and objects

This group of defects comprises either artificially created or naturally occurring defects in actual high-voltage components. The following objects were used in experiments:

1. gas insulated system 400 kV,
2. bushing 10 kV / 300 A,
3. current transformer 2×150 A to 5 A for 50 kV systems,
4. polyethylene cable 6/10 kV,
5. 3-core belted PVC cable 10 kV,
6. bushing 150 kV.

3.3.1 Gas insulated system 400 kV

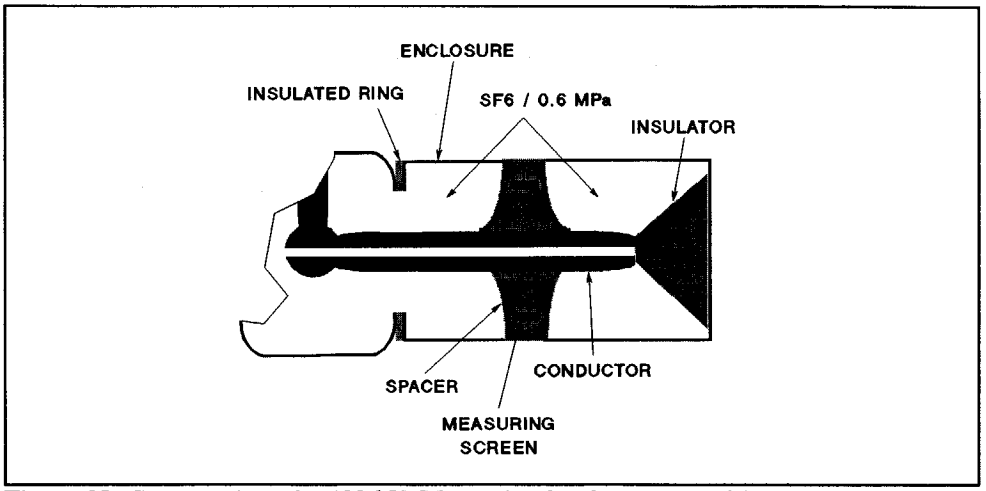

Figure 28. Cross-section of a 400 kV SF_6 gas-insulated system used in experiments.

In this case, a 400 kV gas-insulated system filled with SF_6 at 0.6 MPa was used in experiments, see Figure 28. Fingerprints of the following defects were analyzed [36,58].

1. **Corona discharges in SF_6.** Corona is caused by sharp metallic protrusions at the high voltage or ground potential. Such protrusions in gas-insulated equipment are usually the results of poor production, mechanical damage, or scraping during assembly. Although they do not necessarily cause breakdown during steady-state operating conditions, they can cause failure under lightning impulses [18,93]. Another potential danger of corona or any other type of discharges in SF_6 are decomposition by-products of SF_6, which can be toxic and highly corrosive [120]. Corona discharges were modelled by sharp aluminium splinters situated either at the conductor or on the spacer surface near the conductor. The typical fingerprint of corona discharges in SF_6 is shown in Figure 29.a.

2. **Floating parts I.** Free conducting particles are the most common form of defect in gas-insulated systems [18,22]. The particles acquire charge in the electric field, can move between the conductor and the enclosure, or bounce onto a spacer surface and can cause a breakdown. The danger of a particle depends on its shape and location, *e.g.*, a spherical particle is less dangerous than a long and thin one [93]. This type of defect was modelled by a metal spring from the conductor system with dimensions of 20 mm × 9 mm × 5 mm, which was placed at the bottom of the gas-insulated compartment. A fingerprint of this type of defect can be seen in Figure 29.b.

3. **Floating parts II.** Aluminium splinters, as they may occur when handling and assembling gas-insulated equipment, were loosely laid at the bottom of the test compartment. During the tests, discharges quickly disappeared [58]. This was a result of a particle movement to a field free corner, the place where the particle was found after opening the test compartment. The test arrangement and the corresponding fingerprint is shown in Figure 29.c.

4. **Conducting particle on the spacer near the conductor.** The danger of particles situated on the insulator surfaces is generally accepted [18,22,93]. The particles accumulate charge, which may enhance the failure probability. Furthermore, discharges occurring at the particle result in degradation of the insulator surface, which in the long term can lead to surface tracking and breakdown. This defect was simulated by painting a conductive speck of 2 mm radius on the surface of the spacer near the high-voltage conductor. An example of a fingerprint of this defect type can be seen in Figure 29.d.

5. **Conducting particle on the surface of the spacer.** As in the case above, a conductive particle of 2 mm radius was painted on the surface of the spacer, this time half-way between the conductor and the ground. A fingerprint is shown in Figure 29.e.

6. **Internal discharges in spacer.** This defect was caused by a faulty measuring screen inside a spacer. The measuring screen, made of copper mesh, did not adhere well to the epoxy resin of the spacer. As a result of bad adhesion, air pockets adjacent to the copper mesh were formed. A fingerprint of internal discharges in the spacer is shown in Figure 29.f.

It can be seen that the fingerprints in Figure 29 show remarkable differences. It follows that the recognition of different defects in gas insulated systems is well possible.

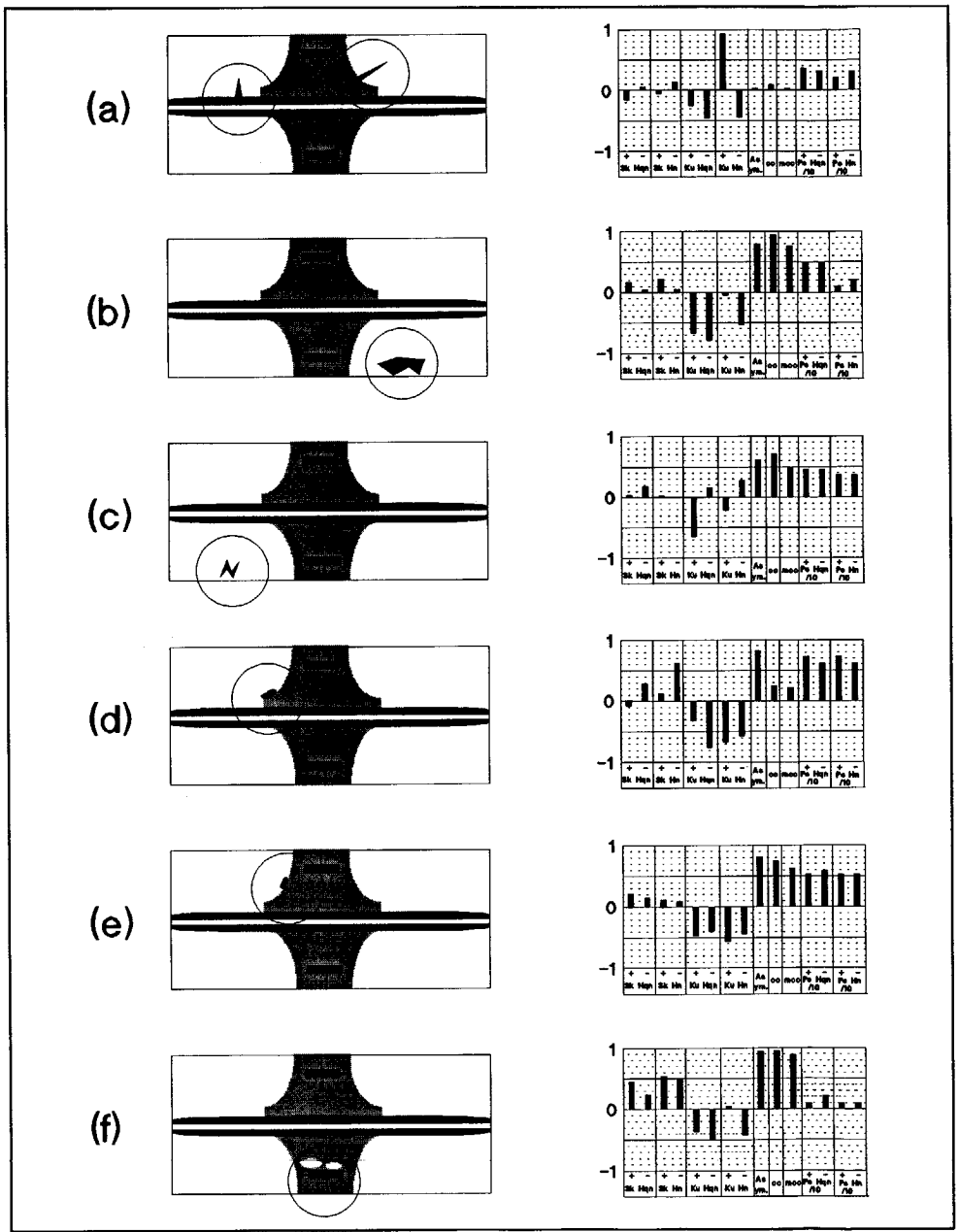

Figure 29. The test arrangements and corresponding fingerprints of the following discharges in SF_6: (a) corona, (b) floating part modelled by a metal spring, (c) floating part modelled by aluminium splinters, (d) conducting particle on the spacer near the conductor, (e) conducting particle on the spacer applied half-way between the conductor and the ground, (f) internal discharges in the spacer. Data after Gulski [36].

3.3.2 Bushing 10 kV / 300 A

This type of bushing provides the measurement of the primary current for medium voltage distribution systems. The apparatus consists of an epoxy resin insulation, current-measuring windings and a grounded casing. The cross-section of the bushing with the critical sites where discharges can occur is shown in Figure 30.

At discharge sites A, the metal casing that makes contact with the epoxy resin insulation may cause surface discharges. At discharge sites B, cavity discharges may occur due to a bad adhesion of the conductive layer at the insulator to the epoxy resin.

In the first case, the complete object was tested. Discharge data were collected for a period of 20 minutes at a test voltage 17 kV. A fingerprint obtained in this test is shown in Figure 30.a.

In the second case, the bushing with removed casing was tested. Discharge data were collected throughout 20 minutes at a test voltage 18 kV. A fingerprint of this discharge test can be seen in Figure 30.b.

The fingerprints as shown in Figure 30 seem to be quite similar. Mathematical analysis is needed to find differences (if there are any) between these two fingerprints.

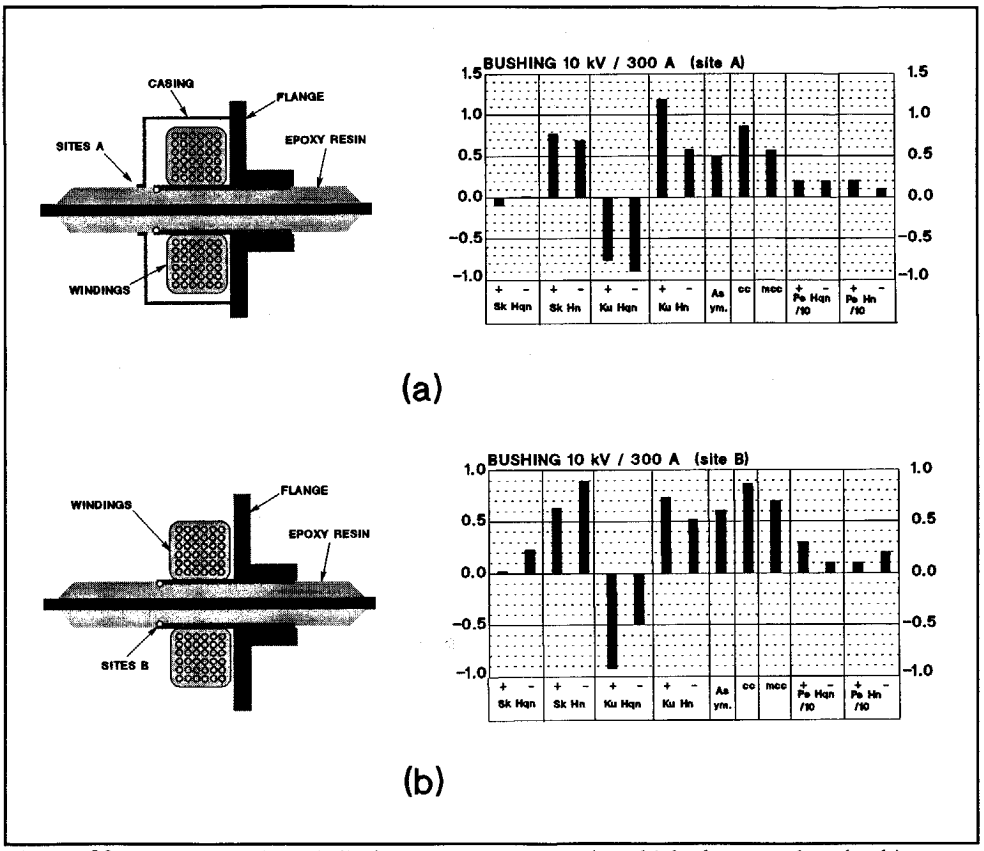

Figure 30. (a) Fingerprint of discharge measurement in which the complete bushing was tested. (b) Fingerprint of discharge measurement in which the bushing with removed casing was tested. Data after Gulski [35].

3.3.3 Current transformer 2 × 150 A to 5 A for 50 kV systems

This current transformer, which is used in 50 kV transmission networks, showed discharges below the operating voltage. Possible causes of discharges are cavities and cracks situated between the current windings and the core in the epoxy insulation, see Figure 31.a. The cracks are a result of high mechanical stresses from a short-circuit test. Discharge data were collected at a test voltage of 42 kV throughout 10 minutes [35]. A fingerprint obtained from the measured data is shown in Figure 31.b.

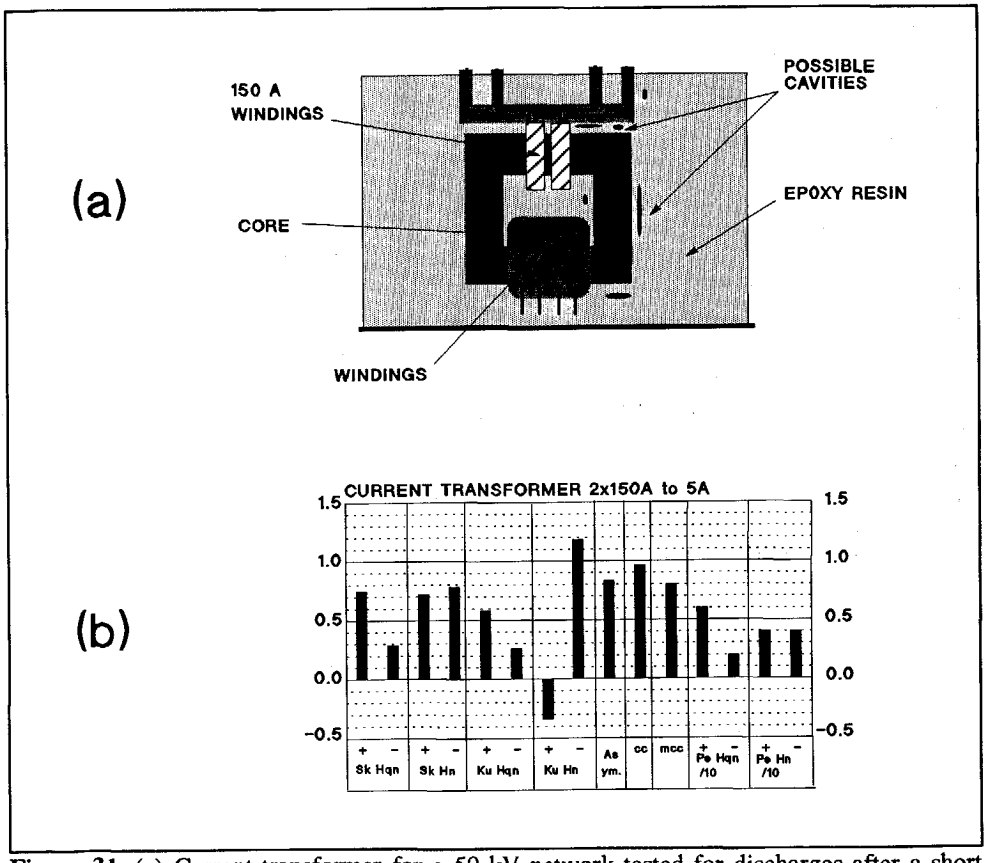

Figure 31. (a) Current transformer for a 50 kV network tested for discharges after a short circuit. (b) Fingerprint of the transformer as calculated from discharge data. Data after Gulski [35].

3.3.4 Polyethylene cable 6/10 kV

Two typical defects in a high-voltage cable were studied: treeing at a sharp electrode and discharges in an electrode bounded cavity. These defects were made artificially and were placed in the middle of a 1m long 6/10 kV cable, see Figure 32.a. To obtain good screening of the measuring electrode, the electrode was covered with insulating paper and a grounded copper screen.

Treeing discharges were initiated by a stainless steel needle with a radius of 50 μm inserted to 1.15 mm depth into the insulation. The cable with the needle was aged for 100 minutes at 28 kV test voltage. Treeing was initiated from the beginning of the test. Discharge data were collected after the ageing for 5 minutes at 42 kV test voltage [35]. The resulting fingerprint of treeing discharges is shown in Figure 32.b.

Discharges in an electrode bounded cavity were modelled with a cylindrical cavity with a 1mm diameter and 1mm height made within the polyethylene insulation, as seen in Figure 32.c. The tests were performed at 42 kV test voltage throughout 20 minutes [35]. A fingerprint of discharges in the electrode bounded cavity is shown in Figure 32.c.

Visual comparison reveals differences between the fingerprint of treeing in this cable and the fingerprint of the electrode bounded cavity in this cable. The differences in values of the kurtosis and the skewness of the $H_n(\varphi)$ discharge distribution are striking, see Figure 32.b and 32.c.

Note that the fingerprint of treeing in the polyethylene cable has some resemblance to that of treeing in a Perspex model as shown in Figure 27. To measure the degree of similarity between the fingerprints, mathematical methods have to be applied.

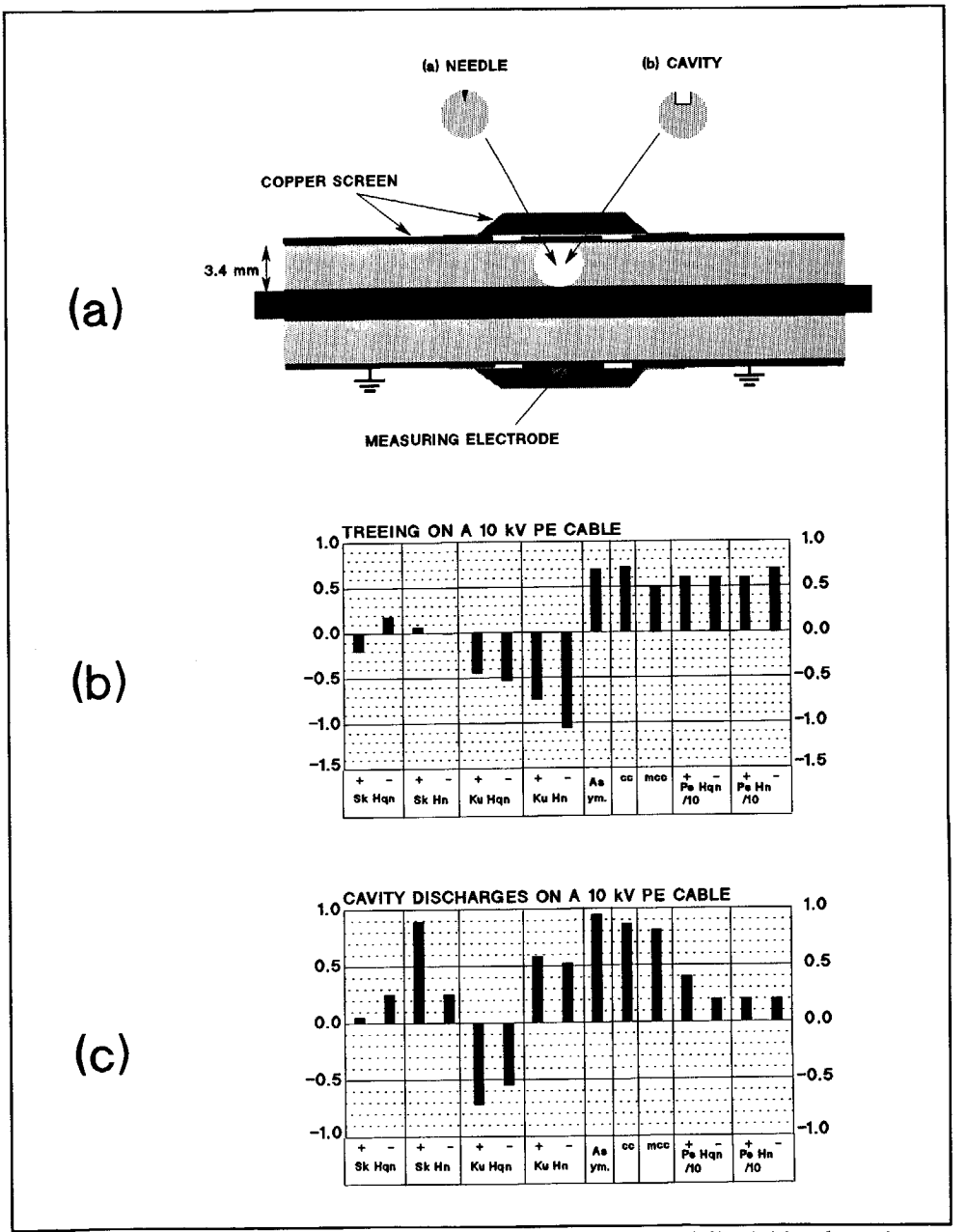

Figure 32. (a) 6/10 kV polyethylene cable with either artificially initiated treeing or artificially made cavity. (b) Fingerprint of treeing discharges in the cable. (c) Fingerprint of cavity discharges in the cable. Data after Gulski [35].

3.3.6 3-core belted PVC cable 10 kV

To analyze discharges in a three-phase configuration, a three-core belted cable rated for 10 kV was tested. Because the electric field in a three-phase constructions rotates and the shape of the field changes continuously, discharge detection is more difficult than in single-phase constructions. In practice, discharges can well be located in one of the cores [57]. It is known that the partial discharges in this type of cable occur in air gaps between the cores, see Figure 33.

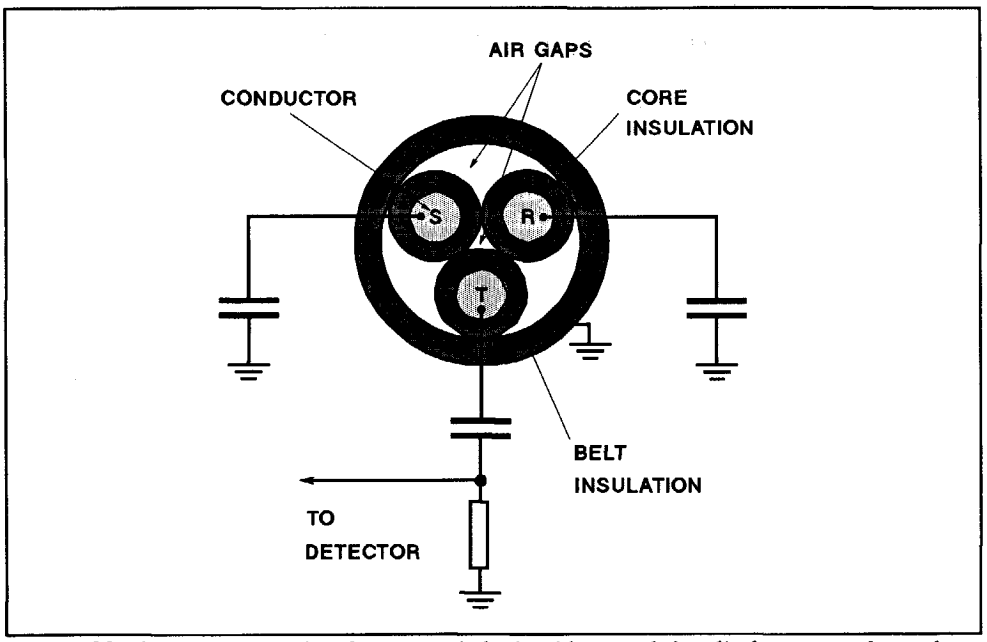

Figure 33. Cross-section of a three-core belted cable tested for discharges at three-phase voltage.

The investigations were carried out on a 6.5 m long cable with discharge-free terminations under oil. The cable was energized at three-phase voltage. Discharge data were collected for each phase separately for a period of 5 minutes at 5 kV test voltage [35]. The resulting fingerprints of each phase are shown in Figure 34. It should be noted that there are unexpected differences between the fingerprints of each phase. Compare, for example, the values of the skewness and the kurtosis of $H_{qn}(\varphi)$ distribution in all three cases, or values of other operators. Mathematical analysis is needed to study these differences.

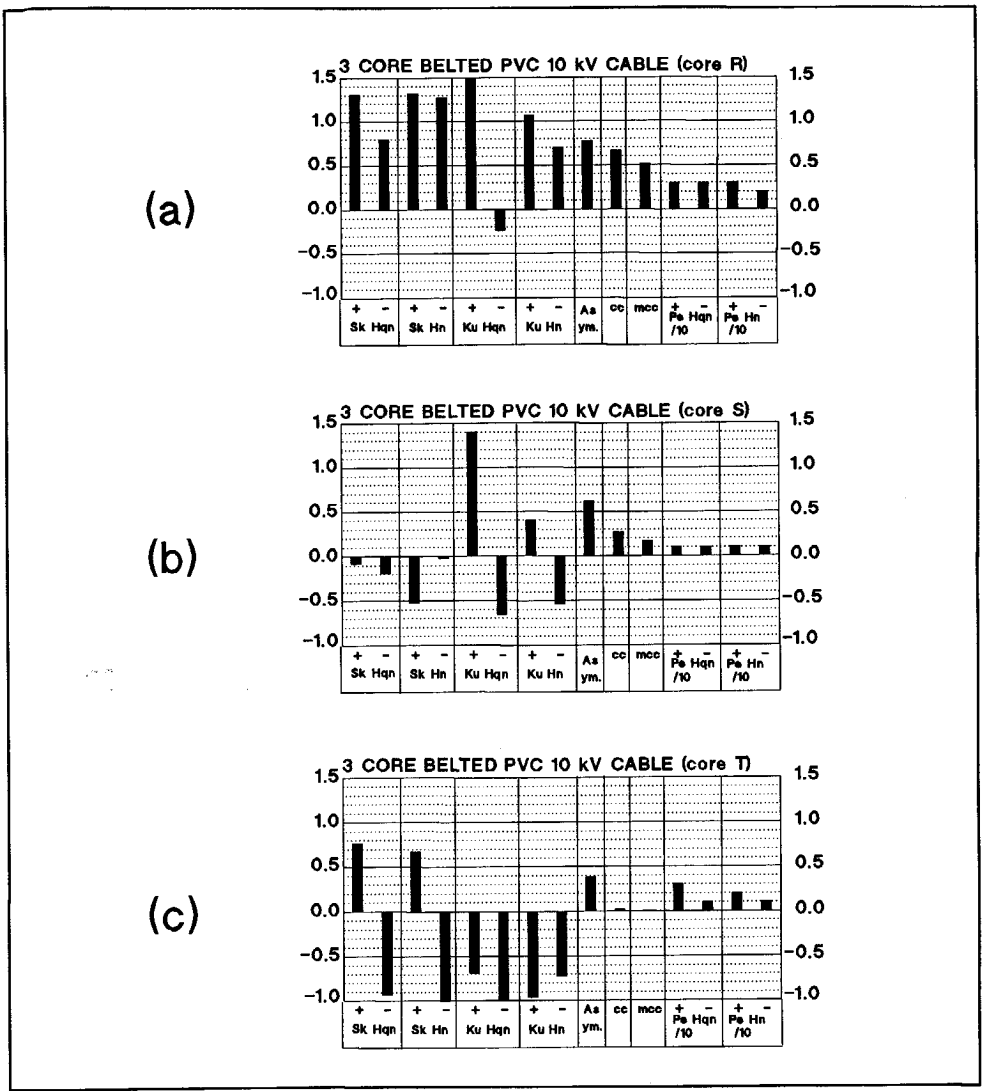

Figure 34. Resulting fingerprints of (a) *R*, (b) *S* and (c) *T* phases of a three-core belted cable tested at three-phase voltage. Data after Gulski [35].

3.3.7 Bushing 150 kV

This bushing is of the well-known capacitor graded type, with oil-impregnated insulation. The bushing is designed for a phase-to-ground voltage of 90 kV. It was rejected from service due to discharges below operating voltage. Two test were carried out.

In the first test, test A, discharge measurements were performed at a test voltage of 90 kV for 20 minutes [35]. The fingerprint calculated from obtained discharge data is shown in Figure 35.a.

The bushing was improved by applying a 0.5 MPa oil pressure to the system. After removal of the oil pressure, the discharge inception voltage increased to 140 kV, a safe value above the operating voltage.

The second test, test B, was then carried out at a voltage level of 160 kV for 20 minutes. The resulting fingerprint of this test is shown in Figure 35.b.

Visual comparison of the fingerprints did not reveal great differences. Further mathematical analysis is required to study the differences between the fingerprints.

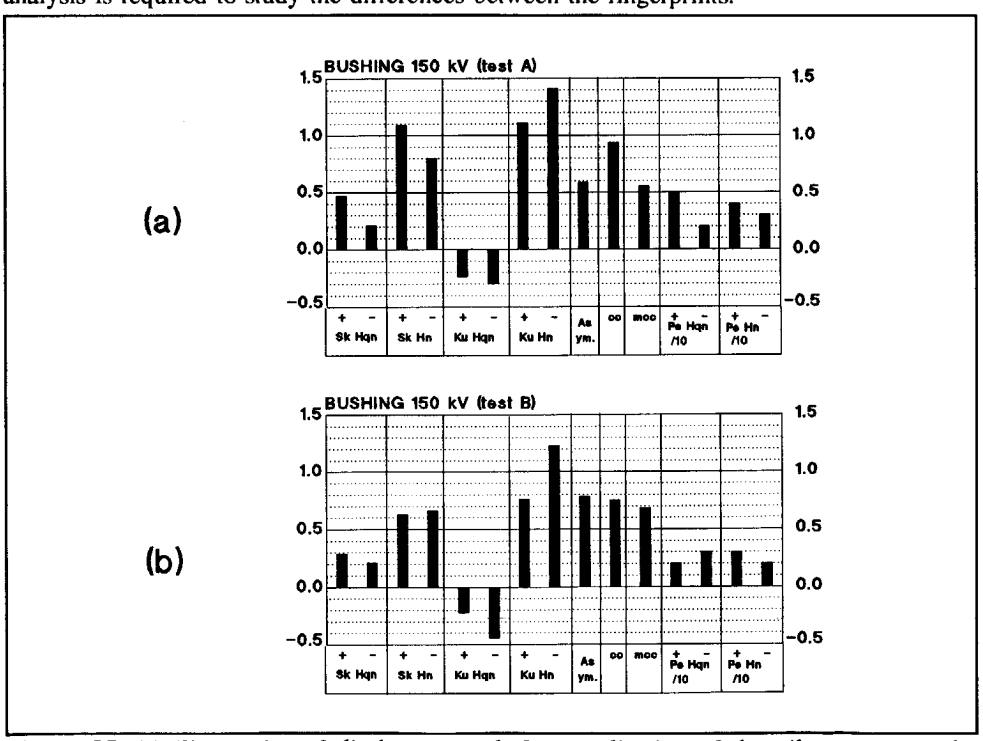

Figure 35. (a) Fingerprint of discharge test before application of the oil pressure to the bushing. (b) Fingerprint of discharge test after application of the oil pressure. Data after Gulski [35].

3.4 Conclusions

In this chapter fingerprints of various discharge sources have been presented. It was shown that different defects gave different fingerprints and the fingerprints were characterized by typical values of statistical operators.

To determine the origin of a fingerprint of unknown origin, a visual comparison could be used. In this case, the comparison is to be made between the fingerprint of unknown origin and the collection of fingerprints of known defects. However, it is quite clear that a real improvement, as compared to the recognition of discharges on an ellipse, has not been achieved. Such a 'by-eye' recognition is time consuming; it depends on a trained expert and mistakes are unavoidable. It follows that automation of the recognition is required to tackle this problem. Such an automated procedure must be fast, reliable, and able to catch all details of the fingerprints. Previous attempts to automate discharge recognition have been summarized in the introduction. This topic is discussed further in Chapter 4.

Chapter 4

Discrimination and classification of discharge patterns

To perform discharge recognition two important items are required:

1. a well-organized data base,
2. reliable tools for classification.

A data base is built by collecting fingerprints of known origin. It should be verified whether fingerprints of various defects differ from each other. For example, do fingerprints of, *e.g.*, corona in air differ from fingerprints of other defects, say cavity discharges, treeing, surface discharges, *etc*? The process of distinguishing groups of fingerprints is called **discrimination.**

Discrimination is also employed to find differences between the fingerprints of the same defect. For example, changes in fingerprints of dielectric bounded cavities during ageing can be examined. In this case, there is no a priori knowledge of the differences between fingerprints, but discrimination techniques can answer the question as to whether the fingerprints of a virgin cavity, a cavity aged for a few minutes, a cavity aged for several hours, *etc*, can be distinguished from each other.

Discrimination techniques are studied in the first part of this chapter, in section 4.1. During the course of this work, a number of procedures were examined. The less successful ones are discussed in Appendix B.1.

The classification of discharges concerns the application of a data base. A fingerprint of unknown origin is compared to all the available defects in a data base. Sometimes, the comparison is made with fewer defects; this is performed when there is *a priori* knowledge of the absence of some types of discharges in insulating constructions. For example, discharges in SF_6 are omitted from a comparison when discharges in oil are studied. The comparison must provide an answer to the following question: Is it possible to assign a fingerprint of unknown origin to that of known defects? This has to be performed with a great degree of reliability. In particular, assignment to a wrong defect must be avoided.

Classification techniques are studied in the second part of this chapter, in section 4.2. A number of methods were investigated. The less successful ones are briefly described in Appendix B.2.

4.1 Discrimination of discharge patterns

A primary purpose of discrimination is to find groups in a data collection, *i.e.*, to distinguish which fingerprints are similar. When this is known, a data base of different defects with similar fingerprints can be created.

Note that in two dimensions, take for example two arbitrary operators, it is relatively easy to identify groups by a simple visual observation of a scatter plot of the data. Because fingerprints as presented in Chapters 2, 3, 4 and 5 consists of 15 or 29 operators, we work in a 15- or 29-dimensional space, and it is more difficult to find clusters of similar fingerprints. Therefore, techniques which transform the multidimensional space to two or three dimensions, with as low as possible loss of information, are applied. Two groups of techniques were studied: mapping and cluster analysis methods.

4.1.1 Mapping techniques

In this case, multidimensional fingerprints are projected on new artificially created axes. The number of new axes is substantially lower than the dimension of original space. More than fifteen methods are available for this purpose [107,108]. In this section, the *principal component analysis* and *discriminant analysis* are investigated. Two other methods studied in this work (*multidimensional scaling* and *Sammon's nonlinear mapping*) are briefly discussed in Appendix B.1.1.

Principal component analysis

This mapping technique reduces the dimensions by finding 'principal components' of the data. 'Principal components' are linear combinations of statistical operators which describe the maximum variance in the data [49,63,77].

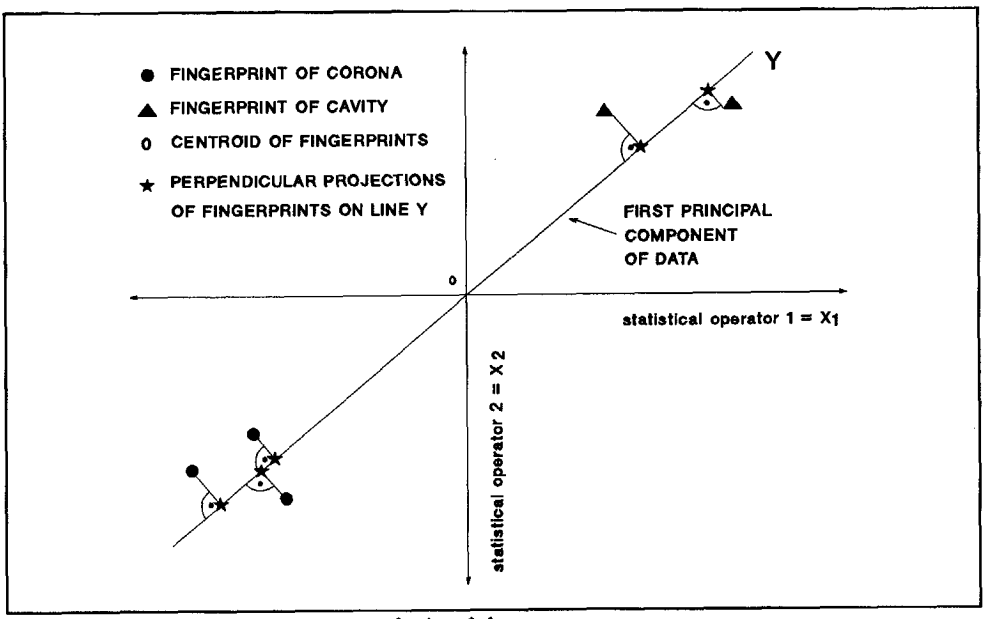

Figure 36. *Principal component* analysis of data.

To understand the principle of this method, five fingerprints in a two-dimensional space are shown in Figure 36. It can be seen that perpendicular projections of the fingerprints onto **one line**, *Y*, give positions of fingerprints with almost the same efficiency as that obtained with two statistical operators. The line, *Y*, which is the 'principal component' of the data, is in this example given by a linear combination of the two statistical operators:

$$Y = a_1 \cdot X_1 + a_2 \cdot X_2 \qquad (9)$$

where X_1 and X_2 are the first and the second operator. The parameters a_1 and a_2 are determined by maximizing the *variance* in the data. No *a priori* knowledge of the membership of individual fingerprints to a particular defect is required in this analysis.

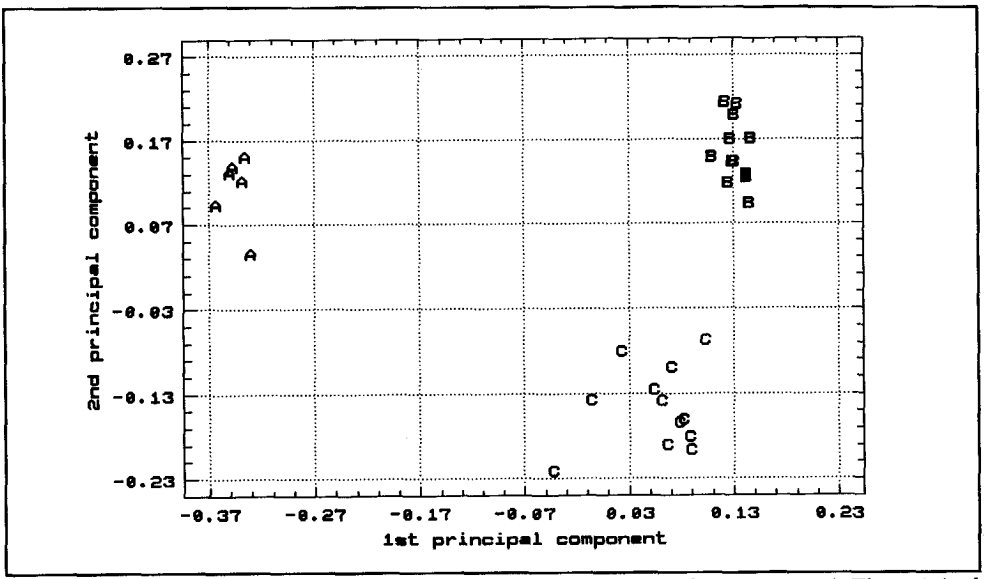

Figure 37. Resulting scatter plot of fingerprints on two 'principal components'. The original 29-dimensional space was reduced to a 2-dimensional space of the 'principal components'. Each letter represents a single fingerprint. The letter *A* labels single point corona in air at the high voltage side, *B* stands for a dielectric bounded cavity and *C* indicates surface discharges in air with a rod at the high voltage potential.

An example of the resulting plot of actual fingerprints on two 'principal components' is shown in Figure 37. Here, the original 29-dimensional space of statistical operators was reduced to a 2-dimensional space of 'principal components'. Each letter represents a single fingerprint. Three main groups can be identified: *A* stands for fingerprints of single point corona in air at the high voltage side, *B* corresponds to a dielectric bounded cavity and *C* indicates surface discharges in air with a rod at the high voltage potential. It can be seen that the first component separates corona discharges from the other defects. The second component separates the dielectric bounded cavities from surface discharges. The separation of groups was successful in this case.

The *principal component* analysis provides a quick way of assessing the structures in data. However, it should be kept in mind that maximizing the *variance* in the data may not necessarily reveal groups in the data, as is shown in the following section on discriminant analysis.

Discriminant analysis

In discriminant analysis, a linear combination of p statistical operators X_1, X_2, ..., X_p:

$$Z = u_1 \cdot X_1 + u_2 \cdot X_2 + \cdots + u_p \cdot X_p \qquad (10)$$

is called the discriminant function [23]. The u's are weights determined by maximizing the *separation* between defects. To perform the analysis, *a priori* knowledge of the membership of individual fingerprints to a particular defect is required.

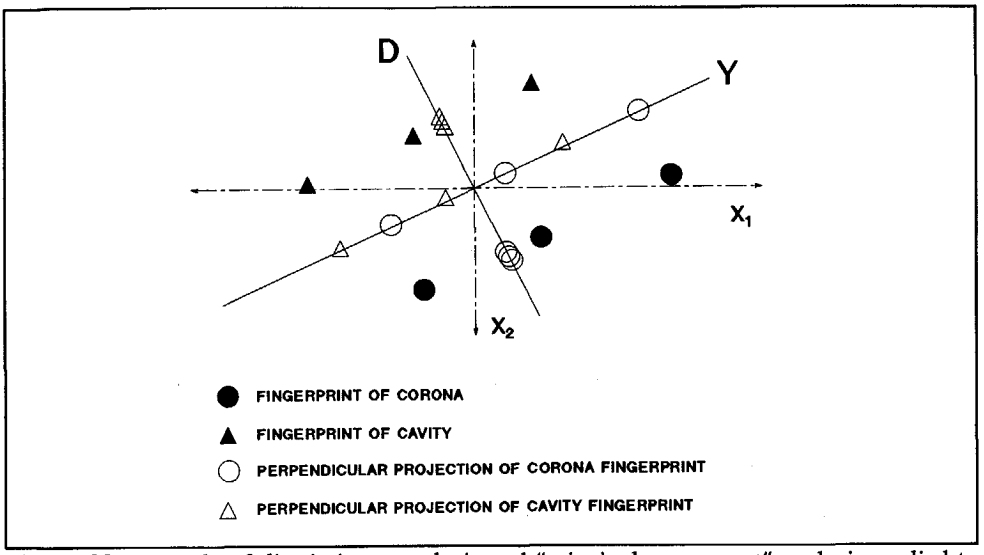

Figure 38. Example of discriminant analysis and "principal component" analysis applied to two-dimensional data. X_1 and X_2 are arbitrary statistical operators, the line D is the discriminant function and the line Y is the "principal component" of the data.

The difference between discriminant analysis and *principal component* analysis is illustrated in Figure 38, where two elongated clusters are shown. Discriminant analysis creates the maximum *separation* between the clusters, which is found at line D. Perpendicular projections of the fingerprints on this line clearly distinguish the clusters. "Principal component analysis" maximizes the *variance* in the data. In this example, perpendicular projections on line Y, which is the "principal component" of the data, do not reveal differences between the clusters.

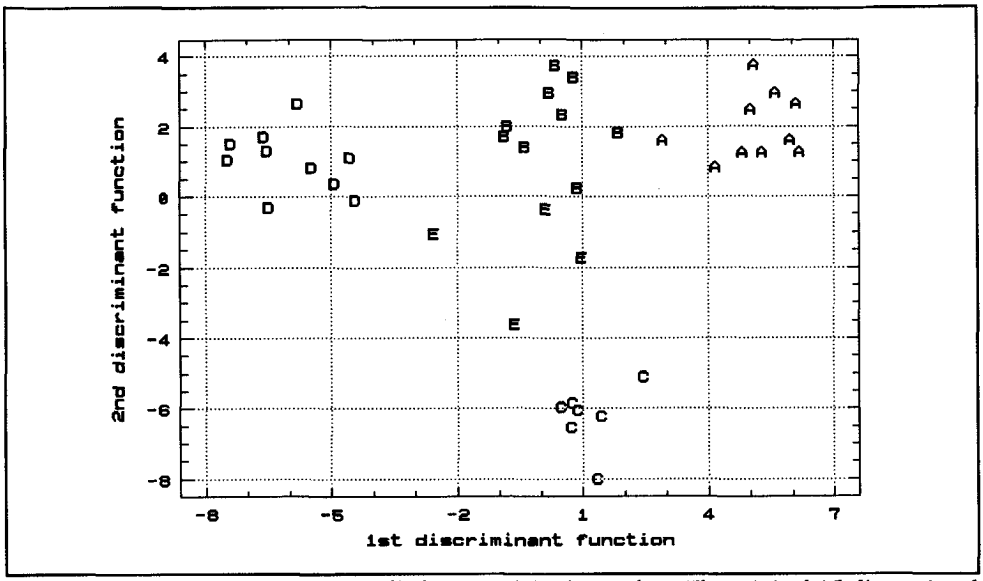

Figure 39. Discriminant analysis applied to actual discharge data. The original 15-dimensional space of statistical operators was reduced to a 2-dimensional space of discriminant functions. Each letter represents a single fingerprint: *A* - dielectric bounded cavity, *B* - surface discharges in air, *C* - surface discharges in oil, *D* - corona in air and *E* - floating parts in air.

An example of discriminant analysis applied to actual discharge data is shown in Figure 39. The fingerprints in the 15-dimensional space of statistical operators were mapped to two dimensions. The two discriminant functions successfully separate the fingerprints of five different defects.

The discriminant analysis yields the best *linear* separation between defects in a multidimensional space. When compared to the "principal component" analysis, the discriminant analysis requires *a priori* knowledge of the membership of individual fingerprints to a particular defect.

4.1.2 Cluster analysis

Cluster analysis tries to recognize groups without *a priori* knowledge. This means that no labels indicating the membership of an individual fingerprint to a particular defect are required. Cluster analysis provides another way to reduce the dimensions of the data. It gives clusters of fingerprints by indicating the group to which a fingerprint belongs. This is the difference between this technique and mapping techniques where a human insight is required to create clusters.

There are more than a hundred algorithms available for the clustering of data and each method would probably give different results [8,29,48,51,63,110]. In this section, *the group*

average and *the furthest neighbour* methods are applied to fingerprints of discharge defects. Other methods investigated during the course of this work are briefly described in Appendix B.1.2.

The group average method and the furthest neighbour method belong to the 'agglomerative' methods of clustering. Final groups in the data are formed as follows [63,69]:

1. Each fingerprint is declared as a group and distances between all groups are calculated.

2. Two groups with the smallest distance are fused together and declared to be one group. In this way the total number of groups in the data is reduced by one.

3. Distances between all groups are again calculated. The choice of distance is important. The group average method calculates the average distance between two groups. The furthest neighbour takes the largest distance between two groups.

4. Steps 2 and 3 are repeated until just one group is left.

The algorithm results in a tree structure, see Figure 40, which allows detailed examination of relationships between individual fingerprints [21,48,63,110]. Originally, such tree structures were used in zoology and botany where the similarity between different species, *e.g.*, apes and humans, was investigated.

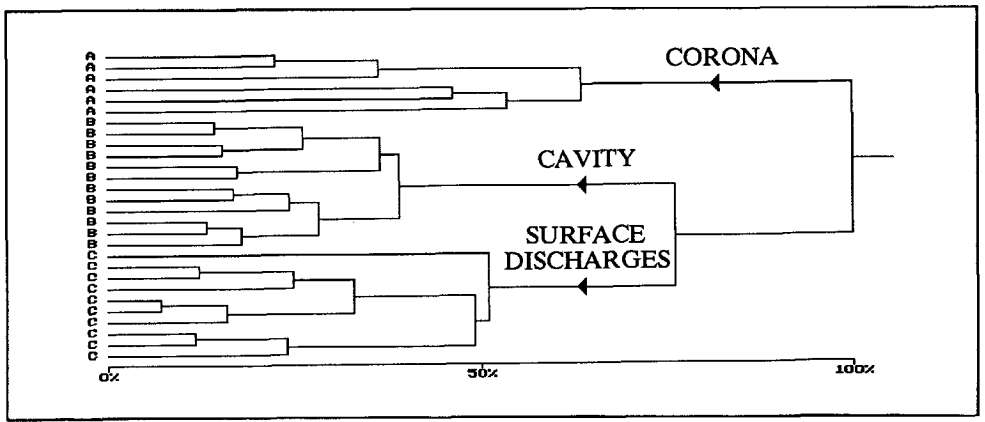

Figure 40. The furthest neighbour clustering method applied to discharge fingerprints. Each letter represents a single fingerprint. Three groups can be clearly identified: *A* - single point corona in air, at the high voltage side, *B* - dielectric bounded cavity and *C* - surface discharges in air with a rod at the high voltage potential.

The scale in the lower part of Figure 40 shows the *dissimilarity* between fingerprints as a percentage of the distance between the last two groups that were fused together. In the example shown in Figure 40 these last two groups were *A* and *BC*. It follows that similar fingerprints will be connected at relatively low dissimilarity levels, whilst differing fingerprints will be connected at relatively high dissimilarity levels. By cutting such a tree-

structure at a certain level, the data can be divided into different groups. This can be seen in Figure 40, where the furthest neighbour method was applied to actual discharge data. Each letter represents a single fingerprint. Three main "branches" of the tree-structure lead to three groups which can clearly be identified as: *A* - single point corona in air, at the high voltage side, *B* - dielectric bounded cavity and *C* - surface discharges in air with a rod at the high voltage potential.

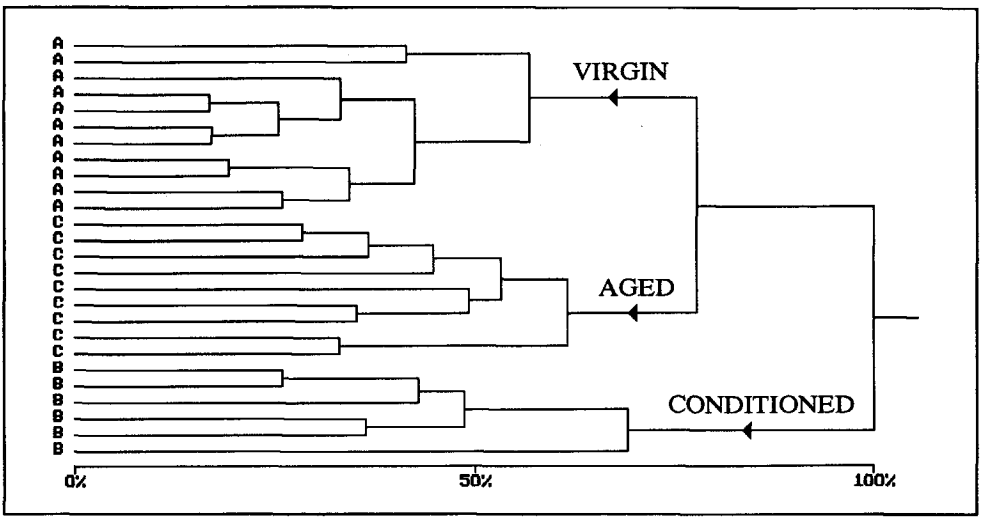

Figure 41. The group average clustering method applied to fingerprints of an electrode bounded cavity at the high voltage side aged for 90 minutes. Each letter represent a single fingerprint. Three main groups of fingerprints can be identified: *A* - cavity in the virgin stage, *B* - cavity aged 5 minutes (conditioned stage) and *C* - cavity aged 90 minutes (aged stage).

In another example, the group average method was applied to fingerprints of an electrode bounded cavity at the high voltage side aged for 90 minutes, see Figure 41. Details of the test procedure are given in Chapter 5. Three main groups of fingerprints can easily be identified as: *A* - cavity in the virgin stage, *B* - cavity aged 5 minutes and *C* - cavity aged 90 minutes. This corresponds with observations on this cavity type where three ageing stages have been found, see Chapter 5.

To asses how well a tree structure reflects the original multidimensional space various statistics are available, calculation details can be found in [48,110]:

1. cophenetic correlation coefficient, *cpcc*, which must be at least 0.6 or greater (maximum value is 1),

2. Δ coefficient, which must be as low as possible.

These statistics were calculated for each case above and are shown in Table 1.

Table 1. Calculated statistics for tree-structures shown in (a) Figure 40 and (b) Figure 41 obtained by the furthest neighbour (FN) method and the group average (GA) method.

	FN	GA
cpcc	0.92	0.96
Δ	0.32	0.11

	FN	GA
cpcc	0.79	0.81
Δ	0.42	0.16

In both cases, the group average method gave better results, suggesting that the relationship between fingerprints in the tree structures are more properly illustrated by this method than the furthest neighbour. During the course of this work, the group average method consistently produced better statistics than the furthest neighbour algorithm. Furthermore, when the number of fingerprints increases, the furthest neighbour method does not necessarily reveal the tree structure correctly [41]. The group average is robust, independent of the number of fingerprints in clusters and presents a relatively safe choice [51,67,84,85].

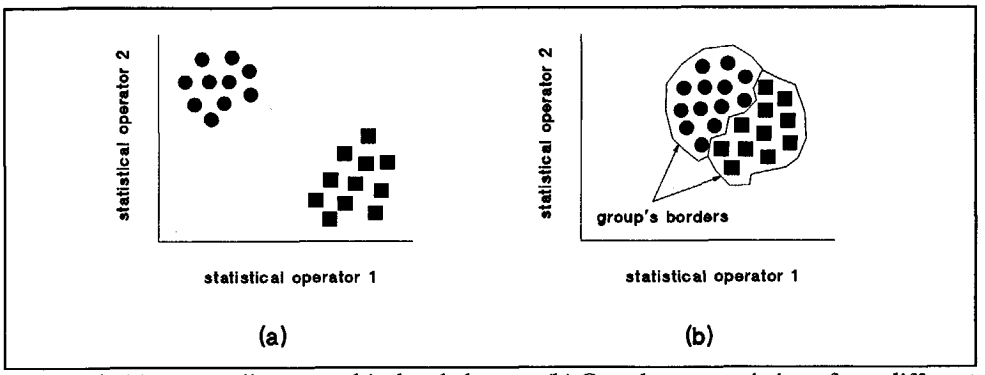

Figure 42. (a) Two-well separated isolated clusters. (b) One cluster consisting of two different groups. Each dot represents one fingerprint.

It should be noted that clustering algorithms usually recognize clusters which are well separated, see Figure 42.a. Sometimes, however, different groups do not form separated clusters, although the groups occupy different positions in space. This situation is shown in Figure 42.b. In such cases, there is *no clustering* method which could distinguish the groups in the data. The *classification* of a fingerprint of unknown origin to the groups can, however, be successful. The groups must then be known a priori, so that borders between the groups are known and satisfactory classification can take place.

Fractal features for discrimination

A completely different approach has been recently suggested by Satish [104]. In contrast to the former discrimination methods this method is not based on the operators of 2-dimensional discharge distributions, such as the skewness, the kurtosis, *etc.* It starts directly from 3-dimensional $H_n(\varphi,q)$ distribution, as shown in Figure 43. Two fractal features are used to quantify the 3-dimensional discharge patterns: *fractal dimension* and *lacunarity.*

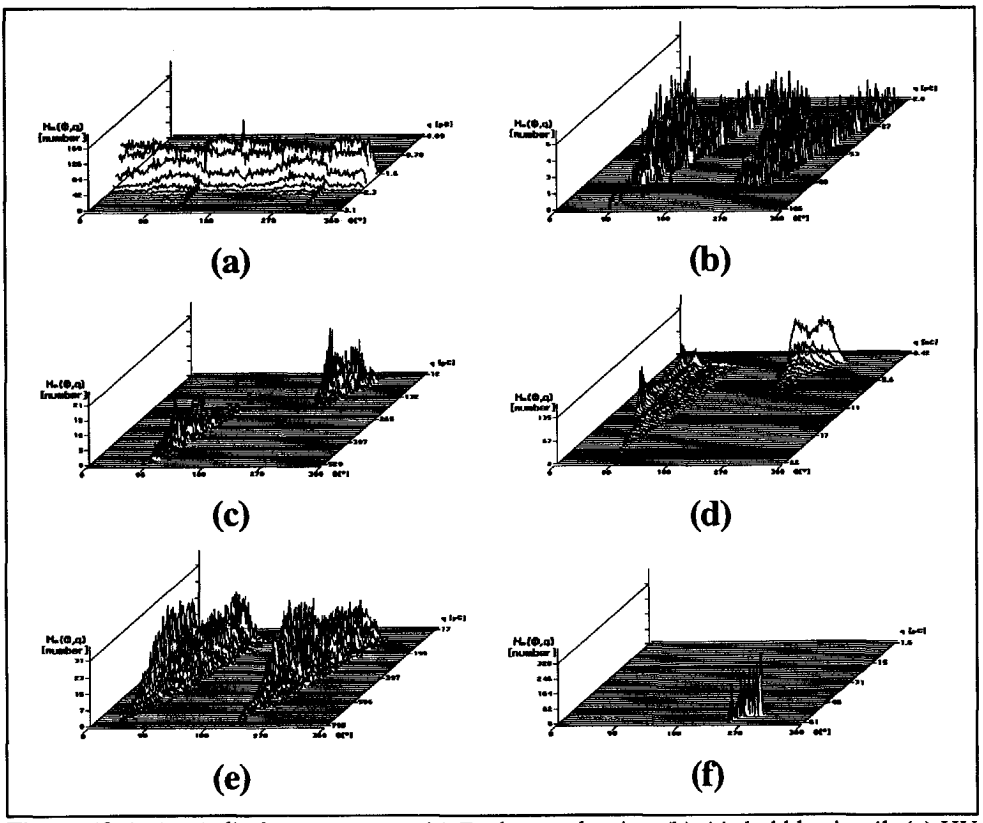

Figure 43. $H_n(\varphi,q)$ discharge patterns. (a) Background noise. (b) Air bubbles in oil. (c) HV single-point corona in oil. (d) HV surface discharges in air. (e) Dielectric bounded cavity in the virgin stage. (f) HV single-point corona in air.

Fractal dimension closely corresponds to surface roughness [76]. For the 3-dimensional discharge patterns it can range from 2 for a flat surface to 3 for a rough surface. This is shown in a simple example in Figure 44.

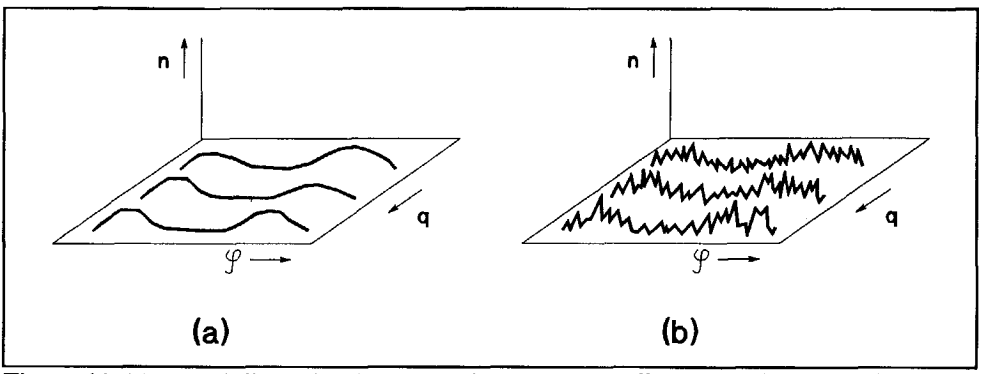

Figure 44. (a) Fractal dimension for a smooth surface is small, say 2.2. (b) Fractal dimension for a rough surface is large, say 2.8.

The second parameter - *lacunarity* - describes the denseness of a surface [76]. For the 3-d discharge patterns it can range from 0 to 1. The lacunarity is small for a dense surface and large for a coarse surface. This is shown in a simple example in Figure 45.

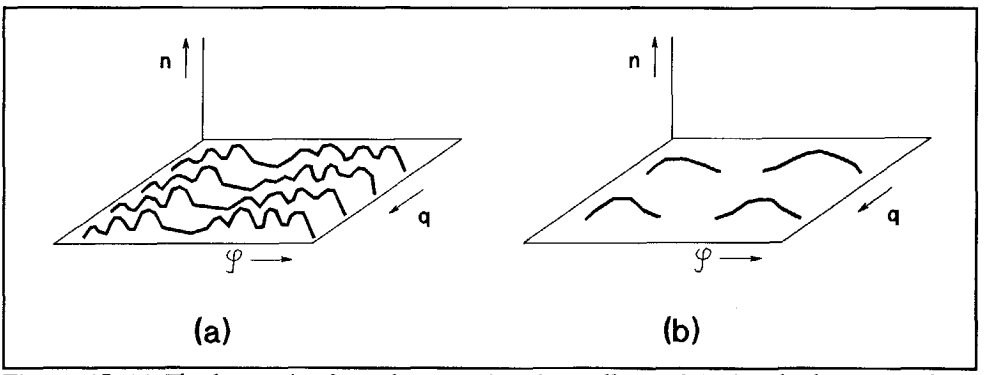

Figure 45. (a) The lacunarity for a dense surface is small, say 0.1. (b) The lacunarity for a coarse surface is large, say 0.9.

Details on the calculation of the fractal features are given in Appendix C.

An example of this approach is shown in Figure 46: both fractal features, the fractal dimension and lacunarity were calculated for 3-dimensional discharge patterns shown in Figure 43. It can be seen that successful discrimination of the discharge patterns took place. Each discharge source has a different position in the two-dimensional fractal space. It follows from these results that the fractal features have a good potential to discriminate between discharge patterns and can be used as an alternative to mapping and cluster analysis techniques.

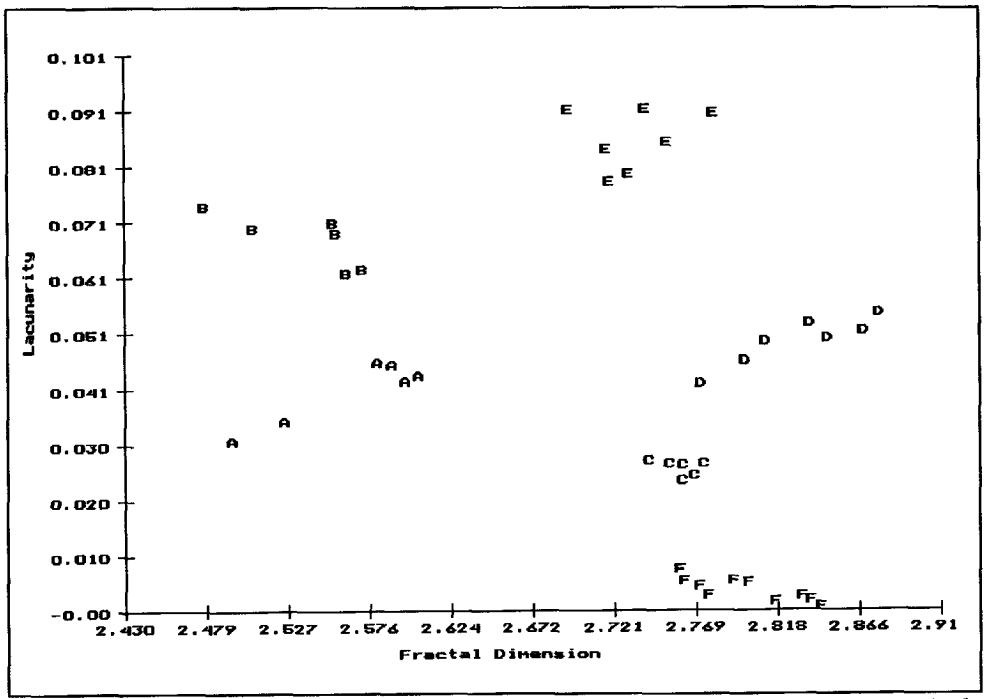

Figure 46. Scatter plot of discharge patterns in fractal space. Each letter represents a single measurement: *A* - background noise, *B* - air bubbles in oil, *C* - HV single-point corona in oil, *D* - HV surface discharges in air, *E* - dielectric bounded cavity in the virgin stage, *F* - HV single-point corona in air.

Scatter plots of discharge patterns in fractal space can be used to create different categories in a data base for discharge recognition. If this is the case, then it should be remembered that the discharge patterns may not be correctly recognized because discharge recognition is at the present time based only on the statistical operators, which represent another form of information extracted from the discharge patterns. Recognition based on both, statistical operators and fractal features, should be investigated in future.

4.1.3 Conclusions

Discovering structures in the data is a difficult problem and there is no 'best' procedure. Each method approaches the data in its own way and it is 'best' according to a criterion which is optimized by the method.

Mapping techniques

One way of exploring the data is to look at it. Scatter plots of fingerprints obtained by mapping techniques give the first impression on the structures in the data. Here, *principal component analysis* and *discriminant analysis* can each serve as a starting point. Other methods, such as *multidimensional scaling* and *Sammon's mapping* are also recommended.

Cluster analysis

Cluster analysis divides given fingerprints into groups. From the methods studied here, *the group average* method is preferred. It produces a tree structure which allows a detailed examination of the data. It is also robust and independent of the number of fingerprints in clusters.

Fractal features

Fractal dimension and lacunarity have also shown a good potential for the discrimination of discharge patterns and can be used as an alternative to other discrimination techniques.

4.2 Classification of discharge patterns

The main aim of classification is to determine the similarity of a fingerprint of unknown origin to the collection of fingerprints of known defects. Two main groups of methods were investigated: conventional classifiers and neural networks.

During the course of this work, data were used which were obtained by the original version of the discharge analyzer (15 statistical operators employed for classification), or the commercial version of the discharge analyzer (29 statistical operators used for classification). This is indicated where appropriate.

In the presentation of the results, a number of acronyms and abbreviations are used. To avoid confusion, a list is given here:

1. COR-AIR - corona discharges in air,
2. COR-SF6 - corona discharges in 0.5MPa SF_6,
3. CAV-SPAC - cavity discharges in spacer,
4. EXTRA-FLAT-DIEL - flat dielectric bounded cavity, 10 mm in diameter, 1 mm height,
5. FLAT-COND - flat electrode bounded cavity, 10 mm in diameter, 1 mm height,
6. FLAT-DIEL - flat dielectric bounded cavity, 5 mm in diameter, 1 mm height,
7. FLOA-AIR - floating parts in air,
8. FLOA-SF6 - floating part in SF_6, a metal spring in gas-insulated system,
9. GIS-SPLI - floating part in SF_6, an aluminium splinter in gas-insulated system,
10. MULT-DIEL - multiple cavities,
11. NARROW-DIEL - narrow dielectric bounded cavity,
12. SPAC-COND - conducting particle on a spacer in gas-insulated system near the conductor,
13. SPAC-MID - conducting particle on a spacer in gas-insulated system applied half-way between the conductor and the ground,
14. SQUARE-DIEL - square dielectric bounded cavity,
15. SUR-AIR - surface discharges in air,

16. SUR-OIL - surface discharges in oil,

17. TREE-COND - treeing discharges initiated by conductor.

A detailed description of each defect can be found in Chapter 3.

4.2.1 Conventional classifiers

Two methods have been examined: *recognition rate* and *centour score*. Some other, less successful, procedures are briefly discussed in the Appendix B.2.

Recognition rate

The use of this method for discharge recognition was suggested by Gulski [35]. It works as follows. Several samples of a known defect are taken and measured for discharges. For each operator, the mean of the measured values is determined. The standard deviation is derived from the scatter of these values. Thus a representative picture can be drawn as shown in Figure 47.a, with each operator having a most probable value between two limits X_1 and X_2:

$$X_1 = M_{SO} - \frac{t \cdot s}{\sqrt{N}}, \qquad X_2 = M_{SO} + \frac{t \cdot s}{\sqrt{N}}, \tag{11}$$

where M_{so} is the arithmetic mean of values of the statistical operator obtained from a series of N observations of one and the same type of defect, s is the standard deviation of this series and t is a statistical test parameter depending on N. Such average fingerprints can be made of many standard or otherwise known defects.

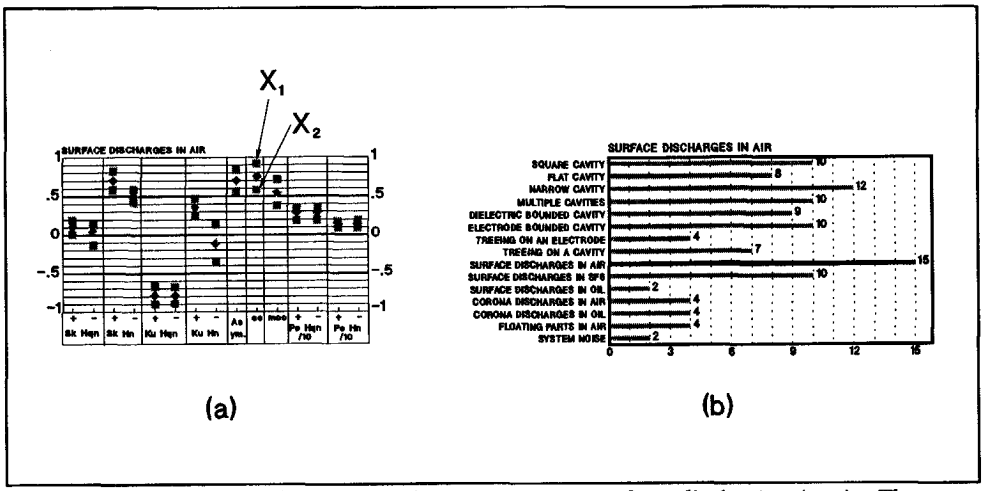

Figure 47. (a) Average fingerprint of many tests on surface discharges in air. The most probable value of each operator varies between the limits X_1 and X_2. (b) Recognition rate for surface discharges in air.

The procedure is now as follows: an unknown defect is measured and each operator is compared to the operators of the known defect. If the operator of the unknown defect falls within the limits of the known defect, a hit is recorded. Thus all operators are compared and the number of hits is recorded. This number is called the *recognition rate*. The recognition rate can vary between the maximum number of operators used for recognition, this is when all operators coincide, and zero, when no operator falls within the limits of the standard deviation. In this example it ranges from 0 to 15. The procedure is repeated, so that an unknown defect is compared with many known defects and the best fit is deemed to represent the cause of the unknown defect, see Figure 47.b. The recognition rate is described in more detail in [35].

Centour score

The other procedure, centour score, works as follows [59,72]. The operators of a known defect are displayed in p-dimensional statistical operator space. In Figure 48, a two-dimensional example of such a display is shown, where a single fingerprint is represented by one dot.

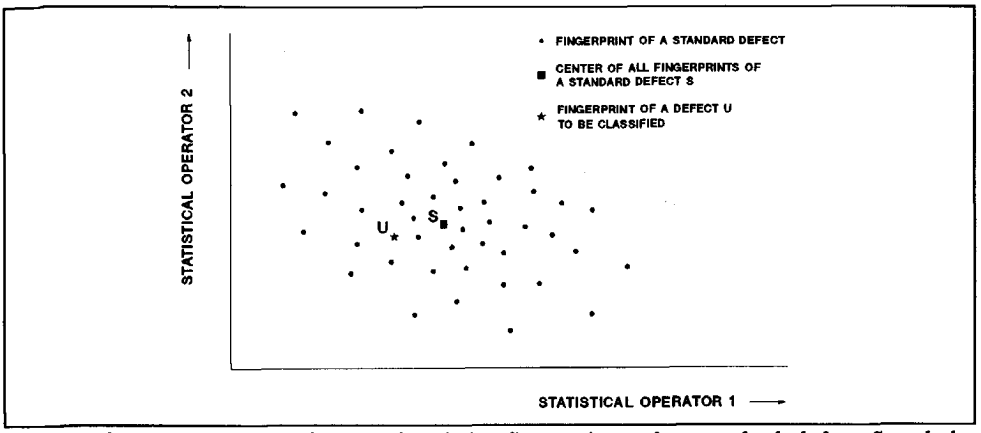

Figure 48. Two-dimensional example of the fingerprints of a standard defect *S* and the fingerprint of one unknown defect *U*.

Again, a number of samples of a known defect are measured and each of the results is displayed, see Figure 48, so that a collection of fingerprints (dots) occurs. The mathematical centre of these fingerprints is determined, and the position of an unknown discharge can be compared with this centre. The centour score is now defined as the percentile rank of the fingerprints (dots) that are further away from the centre of the known discharge population than the measured value. In the simple two-dimensional example given in Figure 48, the unknown defect *U* is compared to the scattered data of a standard defect with centre *S*. The centour score of the unknown defect is now 80%, if eighty percent of the fingerprints of the standard defect are further away from centre *S* than *U* itself.

The centour score can vary from 0% to 100%. This percentage is not the same as the probability that *U* is indeed identical to the standard defect *S*, but it gives us the best possible reflection of it.

The results of a classification of an unknown defect by centour score are given as a list, for instance like that in Table 2, which is studied in the following section. Further calculation details on the centour score are given in the Appendix B.3.

SELF-RECOGNITION

First, it was investigated whether the analysing system could distinguish one type of defect from the others by checking whether it recognizes itself. The average value of the operators of one defect was fed to the system. It was then checked as to whether the average value of that defect was recognized and also whether it was sufficiently distinguished from the other standard defects. The results are shown in Table 2.

The recognition rate is given as the number of operators that coincide with those of the model. The maximum rate is fifteen (data were obtained by the original version of discharge analyzer). Rates going down to eleven are shown, lower values were deemed to give no

information.

The centour score is given in percentages. The maximum obtainable value is 100%, all values above 10% are shown.

The resulting classifications are marked by ++ when the recognition is clear and by + when the main conclusion is supported. The results marked by o and oo are commented on below.

Table 2. Self-recognition of standard defects.

DEFECT	RECOGNITION RATE	VERDICT	CENTOUR SCORE	VERDICT
1. FLAT-DIEL	FLAT-DIEL 15 EXTRA-FLAT-DIEL 14 FLAT-COND 12	++ + o	FLAT-DIEL 100% EXTRA-FLAT-DIEL 47% FLAT-COND 26%	++ +
2. EXTRA-FLAT-DIEL	EXTRA-FLAT-DIEL 15 FLAT-COND 11 FLAT-DIEL 11	++	EXTRA-FLAT-DIEL 100% FLAT-COND 60%	++ o
3. SQUARE-DIEL	SQUARE-DIEL 15 FLAT-DIEL 12 MULT-DIEL 12	++ o	SQUARE-DIEL 100% FLAT-DIEL 64% FLAT-COND 45%	++ o
4. FLAT-COND	FLAT-COND 15 MULT-DIEL 11	++	FLAT-COND 100% FLAT-DIEL 52% SQUARE-DIEL 25%	++ o
5. MULT-DIEL	MULT-DIEL 15 OTHERS ≤ 11	++	MULT-DIEL 100% FLAT-COND 25%	++
6. SUR-AIR	SUR-AIR 15 NARROW-DIEL 12	++ o	SUR-AIR 100% EXTRA-FLAT-DIEL 32% TREE-COND 29%	++ o o
7. SUR-OIL	SUR-OIL 15 OTHERS ≤ 9	++	SUR-OIL 100% TREE-COND 73%	++ oo
8. COR-AIR	COR-AIR 15 NARROW-DIEL 11	++	COR-AIR 100% OTHERS 0%	++
9. TREE-COND	TREE-COND 15 OTHERS ≤ 11	++	TREE-COND 100% OTHERS 0%	++

From this table, it can be concluded that the standard defects from artificial models are well recognized by the system. Two remarks have to be made:

1. The analyzer has apparently also "second" and "third" thoughts: the recognition rate gives several answers at levels below the maximum of fifteen. The centour score gives also extra answers at several levels below the maximum of 100%.

2. Some confusion can be expected when distinguishing between dielectric bounded and electrode bounded cavities, as follows from the extra answers in cases 1,2,3,4 and also in recognizing square cavities, see case 3.

An anomaly oo was found in case 7, surface discharges in oil, where a large content of treeing was found. It was, however, quite possible that tracking or treeing had been developed during the comparatively long period of testing.

A general conclusion can be drawn on the interpretation of these extra answers. This conclusion is used in the section *Industrial models and objects* in this chapter in the form of an algorithm to deal with "extra" answers.

1. Recognition rates that lie three or more numbers below the maximum score are discarded.

2. Centour scores that lie below half the maximum score are discarded as well.

The results reported above were obtained by using 15 statistical operators. During the course of this work, a number of standard defects were also measured with the new version of the discharge analyzer; The data were collected by the author, and 29 statistical operators with the centour score method were used for discharge recognition.

Each standard defect comprised at least 217 fingerprints which were used for the calculation of the mean values and the covariance matrices for the centour score. The fingerprints were collected in the following way. During one session a total of 31 fingerprints were obtained. The 31st fingerprint is the mean value of the last 30 fingerprints. One session took two minutes, so that the measurement time for obtaining one fingerprint was four seconds. After each session a new sample was used. For example, for cavity discharges a new sample with a cavity was built, for surface discharges a new polyethylene slab was used, *etc.* When, *e.g.*, nine samples with a cavity were measured, a total of $9 \times 31 = 279$ fingerprints were collected for this type of defect. The nine mean fingerprints of each session were then used to test the data base. Each fingerprint was individually declared as unknown and compared to the data base. To simulate realistic conditions, the tested fingerprint was excluded from the data base. Four results of classification were defined.

1. Correct classification - the fingerprint is correctly classified, *i.e.*, a fingerprint of cavity discharges is recognized as "Cavity discharges". The following rules were applied: the first centour score must be larger than 30% and the difference between the first and second centour score must be at least 30%. By the "first score" is meant the highest score obtained, where the scores are arranged in the descending order, see for example Figure 49.g,

2. Multiple classification - the fingerprint is classified to more than one category. The first centour score is larger than 30% and the difference between the first and second scores is less than 30%.

3. No recognition - the fingerprint is not assigned to any of the known defects. The

first centour score is less than 30%.

4. Misclassification - the fingerprint is assigned to the wrong discharge. For example, corona discharges are classified as cavity discharges.

The results of the classifications for fingerprints of fourteen standard defects are shown in Figures 49, 50, 51, 52 and Table 3.

Figure 49 gives the centour scores of surface discharges and corona discharges in air. All defects were correctly recognized. In the case of the wire-to-plane corona in air at the high voltage side, the centour score showed resemblance to a single point corona in air at the high voltage potential. As discussed in Chapter 3 this similarity was expected.

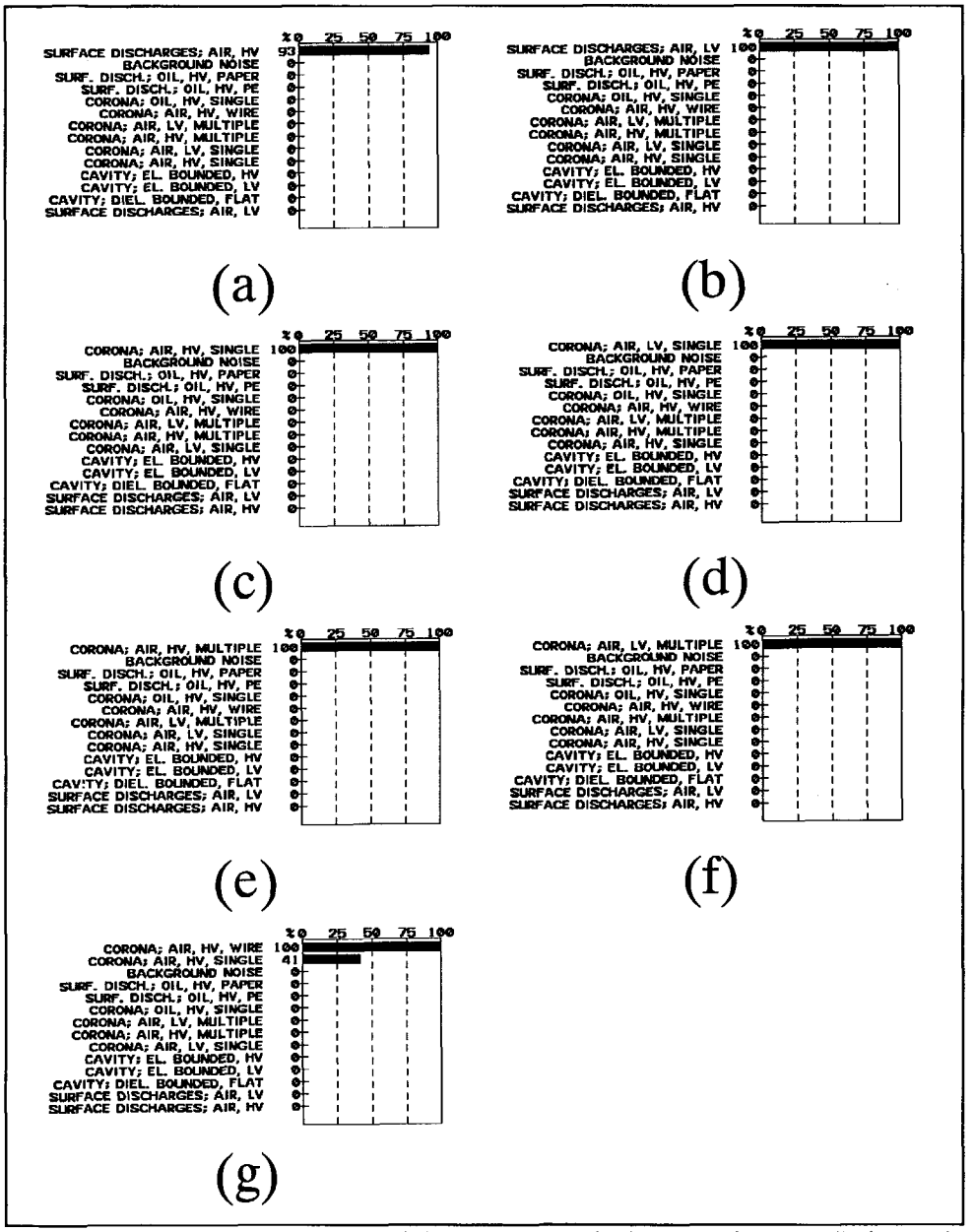

Figure 49. Centour scores of standard defects: surface discharges and corona discharges in air. An arbitrary fingerprint of each defect was tested. (a) Surface discharges in air, with a rod at high voltage potential. (b) Surface discharges in air, with a rod at low voltage potential. (c) Single point corona in air at the high voltage side. (d) Single-point corona in air at the low voltage side. (e) Multiple point corona in air at the high voltage side. (f) Multiple point corona in air at the low voltage side. (g) Wire-to-plane corona in air at the high voltage side.

Figure 50 shows centour scores for surface discharges and corona in oil. Correct recognitions were obtained in all cases.

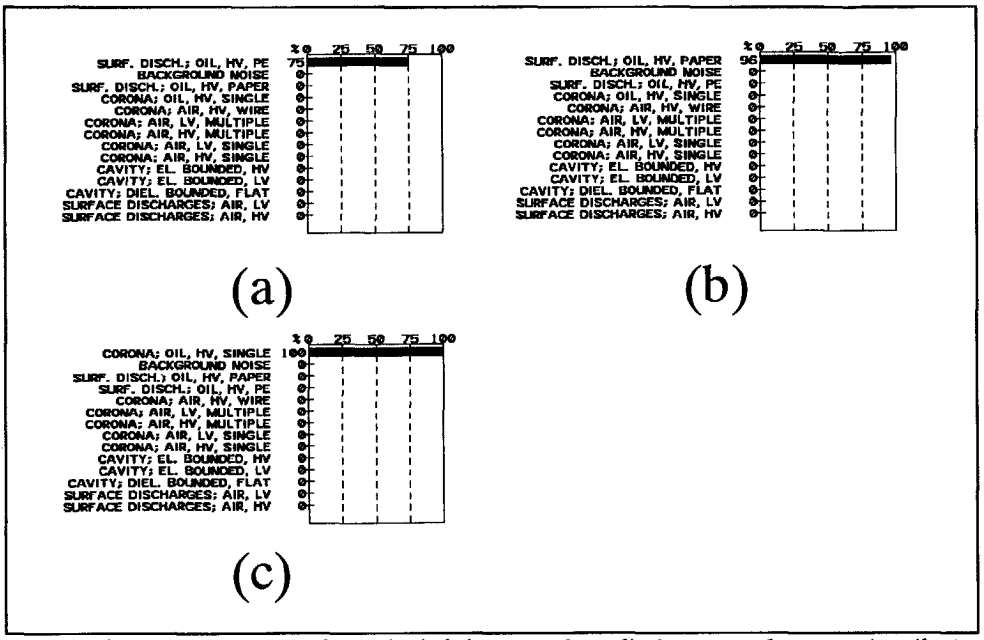

Figure 50. Centour scores of standard defects: surface discharges and corona in oil. An arbitrary fingerprint of each defect was tested. (a) Surface discharges in oil, with a rod at the high voltage side on a polyethylene sheet. (b) Surface discharges in oil, with a rod at the high voltage side on an oil-impregnated sheet. (c) Single point corona in oil at the high voltage side.

In Figure 51, centour scores for cavity discharges are given. No difference was found between fingerprints of dielectric and electrode bounded cavities in the virgin stage, but they were recognized as cavities. Similar results were also obtained by other authors [44], who also suggested that some ageing must take place inside a void before the typical patterns of an electrode bounded cavity appear. This subject is treated further in Chapter 5.

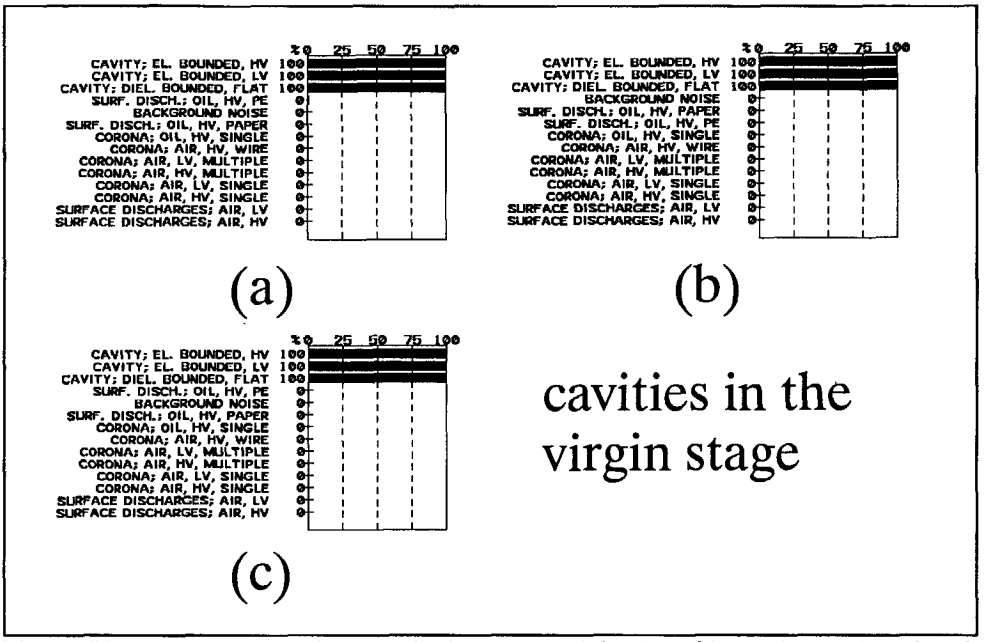

Figure 51. Centour scores of cavity discharges in solids. An arbitrary fingerprint of each defect was tested. (a) Dielectric bounded cavity, flat. (b) Electrode bounded cavity at the high voltage side, flat. (c) Electrode bounded cavity at the low voltage side, flat. Note that no difference was found between dielectric and electrode bounded cavities in the *virgin* stage. The effect of ageing on classification of discharge patterns is studied in Chapter 5.

Figure 52 shows the centour score for background noise. It can be seen that the fingerprint of background noise can be distinguished from the patterns of other discharges.

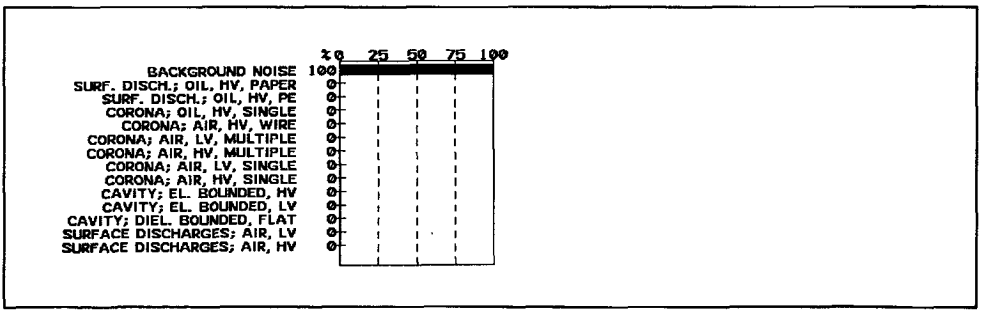

Figure 52. Centour score of background noise. An arbitrary fingerprint was tested.

An overview of obtained results shown in Figures 49, 50, 51 and 52 is given in Table 3.

Table 3. Results of the classification of fourteen standard defects.

Problem	Correctly recognized fingerprints	Multiple recognitions	Fingerprints not recognized	Miss classified fingerprints	Number of mean fingerprints
Surf. disch.; air, HV	10	-	1	-	11
Surf. disch.; air, LV	9	-	-	-	9
Corona; air HV, single	7	-	-	-	7
Corona; air LV, single	10	-	-	-	10
Corona; air HV, multi	10	-	-	-	10
Corona; air LV, multi	17	-	-	-	17
Corona; air HV, wire	9	-	-	-	9
Surf. disch.; oil, HV, PE	9	-	-	-	9
Surf. disch.; oil,HV,paper	10	-	-	-	10
Corona; oil, HV, single	9	-	-	-	9
Cavity; diel. bound., flat	2	10	-	-	12
Cavity; HV el.bound.flat	-	13	-	-	13
Cavity; LV el.bound.flat	1	7	-	-	8
Background noise	14	-	-	-	14

From the presented results, the following can be concluded.

1. Most discharges were correctly recognized, in two cases the classification was broader, see points 2 and 3. **No misclassifications occurred**. This is of great importance with a view to the consequences in industrial applications.

2. Wire-to-plane corona in air, at the high voltage side showed certain similarity with single-point corona in air, at the high voltage potential. As discussed in Chapter 3, this similarity was expected.

3. No difference was found between the fingerprints of dielectric and electrode bounded cavities in the virgin stage, but they were recognized as cavities. Similar results were also obtained by other authors [44], who also suggested that some ageing must take place inside a void before the typical patterns of an electrode bounded cavity appear. This subject is treated further in Chapter 5.

INDUSTRIAL MODELS AND OBJECTS

Six different objects were used, and ten tests at natural defects and six tests at artificial defects in actual high voltage constructions were performed [35,58,59]. The results of the classifications of industrial models and objects have been collected in Table 4. A correct classification is indicated by + and a non-classification by □. An incorrect classification would have been indicated by -, but such a classification did not occur. Fifteen statistical operators were used for discharge recognition.

Table 4. The results of the recognition rate and centour score of tests performed on sixteen industrial objects.

OBJECT	EXPECTED DEFECT	RESULTS			
		RECOGNITION RATE	VERDICT	CENTOUR SCORE	VERDICT
1. BUSHING 10KV/300A CASE A	SURFACE AND INTERNAL DISCHARGES	SUR–AIR 11 FLAT–DIEL 10	+	NO ANSWER	□
2. BUSHING 10KV/300A CASE B	INTERNAL DISCHARGES	FLAT–COND 11 EXTRA–FLAT–DIEL 10	+	EXTRA–FLAT–DIEL 26%	+
3. CURRENT TRANSFORMER	FLAT CAVITY	EXTRA–FLAT–DIEL 11	+	NO ANSWER	□
4. CABLE PHASE R	NONE	CONFUSING	□	NO ANSWER	□
5. CABLE PHASE S	NONE	NO ANSWER	□	NO ANSWER	□
6. CABLE PHASE T	NONE	NO ANSWER	□	NO ANSWER	□
7. 150kV BUSHING – TEST A	FLAT CAVITY	FLAT–COND 12 EXTRA–FLAT–DIEL 11	+	NO ANSWER	□
8. 150kV BUSHING – TEST B	CAVITY	UNCERTAIN	□	FLAT–DIEL 40%	+
9. GIS–SPACER	CAVITY	CAV–SPAC 11	+	CAV–SPAC 89%	+
10. SPRING IN GIS	FLOATING PART	FLOA–SF6 14 GIS–SPLI 13	+	GIS–SPLI 87% FLOA–SF6 76%	+
11. CABLE, TREEING	TREEING	TREE–COND 12	+	TREE–COND 26%	+
12. CABLE, CAVITY	CAVITY AT CONDUCTOR	FLAT–COND 11	+	FLAT–COND 71%	+
13. NEEDLES IN GIS	CORONA	COR–SF6 15	+	COR–SF6 57%	+
14. CONDUCTING PARTICLE MIDDLE OF SPACER	ITSELF AND/OR SURFACE DISCHARGES	CONFUSING	□	SPAC–MID 45%	+
15. CONDUCTING PARTICLE NEAR CONDUCTOR	ITSELF AND/OR SURFACE DISCHARGES	SPAC–COND 13	+	SPAC–COND 80%	+
16. SPLINTER IN GIS	SPLINTER OR FLOATING PART	CONFUSING	□	FLOA–SF6 52%	+

The following results have been obtained.

1. Bushing 10 kV / 300 A.

Case A - the bushing with casing. From the recognition rate, it was concluded that surface and internal discharges were present, in accordance with the expectation. The centour score was very low, thus giving no classification.

Case B - the bushing without casing. The results were interpreted as fairly flat cavities. The surface discharges had apparently disappeared by taking off the casing, in accordance with the expectation.

3. Current transformer 2 x 150 A to 5 A for 50 kV systems.

Cavities between the current winding and core in the insulation were expected. After testing

for discharges, the recognition rate was interpreted as a cavity, probably flat, which agrees with the expectation. The centour score gave no indication.

4. 3-phase belted cable 10 kV.

The results of phase *R* were quite confusing. The recognition rate showed hits for a flat and a square dielectric bounded cavity and a flat electrode bounded cavity with levels of 10, 8 and 9. The centour score gave 14% for the flat electrode bounded cavity, which was interpreted as giving no classification in both cases.

The recognition rates of phases *S* and *T* gave a number of rates at level 4 or 5. This was interpreted as no classification. The centour score of phase *S* was TREEING = 16% and that of phase *T* for all defects $\leq 1\%$. Both cases were interpreted as non-classification.

In all these cases, it was deemed to be correct that no classification could be made. The standard defects to be compared were of an entirely different construction and they were not measured at three-phase voltage either.

7. Bushing 150 kV.

Test A was interpreted as flat cavities, without concluding to electrode bounded or dielectric cavities (uncertainty in making this distinction was expected when discussing the results of self-recognition of standard defects). Ultrasonic detection confirmed this and revealed that discharges were located inside the body of the bushing. The centour score was 3% for FLAT-DIEL, which was accepted as non-classification.

Test B gave confusing results for the recognition rate and clear results for the centour score. The recognition rate showed a square and a flat dielectric bounded and flat electrode bounded cavity at levels 14, 12 and 11. This was interpreted as cavities in general, without classifying the type of cavity. It was regarded as non-classification. The centour score was interpreted as a flat cavity, which could be well in accordance with reality.

9. Internal discharges in a spacer.

A classification was made to compare the spacer with fingerprints of standard defects as well as fingerprints of similar spacers measured before. It was concluded from the recognition rate that the spacer had internal discharges similar to other spacers of the same type, vaguely resembling cavity discharges of other origin (rates at level 7).

The centour score clearly indicated a spacer cavity. The second and third answers were less than half the maximum score and were thus discarded.

10. Floating part in SF_6 - a metal spring in a gas-insulated system.

In this case, the discharge patterns of a metal spring in a gas-insulated switchgear were classified. It was concluded that this pattern did not resemble a floating part in air and that the situation in SF_6 could be well recognized: a high score for both FLOA-SF6 and GIS-SPLI (see case 16).

11. Treeing in a 6/10 kV cable.

It can be concluded that a good recognition of treeing took place. The indication NARROW-DIEL might originate from the stem of the tree.

12. Cavity in a 6/10 kV cable.

This was interpreted as a cavity adjacent to the conductor. The fact that no square cavity was recognized was not surprising, as the set of the studied defects did not include a square cavity at the conductor (see Chapter 3).

13. Corona discharges in SF_6.

Several fingerprints of corona in SF_6 were obtained. An arbitrary fingerprint was then classified. The corona in 5 bar SF_6 was well recognized, a low recognition rate to corona in ambient air was present.

14. Conducting particle on a spacer.

The conducting particle was applied half-way between the conductor and the ground. A number of samples were prepared in this way and an arbitrary sample was then classified. The result of the recognition rate was deemed to be insufficient for recognition. There were rates of 10 for the defect itself and corona discharges in SF_6 and a rate of 9 for floating parts in air. The result was consequently accepted as non-classification.

The centour score gave a better recognition of the cause of the discharges than the recognition rate.

15. Conducting particle on a spacer near the conductor.

In contrast to the former case, this asymmetrically applied defect can be well classified. The asymmetric discharge pattern of this defect can, apparently, be better recognized than that of the former more symmetric one. It did not resemble any of the other defects, which proves the clarity of the recognition.

16. Floating parts in SF_6 - an aluminium splinter in a gas-insulated system.

An arbitrary fingerprint out of many made on this type of defect was classified. The recognition rate was deemed insufficient for correct classification. An explanation could be that the analysing period had been too short, as the splinter had moved in the electric field and was found, after opening the compartment, in a field-free corner (see Chapter 3).

The centour score did better in this short time span. The splinter was clearly recognized as a floating part in SF_6.

Conclusions

It can be seen that quite satisfactory classification results were obtained. Especially the fact that no incorrect classifications took place is appreciable. The following conclusions can be drawn:

1. The results on sixteen full-scale samples as described here show a good potential for the classification of discharges in insulation structures.

2. From the recognition rate and centour score, the latter one is preferred for discharge recognition. It gives better suppression of non-relevant answers.

Further results obtained by the centour score are reported in Chapter 5 and Chapter 6.

4.2.2 Neural networks

Recently, the application of neural networks to discharge recognition has become a trend in the diagnosis of high voltage insulation [45,106,112]. Just as a mankind has learned and developed by means of thousands of trials, errors and improvements from the errors, neural networks also provide brain-like capabilities for solving problems - they learn by example [9,42,73]. Neural networks belong to 'non-parametric' methods. This means that it is usually not necessary to make any assumptions about data structure. In statistics, various preliminary conditions, *e.g.*, data from normal populations, must be fulfilled in order to carry out the analysis.

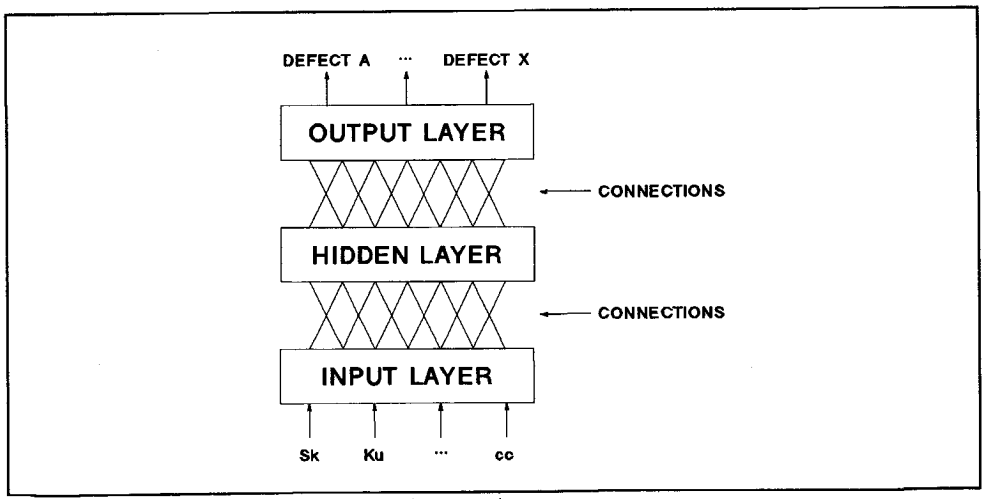

Figure 53. General structure of neural network.

The structure of neural networks is based on a mutually connected three-layer system, see Figure 53: input layer, hidden layer(s) and output layer.

The input layer may have several input neurons or processing elements and is driven by the data obtained by a partial discharge measuring system. In this work the input data were values of operators, although other approaches can also be found [45,106,112].

The hidden layers characterize the typical structure of a neural network and are different for the diverse networks. The main purpose of the hidden layers is to extract classification information from the presented data.

The output layer is defined according to user expectancies. It can be represented by one or more neurons whose outputs indicate the final classification of a fingerprint of unknown origin to the known defects.

The following questions were studied:

1. In comparison with conventional classifiers, do neural networks improve the discharge recognition?

2. Do results depend on the structure of a network?

3. How do neural networks classify fingerprints which deviate completely from the learning fingerprints?

   For example: How will a neural network classify the fingerprint of corona in air when it was only trained to recognize the fingerprints of dielectric and electrode bounded cavities?

4. How long does it take to teach neural networks to recognize fingerprints?

Three commonly used neural networks were examined:

1. back-propagation network,

2. Kohonen self-organizing map,

3. learning vector quantization network.

Although there are many more networks [9,11,47,50,87,98,111,126], to study them was beyond the scope of this thesis.

4.2.2.1 Description of neural networks

Back-propagation network

This type of neural network got its name from the way it handles errors [42,73,125]. It

consists of the input layer, at least one hidden layer and the output layer, see Figure 54.

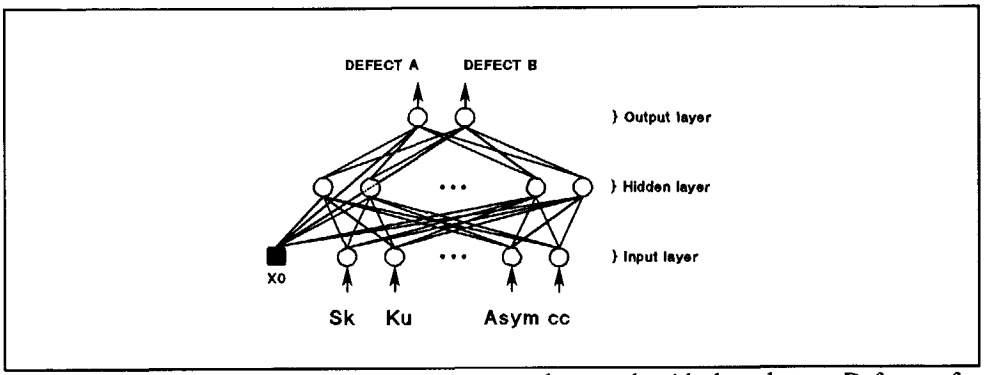

Figure 54. Structure of the back-propagation neural network with three layers. Defects refer to insulation defects which result in partial discharges.

Each layer is fully connected to the succeeding layer. The main purpose of the hidden layer is to extract information on different defects and to pass its knowledge to the output layer (or succeeding hidden layer, if there is more than one hidden layer). The number of neurons in the input layer is equal to the number of statistical operators. The number of neurons in the output layer is equal to the number of defects to be classified. The number of neurons in the hidden layer vary between the number of neurons in the input and the output layer. However, the number of neurons tend to be larger with the complexity of the problem to be solved.

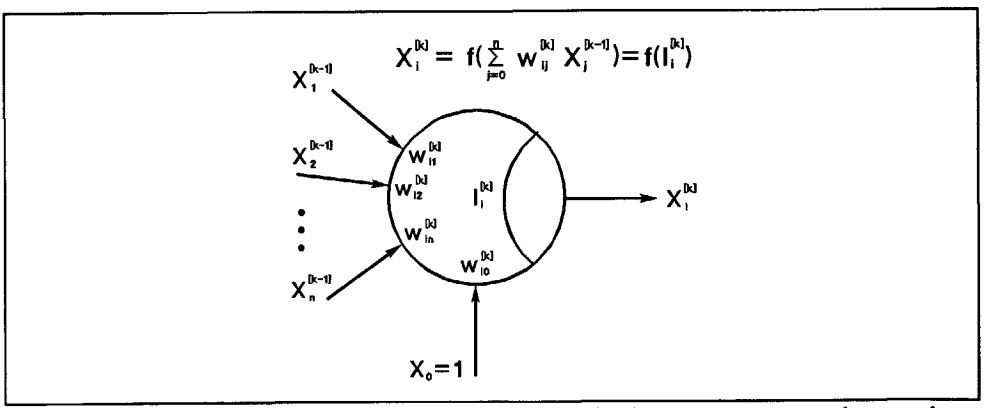

Figure 55. Typical neuron (processing element) of the back-propagation neural network.

A typical neuron is shown in Figure 55, where $X_1^{[k-1]}$, $X_2^{[k-1]}$, ..., $X_n^{[k-1]}$ are n outputs from a preceding layer, $w_{i1}^{[k]}$, $w_{i2}^{[k]}$, ..., $w_{in}^{[k]}$ are weight connections between k - *1* and kth layer and $X_i^{[k]}$ is the output of the ith neuron in the kth layer. The X_0 input to the neuron has always a value of 1 (modified by its weight w_0). Using an analogy, the role of this neuron is the same as that of ground in electrical circuits, *i.e.*, to provide a constant reference value.

The neuron transfers its inputs according to the formulae:

$$X_i^{[k]} = f\left(\sum_{j=0}^{n} w_{ij}^{[k]} \cdot X_j^{[k-1]} \right) = f\left(I_i^{[k]}\right) \tag{12}$$

where f can be a hyperbolic tangent function:

$$f(v) = \frac{e^{v} - e^{-v}}{e^{v} + e^{-v}} \tag{13}$$

see also Figure 56.a, or a sigmoid function:

$$f(v) = \frac{1}{e^{v} + e^{-v}} \tag{14}$$

see Figure 56.b, or any differentiable function. The neuron can be considered to be a simple threshold unit.

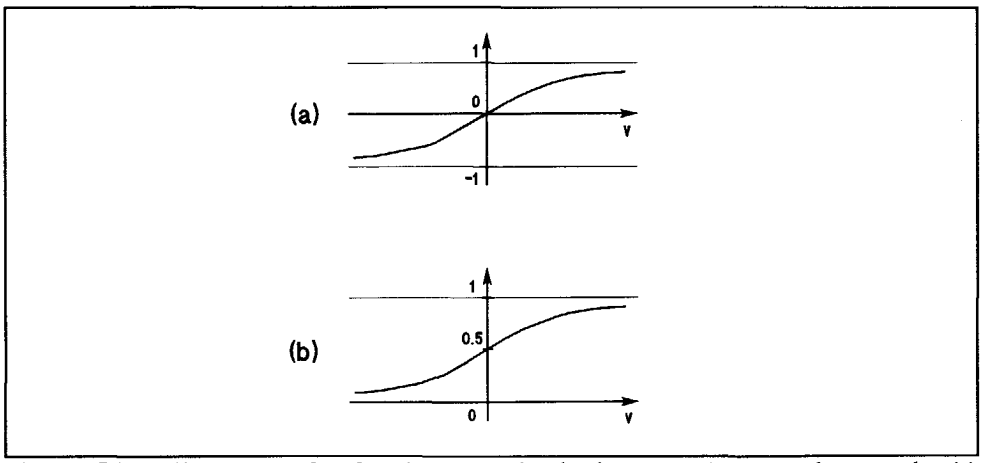

Figure 56. Different transfer functions for the back-propagation neural network: (a) hyperbolic transfer function, (b) sigmoid transfer function.

The learning of the back-propagation network consists of the following steps:

1. The input data flow from the input to the output layer through hidden layer(s).

2. At the output layer the error between desired and computed value is determined. For example, the network is trained for defect A and defect B. If fingerprints of defect A are presented to the network, the desired outputs are: defect A = 1 and at the same time defect B = 0. During learning, the network may compute values, *e.g.*, defect A = 0.7 and defect B = 0.3.

3. The error is back-propagated and weights are adjusted according to the gradient descent algorithm.

The whole procedure is repeated until the root mean square error at the output layer is smaller than a certain number (usually some tenths to some hundredths). This number is called the convergence criterion (CON). The root mean square error is obtained by summing the square of the errors for each neuron in the output layer, dividing it by the number of neurons in the output layer and taking the square root of that average.

The weight connections are randomly generated between -0.1 and 0.1 at the beginning of the learning process.

The scaling of the input data between values -1 and 1 is also required when using a hyperbolic tangent. This is caused by the fact that the hyperbolic tangent becomes saturated when the function argument get larger.

The learning fingerprints of different defects are presented to the network in a random way. This helps the network to learn.

The variant of the basic gradient descent method with a momentum term helps to reinforce general trends in the error function minimization [42,73]. The back-propagation network with the hyperbolic tangent function and a momentum term was used in this work.

It is important to understand how the back-propagation network classifies fingerprints. Mathematical analysis reveals that the network with one hidden layer separates data by hyperplanes [54,70]. The hyperplanes are generated by the neurons in the hidden layer. The weight connections between the hidden layer and the output layer serve as logical functions deciding on which side of a hyperplane the testing fingerprint is. This is shown in Figure 57.a.

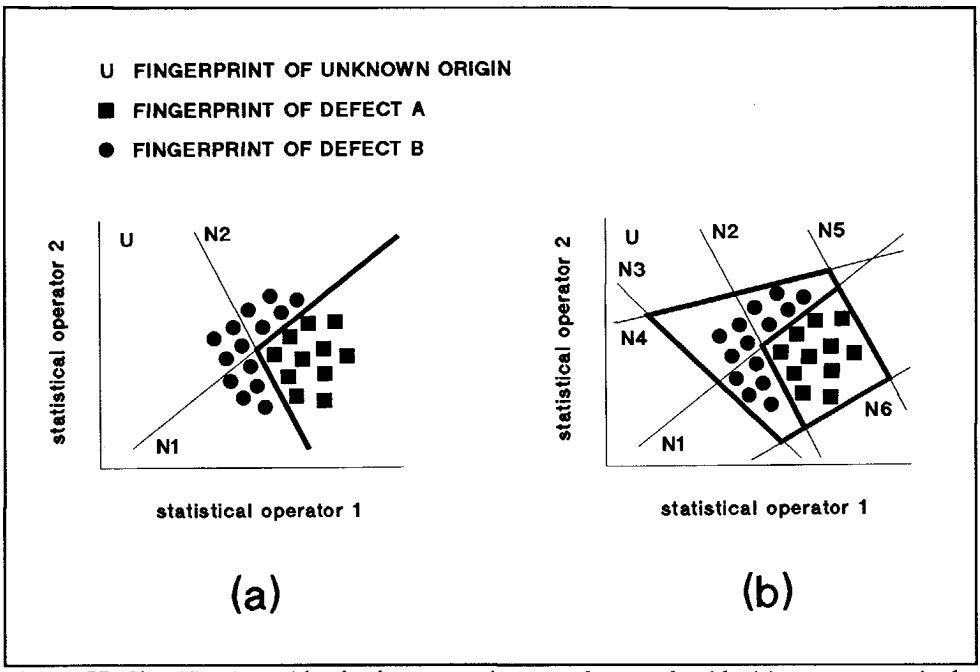

Figure 57. Classification with a back-propagation neural network with: (a) two neurons in the hidden layer, (b) six neurons in the hidden layer. Hyperplanes are generated by the neurons N1 to N6 in the hidden layer. Borders between groups are determined by weight connections between the hidden and the output layer, and they are shown here by thick lines.

Fingerprints of two defects can be in this case separated by the network with two neurons in the hidden layer. The testing fingerprint is then classified according to its position relative to the hyperplanes. Such a classification can cause problems. It can be seen that a fingerprint of unknown origin *U* is in the present situation classified to be defect *B*, yet it apparently does not belong to the defect *B*. It follows that more neurons are required in the hidden layer to separate fingerprints of both defects from the surrounding space, see Figure 57.b. In this case six neurons are used for such a separation of fingerprints. However, in more than two dimensions, the structure of data is unknown and it is difficult to estimate the number of neurons in the hidden layer. Furthermore, even if a sufficient number of neurons is supplied, the hyperplanes can still be generated far away from natural borders between the groups in the data.

The testing of the back-propagation network with actual discharge fingerprints is reported in Section 4.2.2.2.

Kohonen self-organizing map

The Kohonen map transforms a multidimensional input space to the two-dimensional neural network in a non-linear way [53]. It also preserves the topological order of the input data. In other words, two fingerprints that are close to each other will be mapped to neurons that are close to each other in the two-dimensional network layer. The typical arrangement of the Kohonen network is shown in Figure 58. Each neuron at the input and the output layer is fully connected with weight connections to all neurons in the Kohonen layer.

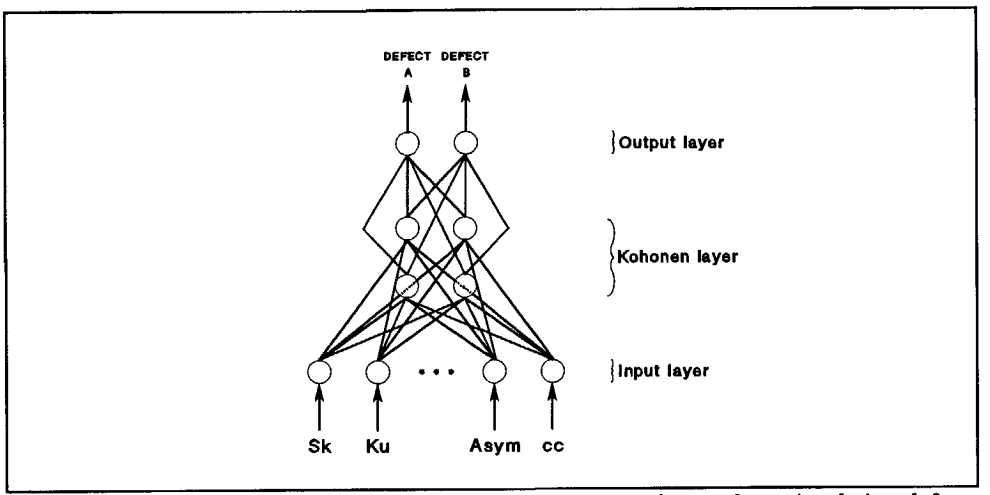

Figure 58. Structure of the Kohonen self-organizing map. Defects refer to insulation defects which result in partial discharges.

Each neuron in the Kohonen layer measures the Euclidean distance between its weights and the input values. That is:

$$d_i = \sqrt{(X_1 - w_{i1})^2 + (X_2 - w_{i2})^2 + \cdots + (X_p - w_{ip})^2}\,, \qquad i = 1, 2, \ldots, N, \quad \textbf{(15)}$$

where X_1, X_2, ..., X_p are p statistical operators, w_{i1}, w_{i2}, ... , w_{ip} are weight connections of ith neuron in the Kohonen layer, N is the number of neurons in the Kohonen layer and p is the number of inputs (in our case p = 15 statistical operators).

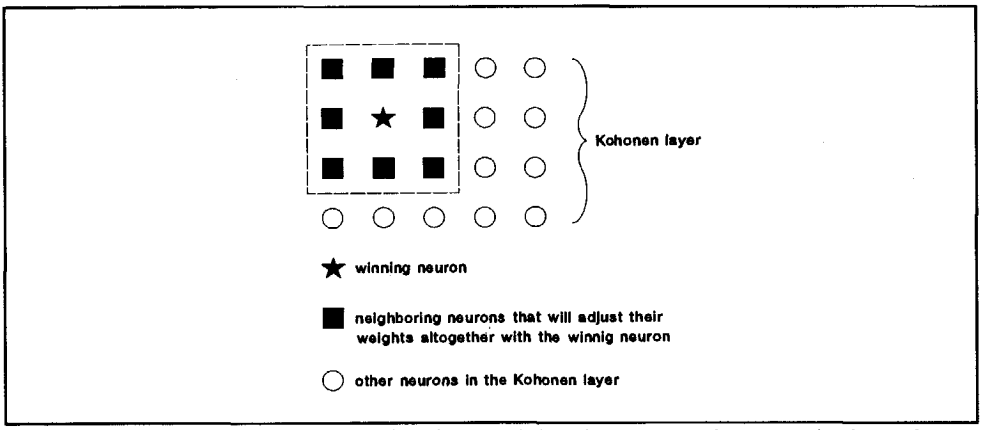

Figure 59. Square-shaped neighbourhood for weight adjustments of neurons in the Kohonen layer.

The weights are randomly generated between -0.1 and 0.1 at the beginning of the learning process. During the learning process, the neuron with the smallest distance adjusts its weights to be closer to the input data. The neighbouring neurons in the Kohonen layer also adjust their weights closer to the same input data. In this case, the square-shaped neighbourhood of weight adjustment was used, see Figure 59.

A problem that is associated with this type of learning is that only one neuron can adjust its weights. For example, if a neuron No.1 adjusted its weights closer to a defect A, then it is much closer to this defect than any other neuron. If another fingerprint of defect A is presented to the neural network, then the neuron No.1 may again adjust its weights to the defect A, *etc.* However, it means that only the neuron No.1 adjusts its weights to defect A while the other neurons simply do not learn. This problem is overcome by introducing the conscience mechanism. If a neuron has won more than average frequency *1/N*, then it is "punished" by increasing its distance from a particular defect. Thus the probability of its winning in the next round is reduced. Also, if a neuron has won less than *1/N* times, its distance is decreased in order to increase its probability to win in the next round.

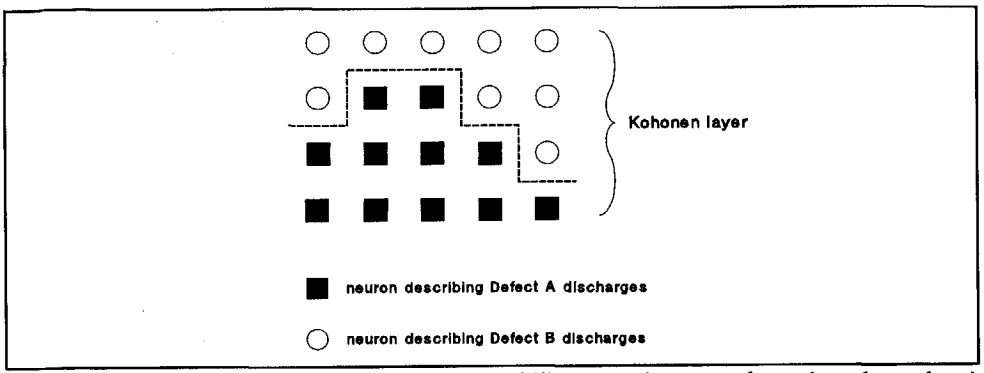

Figure 60. Kohonen self-organizing map after stabilization. The output layer (not shown here) begins to learn which neuron belongs to a particular defect.

At the beginning of the learning process, a sufficient number of learning cycles (LCs) is given to the network for stabilization. The term 'learning cycle' is defined as learning every learning fingerprint once. Throughout that time, the network works in an unsupervised mode. This means that there are no available teaching signals that indicate a particular defect, *e.g.*, that defect A = 1 and at same time defect B = 0, etc. Also the output layer does not learn (learning coefficients in the output layer are set to zero). When learning coefficients in the network become small or zero (thus the learning process in the Kohonen layer is frozen), the output layer begins to learn. It learns which neurons in the Kohonen layer corresponds to a particular defect, see Figure 60. This period of learning requires data with desired outputs.

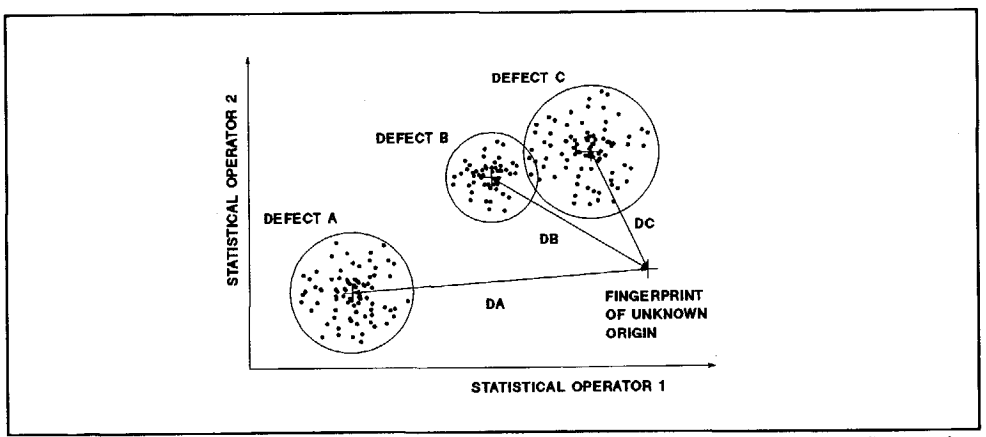

Figure 61. The principle of the smallest distance classifier. One dot represents one fingerprint. A fingerprint of unknown origin is assigned to a defect with the smallest distance between the fingerprint and a defect.

The Kohonen self-organizing map is a smallest distance classifier. This means that a fingerprint is classified to a defect with the smallest distance between the fingerprint and a particular defect. This can cause problems, see Figure 61. It can be seen that a fingerprint of

unknown origin was classified to a defect C, because the distance to this defect is the smallest. Yet, the fingerprint apparently does not belong to the defect C. This can be considered as a potential danger for misclassification.

Testing of the Kohonen neural network with actual discharge patterns is performed in Section 4.2.2.2.

Learning vector quantization network

This type of neural network was originally also suggested by Kohonen [53]. The basic structure is shown in Figure 62. It consists of the input layer, the Kohonen layer with the same number of neurons for each class and the output layer. The learning fingerprint is, in this type of network, called the learning vector.

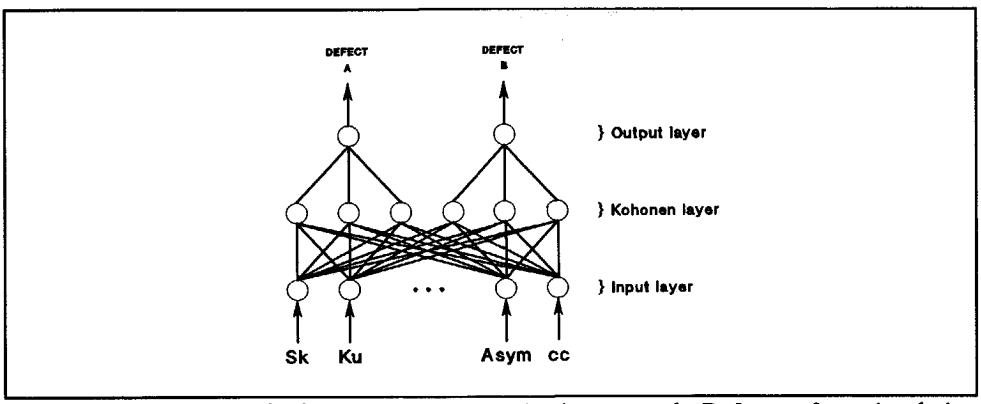

Figure 62. Structure of the learning vector quantization network. Defects refer to insulation defects which result in partial discharges.

The learning process itself is as follows:

1. The Euclidean distance between the learning vector and weight connections of each neuron at the Kohonen layer is calculated.

2. The nearest neuron is declared to be a winner.

3. If the winning neuron is in the class of the learning vector, then its distance to a particular class is decreased by moving the weights of the winning neuron towards the learning vector. Thus the probability of winning in the next round is increased.

4. If the winning neuron is not in the class of the learning vector, then its distance to a particular class is increased by moving the weights of the winning neuron away from the input vector. Thus the probability of winning for this neuron in the next round is decreased.

The whole procedure is repeated until the number of learning cycles is

$$N_{LC} = 3 \div 5 \ \lambda \tag{16}$$

where λ depends on the number of neurons and learning coefficients of the network [90]. It follows that λ determines the time necessary for the training of the network.

In the classification mode, the distance of an unknown input vector to each neuron is computed and again the nearest neuron is declared to be a winner. The classification is made according to a class to which the winning neuron belongs.

Another modification called the extended learning vector quantization network uses not only the nearest neuron for classification but all neurons. This is made by computing the likelihood function for each class:

$$p_j = \sum_{i=1}^{n} e^{-\frac{d_i^2}{2 \cdot const^2}} \tag{17}$$

where n is the number of neurons for each class, d_i is the Euclidean distance between a fingerprint to be classified and ith neuron and *const* is a proportionality constant. The classification is then made to the class with the greatest value of p_j.

The weights are randomly generated between -0.1 and 0.1 at the beginning of the learning process.

The conscience mechanism as described by the Kohonen self-organizing map must here be applied as well.

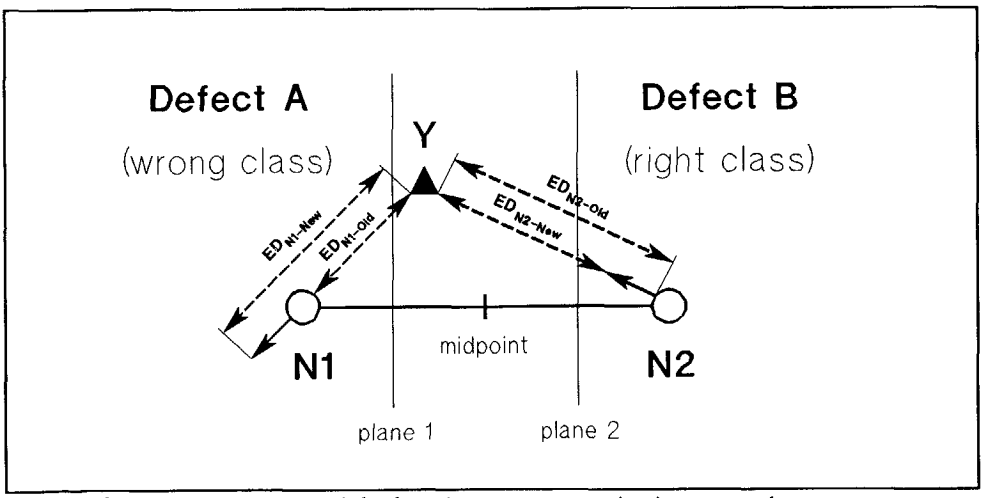

Figure 63. Modified training of the learning vector quantization network.

For a refinement of the solution obtained by the basic algorithm, a variant of the training is used. However, it must be stressed that this variant is limited to the cases when the winning neuron is in the wrong class and the second best neuron is in the right class. The whole situation is, in a simplified form, shown in Figure 63. The learning vector *Y* was assigned to a defect A (while it belongs to defect B) because the Euclidean distance $ED_{N1\text{-}Old}$ between the weights of a neuron *N1* and the learning vector *Y* is smaller than the distance between a neuron *N2* and the learning vector *Y*, $ED_{N2\text{-}Old}$. By adjustment of the weights of both neurons, the learning vector *Y* is moved toward the correct class. The weight adjustments are made such that the distance between a neuron *N1* and the learning vector *Y*, $ED_{N1\text{-}Old}$, is increased to $ED_{N1\text{-}New}$, and distance between a neuron *N2* and the learning vector *Y*, $ED_{N2\text{-}Old}$, is decreased to $ED_{N2\text{-}New}$. However, the learning vector *Y* must be close to the midpoint of a line joining these two neurons, i.e. within a region specified by two planes perpendicular to this line. The details about weight adjustments, determination of planes, *etc.*, are in [90].

The learning vector quantization network is also a smallest distance classifier. As mentioned before, this may cause problems in classification. The testing of these networks with actual discharge fingerprints is reported in Section 4.2.2.2.

4.2.2.2 Classifications with neural networks

In this section attention is drawn to the behaviour of neural networks with a different number of neurons (hidden layers), learning cycles, convergence criterions, *etc.*

Neural networks were trained to recognize defects, where it was known that these defects differ from each other [35,37,58,61]. Learning fingerprints are sets of 15 statistical operators (the original version of the discharge analyzer was used to obtain the data) calculated from $H_{qn}(\varphi)$ and $H_n(\varphi)$ discharge distributions. It should be noted that neural networks are a special case of classifiers and a sufficient number of fingerprints have to be supplied to train neural networks [95,96]. Therefore, four to twenty learning fingerprints of a particular defect were used to train neural networks. The testing fingerprints are the mean values of statistical operators calculated for each defect. The structure of learning and testing fingerprints of defects which the neural networks were taught to recognize, *e.g.*, CAV-SPAC and COR-SF6, is shown in Figure 64.

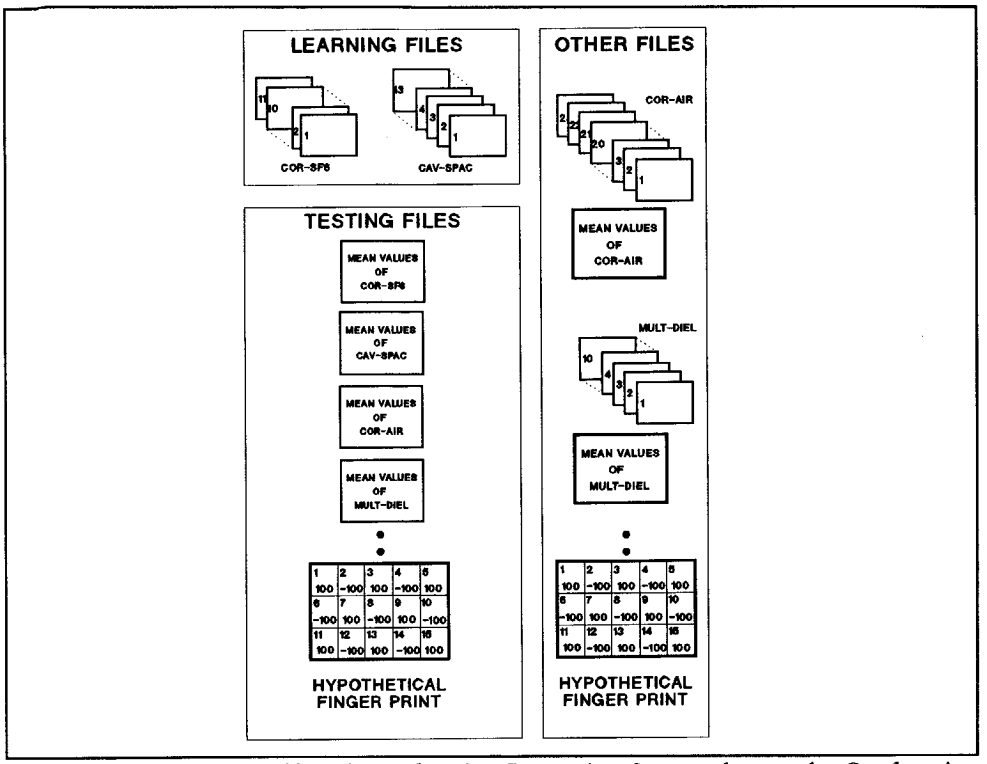

Figure 64. The structure of learning and testing fingerprints for neural networks. One learning fingerprint consists of fifteen statistical operators. One testing fingerprint comprises fifteen mean values of operators of a particular defect and a *hypothetical* fingerprint.

If n_k fingerprints are available for the kth insulation defect, then n_k-1 fingerprints are used to teach neural networks the patterns of kth defect. After the learning process, the testing of the network can, theoretically, be made in two ways. First, as testing fingerprints, the mean values of statistical operators obtained from n_k-1 fingerprints (thus artificially created values) can be used. Second, an actual fingerprint which was omitted from the learning process can be used to test the network. This fingerprint was randomly selected from the set of available fingerprints for each defect. Both have been studied by the author, but no significant differences have been found between results of both ways of testing. For easy reference, only the results obtained when using first method, *i.e.*, using the mean values of the statistical operators, are discussed in this thesis only.

In addition to testing fingerprints of the insulation defects, also a *hypothetical* fingerprint was created. The *hypothetical* fingerprint consists of 15 values of (100,-100,100,-100, ... ,100) and in further text is called the *hypothetical* fingerprint, see Figure 64. The main purpose of creating the *hypothetical* fingerprint was to study the responses of the neural networks to a fingerprint which virtually does not exist.

The neural networks were built according to the recommendations given in [90], *e.g.*, learning

coefficients were changed two or more times during the learning process (from greater values to smaller ones), the values of the learning coefficients were kept small, *e.g.*, from 0.3 to 0.02 in the case of the back-propagation network, *etc.*

The resemblance of an unknown fingerprint to a known defect is given by a value ranging from 0 to 1, see, *e.g.*, values in Table 5. A value of zero means complete lack of resemblance, a value of 1 means total resemblance. Due to a dependence on a convergence criterion, the outputs of the networks can be negative or higher than 1. For the sake of simplicity, the results smaller than 0.2 (lack of resemblance) are presented as empty space, which means zero, and the results higher than 1 (well recognizable) are presented as 1.

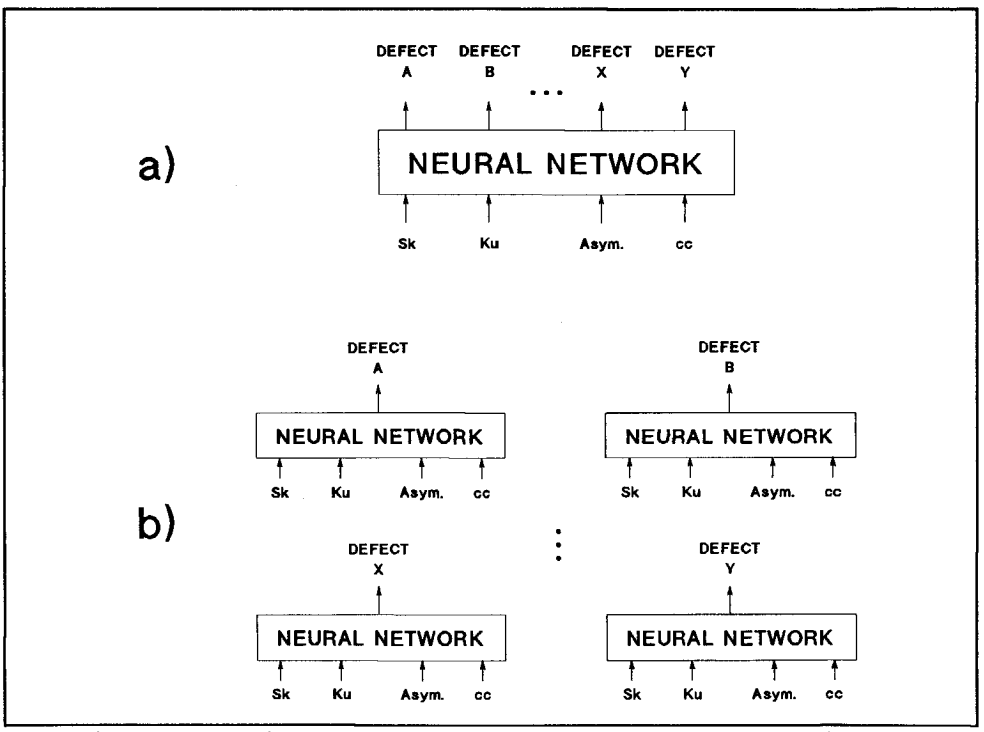

Figure 65. Two approaches of applying of neural networks. (a) First approach - one neural network with the number of outputs equal to the number of studied defects. (b) Second approach - for each defect, a neural network with one output is built. *M* networks are required to recognize *M* different defects.

Two approaches of applying the neural networks were studied, see Figure 65:

First approach - One neural network with the number of outputs equal to the number of studied defects.

Second approach - For each defect, a neural network with one output was built. However,

M networks are necessary for the recognition of *M* defects.

Both approaches are discussed with regard to the reliability of the recognition. Moreover, the calculation times (TIME) which was necessary for teaching neural networks on a 386 personal computer with a mathematical (co)-processor and a clock frequency of 20 MHz are presented. Commercially available software was used to obtain the results presented in this work [90].

Table 5. Results of different neural networks trained to recognize COR-SF6 and CAV-SPAC. Neural networks specifications are: **BP** - the back-propagation network, 1 hidden layer (HL) with 15 neurons, 2 outputs trained for COR-SF6 and CAV-SPAC; CON = 0.05, 297 LCs, TIME = 13 s; **LVQ1** - LVQ network, 2 neurons for each defects: 2×2 = 4 neurons in the Kohonen layer; 2 outputs trained for COR-SF6 and CAV-SPAC, 25000 LCs, TIME = 3.5 min; **LVQ2** - LVQ network, 5 neurons for each defect: 2×5 = 10 neurons in the Kohonen layer, 2 outputs trained for COR-SF6 and CAV-SPAC; 30000 LCs, TIME = 6 min; **LVQ3** - LVQ network, 10 neurons for each defect: 2×10 = 20 neurons in the Kohonen layer, 2 outputs trained for COR-SF6 and CAV-SPAC; 41000 LCs, TIME = 11 min; **KOH1** - Kohonen self-organizing map, 4×3 = 12 neurons in the Kohonen layer, 2 outputs trained for COR-SF6 and CAV-SPAC; 5000 LCs for stabilization, TIME = 1.5 min; **KOH2** - Kohonen self-organizing map, 5×5 = 25 neurons in the Kohonen layer, 2 outputs trained for COR-SF6 and CAV-SPAC; 5000 LCs for stabilization, TIME = 2.5min; **KOH3** - Kohonen self-organizing map network, 5×5 = 25 neurons in the Kohonen layer, 2 outputs trained for COR-SF6 and CAV-SPAC; 10000 LCs for stabilization, TIME = 5.5 min.

TEST DEFECT	BP		LVQ1		LVQ2		LVQ3		KOH1		KOH2		KOH3	
	COR SF6	CAV SPAC	COR SF6	CAV SPAC	COR SF6	CAV SPAC	COR SF6	CAV SPAC	COR SF6	CAV SPAC	COR SF6	CAV SPAC	COR SF6	CAV SPAC
COR SF6	1			1	1		1		0.9				0.9	
CAV SPAC		1		1		1		1		0.9		1		0.9
FLOA SF6		0.9	1			1		1		1		1		0.9
SPAC MID		1	1			1		1		0.9		1		0.9
SPAC COND	0.3	0.7	1			1	1							
MULT DIEL		1		1		1		1		1				0.9
FLAT COND	0.2	0.8		1		1		1						0.9
FLAT DIEL		1		1		1		1		1				0.9
SUR AIR		1		1		1		1		0.9		1		0.9
TREE COND	0.2	0.8		1		1		1						
COR AIR	1		1		1		1		0.9				0.9	
FLOA AIR	0.6	0.4	1		1		1						0.9	
HYPOTHETICAL		1	1			1		1		1		1		0.9

First approach - one network with the number of outputs equal to the number of studied defects. Table 5 shows results for seven networks as described above. Each network has two outputs: first for COR-SF6 and second for CAV-SPAC. These two defects were chosen because of the clear difference between them [35,37,58]. During the teaching process, when learning fingerprints of COR-SF6 were presented to networks, the output for COR-SF6 was set to 1 and the output for CAV-SPAC to 0. When learning fingerprints of CAV-SPAC were presented to networks during the learning, the CAV-SPAC output was taught to produce 1 and at the same time COR-SF6 was taught to produce 0.

To test the networks, a wide variety of fingerprints of different defects was used, see column 'Test defect' in Table 5 and Figure 64.

The back-propagation network learnt the fingerprints of COR-SF6 and CAV-SPAC in a short time: 13 seconds. It classified correctly a testing fingerprint of COR-SF6, see values 1 for COR-SF6 and at the same time 0 for CAV-SPAC in row COR-SF6 in column BP in Table 5. Further, a testing fingerprint of CAV-SPAC shows values 0 for COR-SF6 and 1 for CAV-SPAC, see row CAV-SPAC in column BP in Table 5.

The testing fingerprints of defects for which the back-propagation network was not trained were also classified to COR-SF6 or CAV-SPAC. For example a testing fingerprint of FLOA-SF6 was classified to CAV-SPAC with value of 0.9. The most surprising result was obtained when testing the *hypothetical* fingerprint, which resulted in misclassification to CAV-SPAC with a value of 1. Certainly, the similarities FLAT-DIEL and FLAT-COND and CAV-SPAC are acceptable, but this is out of the question in the case of the *hypothetical* fingerprint.

The back-propagation networks with 10 and 30 neurons in the hidden layer, instead of 15 neurons as in the case above, were also built. The network with 30 neurons in the hidden layer (CON = 0.03, 485 LCs, TIME = 30 s) produced the results, as compared to the case above, with minor differences only. For example, it classified SPAC-COND with values of 0.4 to COR-SF6 (0.3 was the value in the case above) and 0.6 to CAV-SPAC (0.7 in the case above). The network with 10 neurons was unable to learn the fingerprints of COR-SF6 and CAV-SPAC. Several attempts were made to teach this network by varying the learning coefficients and momentum terms, but the root mean square error, as defined before, did not show any sign of decreasing in its value, and the learning process was terminated after 25000 learning cycles.

During the testing of learning vector quantization (LVQ) neural networks, the number of neurons in the Kohonen layer was varied. The networks with 5 and 10 neurons per class in the Kohonen layer classified correctly the testing fingerprints, see columns LVQ2 and LVQ3 in Table 5. The network with 2 neurons per class misclassified a testing fingerprint of COR-SF6 to CAV-SPAC with the value of 1, see column LVQ1 in Table 5.

The extended LVQ networks produced almost identical results in all three cases.

For the classifying of the *hypothetical* fingerprint and fingerprints of unknown origin, the same considerations as those expressed in the results obtained by the back-propagation network are valid.

In all cases the number of learning cycles which was necessary for the training of LVQ networks was calculated according to equation 16, *i.e.*, the number of learning cycles was 5λ.

The calculation times for LVQ networks increased to minutes rather than seconds in the case of the back-propagation network.

The Kohonen map with 12 neurons in the Kohonen layer classified correctly the testing

fingerprints of COR-SF6 and CAV-SPAC with values of 0.9, see column KOH1 in Table 5. When the number of neurons in the Kohonen layer was increased to 25, 5000 learning cycles were insufficient to train the network. A testing fingerprint of COR-SF6 was classified to none of the defects, see row COR-SF6 in column KOH2 in Table 5. By increasing the number of learning cycles to 10000, satisfactory classifications were obtained for testing the fingerprints of COR-SF6 and CAV-SPAC, see column KOH3 in Table 5. Testing of the *hypothetical* fingerprint and fingerprints of unknown origin resulted again in a number of misclassifications. The calculation times for Kohonen self-organizing maps were some minutes.

It can be seen from these results that all three types of network (in a simple arrangement with two outputs) correctly classified the testing fingerprints of trained discharge patterns. The testing of fingerprints of unknown origin and the *hypothetical* fingerprint resulted in a number of misclassifications. It follows that the smallest distance criterion for Kohonen and LVQ networks is not satisfactory. In the case of back-propagation networks, the minimization of error function is not a sufficient criterion for a classification and it resulted in the same type of misclassifications. This conclusion is also supported by other authors [54].

The important factor in obtaining a satisfactory classification was the choice of the correct number of neurons and learning cycles. Teaching times ranged from tens of seconds in the case of back-propagation networks to some minutes in the case of Kohonen and LVQ networks. The testing of neural networks takes only the fractions of second as opposed to the time taken for the teaching of the networks.

Table 6. *First value*: Results for LVQ network trained to recognize 12 defects with 5 neurons for each defect: 12×5 = 60 neurons in the Kohonen layer; 110000 LCs, TIME = 80 min. *Second value*: Results for LVQ network trained for 12 defects with 10 neurons for each defect: 12×10 = 120 neurons in the Kohonen layer; 150000 LCs, TIME = 200 min.

TEST DEFECT	COR SF6	FLOA SF6	CAV SPAC	SPAC MID	SPAC COND	MULT DIEL	FLAT COND	FLAT DIEL	SUR AIR	TREE COND	COR AIR	FLOA PART
COR SF6	/ 1						1 /					
FLOA SF6		1 / 1										
CAV SPAC								1 /	/ 1			
SPAC MID				1 / 1								
SPAC COND					1 / 1							
MULT DIEL						/ 1			1 /			
FLAT COND							1 / 1					
FLAT DIEL						/ 1	1 /					
SUR AIR									1 / 1			
TREE COND									/ 1	1 /		
COR AIR	/ 1					1 /						
FLOA AIR												1 / 1
HYPOTHETICAL		/ 1										1 /

More complicated networks with twelve outputs were also built. To study the effect of the number of neurons, LVQ networks with 5 and 10 neurons per class in the Kohonen layer were built, see the results in Table 6. Note the difference in scores for defects as COR-SF6, CAV-SPAC, MULT-DIEL, FLAT-DIEL, TREE-COND, COR-AIR and the *hypothetical* fingerprint. LVQ and extended LVQ networks produced identical results in both cases. The teaching of these two networks was terminated when the number of learning cycles reached the value 5λ. When LVQ networks with a much higher number of learning cycles than

recommended were built, no significant improvement of the results was achieved in our case. For example, for the network with 10 neurons per class in the Kohonen layer, when the number of learning cycles was determined by 10λ (300000 LCs, TIME = 400 min) and by 15λ (450000 LCs, TIME = 600 min), the results were identical with those for the second value in Table 6, where the number of learning cycles was determined by 5λ, were obtained.

Table 7. *First value.* Results for the back-propagation network trained to recognize 12 defects with 2 hidden layers (HLs), each with 30 neurons; CON = 0.1, 16000 LCs, TIME = 45 min. *Second value.* Results for the back-propagation network trained to recognize 12 defects with 3 HLs, each with 30 neurons; CON = 0.1, 13000 LCs, TIME = 50 min. *Third value.* Results for the back-propagation network trained to recognize 12 defects with 3 HLs, each with 30 neurons; CON = 0.04, 21000 LCs, TIME = 80 min.

TEST DEFECT	COR SF6	FLOA SF6	CAV SPAC	SPAC MID	SPAC COND	MULT DIEL	FLAT COND	FLAT DIEL	SUR AIR	TREE COND	COR AIR	FLOA PART
COR SF6	.9/.9/.9											
FLOA SF6		1 /1 /1										
CAV SPAC			.4/1 /.9			.3/ /		.7/ /				
SPAC MID				1 /1 /1								
SPAC COND					1 /1 /1							
MULT DIEL						1 /.9/1						
FLAT COND			.6/.4/				.4/.7/.9					
FLAT DIEL						.2/ /	.3/ /	.6/1 /1				
SUR AIR			/.2/						1 /.6/1			
TREE COND										1 /1 /1		
COR AIR		.2/ /									1 /1 /1	
FLOA AIR		/.3/								.3/ /		1 /.7/.9
HYPOTHETICAL			/.3/	.9/1 /1	/.3/			.9/ /			.7/ /	

To study the effect of the number of hidden layers and the value of a convergence criterion, three back-propagation networks were built. The results for these networks with twelve outputs are shown in Table 7. Different results were produced by networks with two and three hidden layers, see the first and second value for CAV-SPAC, FLAT-COND, SUR-AIR and the *hypothetical* fingerprint in Table 7. Also the value of the convergence criterion influenced the results, see the second and third value for FLAT-COND, SUR-AIR, FLOA-AIR in Table 7.

Generally, as illustrated by the third value in Table 7, the back-propagation network shows satisfactory results for all the discharge patterns studied here. However, the *hypothetical* fingerprint was misclassified again.

The number of hidden layers (neurons) as well as the number of learning cycles may thus influence the results.

Table 8. *First value.* Results for the Kohonen self-organizing map trained to recognize 12 defects with 5×5 = 25 neurons in the Kohonen layer; 10000 LCs for stabilization, TIME = 4 min. *Second value.* Results for the Kohonen self-organizing map trained to recognize 12 defects with 5×5 = 25 neurons in the Kohonen layer; 40000 LCs for stabilization, TIME = 17 min. *Third value.* Results for the Kohonen self-organizing map trained to recognize 12 defects with 5×5 = 25 neurons in the Kohonen layer; 100000 LCs for stabilization, TIME = 45 min.

TEST DEFECT	COR SF6	FLOA SF6	CAV SPAC	SPAC MID	SPAC COND	MULT DIEL	FLAT COND	FLAT DIEL	SUR AIR	TREE COND	COR AIR	FLOA PART
COR SF6	.7/.7/.6										.3/.3/.4	
FLOA SF6		/ /.2		.9/ /		/.3/.4				/.7/.3		
CAV SPAC			/ /.4			/.3/.2	/.2/	.9/ /.2	/.3/.2			
SPAC MID				.9/.7/.9								
SPAC COND				/.2/.3	.9/.8/.7							
MULT DIEL		.2/ /.3				.5/.3/.3			.3/.4/.4	/.2/		
FLAT COND								1 / /1				
FLAT DIEL			/.3/			/.3/		.9/.3/.9				
SUR AIR		.2/ /.3				.5/.3/.3			.3/.4/.4	/.2/		
TREE COND		.2/ /.2				/ /.4	/.3/		.2/ /	.5/.3/.3		
COR AIR	.4/.3/.4										.5/.7/.6	
FLOA AIR	/.2/	.4/ /.7								.2/ /.3	/.2/	.4/.5/
HYPOTHETICAL		.2/ /	.2/ /					/.4/.2	.3/.3/.5	.2/ /	.7/ /	

Table 9. *First value.* Results for the Kohonen self-organizing map trained to recognize 12 defects with 10×10 = 100 neurons in the Kohonen layer, 20000 LCs for stabilization, TIME = 40 min. *Second value.* Results for the Kohonen self-organizing map trained to recognize 12 defects with 10×10 = 100 neurons in the Kohonen layer, 60000 LCs for stabilization, TIME = 120 min. *Third value.* Results for the Kohonen self-organizing map trained to recognize 12 defects with 10×10 = 100 neurons in the Kohonen layer, 200000 LCs for stabilization, TIME = 400 min.

TEST DEFECT	COR SF6	FLOA SF6	CAV SPAC	SPAC MID	SPAC COND	MULT DIEL	FLAT COND	FLAT DIEL	SUR AIR	TREE COND	COR AIR	FLOA PART
COR SF6							/ /.3	.6/ /	.6/.3/.4	/.4/.3		
FLOA SF6	/ /.9	/.8/										
CAV SPAC								.8/.9/.9				
SPAC MID				.8/.9/.6								/ /.6
SPAC COND					1 /.9/1							
MULT DIEL								/ /.6	.8/.9/.6			
FLAT COND								.8/.9/				
FLAT DIEL								.8/.9/.9				
SUR AIR								.6/ /.6	.6/.9/.6			
TREE COND						/.6/				/.4/		
COR AIR	/ /.9					.8/.6/				/.6/		
FLOA AIR				.8/.6/.9								/.6/
HYPOTHETICAL	.7/1 /									.3/ /.9		

A large number of Kohonen networks were built. Those with 25 neurons in the Kohonen layer were taught 5 times by 10000, 20000, 40000, 60000 and 100000 learning cycles. Only the results for networks which were taught by 10000, 40000 and 100000 learning cycles are shown, see the first, second and third value in Table 8. The Kohonen network with 100 neurons in the Kohonen layer was taught 6 times by 10000, 20000, 40000, 60000, 100000 and 200000 learning cycles. The results for networks which were taught by 20000, 60000 and 200000 learning cycles are shown in Table 9 as the first, second and third values.

Note how the results for the testing fingerprint FLOA-SF6 differ for these variants of the Kohonen network. They range from SPAC-MID=0.9 (see row FLOA-SF6 and the first value in Table 8), through TREE-COND=0.7 (second value in Table 8), MULT-DIEL=0.4 (third value in Table 8), none of the known insulation defects (first value in Table 9), FLOA-SF6=0.8 (second value in Table 9, this is the first correct classification of this testing fingerprint) and COR-SF6=0.9 (third value in Table 9). See also the results for the *hypothetical* fingerprint, which was again wrongly classified.

Using the large number of learning cycles for LVQ and Kohonen networks with 12 outputs, only partially satisfactory results were obtained. Further increase in the number of learning cycles was not performed because of the increase in the calculation time, *e.g.*, it took about 7 hours to teach the Kohonen network with 100 neurons in the Kohonen layer and 200000 learning cycles. The back-propagation networks showed the best ability to learn complicated patterns of twelve defects, see the results in Table 7 for the third value, where it took only 80 minutes (21000 learning cycles) to teach this network to recognize the testing fingerprints of twelve defects correctly. However, the *hypothetical* fingerprint was misclassified again.

Second approach - refers to using M networks for M individual defects with one output only, see Figure 65. To teach neural networks what are 1 and 0 cases *counter defects* must be chosen. If, for example, a neural network is trained to recognize COR-SF6 then a learning fingerprint of COR-SF6 will force the network to produce 1 at the output. All other defects, called in this text *counter defects*, will force the network to produce 0 at the output during the learning process.

Table 10. Results of different neural networks with one output and one *counter defect*, trained to recognize COR-SF6. Neural network specifications are: **BP1** - the back-propagation network, 1 hidden layer (HL) with 15 neurons, 1 output trained for COR-SF6 = 1 and CAV-SPAC = 0; CON = 0.03, 920 LCs, TIME = 33 s; **BP2** - the back-propagation network, 1 HL with 15 neurons, 1 output trained for COR-SF6 = 1 and SPAC-COND = 0; CON = 0.03, 810 LCs, TIME = 30 s; **K1** - Kohonen self-organizing map, 4×4 = 16 neurons in the Kohonen layer, 1 output trained for COR-SF6 = 1 and CAV-SPAC = 0; 5000 LCs for stabilization, TIME = 2 min; **K2** - Kohonen self-organizing map, 5×5 = 25 neurons in the Kohonen layer, 1 output trained for COR-SF6 = 1 and CAV-SPAC = 0; 20000 LCs for stabilization, TIME = 8 min; **K3** - Kohonen self-organizing map, 4×4 = 16 neurons in the Kohonen layer, 1 output trained for COR-SF6 = 1 and SPAC-COND = 0; 10000 LCs for stabilization, TIME = 4 min; **K4** - Kohonen self-organizing map, 5×5 = 25 neurons in the Kohonen layer, 1 output trained for COR-SF6 = 1 and SPAC-COND = 0; 20000 LCs for stabilization, TIME = 9 min.

TEST DEFECT	BP1	BP2	K1	K2	K3	K4
	COR SF6	COR SF6	COR SF6	COR SF6	COR SF6	COR SF6
COR SF6	1	1	1		0.9	0.6
CAV SPAC		0.5			0.9	
FLOA SF6	0.2	0.5	1		0.9	
SPAC MID			1			
SPAC COND	0.4		1			
MULT DIEL		0.5				
FLAT COND	0.2	0.7			0.9	
FLAT DIEL		0.5				
SUR AIR		0.3				
TREE COND	0.2	0.3	1			
COR AIR	1	0.9	1			0.6
FLOA AIR	0.7	0.6				
HYPOTHETICAL			1		1	

The results of six networks trained to recognize COR-SF6 with various *counter defects* are presented in Table 10. The back-propagation networks succeeded in the classification of learnt defects. They produced values of 1 for COR-SF6 and 0 for CAV-SPAC, see column BP1 in Table 10; 1 for COR-SF6 and 0 for SPAC-COND, see column BP2 in Table 10. In both cases, values higher or equal than 0.5 for COR-AIR, FLOA-AIR (BP1) and CAV-SPAC, FLOA-SF6, MULT-DIEL, FLAT-COND, FLAT-DIEL, COR-AIR, FLOA-AIR (BP2) were obtained. Moreover, the BP1 network (taught to recognize COR-SF6 with *counter defect* CAV-SPAC) classified a testing fingerprint of FLAT-COND with a value of 0.2 while the BP2 network (taught to recognize COR-SF6 with *counter defect* SPAC-COND) classified FLAT-COND with a value of 0.7. This means that different outputs were obtained for the same testing fingerprint when the networks were trained with two different *counter defects.*

The Kohonen network with 16 neurons in the Kohonen layer needed only 5000 learning cycles to classify correctly a testing fingerprint of COR-SF6 with a value of 1 and testing fingerprint of *counter defect* CAV-SPAC with value of 0, see column K1 in Table 10. Testing fingerprints of FLOA-SF6, SPAC-MID, SPAC-COND, TREE-COND, COR-AIR and the *hypothetical* fingerprint were also classified as COR-SF6.

Several attempts were made to teach Kohonen networks with 25 neurons in the Kohonen layer to recognize fingerprints of COR-SF6. The network taught by 20000 LCs had output 0 for all of the testing fingerprints, see column K2 in Table 10. By increasing the number of learning cycles to 40000, the results were identical to those in column K2 in Table 10.

When Kohonen networks with 16 neurons in the Kohonen layer were taught to recognize fingerprints of COR-SF6 and SPAC-COND, 10000 learning cycles were necessary to obtain correct classifications of these defects. The network showed value 0.9 for a testing fingerprint of COR-SF6 and 0 for a testing fingerprint of SPAC-COND, see column K3 in Table 10. Testing fingerprints of CAV-SPAC, FLOA-SF6, FLAT-COND and the *hypothetical* fingerprint were also classified to COR-SF6.

Kohonen networks with 25 neurons in the Kohonen layer classified a testing fingerprint of COR-SF6 with a value of 0.6 and a testing fingerprint of SPAC-COND with a value of 0, see column K4 in Table 10. In this case, also a testing fingerprint of COR-AIR was classified to COR-SF6 with a value of 0.6. When the network was taught by 10000 learning cycles, it classified all testing fingerprints with a value of 0 to COR-SF6. When the number of learning cycles was increased to 40000, the network classified testing fingerprints of COR-SF6 and also that of COR-AIR with a value of 0.7 to COR-SF6; all other testing fingerprints were classified with the value of 0 to COR-SF6.

Table 11. Results of different neural networks with one output and eleven *counter defects*. Neural networks specifications are: **BP1** - the back-propagation network, 1 hidden layer (HL) with 15 neurons, 1 output trained for COR-SF6 = 1 and ALL OTHER DEFECTS = 0; CON = 0.03, 5880 LCs, TIME = 4.5 min; **BP2** - the back-propagation network, 1 HL with 30 neurons, 1 output trained for COR-SF6 = 1 and ALL OTHER DEFECTS = 0; CON = 0.03, 170 LCs, TIME = 13 s; **K1** - Kohonen self-organizing map, 4×4 = 16 neurons in Kohonen layer, 1 output trained for COR-SF6 = 1 and ALL OTHER DEFECTS =0; 20000 LCs for stabilization, TIME = 7 min; **K2** - Kohonen self-organizing map, 5×5 = 25 neurons in Kohonen layer, 1 output trained for COR-SF6 = 1 and ALL OTHER DEFECTS = 0; 40000 LCs for stabilization, TIME = 17 min; **BP3** - the back-propagation network, 1 HL with 15 neurons, 1 output trained for FLOA-SF6 = 1 and ALL OTHER DEFECTS = 0; CON = 0.05, 9100 LCs, TIME = 8 min.

TEST DEFECT	BP1	BP2	K1	K2	BP3
	COR SF6	COR SF6	COR SF6	COR SF6	FLOA SF6
COR SF6	0.8				
CAV SPAC					
FLOA SF6					0.9
SPAC MID					
SPAC COND					
MULT DIEL					
FLAT COND					
FLAT DIEL					
SUR AIR					
TREE COND					
COR AIR					
FLOA AIR			0.3		
HYPOTHETICAL				0.5	1

The back-propagation and Kohonen networks were also trained for COR-SF6 with all available (in this case eleven) *counter defects*. The back-propagation network with 15 neurons in the hidden layer classified correctly a testing fingerprint of COR-SF6 with the value of 0.8 and all other testing fingerprints with the value of 0 to COR-SF6, see column BP1 in Table 11. The back-propagation network with 30 neurons in the hidden layer needed only 13 seconds to learn, as opposite to 4.5 minutes in the previous case, but it classified all testing fingerprints with a value of 0 to COR-SF6, see column BP2 in Table 11.

Several attempts were made to teach the Kohonen network to recognize the fingerprints of COR-SF6 while fingerprints of other defects were *counter defects*. The network with 16 neurons in the Kohonen layer was taught by 10000, 20000 and 50000 learning cycles. The network with 25 neurons in the Kohonen layer was taught by 10000, 20000, 40000 and 70000 learning cycles. None of these networks was able to classify correctly the testing fingerprints, see columns K1 and K2 in Table 11.

The back-propagation network, which was taught to recognize fingerprints of FLOA-SF6 while fingerprints of other defects were *counter defects*, classified correctly the testing fingerprints for which it was trained, see column BP3 in Table 11. However, the *hypothetical* fingerprint was also recognized as FLOA-SF6 with the value of 1.

It can be seen from these results that also the *second approach* to the building of neural networks has pitfalls. Not only do the number of neurons, the number of learning cycles, the value of a convergence criterion have a role in classification, but so does also the choice of *counter defects*. Even when fingerprints of all other defects are used as *counter defects*, the misclassification of a testing fingerprint which deviates completely from the learning fingerprints may still occur.

Conclusions

The back-propagation network, Kohonen self-organizing map and the learning vector quantization network were applied to the recognition of discharge patterns, using statistical operators as the input data. The following can be concluded:

1. In a simple arrangement with two defects to classify, the trained patterns were correctly recognized. In an arrangement with twelve different defects to classify, the best ability to learn was demonstrated by the back-propagation network.

2. The results of classification depend on the number of neurons (hidden layers), the number of learning cycles and the value of a convergence criterion.

3. A fingerprint which completely deviates from the learning fingerprints can erroneously be recognized as one of the known fingerprints. This is a serious disadvantage when using the neural networks for industrial purposes.

4. Training times depend on the type of neural network, the number of neurons, the number of learning cycles and the number of defects to be classified. It took a few minutes to recognize the fingerprints of two defects, but the training times to recognize the fingerprints of twelve defects were some hours.

5. Neural networks have always to be trained and retrained if a new defect is added to the collection of known defects. Long training times limit the use of the networks.

4.3 Conclusions

In this chapter mathematical methods for the discrimination and classification of discharge patterns have been investigated.

Discrimination

The experience reported in this chapter showed that discrimination between fingerprints of various defects is well possible. **Agglomerative clustering methods**, which provide a tree structure of the data are very attractive. A distinction between fingerprints where no *a priori* knowledge is available can be carried out in this way. To build such a tree structure, *the group average method* (among many others) is favoured.

Fractal dimension and lacunarity have also shown a good potential for the discrimination of discharge patterns and can be used as an alternative to other discrimination techniques.

Classification

Neural networks did not prove to be a valuable tool for discharge recognition. The results obtained from the back-propagation network, the Kohonen self-organizing map and the learning vector quantization network were dependent on the type of neural network, the structure of the neural network and the number of learning cycles, *etc.* Furthermore, a fingerprint that deviates completely from the learning fingerprints can erroneously be recognized as one of the known fingerprints.

Conventional classifiers were more successful in discharge recognition. The **centour score** in particular showed a good potential against misclassification. This is of a great importance, because of the consequences in industrial applications.

Chapter 5

Discharge patterns during ageing of insulation

The problem of the ageing of insulation has long been a subject of numerous investigations [7,19,26,30,31,78,79,81,114]. There are several mechanisms of ageing, *e.g.*, thermal, mechanical, electrical, and partial discharges have been considered one such ageing mechanism. Discharges cause physical and chemical changes in insulating materials which in the end can lead to the breakdown of the insulation [122]. Recent research on partial discharges in cavities has revealed that at least three consecutive stages of the insulation degradation take place [89]. These ageing stages differ by the pulse shape as observed by the ultra-wide band (time resolved) techniques, the optical appearance of discharges, phase-related discharge distributions obtained by the conventional discharge detection (IEC 270) and the degree of degradation of insulating material [60]. In the third stage, formation of pits on the cavity surface was observed which can be considered as a predecessor to a final breakdown of the insulation.

In this chapter, discharge patterns obtained during the ageing of some standard defects and of some industrial objects are presented. The aim of this work was to observe:

1. changes in the discharge patterns during the ageing period,
2. damage of the insulation caused by discharges.

Discharges were measured with a *conventional* discharge detector extended with a statistical discharge analyzer (see Chapter 2) and the discharge signals were analyzed by pattern recognition techniques. All data were collected by the author.

5.1 Standard defects

5.1.1 Cavity discharges

Two types of ageing tests were performed on cavities:

1. short-term ageing - up to 90 minutes,
2. long-term ageing - up to several hundreds hours.

Short-term ageing

In this case, discharge patterns obtained during 1.5 hours of ageing of cavities in polyethylene were studied [62]. Two aspects were taken into account:

1. ageing due to discharges,
2. the location of the cavity - dielectric or electrode bounded.

Air filled cavities with a diameter 5-9 mm and a height 0.4-0.5 mm were used in this work. Figure 66 shows the cavity types studied.

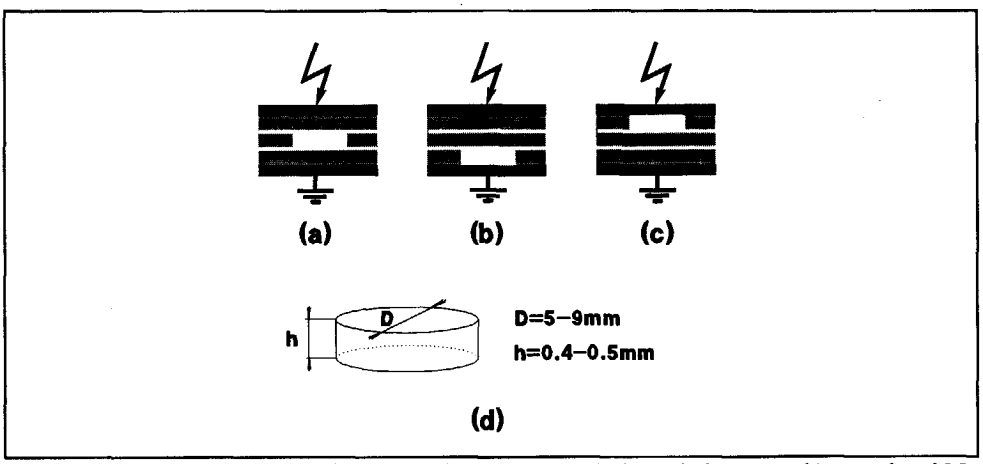

Figure 66. Cavity types studied: (a) sample of a dielectric bounded cavity, (b) sample of LV electrode bounded cavity, (c) sample of HV electrode bounded cavity. (d) Cavity parameters; 6-13 samples per case were measured.

Three stages of ageing due to partial discharges were defined according to Figure 67:

1. virgin - first 2 minutes after the voltage has reached its test value,
2. conditioned - 5-10 minutes from the beginning of the test,
3. aged - 90 minutes from the beginning of test.

Fingerprints of each ageing stage were collected at the test voltage 50-80% over the discharge inception voltage over a period of 2 minutes. The schematic diagram of the fingerprint collection is shown in Figure 67.

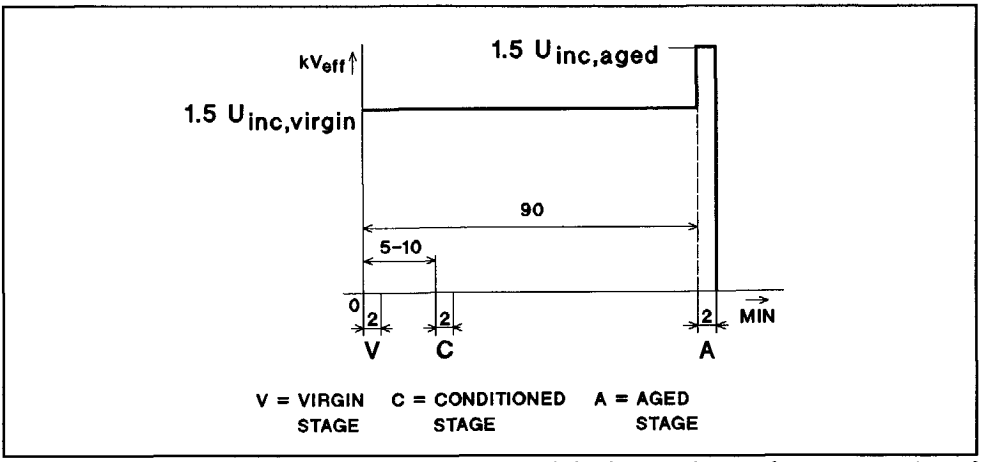

Figure 67. Procedure for the measurement of partial discharges during short-term ageing of cavities.

For pattern recognition purposes, three categories for each ageing stage are distinguished: dielectric bounded cavity, HV, and LV electrode bounded cavity. It follows that a total of nine, presumably different, categories were formed, see Table 12. Each category was represented by a number of fingerprints which were measured at one of the studied defects. Tree structure for fingerprints of HV electrode bounded cavity in the virgin, conditioned and aged stage obtained by the group average method is shown in Figure 41 in Chapter 4.

Table 12. Result of fingerprint classifications of dielectric bounded and electrode bounded cavities in virgin, conditioned and aged stage.

Cavity type	Correctly recognized fingerprints	Multiple recognitions	Fingerprints not recognized	Mis classified fingerprints	Number of fingerprints
Diel. bounded, virgin stage	2	10	-	-	12
HV el.bounded virgin stage	-	13	-	-	13
LV el.bounded virgin stage	1	7	-	-	8
Diel. bounded, conditioned stage	9	1	2	-	12
HV el.bounded conditioned stage	8	1	-	-	9
LV el.bounded conditioned stage	11	1	-	-	12
Diel. bounded, aged stage	8	1	-	-	9
HV el.bounded aged stage	9	4	-	-	13
LV el.bounded aged stage	7	2	-	-	9

Results

Virgin stage

For dielectric and electrode bounded cavities in the virgin stage the discharge patterns resembled each other to a high degree, see Figure 68. Especially remarkable was the fact that the asymmetry operator for $H_{qmax}(\varphi)$, $H_{qn}(\varphi)$ and $H_n(\varphi)$ discharge distributions had a value of zero, thus indicating no asymmetry, for electrode bounded cavities. This was also observed at the oscilloscope screen where discharges with approximately equal magnitude and repetition rate were seen in both half-cycles of the test voltage for all cavity types studied [62]. Similar observations were also made by other authors [44] who suggested that before the typical asymmetric discharge pattern of the electrode bounded cavity appears, some ageing

must take place inside the void. A possible explanation for this phenomenon could be the presence of a metallic oxide layer on the surface of a metallic electrode. It should be kept in mind that the oxide layer may have other dielectric properties than the metal itself and it might behave as an insulator at the beginning of the test. This results in a discharge pattern of the electrode bounded cavity which resembles that of a dielectric bounded cavity in the virgin stage.

Figure 68 shows an example of the recognitions of the cavity types studied in the virgin stage. Further evaluation of the results is shown in Table 12. It can be seen that a number of multiple classifications occurred in the virgin stage due to the high resemblance of the fingerprints of dielectric and electrode bounded cavities, see text above. Although the ageing stage was correctly determined, discrimination between the dielectric and electrode bounded cavities was not possible in the virgin stage.

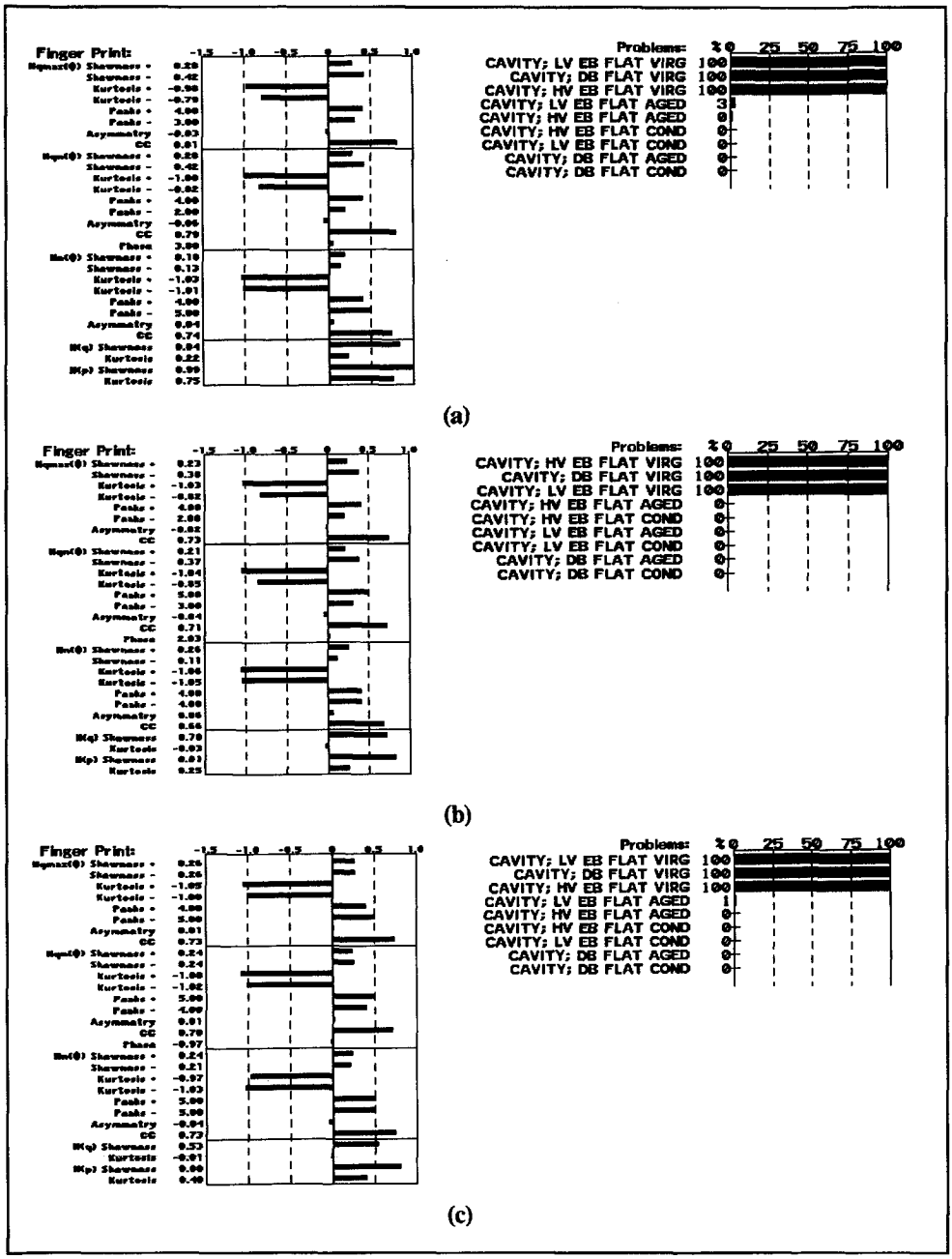

Figure 68. Typical fingerprints and recognitions of (a) dielectric bounded cavity, (b) HV electrode bounded cavity and (c) LV electrode bounded cavity in *the virgin stage*. Note that no difference was found between fingerprints of dielectric and electrode bounded cavities in *the virgin stage*.

Conditioned stage

After 5-10 minutes from the beginning of the test, the discharge patterns changed rapidly. For the electrode bounded cavities, asymmetry in the discharge magnitude (between the positive and the negative half of the voltage cycle) became apparent. This was reflected in the asymmetry operator of the $H_{qmax}(\varphi)$ and $H_{qn}(\varphi)$ discharge distributions which had a value of about -0.25 and 0.25 for HV and LV electrode bounded cavities, see Figure 69. Although differences in asymmetry up to a factor of 10 have been observed [78], in these measurements this factor did not exceed 3. The appearance of asymmetric patterns in the case of electrode bounded cavities could be the result of a 'burn-out' of a metallic oxide layer on the surface of a metallic electrode by discharges as discussed above.

The patterns of the dielectric bounded cavity changed as well. Compare, for example, the values of the skewness operator of the $H^{+}_{qn}(\varphi)$ distributions. They changed from 0.28 in the virgin stage, see Figure 68, to 0.68 in the conditioned stage, see Figure 69. The skewness of $H^{-}_{qn}(\varphi)$ distribution changed from 0.4 in the virgin stage to 0.62 in the conditioned stage.

Recognitions of typical fingerprints are shown in Figure 69. The determination of the ageing stages and the cavity types, as compared to the virgin stage, were clear. Two fingerprints of the dielectric bounded cavity in the conditioned stage were not recognized, see Table 12.

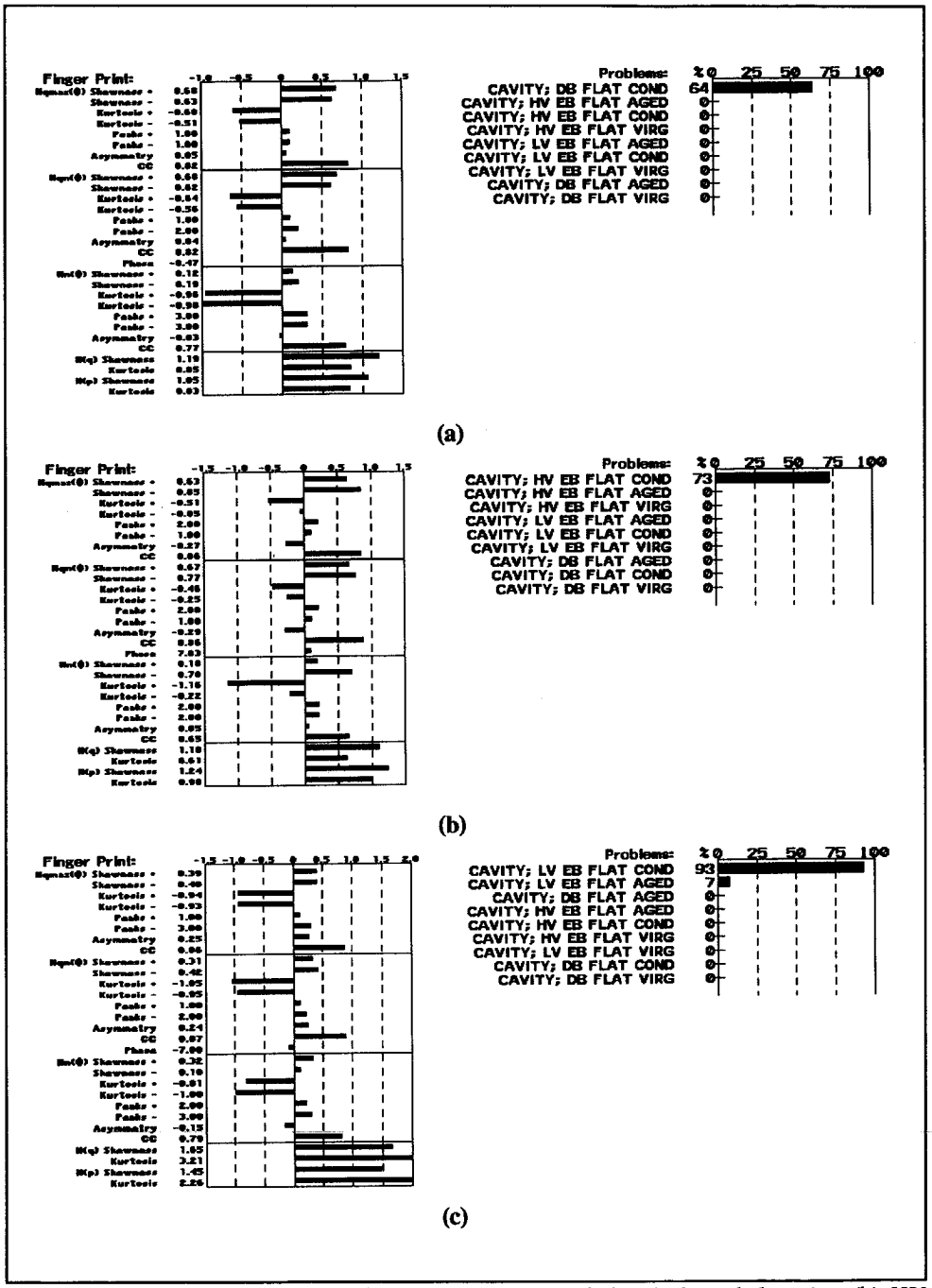

Figure 69. Typical fingerprints and recognitions of (a) dielectric bounded cavity, (b) HV electrode bounded cavity and (c) LV electrode bounded cavity in *the conditioned stage.*

Aged stage

After 90 minutes of ageing at about 1.5 inception voltage of the virgin stage, the discharges in many cases extinguished. Such a self-extinction of discharges could be explained by the formation of semi-conducting deposits on cavity walls [40,80,82,99,101,113]. The deposits are the result of complex chemical reactions initiated by the discharges. There could be also other modes of discharge extinction. For example, the gas composition, pressure and temperature may change during ageing as a result of discharge-induced processes [5,113]. This might influence discharge behaviour during the ageing time and result in a self-extinction of discharges.

To obtain the fingerprints under similar conditions as in the virgin and conditioned stage, the test voltage was increased. The inception voltage in the aged stage was about 20-50% higher than in the virgin stage.

Typical fingerprints of cavities in the aged stage are shown in Figure 70. Note that the discharge patterns again changed and are different from those obtained in the virgin and in the conditioned stage. Compare, for example, the values of the skewness of the $H^{-}_{qn}(\varphi)$ distributions. It changed from 0.42 in the virgin stage, see Figure 68, to 0.62 in the conditioned stage, see Figure 69, and reached a value of 0.19 in the aged stage, see Figure 70.

As in the conditioned stage, the electrode bounded cavities showed typical asymmetric patterns. This can be seen in the values of the asymmetry operator of the $H_{qmax}(\varphi)$ and $H_{qn}(\varphi)$ discharge distributions of HV and LV electrode bounded cavities. It had values of about -0.25 and 0.25 for these studied cases, see Figure 70.

Recognition of typical fingerprints is shown in Figure 70. Similar to the conditioned stage, the determination of the ageing stages and cavity types were clear. Of four multiple recognitions in the case of HV electrode bounded cavities in the aged stage, see Table 12, three had first centour scores indicating this category and second centour scores indicating the dielectric bounded cavity in the aged stage. In the case of LV electrode bounded cavities in the aged stage, both multiple recognitions had first centour scores indicating this category, and second centour scores indicating the dielectric bounded cavity in the aged stage.

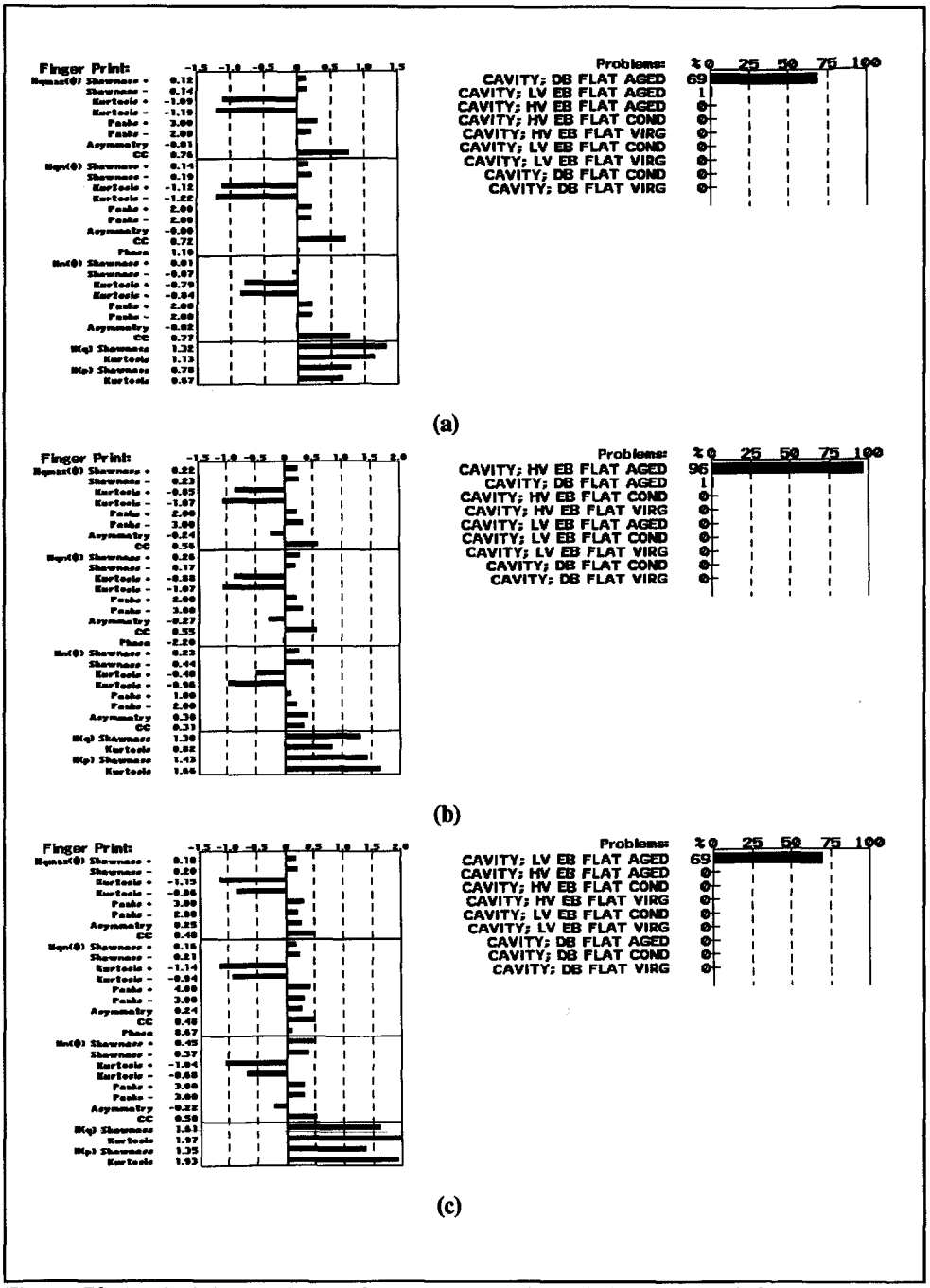

Figure 70. Typical fingerprints and recognitions of (a) dielectric bounded cavity, (b) HV electrode bounded cavity and (c) LV electrode bounded cavity in *the aged stage*.

Rapid changes in discharge patterns as observed during 90 minutes of ageing are generally explained by rapid changes of an environment where discharges take place. Bombardment of the cavity surface by energetic electrons can break molecular bonds of the insulating material and in such a way freed species can participate in chemical reactions [79,82,114,122]. The chemical reactions initiated by discharges may change the resistivity of the cavity surface [34,46,55,80,88,101,113], the gas composition, pressure and temperature [5,33,43,82,127]. Such changes may effect discharge process and thus the discharge patterns.

Conclusions

Discharge patterns of dielectric and electrode bounded flat cavities embedded in polyethylene were observed during a period of 90 min. The following conclusions can be drawn.

1. A relatively short voltage application causes ageing in the discharge site. As a result, the discharge patterns changed during the measurement period.

2. Using the fingerprint technique, it was possible to follow the changes in discharge patterns during ageing and to recognize ageing stages.

3. No differences were found between the discharge patterns of *dielectric* and *electrode bounded cavities* in *the virgin stage*, *i.e.*, in the first minutes of the measurement.

4. A clear recognition of dielectric and electrode bounded cavities in *the conditioned* and *aged stages* was achieved.

Transformation of statistical parameters

When defects with asymmetry in the layout are studied, *e.g.*, electrode bounded cavities at the low voltage or at the high voltage electrode, it should be possible to measure one of the two cases only, the other one can be obtained numerically. As has been discussed in Chapter 3 in section *Single point-to-plane corona in air*, this goal can be achieved by a simple transformation of statistical operators. For this purpose, the following transformation of statistical operators was studied:

1. skewness, kurtosis, number of peaks of $H_{qmax}(\varphi)$, $H_{qn}(\varphi)$ and $H_n(\varphi)$ discharge distributions for the positive and the negative half of the voltage cycle were mutually exchanged;

2. asymmetries of $H_{qmax}(\varphi)$, $H_{qn}(\varphi)$ and $H_n(\varphi)$ discharge distributions and phase factor of $H_{qn}(\varphi)$ distribution were changed in sign.

To verify this transformation, data as obtained during the short-term ageing of cavities were used. First, the transformed fingerprints of LV and HV electrode bounded cavities were used to create new artificial defects - HV electrode bounded cavity (see category CAVITY; HV EB - CREATED FROM LV, in Figure 71) and LV electrode bounded cavity (see category

CAVITY; LV EB - CREATED FROM HV, in Figure 71) - in both the conditioned and aged stages. Second, for actually measured LV and HV electrode bounded cavities in the conditioned and aged stages the mean fingerprints were calculated. These mean fingerprints were then classified using the data base consisting of the following categories: HV and LV electrode bounded cavities (measured data) and HV and LV electrode bounded cavities (artificially created data).

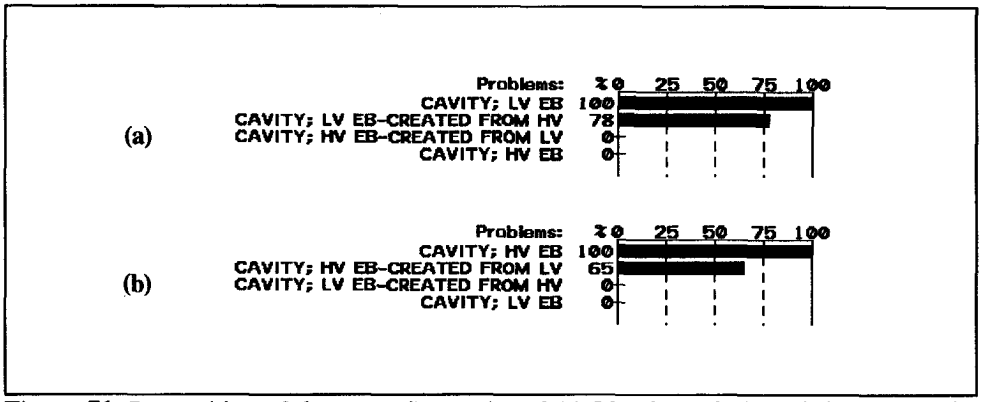

Figure 71. Recognition of the mean fingerprint of (a) LV electrode bounded cavity in the conditioned stage, (b) HV electrode bounded cavity in the conditioned stage, in the cases of measured and artificially created defects.

Figure 71.a shows the recognition in the case of the mean fingerprint of an LV electrode bounded cavity in the conditioned stage. The resemblance to the artificially created defect of the LV case (from the HV case) is considerable - 78%. This means that there is a high correlation between measured and artificially created data. A similar result was obtained in the case of the HV electrode bounded cavity in the conditioned stage. The resemblance to the artificially created cavity of the HV case (from the LV case) was 65%, see Figure 71.b.

Conclusions

It follows from these results that for discharge patterns where the asymmetry between the positive and the negative half of the voltage cycle is characteristic, the transformation of the statistical operators can be used to simulate artificial defects at the opposite side of the electrode. Fingerprints created in such way can be used for discharge recognition purposes.

Long-term tests

Several tests with a duration of up to 650 hours were performed at a flat cavity in polyethylene (cavity dimensions: diameter = 6 mm, height = 0.2 mm). The ageing voltage was increased in steps from 14 kV to 20 kV during the ageing period, see Figure 72. The test voltage for the collection of fingerprints was 14 kV. This voltage level corresponded to an average field strength of about 15 kV/mm in polyethylene.

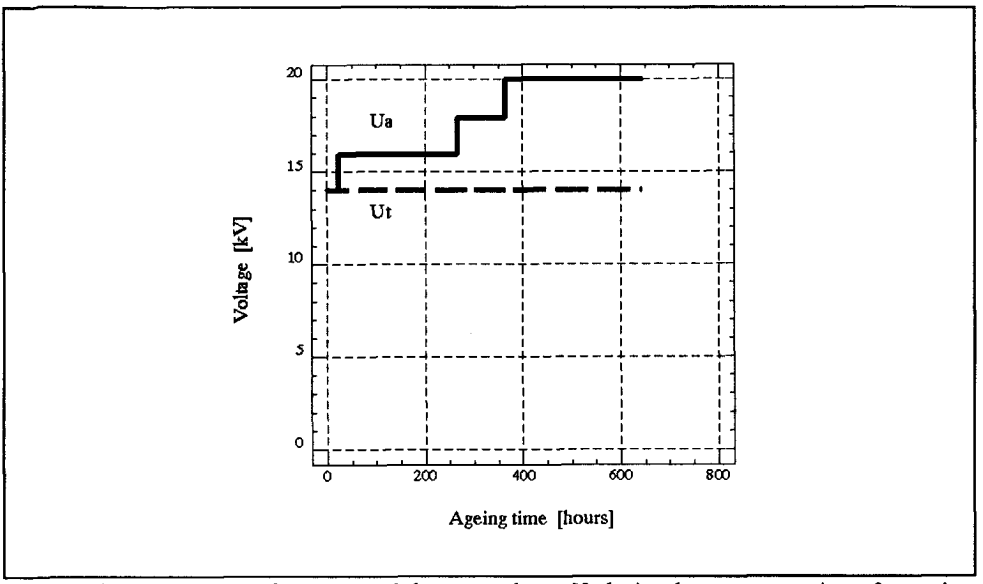

Figure 72. The ageing voltage U_a and the test voltage U_t during long-term ageing of a cavity.

The behaviour of the maximum discharge magnitude during ageing is shown in Figure 73. Trends can be clearly seen: after an initial transient response where the discharge magnitude increased from about 200 pC to 600 pC, the discharge magnitude tended to decrease with time. After about 360 hours of ageing, there were no discharges detectable at the voltage level of 14 kV (the sensitivity of the measurement was 0.1 pC). As has been discussed previously several mechanisms may be responsible for this behaviour. Discharges were, however, observed at the voltage level of 20 kV. After several days of ageing at 20 kV, the number of discharges and also the discharge magnitude decreased at this voltage level so that in the end phase of the test only several discharges per second were observed. However, from about 500 hours on, discharges with a high repetition rate and small discharge magnitude (0.2 - 5 pC) were occasionally observed on an oscilloscope screen.

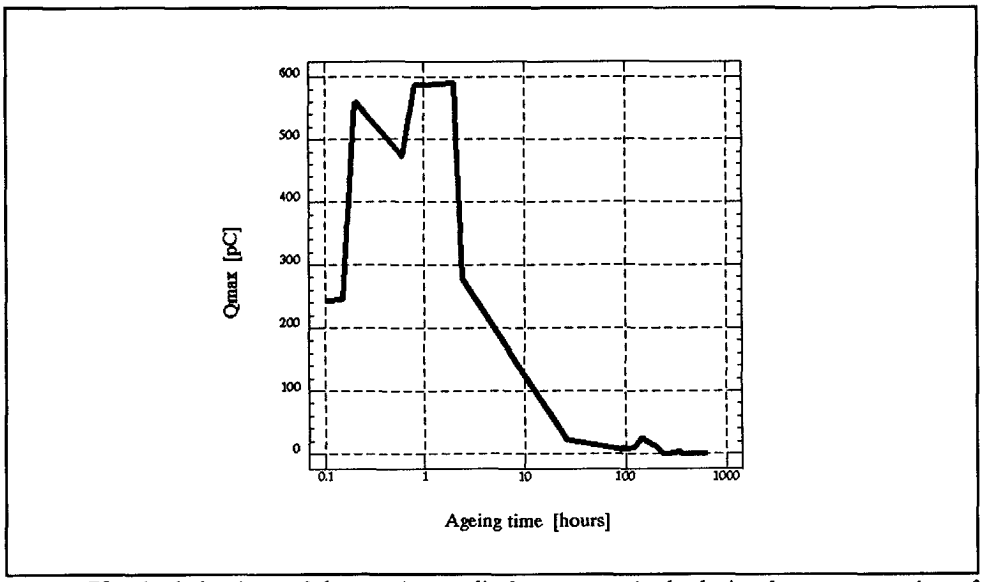

Figure 73. The behaviour of the maximum discharge magnitude during long-term ageing of a cavity.

A total of 28 *mean* fingerprints were collected during this ageing period. As has been mentioned in Chapter 4, one *mean* fingerprint is the mean value of 30 fingerprints obtained during one data collection session. One session took typically 10 minutes. It follows that a total of 28×31=868 fingerprints were collected during the ageing period. To reduce the amount of the data for processing, the *mean* fingerprints were analyzed only. The fingerprints were analyzed by the group average method. The resulting tree structure is shown in Figure 74.

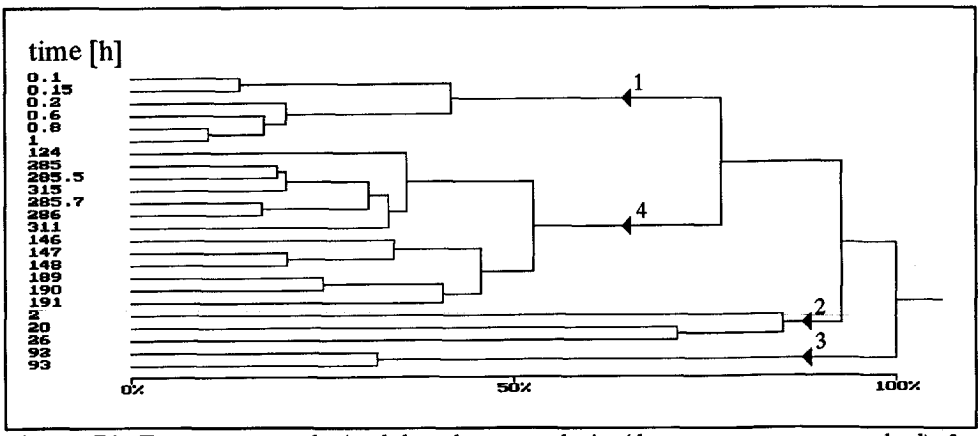

Figure 74. Tree-structure obtained by cluster analysis (the group average method) for fingerprints of cavity discharges during long-term ageing. The numbers on the left side of the figure indicate the time at which the fingerprints were collected.

Four different groups of fingerprints were distinguished. These are shown as a function of ageing time in Figure 75. It can be seen that especially in the beginning of the test rapid changes occurred. Visual inspection revealed that in the fourth stage the degradation of the cavity surface in the form of discharge by-products and small recesses was observed.

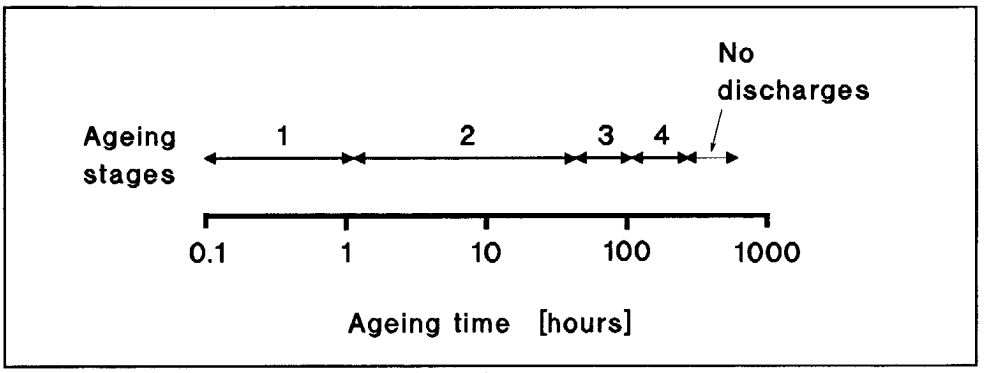

Figure 75. Ageing stages of a cavity during long-term test.

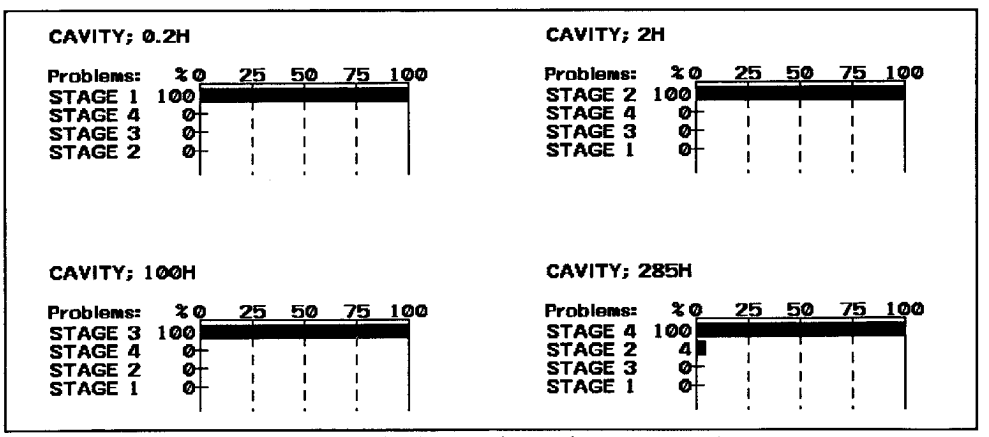

Figure 76. Recognitions of cavity discharges during long-term ageing.

The recognitions of fingerprints of each ageing stage are shown in Figure 76.

Detailed evaluation of the results is given in Table 13. It can be seen that satisfactory recognitions took place. One fingerprint in stage 1 which was 'not recognized' had a centour score of 15% to this stage. As discussed in Chapter 4, recognitions with the centour score lower than 30% are considered to be not recognized. One multiple recognition of a fingerprint in stage 4 was the result of an overlap with fingerprints in stage 3. There were no misclassifications.

Table 13. Results of fingerprint classifications of cavity discharges during long-term ageing.

Stage	Correctly classified fingerprints	Multiple recognitions	Fingerprints not recognized	Mis classified fingerprints	Number of mean fingerprints
1	5	-	1	-	6
2	3	-	-	-	3
3	2	-	-	-	2
4	11	1	-	-	12

In long-term tests performed in this work, the surface of a cavity was observed for any sign of degradation. Photographs of the cavity surface as taken after 50, 330 and 650 hours of ageing are shown in Figures 77 and 78 (after opening of the cavity a new sample was used in the test). It can be seen that after about 50 hours of ageing, discharge by-products in the form of single crystals of oxalic acid [80,99] started to form on the cavity surface, see Figures 77.a. and 77.b. The crystals with the presence of moisture are of a conductive nature and have sharp edges. In this way the field at the crystals is enhanced and increased discharge activity can be observed at the crystals [89]. The increased discharge activity results in more crystals, *etc.* After about 330 hours, clusters of crystals were observed on the cavity surface, see Figure 77.c. An overview of the whole cavity surface, see Figure 77.d, reveals that the number and also the size of the crystals substantially increased when compared to the first case, see Figure 77.b. At such clusters of crystals, the erosion of the cavity surface starts as a result of increased discharge activity caused by the field intensification at the crystals edges [89]. This leads to the formation of small pits or craters at clusters of crystals. This was actually observed after about 650 hours when small recesses near crystals were found. The recess can be seen in Figure 78.a as a grey area around white crystals. The erosion of the cavity surface is schematically drawn in Figure 79. Overview of the whole cavity area after 650 hours of ageing, see Figure 78.b, reveals that the number and the size of the crystals again increased when compared to the first and the second case, see Figures 77.b and 77.d.

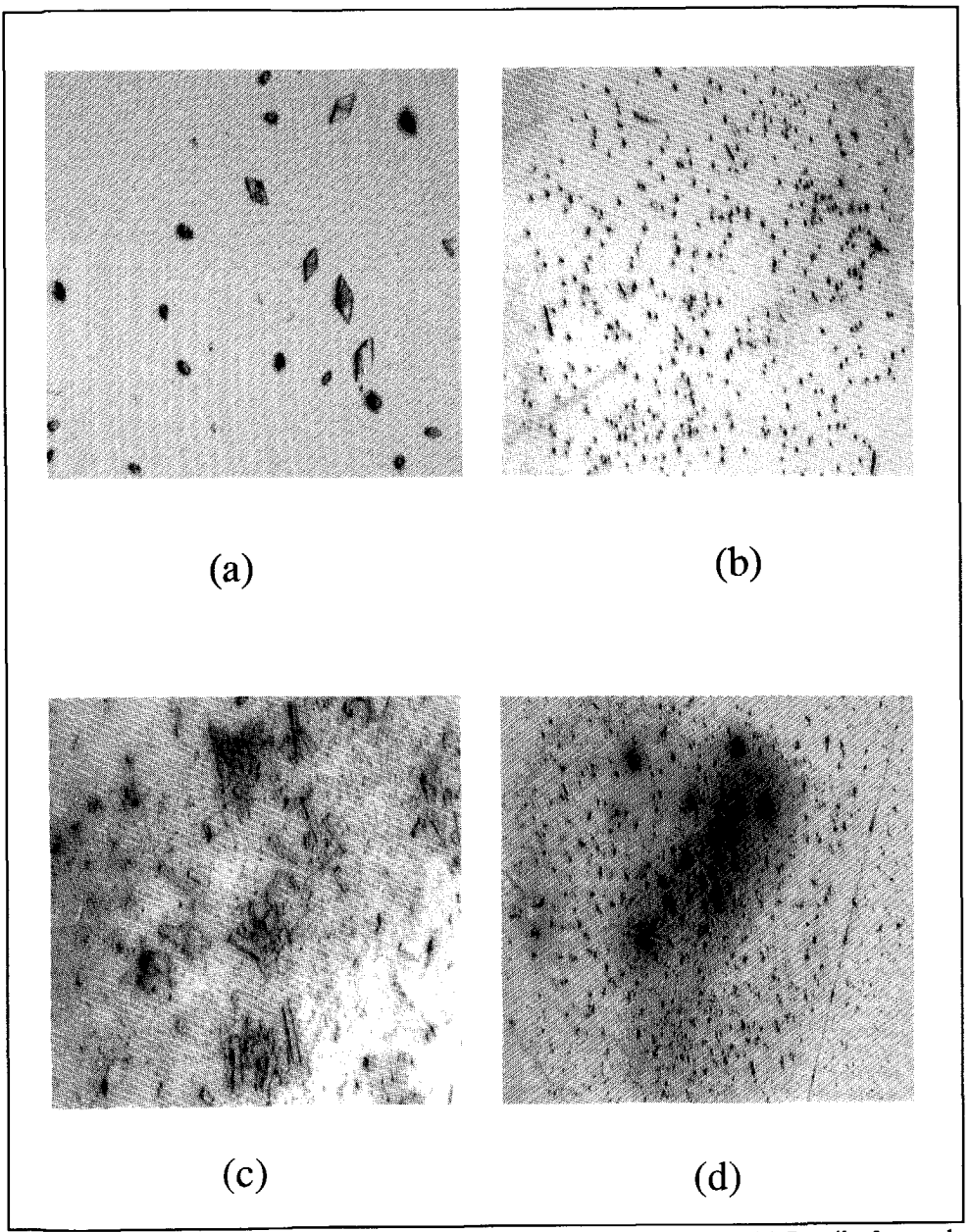

Figure 77. The surface of a cavity as observed during long-term tests. (a) Detail of crystals of oxalic acid on the cavity surface after 50 hours of ageing. The width of the figure corresponds to 1 mm. (b) An overview of the whole cavity surface after 50 hours of ageing. Cavity diameter = 6 mm. (c) Detail of clusters of crystals of oxalic acid on the cavity surface after 330 hours of ageing. The width of the figure corresponds to 1 mm. (d) An overview of the whole cavity surface after 330 hours of ageing. Cavity diameter = 6 mm.

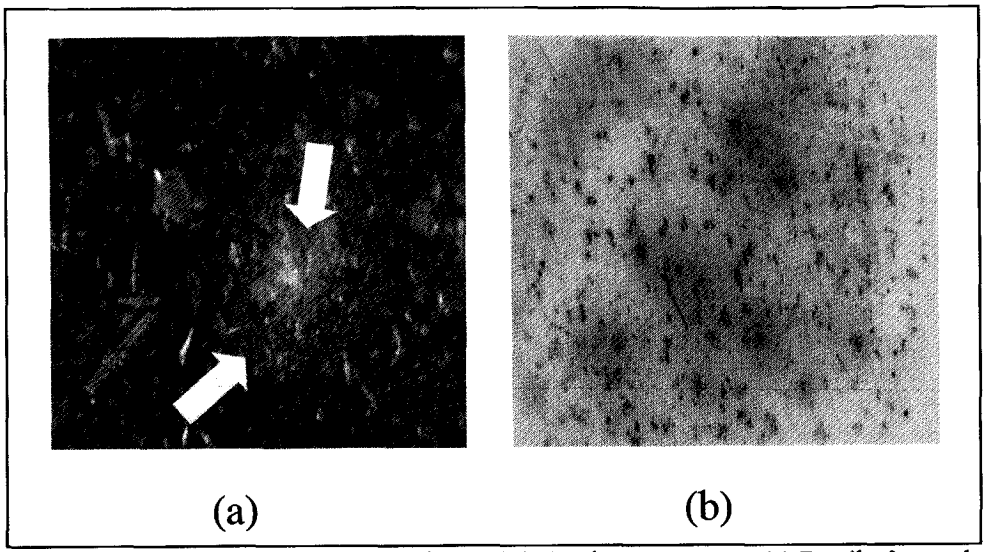

Figure 78. The surface of a cavity as observed during long term tests. (a) Detail of crystals of oxalic acid on the cavity surface after 650 hours of ageing. The arrows mark the top of a cluster of crystals and a recess around it. The width of the figure corresponds to 1 mm. (b) An overview of the whole cavity surface after 650 hours of ageing. Cavity diameter = 6 mm.

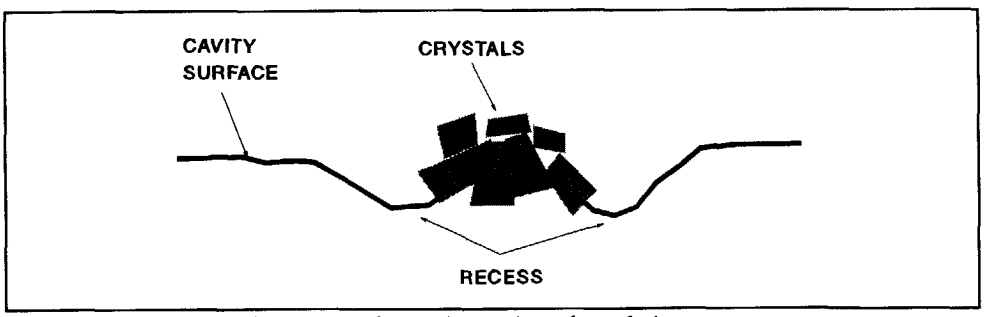

Figure 79. Schematic drawing of the cavity surface degradation.

Conclusions

Discharges in a cavity were observed during long-term tests up to 650 hours at 15 to 20 kV/mm. The discharge patterns changed several times during the ageing period. The changes in discharge patterns can be correlated with the degradation of the cavity surface. Such a degradation was manifested by the formation of discharge by-products in the form of crystals of oxalic acid and small depressions on the cavity surface, as known from literature. Using pattern recognition techniques, we have been able to detect the changes in the discharge patterns and correctly classify the fingerprints of each ageing stage.

5.1.2 Surface discharges in air

A rod-plane configuration was used to model surface discharges. A copper ring with a diameter of 35 mm and rounded edges was placed on the top of a 10 mm thick Perspex plate with three 100 μm thick polyethylene sheets on it, see Figure 80.

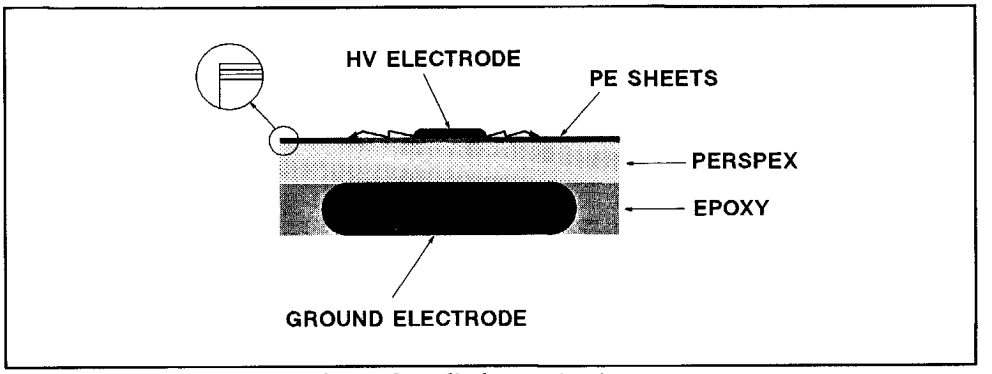

Figure 80. Test arrangement for surface discharges in air.

Two types of test were carried out:

1. short-term tests - up to 100 hours,
2. long-term tests - up to 1230 hours.

Short-term tests

The main purpose of the short-term ageing tests was to observe the basic discharge quantities, such as the maximum discharge magnitude and the discharge repetition rate during ageing. Further, the formation of discharge by-products and degradation of the polyethylene surface was observed. The duration of the tests did not exceed 100 hours. The test voltage was chosen to be 9 kV, which was 50% above the discharge inception at the beginning of the test. In Figure 81, the behaviour of the maximum discharge magnitude and the number of discharges in the positive and in the negative half-cycle of the test voltage as a function of the ageing time is shown. It is clearly visible that both quantities varied significantly during the test period.

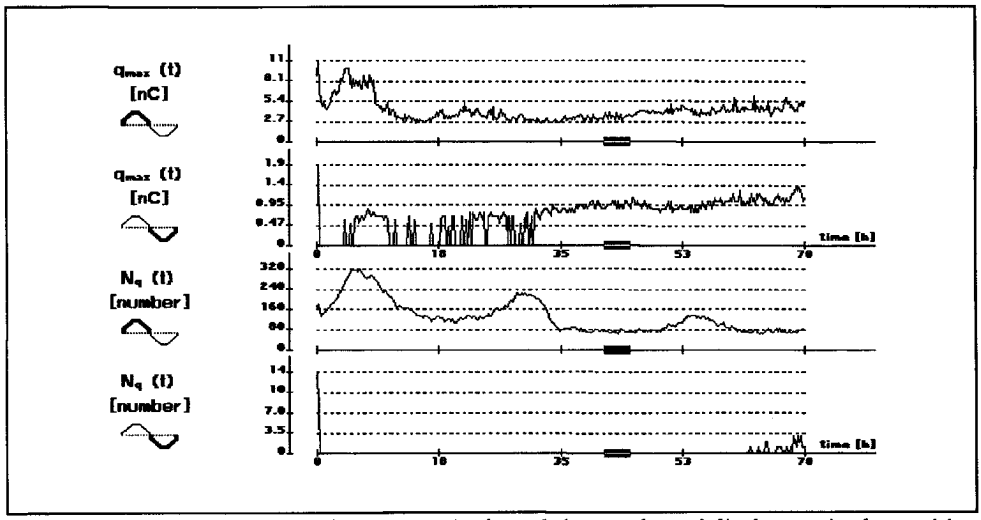

Figure 81. The maximum discharge magnitude and the number of discharges in the positive and in the negative half-cycle of the test voltage of surface discharges in air as a function of the ageing time.

Observation of the surface exposed to surface discharges revealed the formation of discharge by-products mostly in the form of crystals of oxalic acid [80,99]. The number, the size of the crystals and the area, which these crystals covered, increased with the test time, see Figure 82.

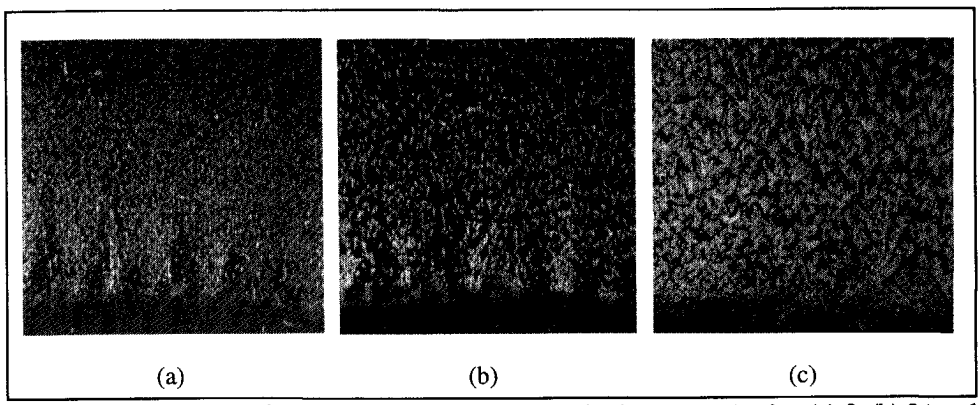

Figure 82. Surface of polyethylene exposed to surface discharges in air after (a) 8, (b) 24 and (c) 100 hours of ageing. The black area at the bottom of the figure marks the place where the high voltage electrode was situated. The width of the figure corresponds to 3.5 mm.

After 100 hours of ageing, three different rings of discharge by-products were found on the surface of the polyethylene near the high voltage electrode, see Figures 83 and 84.

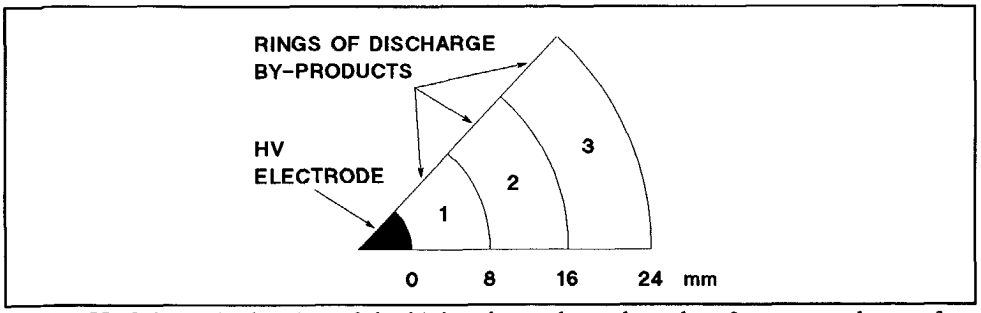

Figure 83. Schematic drawing of the high voltage electrode and surface exposed to surface discharges with three different rings of discharge by-products as they occurred after 100 hours of ageing.

In the first ring, up to 8 mm from the high voltage electrode, large crystal 'flakes' having a tree form can be seen, see Figure 84.a.

In the second ring, from about 8 to 16 mm from the high voltage electrode, the surface had a greyish colour and the density of large crystals decreased substantially, see Figure 84.b.

In the third ring, ranging from about 16 to 25 mm, tiny crystals were observed which were ten or more times smaller than those in the first ring, see Figure 84.c.

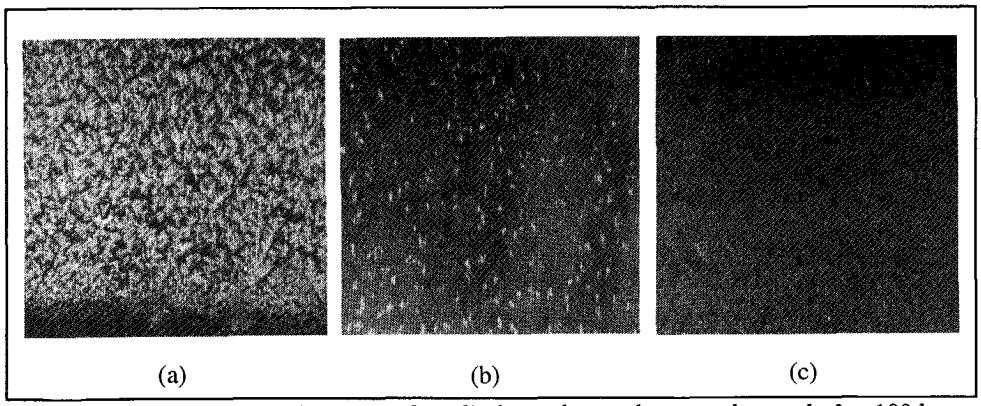

Figure 84. Three different rings of surface discharge by-products as observed after 100 hours of ageing. (a) 1st ring, 0-8 mm from the HV electrode. (b) 2nd ring, 8-16 mm from the HV electrode. (c) 3rd ring, 16-25 mm from the HV electrode.

The fact that discharge by-products may be of a conductive nature is well known [46,80,88,113]. As the discharge by-products are gradually formed on the surface of polyethylene, they may change the electric field around the electrode. It is believed that the fluctuations in the discharge magnitude and the number of discharges as seen in Figure 81 are caused by the formation of these discharge by-products.

The condition of a surface, for example its contamination, also influences the propagation of surface discharges. This is shown in Figure 85. A textile fibre left on a polyethylene sheet in an almost radial direction to the high voltage electrode absorbed liquid discharge by-products and changed the electric field around it. This resulted in increased discharge activity at its ends with the formation of a large number of crystals at both ends of the fibre. Note that as the fibre absorbed discharge by-products, no crystals could be found next to and along the length of the fibre and the fibre was heavily crystallized.

Figure 85. A textile fibre exposed to surface discharges in air. The fibre was left on a polyethylene sheet in almost radial direction to a high voltage electrode. The length of the fibre was about 3.5 mm. The black area in the lower right corner marks the place where the high voltage electrode was situated.

Long-term tests

In the long-term test, polyethylene sheets were continuously exposed to surface discharges during a period of 1230 hours. In the first thousand hours, the ageing voltage U_a was chosen to be 9kV, which corresponded to 1.5 inception voltage at the beginning of the test. After about one thousand hours the ageing voltage was increased every 48 hours by 3kV. This procedure was repeated until a partial breakdown of the polyethylene sheet was observed.

The test voltage U_t for the measurement of discharges was always 50% above the discharge inception at the time of measurement. The ageing voltage U_a and the test voltage U_t as a function of the ageing time are shown in Figure 86.a. It should be observed that the test voltage U_t was up to 900 hours about the same - 9 kV. Then it gradually decreased to a value of about 4 kV in the end of the test.

The maximum discharge magnitude dropped from about 15 nC to about 1-3 nC during the first hours of the test, see Figure 86.b. Then it remained approximately constant till 1000 hours. At the end phase of the test it decreased again to about 4 pC. The last drop in the discharge magnitude could be explained by the fact that in the end phase of the test the measurements were carried out with the decreased test voltage - 4 kV. At the test voltage level of 9 kV, however, discharges with magnitude of 1-3 nC were registered.

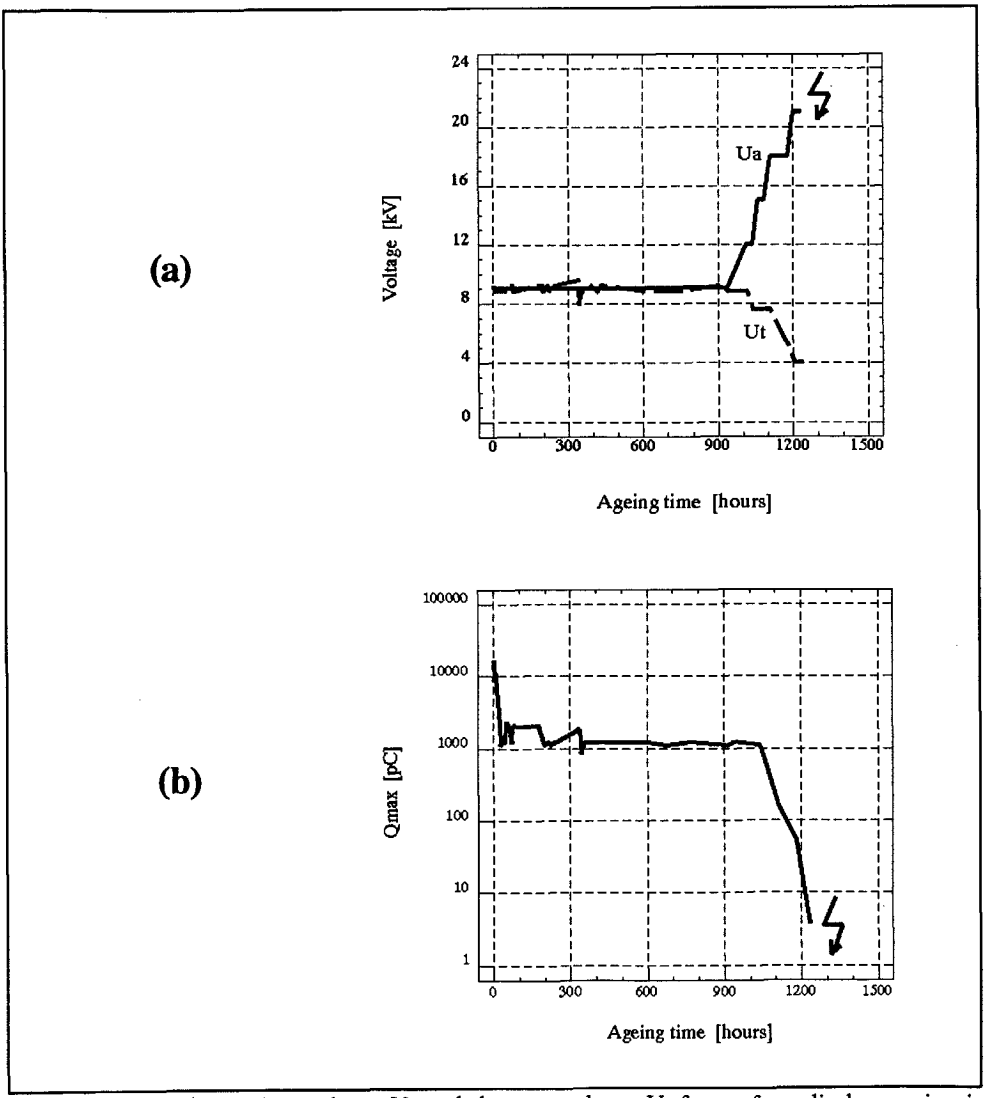

Figure 86. (a) The ageing voltage U_a and the test voltage U_t for surface discharges in air during long-term ageing. (b) The maximum discharge magnitude of surface discharges in air as a function of the ageing time.

A total of 39 *mean* fingerprints were made during the ageing period. As mentioned before, one *mean* fingerprint is the mean value of 30 fingerprints obtained during one data collection session. One session took 2 minutes. It follows that a total of 39×31=1209 fingerprints were collected during the ageing period. To reduce the amount of data for processing, only the *mean* fingerprints were analyzed.

By means of cluster analysis (the group average method) a tree structure of the data was made, see Figure 87. As explained in Chapter 4, the main 'branches' in such a tree are sought to distinguish between different groups of fingerprints. In this case, four groups of fingerprints referencing four ageing stages were identified during the long-term test. There is some space left in the interpretation of such tree structures. For example, the third group in Figure 87 may be divided to two subgroups, 3a and 3b, which would in this case result in five (as opposed to four) ageing stages. By dividing a tree structure into more 'branches', a more refined picture of ageing stages can be obtained, but it can be doubtful whether these stages are related to actual physical differences of the insulating material during ageing.

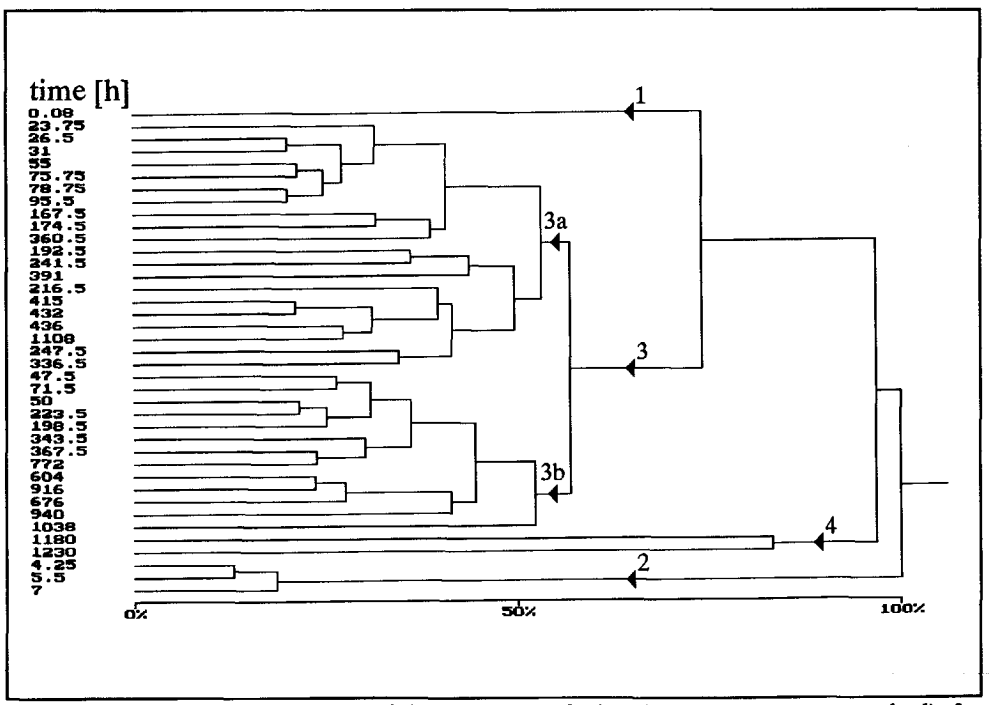

Figure 87. Tree structure obtained by cluster analysis (the group average method) for fingerprints of surface discharges in air during long-term ageing. The numbers on the left side of the figure indicate the time at which the fingerprints were collected.

The ageing stages identified by the tree structure are shown as a function of the ageing time in Figure 88. It can be seen that the first stage lasted about one hour only. The second stage took several hours. Then a long period with a duration of several hundred hours followed. The fourth stage, where the partial breakdown of the insulation occurred, was observed in the last dozens of hours.

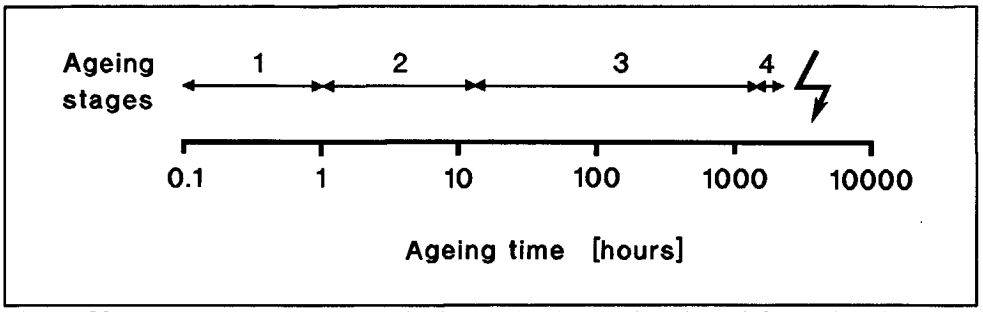

Figure 88. Ageing stages of surface discharges in air as a function of the ageing time.

A data base consisting of representative fingerprints of each stage was then built. The results of the classifications are shown in Figure 89 and Table 14. Most of the fingerprints were classified correctly. There were no misclassifications.

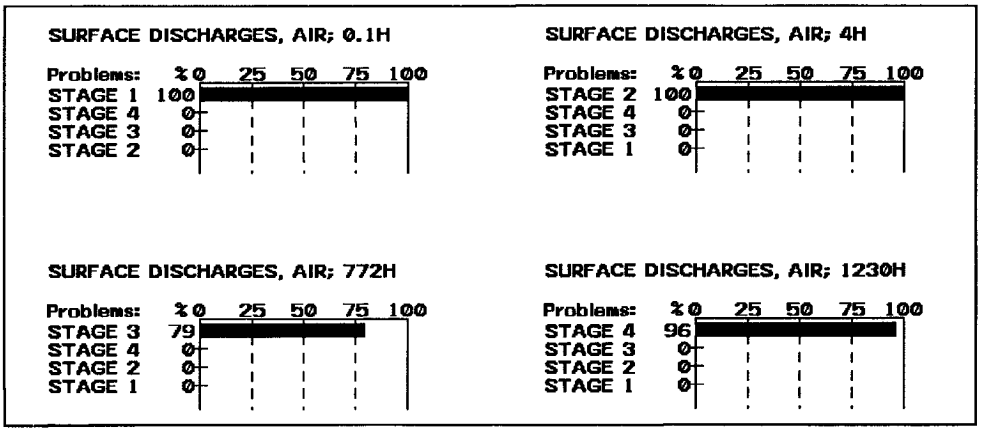

Figure 89. Recognitions of surface discharges in air during long-term ageing.

Table 14. Result of fingerprint classifications of surface discharges in air during long term ageing.

Stage	Fingerprints correctly recognized	Multiple recognitions	Fingerprints not recognized	Mis-classified fingerprints	Number of mean fingerprints
1	1	-	-	-	1
2	3	-	-	-	3
3	32	-	1	-	33
4	2	-	-	-	2

One remark has to be made concerning the collection of fingerprints in the last - fourth - stage. In this stage, the fingerprints were collected at a voltage level of about 4 kV, which corresponded to 1.5 discharge inception voltage, see Figure 86. When the test voltage was increased to 9 kV, which corresponds to a situation of constant test voltage from the beginning to the end, discharge patterns similar to those in stage 3 were observed on an oscilloscope screen. This emphasizes the influence of the test voltage on the collection of discharge patterns. If the fingerprints were taken at the constant voltage level, say 9 kV, it would not be possible to detect damage to the insulation by means of discharge patterns. By collecting data at 1.5 inception voltage, it was possible to detect changes in discharge patterns and relate them to damage to the insulation.

Several defects were observed on the surface of the polyethylene sheet in the last - fourth stage, see Figure 90. The formation of such defects is caused by a constant bombardment of the polyethylene surface by energetic electrons, chemical degradation caused by discharge by-products, *etc.* With the high discharge repetition rate, also the temperature of the surface may rise considerably and thermal ageing might take place [30,31,79,80,109,119].

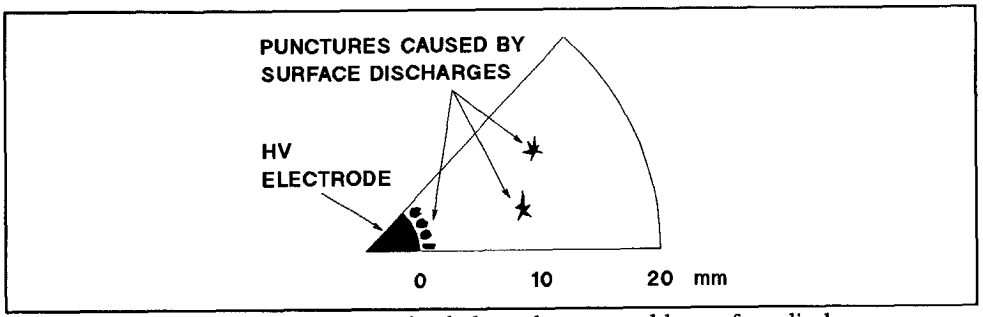

Figure 90. A view of defects on a polyethylene sheet caused by surface discharges.

As expected, a number of punctures occurred near the electrode, see Figures 90 and 91.a. This was also the place where the most intense light was observed. Three other punctures were observed at a distance of about 10 mm from the electrode, see Figures 90 and 91. The structures of these defects were also different, oval as opposed to star-shaped, see Figure 91. The breakdowns off the electrode could be caused by, *e.g.*, dust deposits on the surface or other local inhomogenities.

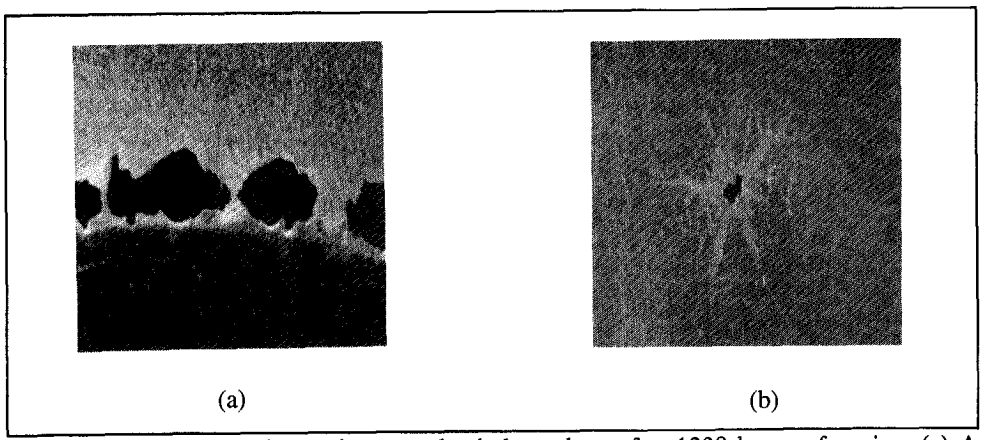

Figure 91. Defects as observed on a polyethylene sheet after 1230 hours of ageing. (a) A puncture as observed around the electrode. (b) A puncture as observed about 10 mm off the electrode. The width of the figure corresponds to 3.5 mm.

As those punctures occurred, the discharges propagated not only on the top of the first sheet, but also between the first and the second sheet. Crystals of discharge by-products, which were found on the top of the second sheet, see Figure 92, are evidence of this.

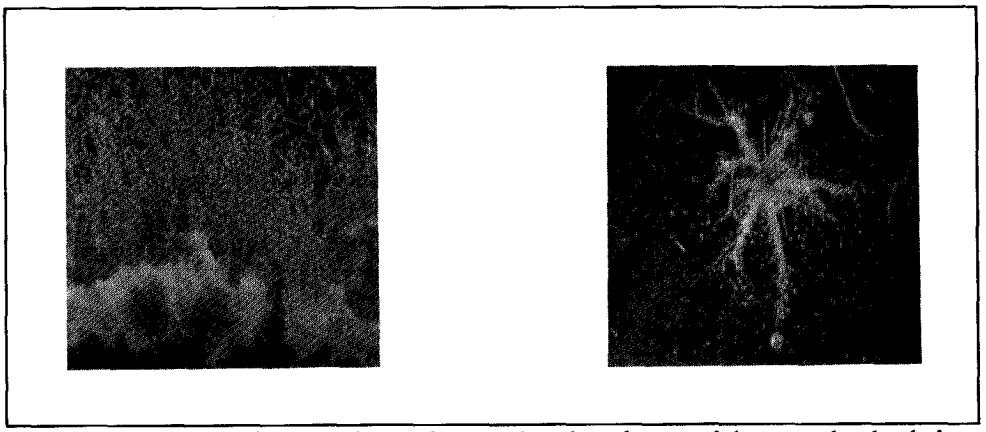

Figure 92. Crystals of discharge by-products as found on the top of the second polyethylene sheet at the places where punctures occurred. (a) The crystals around the electrode. (b) The crystals at puncture which occurred 10 mm off the electrode.

Also, tree-like channel structures covered with crystals were observed on the top of the second and at the bottom of the first sheet in the places where the breakdown of the first sheet occurred, see Figure 93.

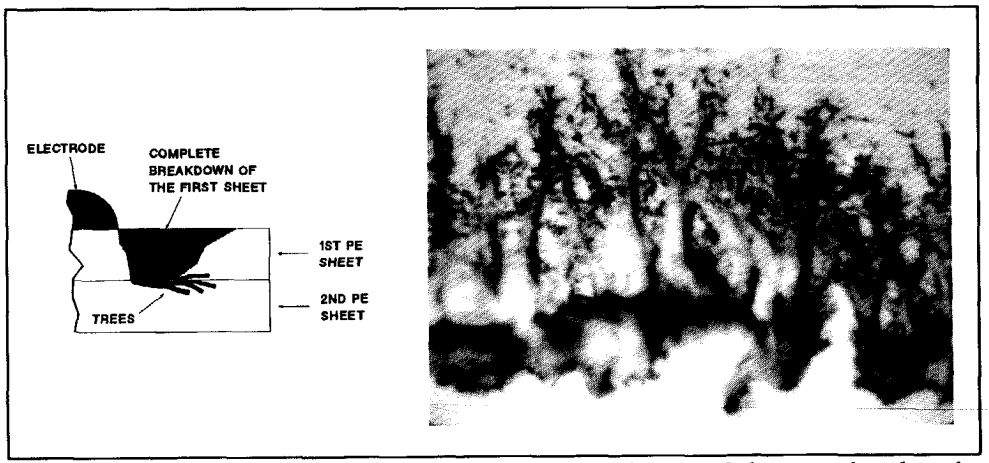

Figure 93. Tree-like channel structures as observed on the top of the second and at the bottom of the first polyethylene sheet in the places where the breakdown of the first sheet occurred. The white area at the bottom of the figure marks the place where the electrode was situated. The width of the figure corresponds to 3.5 mm.

Conclusions

Discharge patterns of surface discharges in air were observed during long-term ageing up to 1200 hours. The discharge patterns changed several times during the ageing period. The changes in the discharge patterns went together with the degradation of the dielectric exposed to surface discharges which was manifested by the formation of discharge by-products on the surface of the dielectric and partial breakdowns of the dielectric. With the aid of pattern recognition techniques, we have been able to detect changes in discharge patterns during ageing and correctly determine ageing stages of the dielectric.

5.1.3 Surface discharges in oil

A rod-plane configuration was used to model surface discharges in oil (Diala C by Shell). A 1 mm thin copper ring with rounded edges was placed on the top of a 2 mm thick polyethylene slab, see Figure 94.

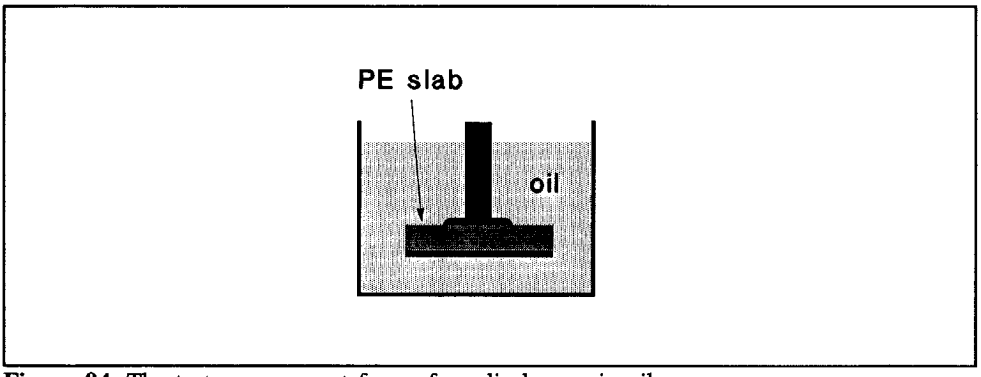

Figure 94. The test arrangement for surface discharges in oil.

Ageing of the insulation took 460 hours and proceeded in voltage steps of 4 kV (from 13 kV to 25 kV) at time intervals of about 120 hours, see Figure 95. The test voltage for a collection of fingerprints was chosen to be constant at 13 kV which corresponds to 1.5 U_{inc} of the virgin sample.

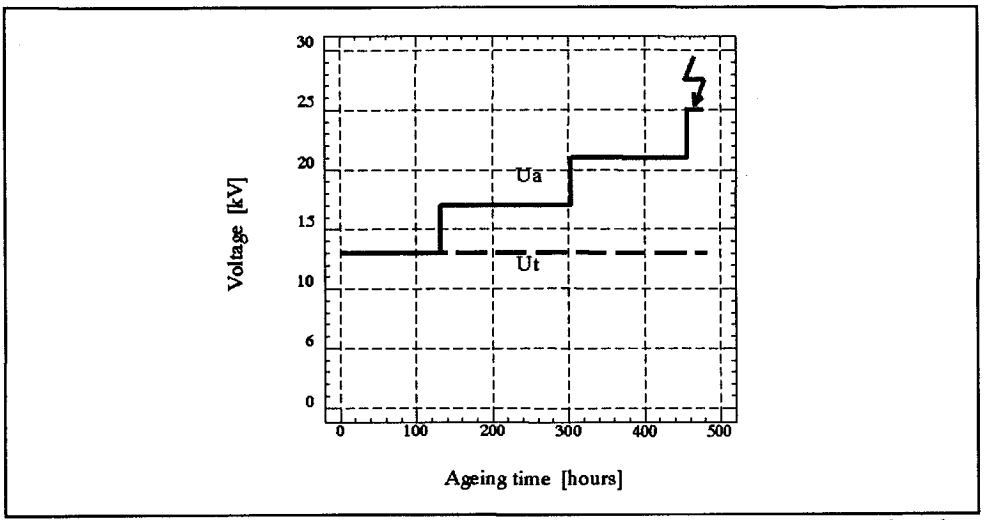

Figure 95. The ageing voltage U_a and the test voltage U_t for a measurement of surface discharges in oil during long-term ageing.

The behaviour of the maximum discharge magnitude as a function of the ageing time is shown in Figure 96. The discharge magnitude increased during the first tens hours. Then it dropped to a value observed at the beginning of the test and remained about constant till the end of the test.

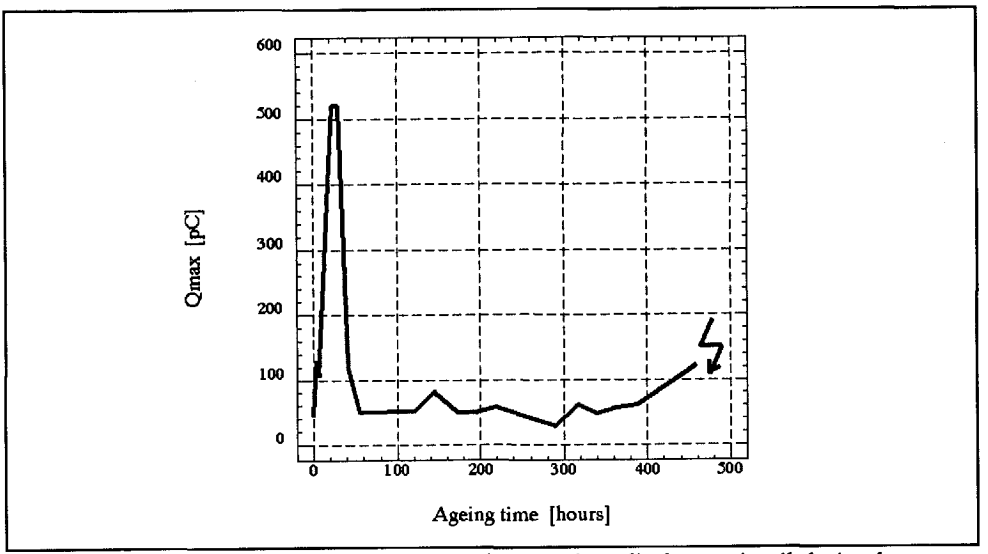

Figure 96. The maximum discharge magnitude of surface discharges in oil during long-term ageing.

A total of 16 *mean* fingerprints were collected during the ageing period. It follows that a total of 16×31=496 fingerprints were collected. As previously mentioned, to reduce the amount of data for processing, only the *mean* fingerprints were analyzed. The fingerprints were analyzed by cluster analysis (the group average method). The resulting tree structure is shown in Figure 97.

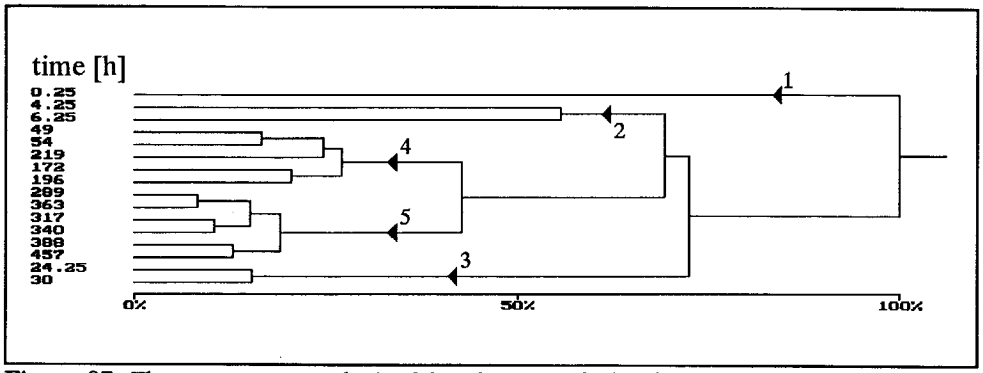

Figure 97. The tree structure obtained by cluster analysis (the group average method) for fingerprints of surface discharges in oil. The numbers on the left side of the figure indicate the time at which the fingerprints were collected.

By looking for main 'branches' in the tree as explained before, five different groups of fingerprints were distinguished, see Figure 97. These groups - the ageing stages are shown as a function of the ageing time in Figure 98. It can be seen that in the first 50 hours discharge patterns changed rapidly, which resulted in four ageing stages. After about 50 hours the discharge patterns stabilized.

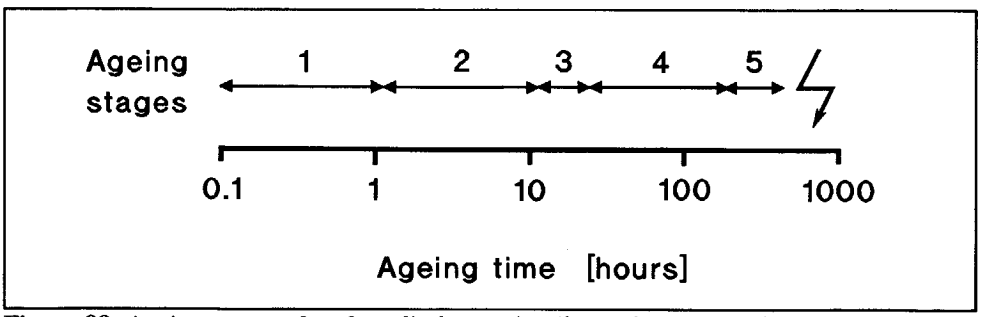

Figure 98. Ageing stages of surface discharges in oil as a function of the ageing time.

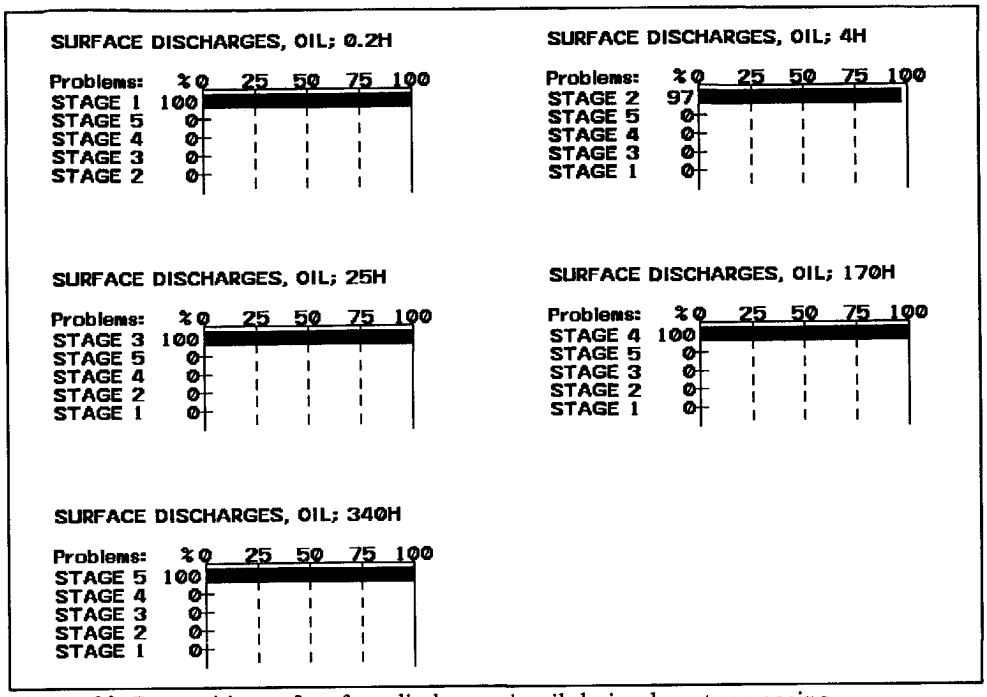

Figure 99. Recognitions of surface discharges in oil during long-term ageing.

Figure 99 show recognitions of fingerprints in each stage. Detailed evaluation of results is given in Table 15. It can be seen that all fingerprints were correctly recognized. There were no misclassifications to other ageing stages.

Table 15. Result of fingerprint classifications of surface discharges in oil during long term ageing.

Stages	Correctly classified fingerprints	Multiple recognitions	Fingerprints not recognized	Mis classified fingerprints	Number of mean fingerprints
1	1	-	-	-	1
2	2	-	-	-	2
3	2	-	-	-	2
4	5	-	-	-	5
5	6	-	-	-	6

One remark has to be made concerning the breakdown of the insulation. The breakdown occurred within a period of 24 hours after the increase of the ageing voltage from 21 kV to 25 kV, see Figure 95. Because the fingerprints were collected during a time interval of about 24 hours no rapid change in discharge patterns was detected before the breakdown. It should be kept in mind that treeing tracks, such as those shown in Figure 100.c, can lead to the breakdown of the insulation rather quickly, in seconds or minutes, after its initiation [57].

Degradation of a polyethylene surface near the electrode was observed during the test, see Figure 100.a. It consisted of uniform 'wear-out' of the insulation in the form of carbonized spots around the electrode, see Figure 100.b., and traces of treeing, see Figure 100.c. Treeing of the insulation could have been the cause of the breakdown of the insulation near the electrode, see Figure 100.d.

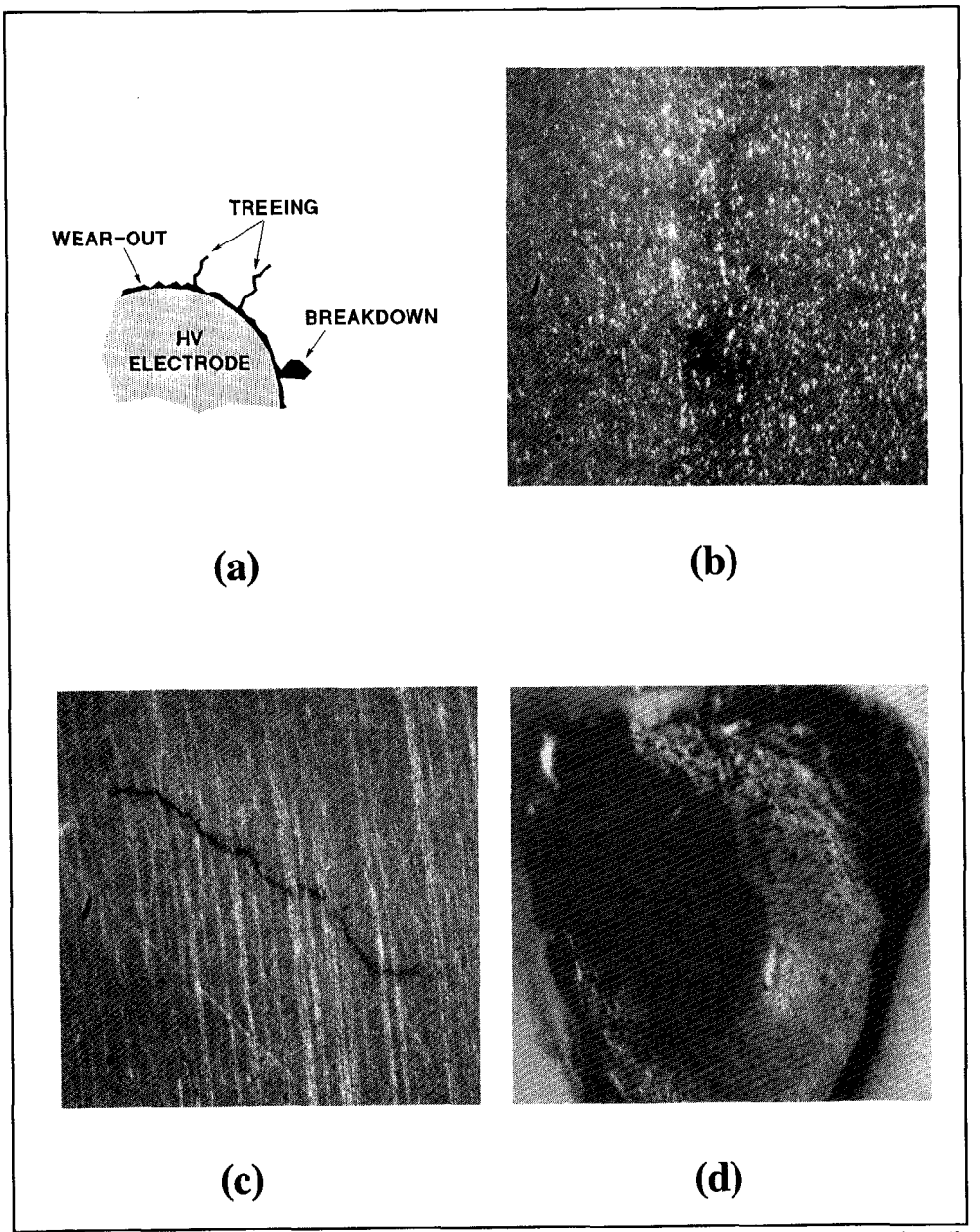

Figure 100. Degradation of a polyethylene surface exposed to surface discharges under oil. (a) An overview of the insulation degradation. (b) Carbonized spots found around the electrode (see black spots in the vertical direction approximately in the middle of the figure). The width of the figure corresponds to 2 mm. (c) Treeing traces near the electrode. The width of the figure corresponds to 4 mm. (d) The breakdown of a polyethylene slab. The width of the figure corresponds to 6 mm.

Conclusions

Discharge patterns obtained during long-term ageing of a dielectric exposed to surface discharges in oil were studied. The discharge patterns changed several times during ageing. Discharges resulted in a degradation of the dielectric which finally led to the breakdown of the dielectric. Using pattern recognition techniques, it was possible to detect changes in discharge patterns and correctly classify the fingerprints of each ageing stage.

5.2 Industrial objects

5.2.1 12 kV current transformer

A 12 kV current transformer used in 10/12 kV distribution networks showed discharges at a voltage level of 28 kV. Possible cause of discharges are cavities and cracks situated in the epoxy insulation, see Figure 101. The cavities could have been originated during the casting of the epoxy insulation. The cracks may have resulted from a short-circuit test that was performed before the ageing test described here.

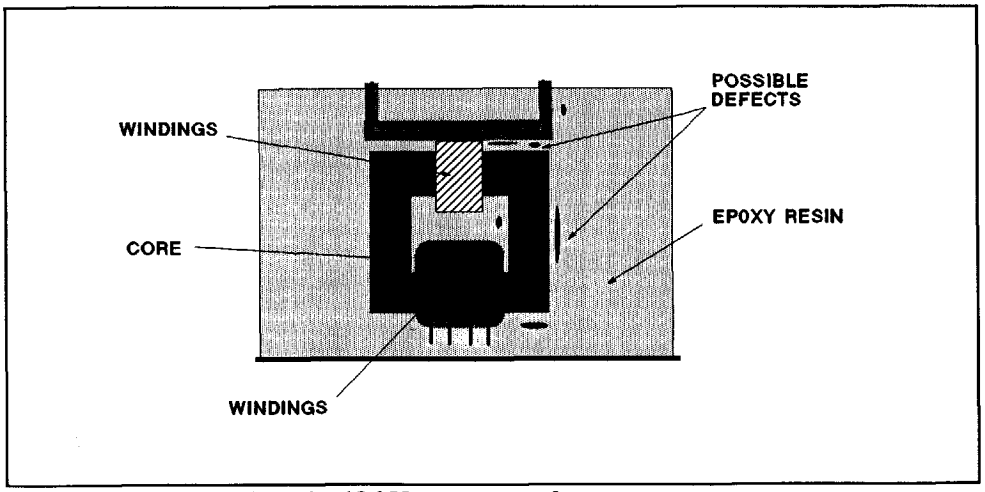

Figure 101. Cross-section of a 12 kV current transformer.

The transformer was continuously aged till breakdown during a period of 900 hours. The ageing voltage U_a was increased in steps from 45 to 90 kV, see Figure 102. The test voltage at which fingerprints were collected was 40 kV at the beginning of the test and 65 kV at the end of the test, see text below.

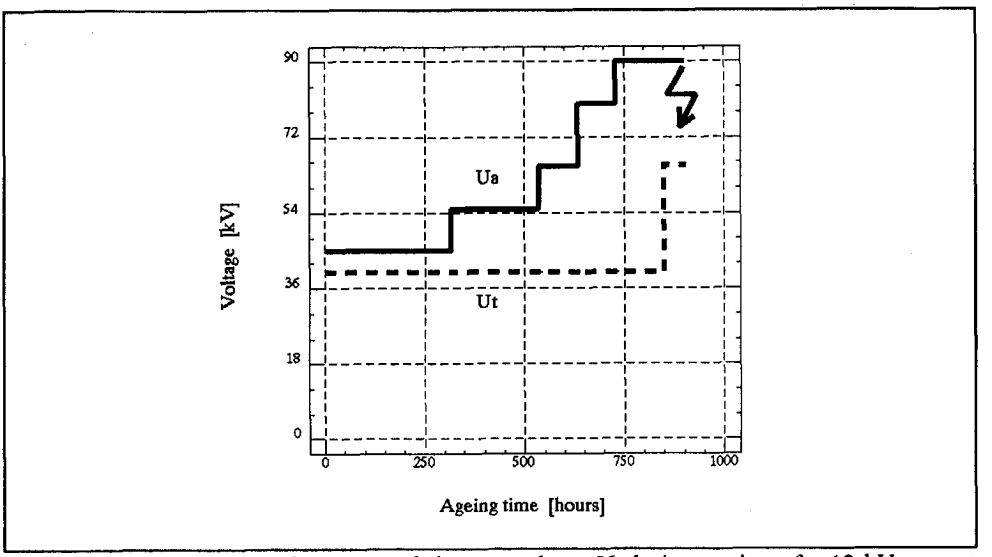

Figure 102. The ageing voltage U_a and the test voltage U_t during ageing of a 12 kV current transformer.

The behaviour of the maximum discharge magnitude during ageing time is shown in Figure 103. Discharges with a magnitude of about 8 pC were detected at the beginning of the test. As the test voltage was gradually increased from 0 to 40 kV, several defects began to discharge at different voltage levels. At the test voltage of 40 kV, three defects with three different discharge magnitudes were observed on an oscilloscope screen. After few hours the discharges extinguished. The transformer was then checked for discharges every day with the test voltage up to 90 kV, but there were no detectable discharges (the sensitivity of the measurement was 1 pC). After about 850 hours of ageing discharges reappeared. The test voltage, however, had to be increased from 40 to 65 kV because there were no discharges detectable at the test voltage level of 40 kV. At the test voltage of 65 kV discharges with magnitude of about 110 pC were measured. This time only one defect discharged. After another 50 hours of ageing the transformer broke down.

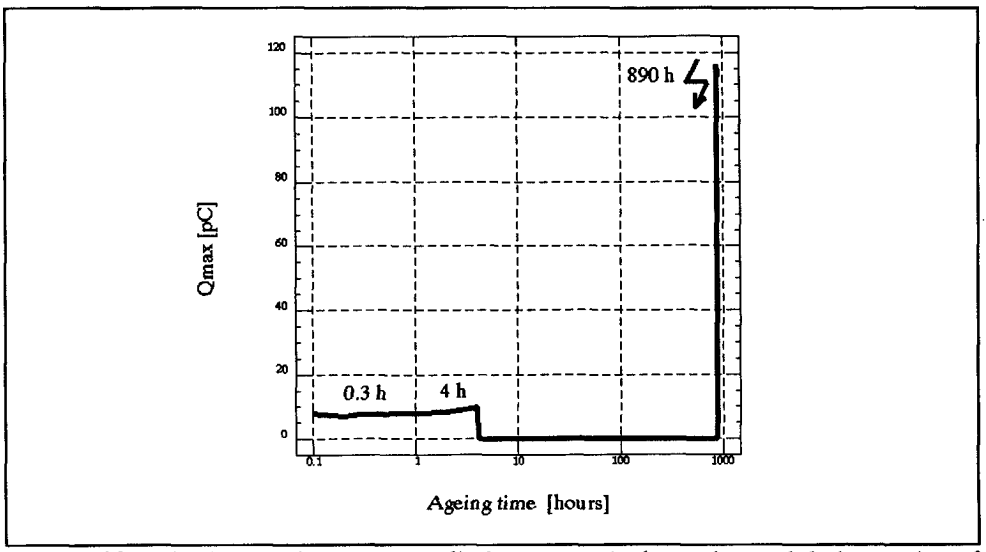

Figure 103. Behaviour of the maximum discharge magnitude as observed during ageing of a 12 kV current transformer.

A total of 12 *mean* fingerprints were collected. It follows that a total of 12×31=371 fingerprints were collected during the ageing period. The fingerprints were analyzed by cluster analysis (the group average method). By looking for main 'branches' in a tree structure, see Figure 104, three different groups of fingerprints were distinguished.

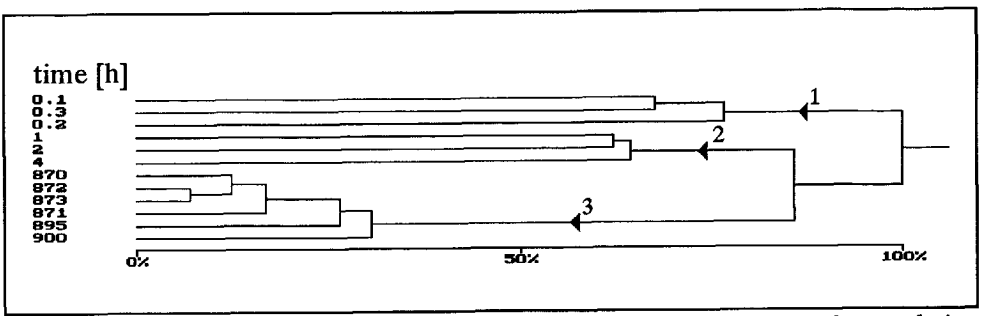

Figure 104. Tree structure obtained for fingerprints of a 12 kV current transformer during long-term ageing. The numbers on the left side of the figure indicate the time at which the fingerprints were collected.

These groups - the ageing stages are shown in Figure 105 as a function of the ageing time. It can be seen that the first stage lasted one hour only. The second stage took several hours from the end of the first stage. After the second stage, a long period with a duration of several hundred hours followed where no discharges were detected. Note that with the sensitivity of the measurement of about 1 pC discharges with the smaller magnitude remained undetected. Yet the discharges could substantially deteriorate the insulation, as shown in [60,89]. After about 850 hours of ageing, the third stage with the duration of about 50 hours took place, after which breakdown of the transformer occurred.

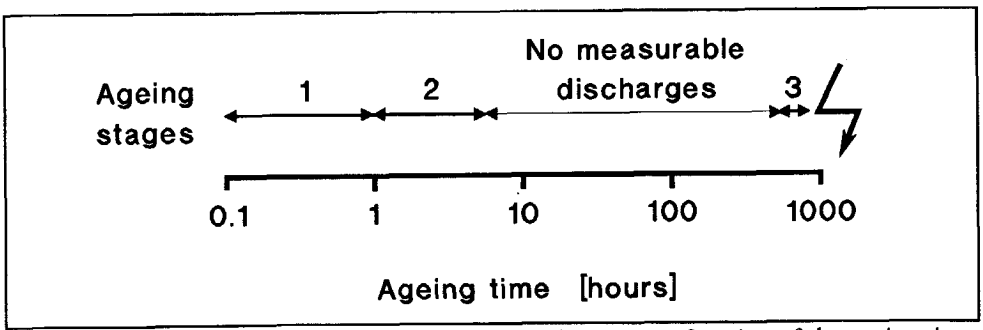

Figure 105. Ageing stages of a 12 kV current transformer as a function of the ageing time.

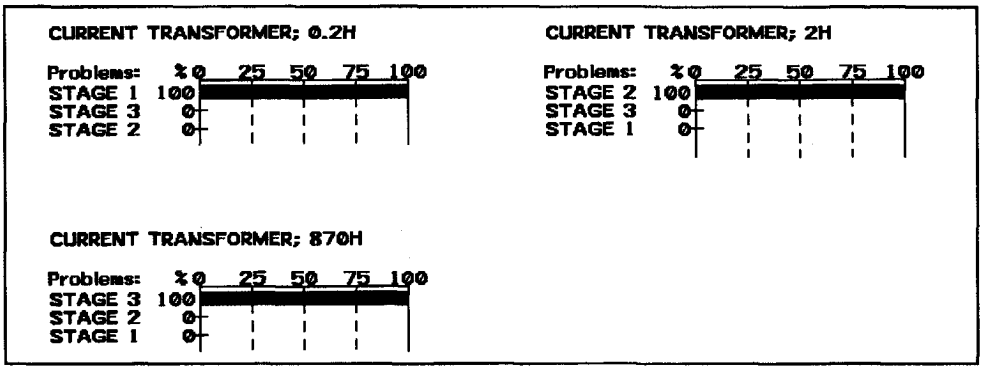

Figure 106. Recognition of discharge patterns of a 12 kV current transformer during long-term ageing.

Recognitions of fingerprints of each ageing stage are shown in Figure 106. Detailed evaluation of results is given in Table 16. It can be seen that satisfactory recognitions took place. There were no misclassifications to other ageing stages.

Table 16. Result of fingerprint classifications of a 12 kV current transformer during long-term ageing.

Stage	Correctly classified fingerprints	Multiple recognitions	Fingerprints not recognized	Mis-classified fingerprints	Number of mean fingerprints
1	3	-	-	-	3
2	3	-	-	-	3
3	6	-	-	-	6

Conclusions

A 12 kV current transformer was aged till breakdown for a period of 900 hours. After several hours the discharges extinguished. The discharges appeared again after about 850 hours and the transformer broke down after another 50 hours of ageing. By means of cluster analysis techniques, three different discharge patterns were distinguished during the ageing of the transformer. Fingerprints of each ageing stage were then successfully classified to the corresponding stage. There were no misclassifications. The disappearance of detectable discharges during long period of the test time presents a considerable disadvantage in using this method for the prediction of insulation breakdown.

5.2.2 23 kV epoxy insulator

A 23 kV epoxy insulator, see Figure 107, was aged for a period of 1600 hours. This insulator showed discharges below operating voltage. A possible cause of discharges are the cavities formed in the body of the insulator during the casting of the epoxy insulation.

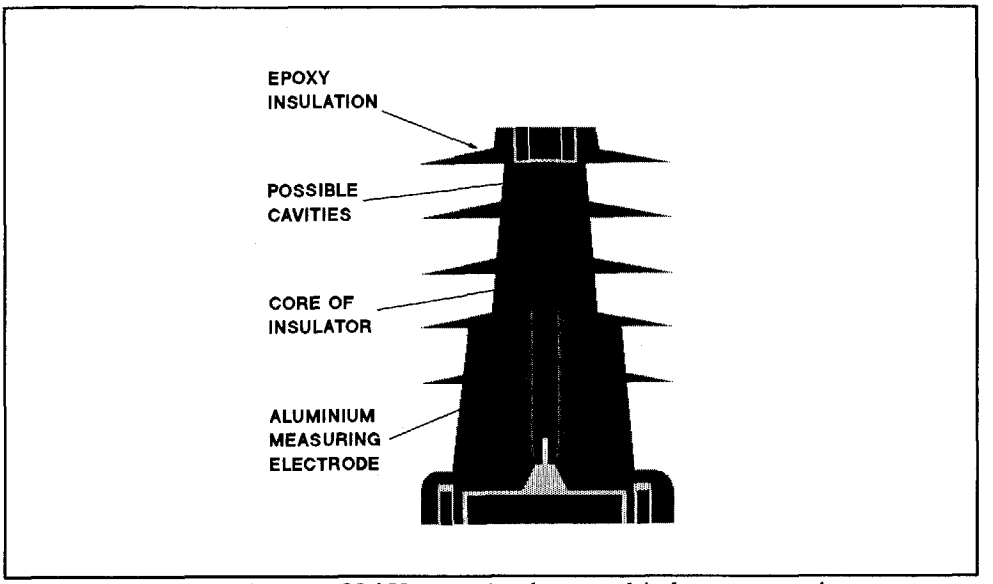

Figure 107. Cross-section of a 23 kV epoxy insulator used in long-term ageing.

The ageing voltage was increased in 5 kV steps (from 28 kV to 82 kV) about every 120 hours, see Figure 108. The test voltage for collecting of fingerprints was 23 kV - the operating voltage of the epoxy insulator.

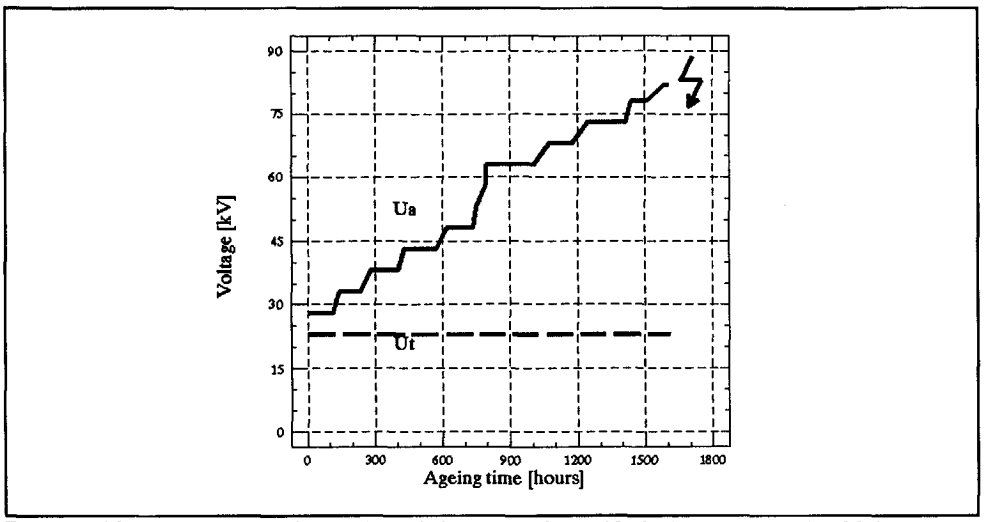

Figure 108. The ageing voltage U_a and the test voltage U_t during ageing of a 23 kV epoxy insulator.

The behaviour of the maximum discharge magnitude during the ageing time is shown in Figure 109. It remained about constant at level 40 pC up to about 1000 hours, then it increased to about 100 pC and in the end phase of the test it dropped to level 30 pC.

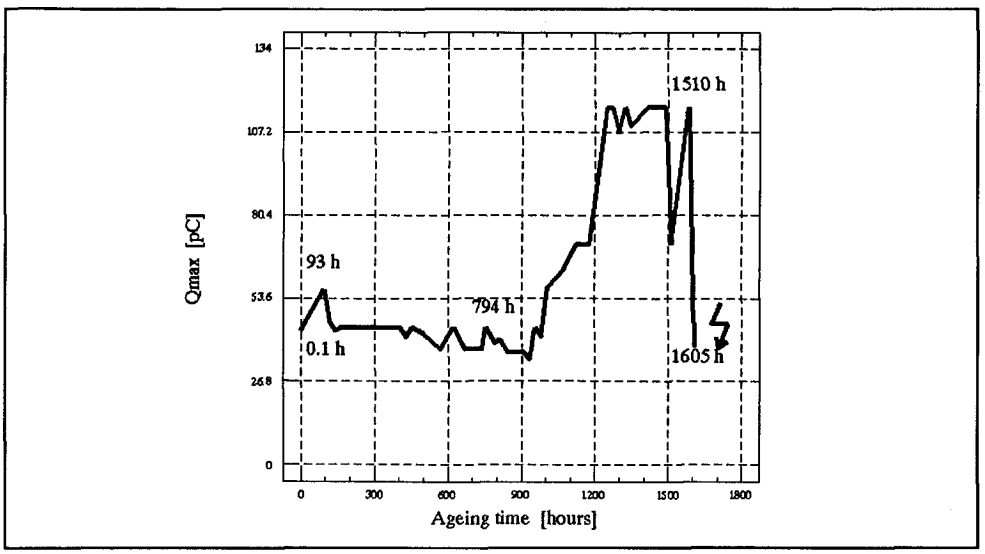

Figure 109. The maximum discharge magnitude obtained during long-term ageing of a 23 kV epoxy insulator.

A total of 45 *mean* fingerprints were collected during the ageing period. It follows that a total of 45×31=1395 fingerprints were collected. The differences between the fingerprints are shown in the form of a tree structure obtained by cluster analysis (the group average method). By looking for main 'branches' in the tree structure, see Figure 110, five groups of fingerprints were distinguished.

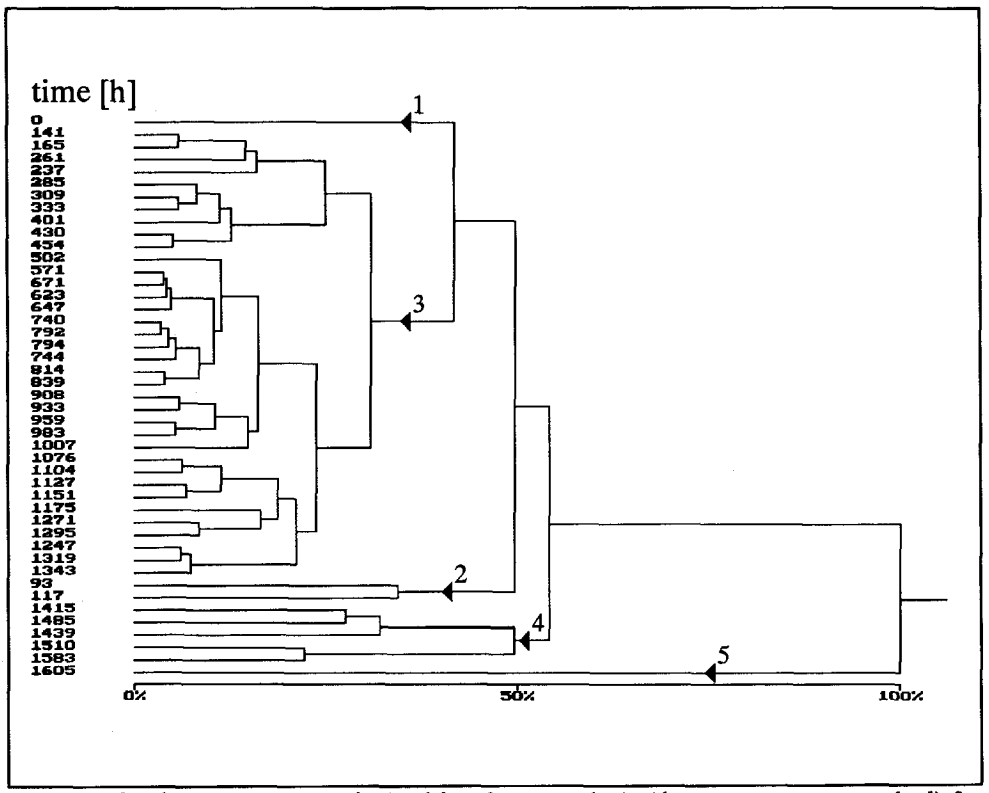

Figure 110. The tree structure obtained by cluster analysis (the group average method) for a 23 kV epoxy insulator. The numbers on the left side of the figure indicate the time at which the fingerprints were collected.

These groups - the ageing stages are shown in Figure 111 as a function of the ageing time. In the last stage - after about 1600 hours of ageing - a partial breakdown of the insulator took possibly place. The insulator could withstand its operating voltage but intense acoustic noise was heard along the body of the insulator.

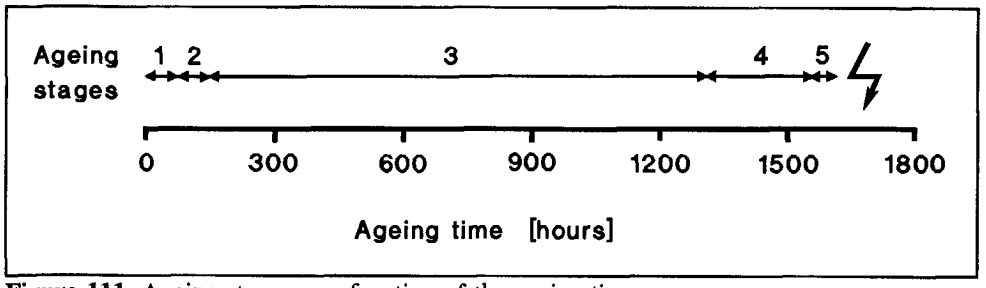

Figure 111. Ageing stages as a function of the ageing time.

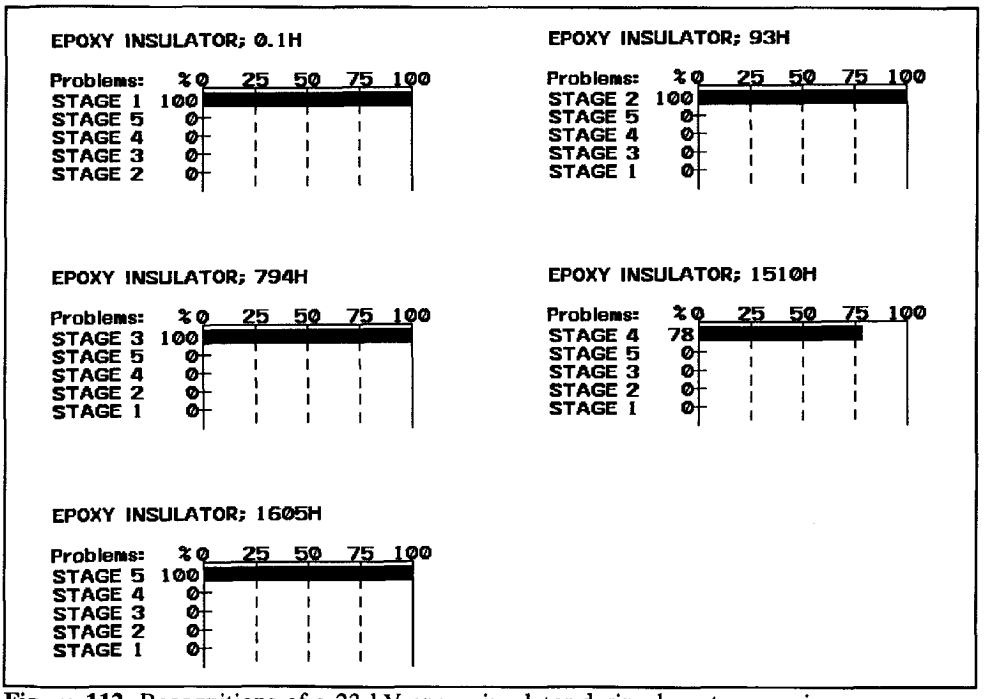

Figure 112. Recognitions of a 23 kV epoxy insulator during long term ageing.

Recognitions of fingerprints of each ageing stage are shown in Figure 112.

Detailed statistical evaluation of results is given in Table 17. It can be seen that satisfactory recognitions took place. Three fingerprints which were not recognized had centour scores lower than 30% but to a correct stage.

Table 17. Result of fingerprint classifications of a 23 kV epoxy insulator during long term ageing.

Stage	Correctly recognized fingerprints	Multiple recognitions	Fingerprints not recognized	Mis classified fingerprints	Number of mean fingerprints
1	1	-	-	-	1
2	2	-	-	-	2
3	33	-	3	-	36
4	5	-	-	-	5
5	1	-	-	-	1

Conclusions

A 23 kV epoxy insulator was aged during a period of 1600 hours. Several changes in discharge patterns were observed during this ageing period. Using pattern recognition techniques we have been able to distinguish these changes and correctly classify fingerprints of each ageing stage.

5.3 Conclusions

In this chapter the effect of ageing on discharge patterns was studied. The following can be concluded.

1. Discharge patterns as observed during long-term ageing of standard defects and industrial high voltage components changed several times during the ageing period.

2. Most of the changes in discharge patterns occurred at the beginning of the accelerated long-term tests, in the first minutes or hours. After that relatively stable patterns with a duration of several hundred hours were observed.

3. The changes in discharge patterns during ageing have implications for discharge recognition because patterns which occur at the beginning of a test differ from those at the end of the test. A separate category in a data base should be created for each ageing stage.

4. The tree structures of the group average method proved to give a good discrimination between different ageing stages during long-term tests.

5. Using the centour score method a successful recognition of fingerprints according to ageing stages took place. There were no misclassifications.

6. Tests on actual high voltage components indicate that the selected recognition tools (the group average method, the centour score method) have a good potential for industrial application, such as the periodic testing of electrical insulation in high voltage components.

Chapter 6

Conclusions and suggestions

6.1 Conclusions

The aim of this study was to improve the existing tools for the recognition of partial discharges. The main tasks were:

1. improvement of the **classification** of fingerprints.
2. introduction of **discrimination** methods.
3. testing of the classification and discrimination methods with data from laboratory samples and industrial high voltage components.
4. application of classification and discrimination methods for the periodic testing of the **ageing** of dielectrics.

Classification of discharge patterns

Many methods were studied: neural networks and conventional classifiers.

1. Neural networks did not prove to be a valuable tool for discharge recognition. The results were too much dependent on the type of neural network, the structure of the neural network, the number of learning cycles, *etc.*

   Furthermore, a fingerprint that deviates completely from learning fingerprints can erroneously be recognized as one of the known fingerprints. Such an erroneous classification is unacceptable in industrial applications.

2. Conventional classifiers are more successful in discharge recognition. Especially **the centour score method** has shown a good potential against misclassifications. This is of importance because of its consequences in industrial applications.

Discrimination of discharge patterns

Also in this case many methods were examined. The following can be concluded.

1. To discriminate between fingerprints where no *a priori* knowledge is available, agglomerative clustering methods which provide a tree structure of data are attractive. To build such a tree structure, **the group average method** is favoured.

2. Fractal dimension and lacunarity have also shown a good potential for the discrimination of discharge patterns and can be used as an alternative to other discrimination techniques.

Ageing stages of insulation

The effect of ageing on discharge patterns was studied.

1. Discharge patterns as observed during long-term ageing of standard defects and industrial high voltage components changed several times during the ageing period.

2. Most of the changes in discharge patterns occurred at the beginning of the accelerated long-term tests, in the first minutes or hours. After that relatively stable patterns with a duration of several hundreds hours were observed.

3. The changes in discharge patterns during ageing have implications for discharge recognition because patterns which occur at the beginning of a test differ from those at the end of the test. A separate category in a data base should be created for each ageing stage.

4. The tree structures of the group average method, proved to give a good discrimination between different ageing stages during long-term tests.

5. Using the centour score method a successful recognition of fingerprints according to ageing stages took place. There were no misclassifications.

6. Tests on actual high voltage components indicate that the selected recognition tools (the group average method, the centour score method) have a good potential for industrial application, such as the periodic testing of electrical insulation in high voltage components.

6.2 Suggestions

Results obtained in this study raise several issues which it might be worthwhile to explore in future.

1. The present work was concentrated on the recognition of *single* discharge sources. It would be useful to explore the possibilities of the recognition of *multiple* discharge sources.

2. Further improvement of the discharge recognition techniques could be studied. The improvement might be achieved by using fewer but more efficient operators.

3. The ageing tests performed in this work were based on a few samples only. Tests with a larger number of samples should be made. Industrial experience with actual high voltage components is especially required.

Bibliography

[1] Al-Arainy, A.A., Malik, N.H., Al-Bahloul, M.K., "Statistical Variation of AC Corona Pulse Amplitudes in Point-to-plane Air Gaps", IEEE Trans. on Electrical Insulation, Vol.24, pp. 681-687, 1989.

[2] Anderson, T.W., **An Introduction to Multivariate Statistical Analysis**, Wiley, 1958.

[3] Aurud, T., Lundgaard, L.E., Telstad, T., Skyberg, B., "Electric and Acoustic Measurements of Moving Particles in GIS", Nordic Insulation Symposium, Vaasa, Finland, pp. 267-276, 1994.

[4] Babula, E., Sierota, A., Zoledziowski, S., Calderwood, J.H., "Surface Partial Discharges in Moist Dielectric Liquids", IEEE Trans. on Electrical Insulation, Vol.20, pp. 299-302, 1985.

[5] Bartnikas, R., "Some Observations on the Character of Corona Discharges in Short Gap Spaces", IEEE Trans. on Electrical Insulation, Vol.6, pp. 63-75, 1971.

[6] Bartnikas, R., "Corona Pulse Probability Density Function Measurements on Primary Distribution Power Cabels", IEEE Trans. on Power Apparatus and Systems, Vol.94, pp. 716-723, 1975.

[7] Bartnikas, R., McMahon, E.J., *eds.*, **Engineering Dieletrics, Vol.I, Corona Measurement and Interpretation**, ASTM, 1979.

[8] Bezdek, J.C., **Pattern Recognition with Fuzzy Objective Function Algorithms**, Plenum Press, 1981.

[9] Bishop, C.M., "Neural Networks and Their Applications", Review of Scientific Instruments, Vol.65, pp. 1803-1832, 1994.

[10] Bishop, C.M., "Novelty Detection and Neural Network Validation", IEE Proceedings on Vision and Image Signal Processing, Vol.141, pp. 217-222, 1994.

[11] Carpenter, G.A., Grossberg, S., Markuzon, N., Reynolds, J.H., Rosen, D.B., "Fuzzy ARTMAP: A Neural Network Architecture for Incremental Supervised Learning of Analog Multidimensional Maps", IEEE Trans. on Neural Networks, Vol.3, pp. 698-713, 1992.

[12] Chadband, W.G., "Electrical Breakdown - from Liquid to Amorphous Solid", Journal of Physics D: Applied Physics, Vol.24, pp. 56-64, 1991.

[13] Champion, J.V., Dodd, S.J., Stevens, G.C., "Long-term Light Emission Measurement and Imaging during the Early Stages of Electrical Breakdown in Epoxy Resin", Journal of Physics D: Applied Physics, Vol.27, pp. 604-610, 1994.

[14] Chang, D.D., Sudarshan, T.S., Thompson, J.E., "Analysis of Electric Stress Distribution in Cavities Embedded Within Dielectric Structures", IEEE Trans. on Electrical Insulation, Vol.21, pp. 213-219, 1986.

[15] Contin, A., Rabach, G., "Partial Discharge Analysis of Rotating AC Machines", IEEE Trans. on Electrical Insulation, Vol.28, pp. 1033-1042, 1993.

[16] Černák, M., Hosokawa, T., Odrobina, I., "Experimental Confirmation of Positive-streamer-like Mechanism for Negative Corona Current Pulse Rise", Journal of Physics D: Applied Physics, Vol.26, pp. 607-618, 1993.

[17] Devins, J.C., "The Physics of Partial Discharges in Solid Dieletrics", IEEE Trans. on Electrical Insulation, Vol.19, pp. 475-494, 1984.

[18] "Diagnostic Methods for GIS Insulating Systems", CIGRE, Paris, France, Paper 15/23-01, 1992.

[19] Dissado, L.A., Fothergill, J.C., **Electrical Degradation and Breakdown in Polymers**, Peregrinus, 1992.

[20] Duda, R., Hart, P.E., **Pattern Classification and Scene Analysis**, Wiley, 1973.

[21] Edelbrock, C., "Mixture Model Tests of Hierarchical Clustering Algorithms: The Problem of Classifying Everybody", Multivariate Behavioural Research, Vol.14, pp. 367-384, 1979.

[22] "Effects of Particles on GIS Insulation and the Evaluation of Relevant Diagnostic Tools", CIGRE, Paris, France, Paper 15-103, 1994.

[23] Fisher, R.A., "The Use of Multiple Measurements in Taxonomic Problems", Annals of Eugenics, Vol.3, pp. 179-188, 1936.

[24] Forster, E.O., "Partial Discharges and Streamers in Liquid Dieletrics", IEEE Trans. on Electrical Insulation, Vol.28, pp. 941-946, 1993.

[25] Fothergill, J.C., Dissado, L.A., Sweeney, P.J.J., "A Discharge-avalanche Theory for the Propagation of Electrical Trees", IEEE Trans. on Dielectrics and Electrical Insulation, Vol.1, pp. 474-486, 1994.

[26] Fruth, B., Fuhr, J., "Partial Discharge Pattern Recognition - A Tool for Diagnosis and Monitoring of Ageing", CIGRE, Paris, France, Paper 15/33-12, 1990.

[27] Fruth, B., Niemeyer, L., "The Importance of Statistical Characteristics of Partial Discharge Data", IEEE Trans. on Electrical Insulation, Vol.27, pp. 60-69, 1992.

[28] Fruth, B., Gross, D.W., "Combination of Frequency Spectrum Analysis and Partial Discharge Pattern Recording", IEEE International Symposium on Electrical Insulation, Pittsburgh, USA, pp. 296-300, 1994.

[29] Fukunaga, K., **Introduction to Statistical Pattern Recognition**, Academic Press, 1990.

[30] Gamez-Garcia, M., Bartnikas, R., Wertheimer, M.R., "Synthesis Reactions Involving XLPE Subjected to Partial Discharges", IEEE Trans. on Electrical Insulation, Vol.22, pp. 199-205, 1987.

[31] Gamez-Garcia, M., Bartnikas, R., Wertheimer, M.R., "Modification of XLPE Exposed to Partial Discharges at Elevated Temperature", IEEE Trans. on Electrical Insulation, Vol.25, pp. 688-692, 1990.

[32] Gassaway, J.D., Jacob, P.B., Vassiliadis, C.A., Reynolds, P.H., "Computer-aided Partial Discharge Measurement and Recognition", 5th International Symposium on High Voltage Engineering, Braunschweig, Germany, Paper 41.03, 1987.

[33] Gjærde, A.C., "Measurements of Void Gas Pressure During Combined Thermal and Partial Discharge Ageing of Epoxy", IEE Proc. on Science, Measurements and Technology, Vol.142, No.1, 17-21, 1995.

[34] Goldman, M., Goldman, A., Gatellet, J., "Physical and Chemical Aspects of Partial Discharges and Their Effects on Materials", IEE Proc. on Science, Measurements and Technology, Vol.142, No.1, 11-16, 1995.

[35] Gulski, E., **Computer-aided Recognition of Partial Discharges Using Statistical Tools**, Delft University Press, 1991.

[36] Gulski, E., "Computer-aided Measurement of Partial Discharges in HV Equipment", IEEE Trans. on Electrical Insulation, Vol.28, pp. 969-983, 1993.

[37] Gulski, E., Krivda, A., "Neural Networks as a Tool for Recognition of Partial Discharges", IEEE Trans. on Electrical Insulation, Vol.28, pp. 984-1001, 1993. *Errata* in IEEE Trans. on Dielectrics and Electrical Insulation, Vol.1, p. 351, 1994.

[38] Gulski, E., Seitz, P., "Computer-aided Registration and Analysis of Partial Discharges in High Voltage Equipments", 8th International Symposium on High Voltage Engineering, Yokohama, Japan, Paper 60.04, 1993.

[39] Gustafson, D.E., Kessel, W., "Fuzzy Clustering with a Fuzzy Covariance Matrix", Proceedings of the 1978 IEEE Conference on Decision and Control, San Diego, USA, pp. 761-766, 1979.

[40] Hall, H.C., Russek, R.M., "Discharge Inception and Extinction in Dielectric Voids", Proc. IEE, Part II, Vol.101, pp. 47-55, 1954.

[41] Hartigan, J.A., "Statistical Theory in Clustering", Journal of Classification, Vol.2, pp. 63-76, 1985.

[42] Hecht-Nielsen, R., **Neurocomputing**, Addison-Wesley, 1991.

[43] Hikita, M., Komori, F., Nishiguchi, N., Mizutani, T., "Phase-resolved and Time-sequential Partial Discharge Pulse Measurements in a Metal-void-insulator System Using a Personal Computer", Journal of Physics D: Applied Physics, Vol.27, pp. 1220-1228, 1994.

[44] Holbøll, J.T., Braun, J.M., Fujimoto, N., Stone, G.S., "Partial Discharges in Flat, Dielectric/Metallic Bounded Cavities", International Conference on Partial Discharges, Canterbury, England, IEE Publication 378, pp. 39-40, 1993.

[45] Hozumi, N., Okamoto, T., Imajo, T., "Discrimination of Partial Discharge Patterns Using a Neural Network", IEEE Trans. on Electrical Insulation, Vol.27, pp. 550-556, 1992.

[46] Hudon, C., Bartnikas, R., Wertheimer, M.R., "Spark-to-glow Discharge Transition due to Increased Surface Conductivity on Epoxy Resin Specimens", IEEE Trans. on Electrical Insulation, Vol.28, pp. 1-8, 1993.

[47] Jacobs, R.A., Jordan, M.I., Nowlan, S.J., Hinton, G.E., "Adaptive Mixtures of Local Experts", Neural Computation, Vol.3, pp. 79-87, 1991.

[48] Jain, A.K., Dubes, R.C., **Algorithms for Clustering Data**, Prentice Hall, 1988.

[49] Jambu, M., **Exploratory and Multivariate Data Analysis**, Academic Press, 1991.

[50] Jordan, M.I., Jacobs, R.A., "Hierarchies of Adaptive Experts", Advances in Neural Information Processing Systems, Vol.4, pp. 985-992, 1992.

[51] Kaufman, L., Rousseeuw, P.J., **Finding Groups in Data: An Introduction to Cluster Analysis**, Wiley, 1990.

[52] Keller, J.M., Chen, S., Crowover, R.M., "Texture Description and Segmentation through Fractal Geometry", Computer Vision, Graphics, and Image Processing, Vol. 45, pp. 150-166, 1989.

[53] Kohonen, T., "The Self-Organizing Map", Proc. of the IEEE, Vol. 78, pp. 1464-1480, 1990.

[54] Kramer, M.A., Leonard, J.A., "Diagnosis Using Back-propagation Neural Networks - Analysis and Criticism", Computers and Chemical Engineering, Vol.14, pp. 1323-1338, 1990.

[55] Kranz, H.G., "Partial Discharge Evaluation of Polyethylene Cable-material by Phase Angle and Pulse Shape Analysis", IEEE Trans. on Electrical Insulation, Vol.17, pp. 151-155, 1982.

[56] Kranz, H.G., Krump, R., "Partial Discharge Diagnosis Using Statistical Optimization on a PC-based System", IEEE Trans. on Electrical Insulation, Vol.27, pp. 93-98, 1992.

[57] Kreuger, F.H., **Discharge Detection in High Voltage Equipment**, Temple Press, American Elsevier, 1964; Butterworths, 1989.

[58] Kreuger, F.H., Gulski, E., Sonneveld, W.A., "Diagnosis in GIS by Statistical Analysis of Discharges", CIGRE, Paris, France, Paper 15/23-04, 1992.

[59] Kreuger, F.H., Gulski, E., Krivda, A., "Classification of Partial Discharges", IEEE Trans. on Electrical Insulation, Vol.28, pp. 917-931, 1993.

[60] Kreuger, F.H., Morshuis, P.H.F., Gulski, E., "Evaluation of Discharge Damage by Fast Transient Detection and Statistical Analysis", CIGRE, Paris, France, Paper 15-106, 1994.

[61] Krivda, A., Gulski, E., "Neural Networks as a Tool for Recognition of Partial Discharges", International Conference on Partial Discharge, Canterbury, England, IEE Publication 378, pp. 84-85, 1993.

[62] Krivda, A., Gulski, E., "Influence of Aging on Classification of Partial Discharges in Cavities", Japanese Journal of Applied Physics, Part I, Vol. 33, pp. 5942-5949, 1994.

[63] Krzanowski, W., **Principles of Multivariate Analysis, A User's Perspective**, Clarendon Press, 1988.

[64] Krump, R., **Ein Störsignalresistentes Verfahren Zur Computergestützten Teilentladungs Diagnostik in SF6-isolierten Schaltanlagen**, Bergische Universität Wuppertal, 1989.

[65] Kruskal, J.B., "Multidimensional Scaling by Optimizing Goodness of Fit to a Nonmetric Hypothesis", Psychometrika, Vol.29, pp. 1-27, 1964.

[66] Kruskal, J.B., "Nonmetric Multidimensional Scaling: A Numerical Method", Psychometrika, Vol.29, pp. 115-129, 1964.

[67] Kuiper, F.K., Fisher, L., "A Monte Carlo Comparision of Six Clustering Procedures", Biometrics, Vol.31, pp. 777-783, 1975.

[68] Lama, W.L., Gallo, C.F., "Systematic Study of the Electrical Characteristics of the Trichel Current Pulses from Negative Needle-to-plane Coronas", Journal of Applied Physics, Vol.45, pp. 103-113, 1974.

[69] Lance, G.N., Williams, W.T., "A General Theory of Classificatory Sorting Strategies, 1. Hierarchical Systems", Computer Journal, Vol.9, pp. 373-380, 1966.

[70] Leonard, J.A., Kramer, M.A., "Radial Basis Function Networks for Classifying Process Faults", IEEE Control Systems Magazine, Vol.11, No.3, pp. 31-38, 1991.

[71] Lewis, T.J., "Basic Electrical Processes in Dielectric Liquids", IEEE Trans. on Dielectrics and Electrical Insulation, Vol.1, pp. 630-643, 1994.

[72] Lindeman, R.H., Merenda, P.F., Gold, R.Z., **Introduction to Bivariate and Multivariate Analysis**, Scott, Foresman and Company, 1980.

[73] Lippmann, R.P., "An Introduction to Computing with Neural Nets", IEEE Acoustics, Speech and Signal Processing Magazine, Vol.4, No.2, pp. 4-22, 1987.

[74] Lundgaard, L.E., Tangen, G., Skyberg, B., Faugstad, K., "Acoustic Diagnosis of GIS; Field Experience and Development of Expert System", IEEE Trans. on Power Delivery, Vol.7, pp. 287-294, 1992.

[75] MacQueen, J., "Some Methods for Classification and Analysis of Multivariate Observations", in **Proceedings of the 5th Berkeley Symposium on Mathematical Statistics and Probability**, *eds.* Le Cam, L.M., Neyman, J., Vol.1, pp. 281-297, University of California Press, 1967.

[76] Mandelbrot, B.B., **The Fractal Geometry of Nature**, Freeman, 1983.

[77] Mardia, K.V., Kent, J.T., Bibby, J.M., **Multivariate Data Analysis**, Academic Press, 1980.

[78] Mason, J.H., "The Deterioration and Breakdown of Dieletrics Resulting from Internal Discharges", Proc. IEE, Vol.98, pp. 44-59, 1951.

[79] Mayoux, C., "Partial-discharge Phenomena and the Effect of Their Constituents on Polyethylene", IEEE Trans. on Electrical Insulation, Vol.11, pp. 139-149, 1976.

[80] McMahon, E.J., Perkins, J.R., "Surface and Volume Phenomena in Dielectric Breakdown of Polyethylene", IEEE Trans. on Power Apparatus and Systems, Vol.82, pp. 1128-1136, 1963.

[81] McMahon, E.J., "The Chemistry of Corona Degradation of Organic Insulating Materials in High Voltage Fields and Under Mechanical Strain", IEEE Trans. on Electrical Insulation, Vol.3, pp. 3-10, 1968.

[82] Meats, R.J., Stannett, A.W., "Degradation of Insulation Materials by Electrical Discharges", IEEE Trans. on Power Apparatus and Systems, Vol.83, pp. 49-54, 1964.

[83] Merrill, F.H., Von Hippel, A., "The Atomphysical Interpretation of Lichtenberg Figures and Their Application to the Study of Gas Discharge Phenomena", Journal of Applied Physics, Vol.10, pp. 873-887, 1939.

[84] Milligan, G.W., "An Examination of the Effect of Six Types of Error Perturbation on Fifteen Clustering Algorithms", Psychometrika, Vol.45, pp. 325-342, 1980.

[85] Milligan, G.W., Soon, S.C., Sokol, L.M., "The Effect of Cluster Size, Dimensionality and the Number of Clusters on Recovery of True Cluster Structure", IEEE Trans. on Pattern Analysis and Machine Intelligence, Vol.5, pp. 40-47, 1983.

[86] Milligan, G.W., Cooper, M.C., "An Examination of Procedures for Determining the Number of Clusters in a Data Set", Psychometrika, Vol.50, pp. 159-179, 1985.

[87] Moody, J., Darken, C.J., "Fast Learning in Networks of Locally-tuned Processing Units", Neural Computation, Vol.1, pp. 281-294, 1989.

[88] Morshuis, P.H.F., Kreuger, F.H., "Transition from Streamer to Townsend Mechanisms in Dielectric Voids", Journal of Physics D: Applied Physics, Vol.23, pp. 1562-1568, 1990.

[89] Morshuis, P.H.F., **Partial Discharge Mechanisms**, Delft University Press, 1993.

[90] "NeuralWorks Professional II/PLUS", NeuralWare, Inc., Pittsburgh, USA, 1993.

[91] Okamoto, T., Tanaka, T., "Novel Partial Discharge Measurement Computer-aided Measurement Systems", IEEE Trans. on Electrical Insulation, Vol.21, pp. 1015-1019, 1986.

[92] **Partial Discharge Measurements**, IEC Standard, Publication 270, 1981.

[93] "Partial Discharge Testing of Gas Insulated Substations", IEEE Trans. on Power Delivery, Vol.7, pp. 499-506, 1992.

[94] Petersen, W., "Beiträge zur Berechnung der Hochspannungsisolierung", Archif für Elektrotechnik, Vol.1, No.1, pp. 28-33, 1912.

[95] Raudys, S.J., Jain, A.K., "Small Sample Size Problems in Designing Artificial Neural Networks", in **Artificial Neural Networks and Statistical Pattern Recognition, Old and New Connections**, *ed.* Sethi, I.K., Jain, A.K., pp. 33-50, Elsevier Science Publishers, 1991.

[96] Raudys, S.J., Jain, A.K., "Small Sample Size Effects in Statistical Pattern Recognition: Recommendations for Practitioners", IEEE Trans. on Pattern Analysis and Machine Intelligence, Vol.13, pp. 252-264, 1991.

[97] "Recognition of Discharges", CIGRE, Electra, No.11, pp. 61-98, 1969.

[98] Reilly, D.L., Cooper, L.N., Elbaum, C., "A Neural Model for Category Learning", Biological Cybernetics, Vol.45, pp. 35-41, 1982.

[99] Reynolds, S.I., "On the Behaviour of Natural and Artificial Voids in Insulation Under Internal Discharge", AIEE Trans., Part III, Vol.77, pp. 1604-1608, 1959.

[100] Robinson, D.M., **Dielectric Phenomena in High Voltage Cables**, Chapman and Hall, 1936.

[101] Rogers, E.C., "The Self-extinction of Gaseous Discharges in Cavities in Dielectrics", Proc. IEE, Part A, Vol.105, pp. 621-630, 1958.

[102] Sammon, J.W., "A Nonlinear Mapping for Data Structure Analysis", IEEE Trans. on Computers, Vol.18, pp. 401-409, 1969.

[103] Satish, L., Gururaj, B.I., "Use of Hidden Markov Models for Partial Discharge Pattern Classification", IEEE Trans. on Electrical Insulation, Vol.28, pp. 172-182, 1993.

[104] Satish, L., Zaengl, W.S., "Can Fractal Features be used for Recognizing 3-d Partial Discharge Patterns", accepted for publication in IEEE Trans. on Dielectrics and Electrical Insulation.

[105] Schifani, R., "A Novel Histogram for Partial Discharge Signals in HV Insulating Systems", IEEE Trans. on Electrical Insulation, Vol.21, pp. 89-99, 1986.

[106] Schnettler, A., Tryba, V., "Artificial Self-Organizing Neural Network for Partial Discharge Recognition", Archiv für Elektrotechnik, Vol. 76, pp. 1-6, 1993.

[107] Siedlecki, W., Siedlecka, K., Sklansky, J., "An Overview of Mapping Techniques for Exploratory Pattern Analysis", Pattern Recognition, Vol.21, pp. 411-429, 1988.

[108] Siedlecki, W., Siedlecka, K., Sklansky, J., "Experiments on Mapping Techniques for Exploratory Pattern Analysis", Pattern Recognition, Vol.21, pp. 431-438, 1988.

[109] Sierota, A., Calderwood, J.H., "Degradation and Breakdown of Solid Dieletric Materials Resulting from Surface Discharges in Air and in Insulating Liquids", IEEE Trans. on Electrical Insulation, Vol.23, pp. 993-998, 1988.

[110] Sneath, P.H.A., Sokal, R.R., **Numerical Taxonomy: The principles and Practice of Numerical Classification**, Freeman and Company, 1973.

[111] Specht, D.F., "Probabilistic Neural Networks", Neural Networks, Vol.3, pp. 109-118, 1990.

[112] Suzuki, H., Endoh, T., "Pattern Recognition of Partial Discharge in XLPE Cables Using a Neural Network", IEEE Trans. on Electrical Insulation, Vol.27, pp. 543-549, 1992.

[113] Tanaka, T., Ikeda, Y., "Internal Discharges in Polyethylene with an Artificial Cavity", IEEE Trans. on Power Apparatus and Systems, Vol.90, pp. 2692-2702, 1971.

[114] Tanaka, T., "Internal Partial Discharge and Material Degradation", IEEE Trans. on Electrical Insulation, Vol.21, pp. 899-905, 1986.

[115] Tanaka, T., "Charge Transfer and Tree Initiation in Polyethylene Subjected to AC Voltage Stress", IEEE Trans. on Electrical Insulation, Vol.27, pp. 424-431, 1992.

[116] Thanh, L.C., "Negative Corona in a Multiple Interacting Point-to-plane Gap in Air", IEEE Trans. on Industry Applications, Vol.21, pp. 518-522, 1985.

[117] Trauwaert, E., "L_1 in Fuzzy Clustering", in **Statistical Data Analysis Based on the L_1 Norm and Related Methods**, *ed.* Dodge, Y., pp. 417-426, Elsevier Science Publishers, 1987.

[118] Trichel, G.W., "The Mechanism of the Negative Point to Plane Corona Near Onset", Physical Review, Vol.54, pp. 1078-1084, 1938.

[119] Toriyama, Y., Okamoto, H., Kanazashi, M., "Breakdown of Insulating Materials by Surface Discharge", IEEE Trans. on Electrical Insulation, Vol.6, pp. 124-129, 1971.

[120] Van Brunt, R.J., Herron, J.T., "Fundamental Processes of SF_6 Decomposition and Oxidation in Glow and Corona Discharges", IEEE Trans. on Electrical Insulation, Vol.25, pp. 75-94, 1990.

[121] Van Brunt, R.J., "Stochastic Properties of Partial-discharge Phenomena", IEEE Trans. on Electrical Insulation, Vol.26, pp. 902-948, 1991.

[122] Van Brunt, R.J., "Physics and Chemistry of Partial Discharge and Corona. Recent Advances and Future Chalenges", IEEE Trans. on Dielectrics and Electrical Insulation, Vol.1, pp. 761-784, 1994.

[123] Ward, H.W., "Digital Techniques for Partial Discharge Measurements", IEEE Trans. on Power Deliwery, Vol.7, pp. 469-479, 1992.

[124] Watson, P.K., Chadband, W.G., Sadeghzadeh-Araghi, M., "The Role of Electrostatic and Hydrodynamic Forces in the Negative-point Breakdown of Liquid Dieletrics", IEEE Trans. on Electrical Insulation, Vol.26, pp. 543-559, 1991.

[125] Widrow, B., Lehr, M.A., "30 Years of Adaptive Neural Networks: Perceptron, Madaline and Backpropagation", Proc. of the IEEE, Vol. 78, pp. 1415-1442, 1990.

[126] Wilensky, G.D., Manukian, N., "The Projection Neural Network", International Joint Conference on Neural Networks, Baltimore, USA, Vol.2, pp. 358-367, 1992.

[127] Wolter, K.D., Tanaka, J., Johnson, J.F., "A Study of the Gaseous Degradation Products of Corona-exposed Polyethylene", IEEE Trans. on Electrical Insulation, Vol.17, pp. 248-252, 1982.

[128] Wootton, R.E., "Computer Assistance for the Performance and Interpretation of High Voltage AC Discharge Tests", 5th International Symposium on High Voltage Engineering, Braunschweig, Germany, Paper 41.12, 1987.

Appendix A

Discharge distributions of various insulation defects

In this appendix discharge distributions of standard defects and industrial HV components collected by the author during the course of this work are presented.

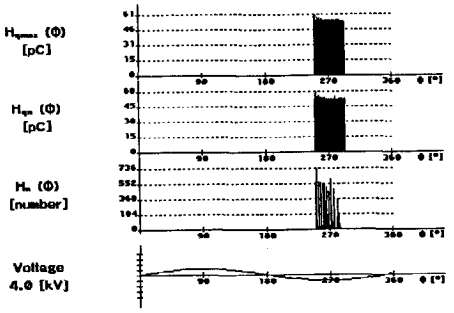

Figure 113. HV single-point corona in air.

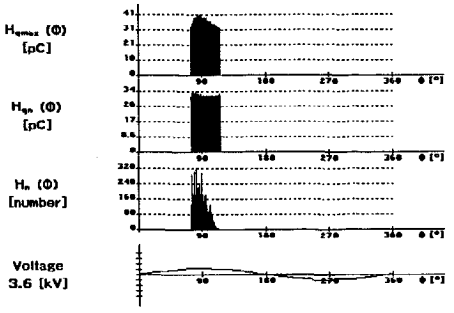

Figure 114. LV single-point corona in air.

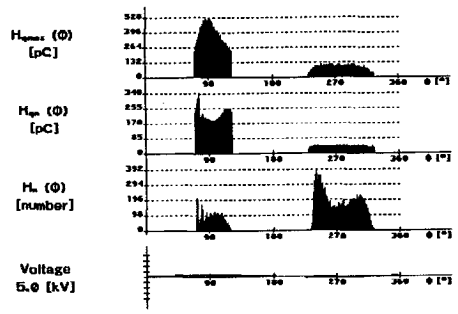

Figure 115. HV multiple-point corona in air.

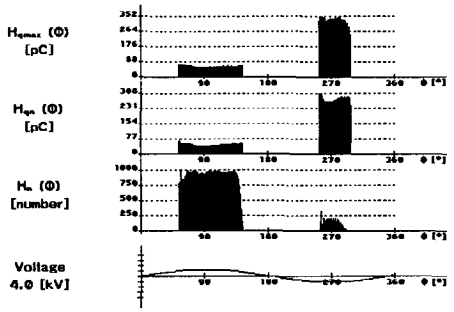

Figure 116. LV multiple-point corona in air.

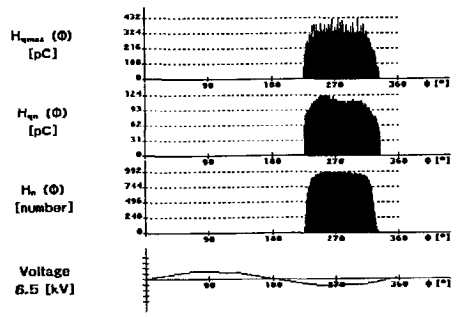

Figure 117. HV wire-to-plane corona in air.

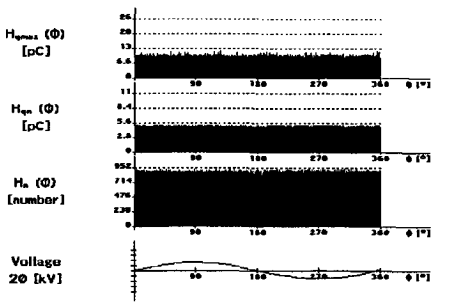

Figure 118. Background noise.

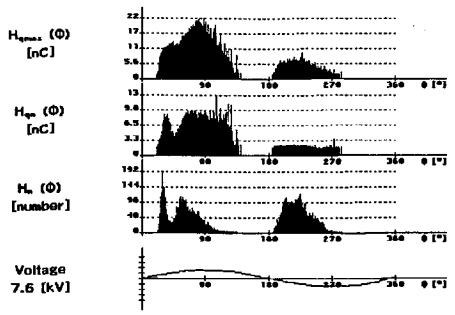

Figure 119. HV surface discharges in air.

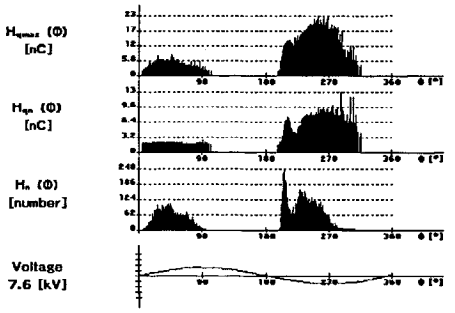

Figure 120. LV surface discharges in air.

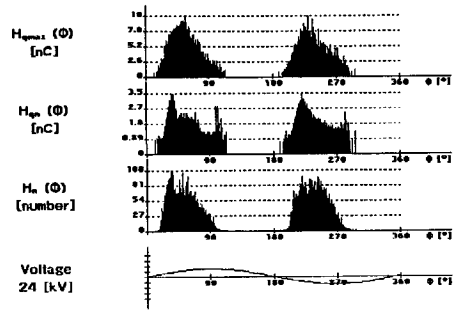

Figure 121. HV surface discharges in oil on a PE slab.

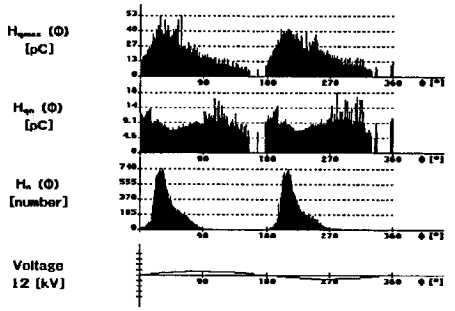

Figure 122. HV surface discharges in oil on an oil-impregnated paper.

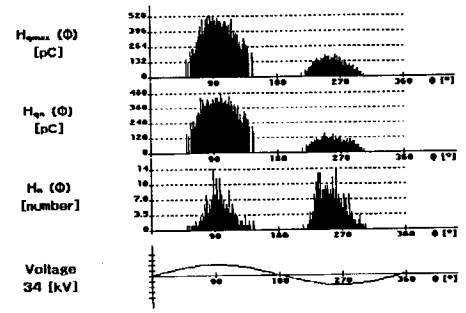

Figure 123. HV single-point corona in oil.

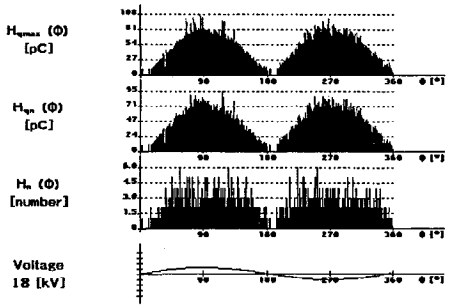

Figure 124. Air bubbles in oil.

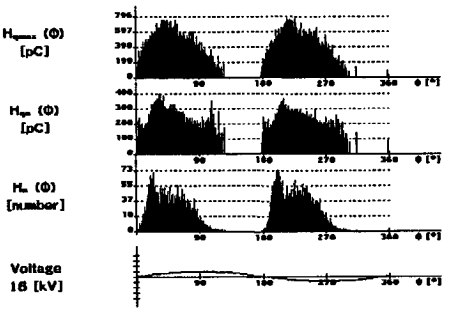

Figure 125. Dielectric bounded cavity in the virgin stage.

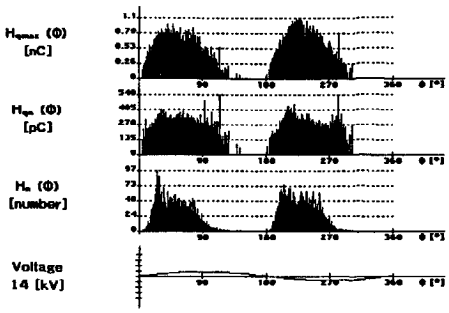

Figure 126. HV electrode bounded cavity in the virgin stage.

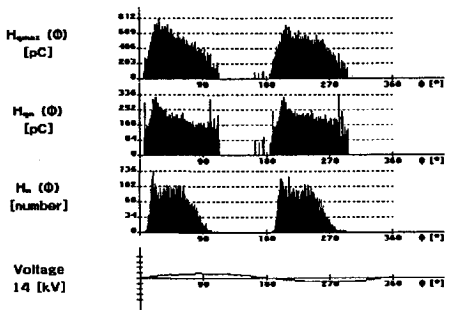

Figure 127. LV electrode bounded cavity in the virgin stage.

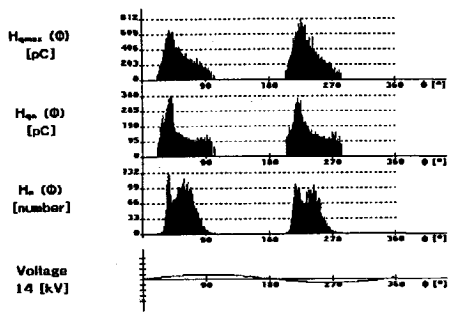

Figure 128. Dielectric bounded cavity in the conditioned stage.

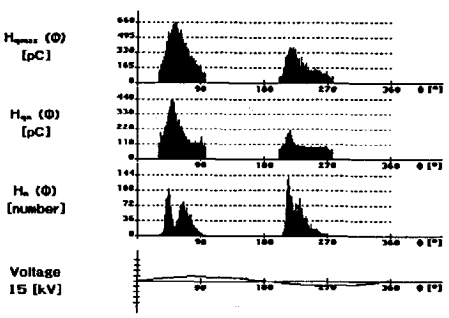

Figure 129. HV electrode bounded cavity in the conditioned stage.

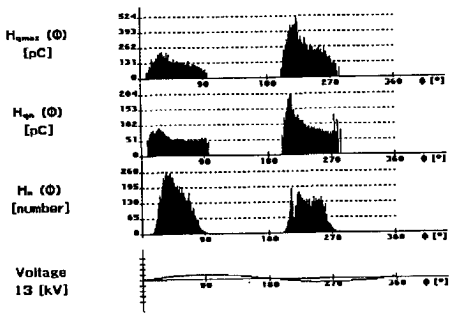

Figure 130. LV electrode bounded cavity in the conditioned stage.

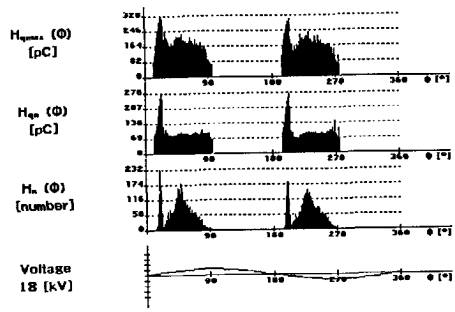

Figure 131. Dielectric bounded cavity in the aged stage.

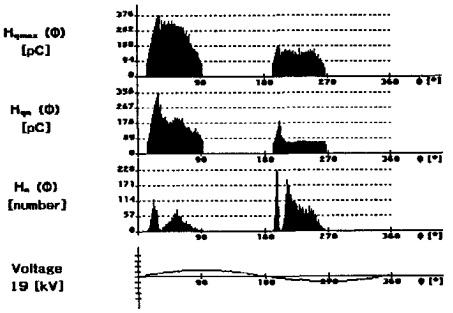

Figure 132. HV electrode bounded cavity in the aged stage.

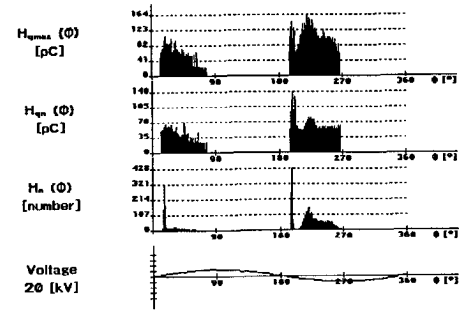

Figure 133. LV electrode bounded cavity in the aged stage.

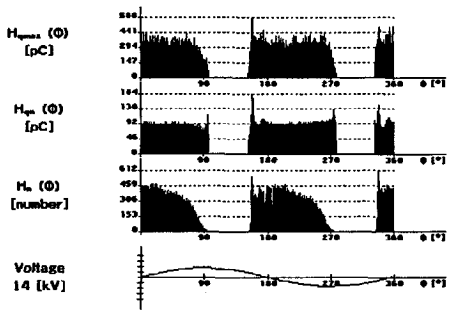

Figure 134. Dielectric bounded cavity; stage 1 - 0.2 h.

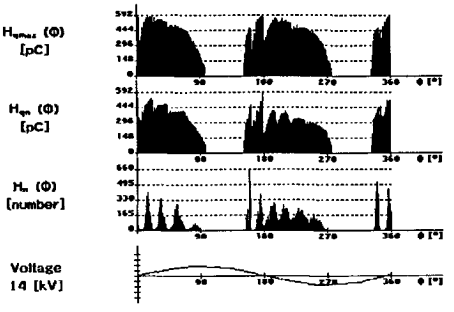

Figure 135. Dielectric bounded cavity; stage 2 - 2 h.

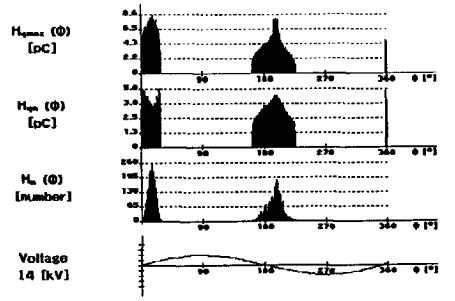

Figure 136. Dielectric bounded cavity; stage 3 - 93 h.

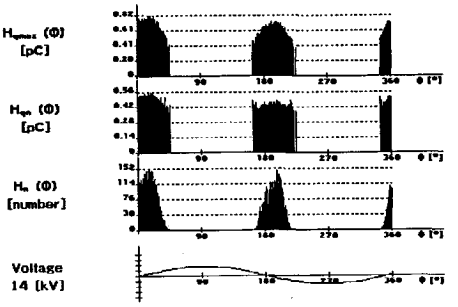

Figure 137. Dielectric bounded cavity; stage 4 - 285 h.

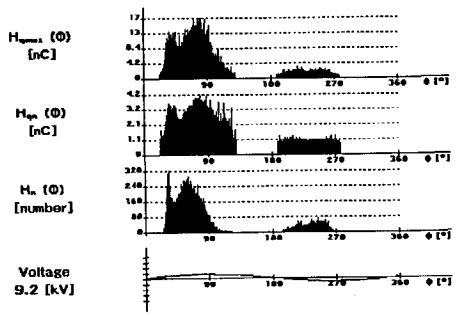

Figure 138. Surface discharges in air; stage 1 - 0.1 h.

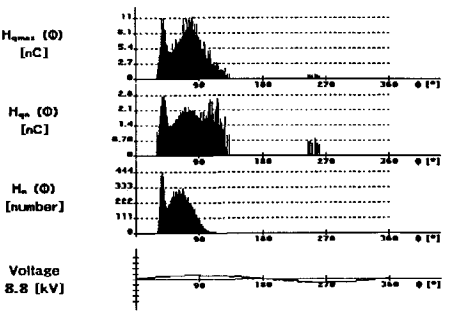

Figure 139. Surface discharges in air; stage 2 - 4 h.

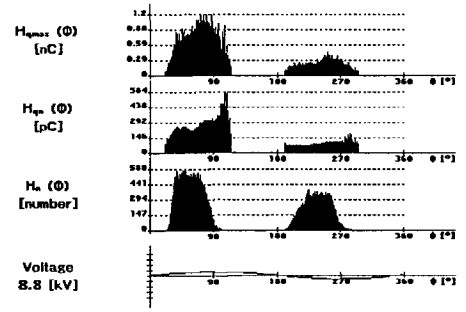

Figure 140. Surface discharges in air; stage 3 - 772 h.

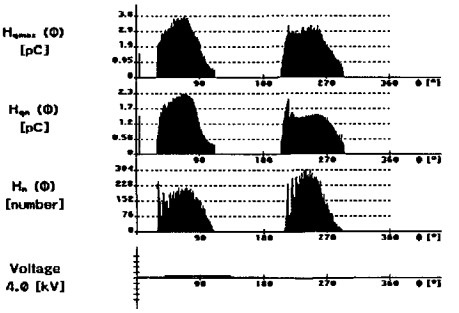

Figure 141. Surface discharges in air; stage 4 - 1230 h.

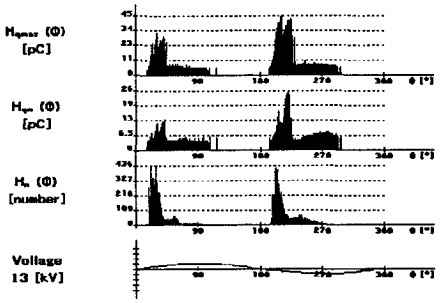

Figure 142. Surface discharges in oil; stage 1 - 0.2 h.

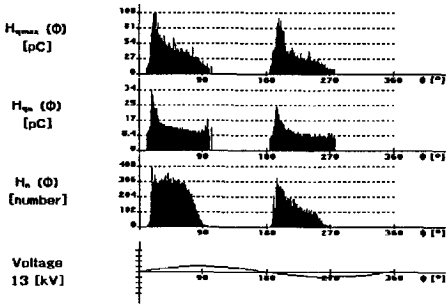

Figure 143. Surface discharges in oil; stage 2 - 4 h.

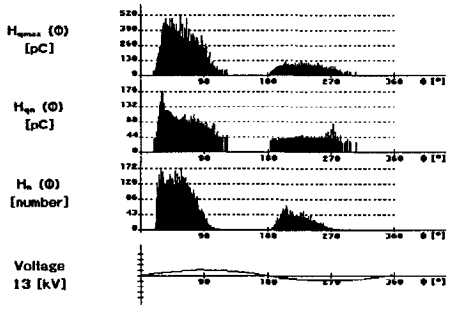

Figure 144. Surface discharges in oil; stage 3 - 25 h.

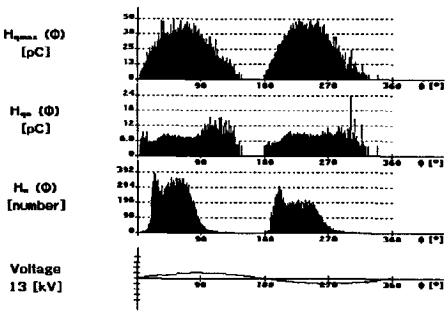

Figure 145. Surface discharges in oil; stage 4 - 170 h.

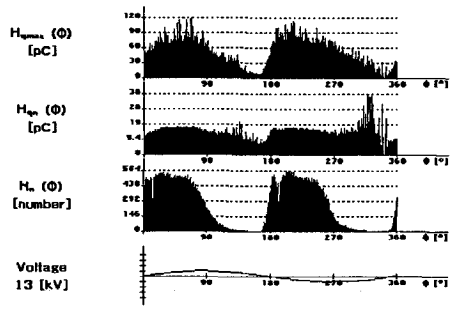

Figure 146. Surface discharges in oil; stage 5 - 340 h.

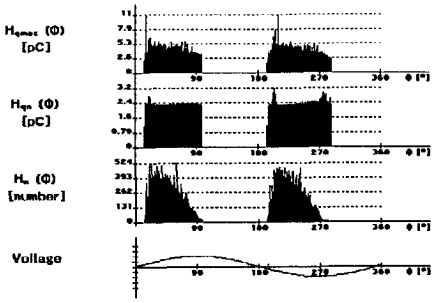

Figure 147. A 12 kV current transformer; stage 1 - 0.2 h.

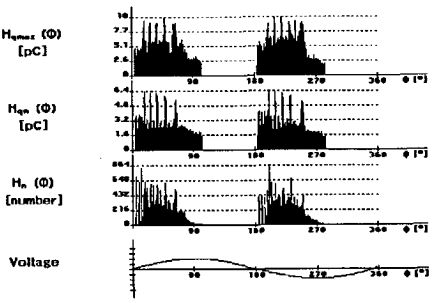

Figure 148. A 12 kV current transformer; stage 2 - 2 h.

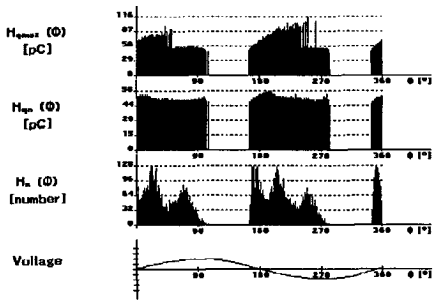

Figure 149. A 12 kV current transformer; stage 3 - 870 h.

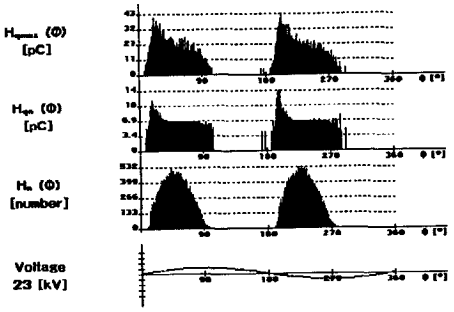

Figure 150. A 23 kV epoxy insulator; stage 1 - 0.1 h.

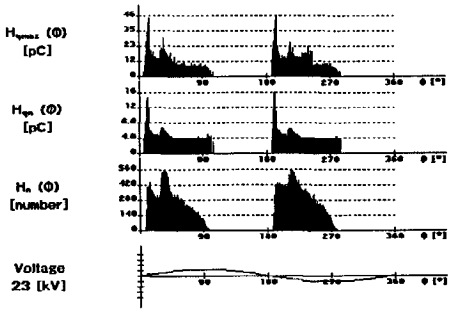

Figure 151. A 23 kV epoxy insulator; stage 2 - 93 h.

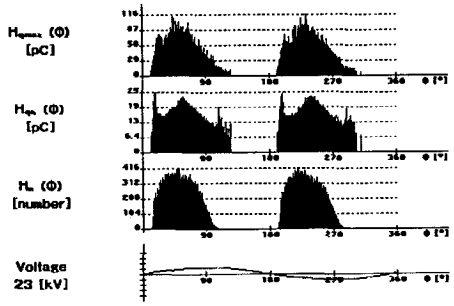

Figure 152. A 23 kV epoxy insulator; stage 3 - 794 h.

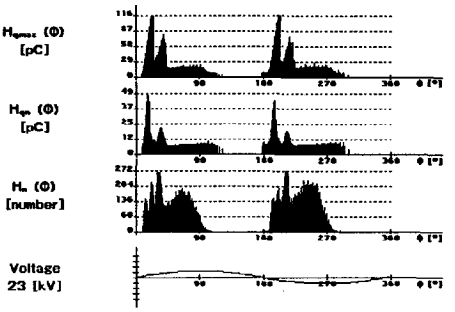

Figure 153. A 23 kV epoxy insulator; stage 4 - 1510 h.

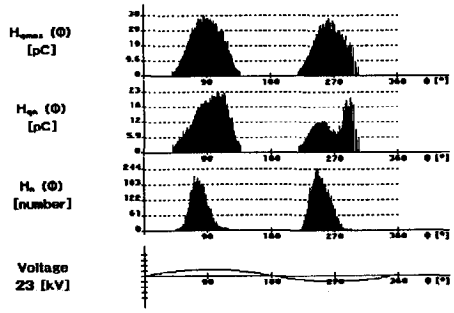

Figure 154. A 23 kV epoxy insulator; stage 5 - 1605 h.

Appendix B

Discrimination and classification of discharge patterns

The most promising methods for the discrimination and classification of discharge patterns are described in Chapter 4. Other methods which appeared to be *less successful* in these tasks are described in Appendix B.1 and B.2. Appendix B.3 gives the computational details on the calculation of centour scores.

B.1 Discrimination of discharge patterns

B.1.1 Mapping techniques

In Chapter 4 "principal component" analysis and discriminant analysis were used to reduce an original multidimensional space to two dimensions. These are linear methods, *i.e.*, they separate data in a linear fashion. To separate data in a nonlinear way, other methods have to be used, *e.g.*, multidimensional scaling, Sammon's nonlinear mapping, *etc.* [63,107,108].

Multidimensional scaling

The method is based on the principle that the distances between fingerprints in a multidimensional space must be the same in the lower dimensional space [65,66]. This means that large distances in the multidimensional space match large distances in the low dimensional space. Similarly, small distances in the multidimensional space match small distances in the low dimensional space. At the beginning of the procedure, coordinates in the low dimensional space are randomly generated. Then the coordinates are moved in steps to new positions in a manner which in the end should satisfy a linear relationship between the distances in the multidimensional and in the low dimensional space. The gradient descent method is used to adjust the coordinates of fingerprints to new positions. This is illustrated in Figure 155, where multidimensional scaling was applied to actual discharge data. At the beginning of the procedure, see Figure 155.a, the distances between the fingerprints in the low dimensional space are randomly distributed. At the end of the procedure, see Figure 155.b, the distances in the low dimensional space roughly match those in the multidimensional space.

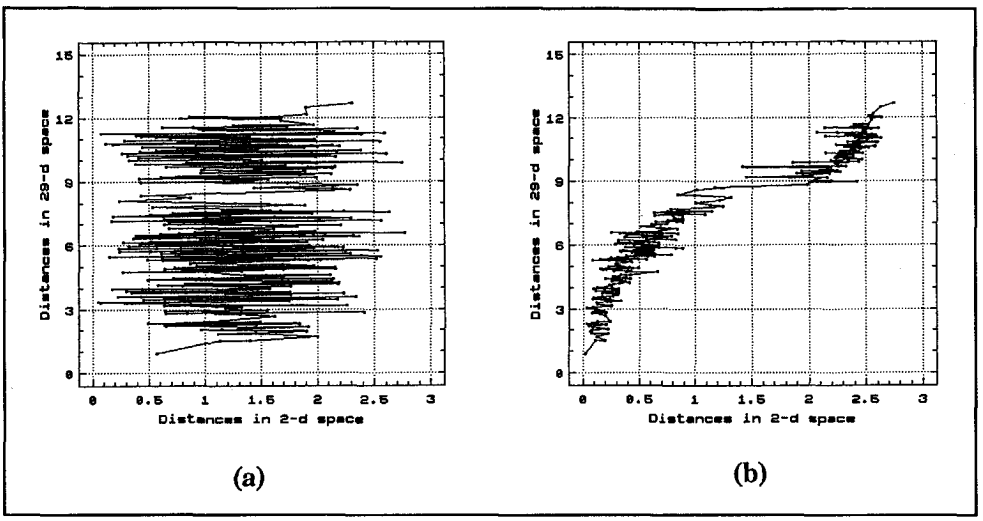

Figure 155. Distances in a multidimensional and a low dimensional space (a) at the beginning and (b) at the end of the multidimensional scaling.

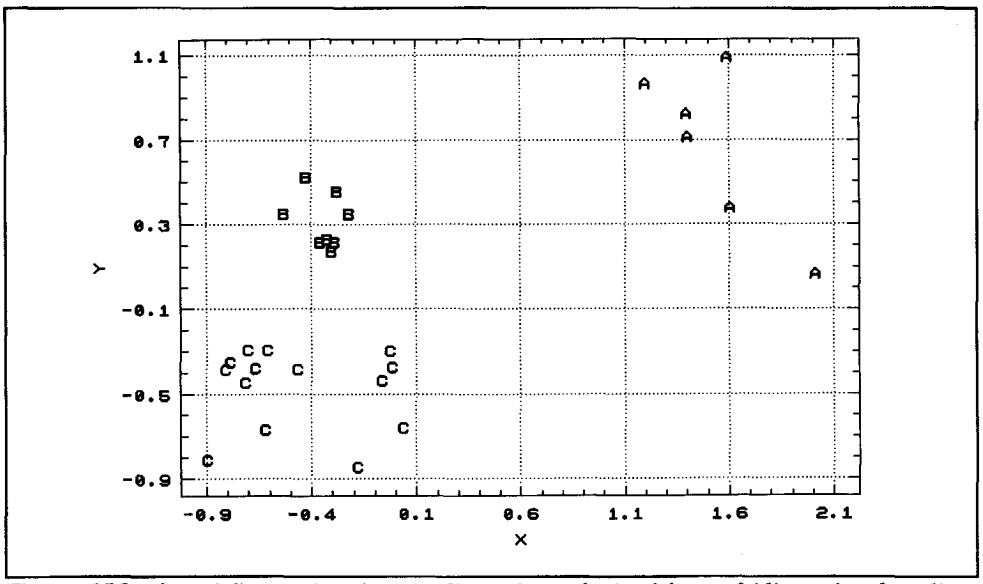

Figure 156. Plot of fingerprints in two dimensions obtained by multidimensional scaling. Original 29-dimensional space of statistical operators was reduced to two dimensions. Each letter represents one fingerprint: *A* - single point corona in air at the high voltage side, *B* - single point corona in oil at the high voltage side, *C* - surface discharges in oil propagated on a polyethylene sheet, with a rod at the high voltage potential.

In order to evaluate this match, a criterion called *stress* has been developed; calculation details can be found in [65,66]. In this example, the *stress* was 8%, which indicates a satisfactory match. If the stress is larger than 10%, the two-dimensional scatter plot of the data gives rise to doubts. The best value for the *stress* is, of course, 0%. This means that a perfect linear relationship between the distances in the multidimensional and the low dimensional space is obtained. Experience has shown that if a low *stress* value is obtained, plots of the data are usually very reliable.

The resulting scatter plot of the discharge data in a new low dimensional space is shown in Figure 156. It can be seen that all three groups are well separated from each other.

Sammon's nonlinear mapping

This method is somewhat similar to multidimensional scaling [102]. It minimizes the following function:

$$E = \frac{1}{\sum_{i<j}^{N} d_{ij}^{*}} \cdot \sum_{i<j}^{N} \frac{(d_{ij}^{*} - d_{ij})^2}{d_{ij}^{*}} \qquad (18)$$

where d^*_{ij} is the distance between ith and jth fingerprint in multidimensional space, d_{ij} is the distance between ith and jth fingerprint in low space and N is the number of fingerprints. The summation is made for all possible distances between the fingerprints. The gradient descent method is used to minimize the E function.

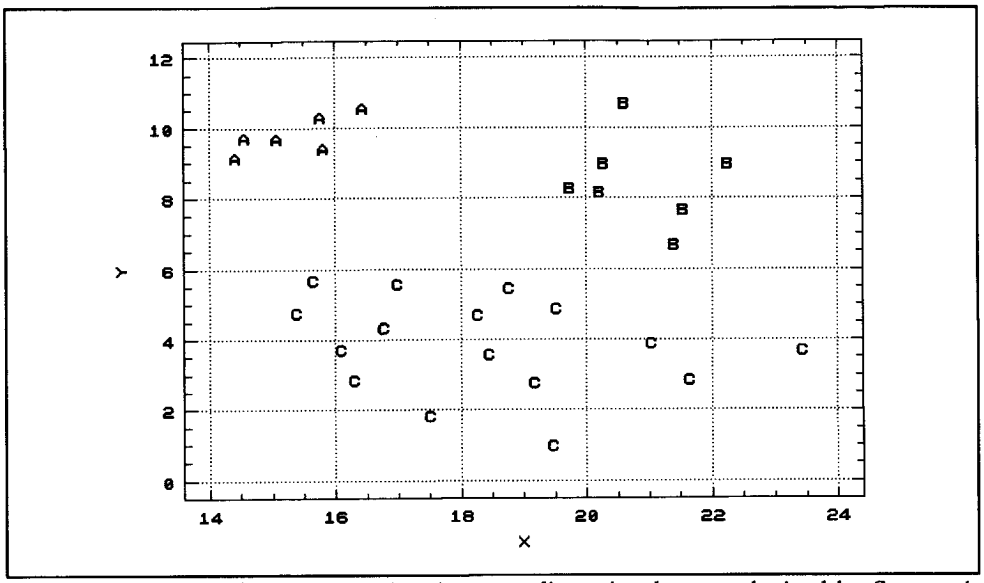

Figure 157. Scatter plot of fingerprints in a two-dimensional space obtained by Sammon's nonlinear mapping. Original 15-dimensional space of statistical operators was reduced to two dimensions. Each letter represents one fingerprint: *A* - corona discharges in SF_6, *B* - cavity discharges in a spacer, *C* - conducting particle on a spacer applied half-way between the conductor and the ground.

Sammon's mapping was applied to fingerprints of three defects in gas-insulated switchgear. Minimization was stopped when the *E* function reached the value 10^{-6}. The resulting scatter plot of the data in the new two dimensional space is shown in Figure 157. It can be seen that the fingerprints of these defects occupy different positions in space and can be clearly distinguished.

Multidimensional scaling and Sammon's nonlinear mapping are iterative techniques in nature, which is the practical limitation of these methods.

B.1.2 Cluster analysis

Except for the furthest neighbour and the average clustering methods, which have been discussed in Chapter 4, also other clustering algorithms have been applied during the course of this work. They are briefly described in this Appendix.

Agglomerative clustering

Two methods of agglomerative hierarchical clustering, the furthest neighbour and the average clustering methods, have been discussed in Chapter 4. Other possibilities are [48,63,69]:

1. *the nearest neighbour method*, which takes the smallest distance between two groups,

2. *the centroid method*, which calculates the squared Euclidean distance (obtained from Pythagoras theorem) between the centroids of two groups,

3. *the median method*, which calculates the distance between medians of two groups in its geometric representation.

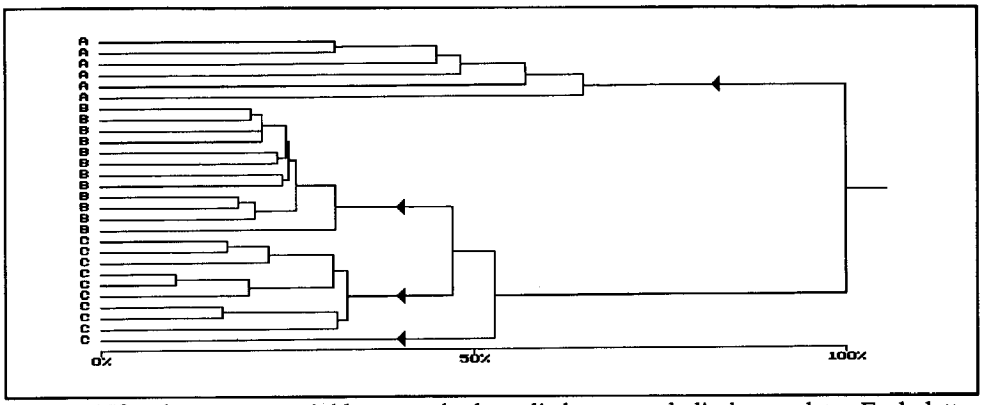

Figure 158. The nearest neighbour method applied to actual discharge data. Each letter represents one fingerprint: *A* - single point corona in air, at the high voltage side, *B* - dielectric bounded cavity, *C* - surface discharges in air with a rod at the high voltage potential.

Application of the nearest neighbour method to actual discharge data is shown in Figure 158. It can be seen that all three defects can be distinguished, although the tree structure differs from that obtained by the furthest neighbour method obtained for the same data, see Figure 40 in Chapter 4. The obtained statistics (see Chapter 4) for this tree structure were: cophenetic correlation coefficient - 0.95 and Δ coefficient - 0.24. This indicates that this tree structure matches well the original 29-dimensional space. When the statistics of the agglomerative methods are mutually compared for this example, see Table 1.a in Chapter 4, it can be seen that the best statistics were yielded by the group average method, followed by the nearest neighbour method and the furthest neighbour method. It follows that, from these three methods, the tree structure of the group average method gives the best insight to the data in this example. It is followed by the tree structure obtained by the nearest method and the furthest neighbour method.

The nature of the produced clusters varies with the method. The group average, the furthest neighbour and the centroid methods lead to spherical clusters. The nearest neighbour method often gives long elongated clusters. The furthest neighbour method results in clusters of equal diameter [63].

Nonhierarchical clustering methods

In this category, two methods have been applied to discharge data: Forgy's and MacQueen's *k*-means clustering [48,75]. These methods have the following algorithm:

1. Specify the number of desired clusters. Assign each fingerprint to a particular cluster.

2. Generate a new partition by allocating fingerprints to their nearest cluster centre.

3. Compute new cluster centres as the centroids of fingerprints.

4. Repeat steps 2 and 3 until fingerprints do not migrate from one cluster to another.

In Forgy's method, the clusters centres are recomputed after all fingerprints have been examined. In MacQueen's method, the centres are recomputed after each new allocation of a fingerprint.

The crucial parameters with these methods are the initial partition of fingerprints to clusters and the number of clusters. Different initial partitions can lead to different final clusterings, because the algorithm can converge to a local minimum [48]. It is therefore important to run the algorithm several times with different initial partitions. If all runs produce the same final clustering, then the partition can be considered to be relatively reliable.

The second parameter is the initial number of clusters. The choice of the correct number of clusters is one of the most difficult problems in cluster analysis and no unique solution exists [51]. If the structure of data is unknown, how can we supply this parameter to clustering algorithms? Various indices have been developed to indicate the number of groups in the given data [48,51,86]. The usual method is to run an algorithm several times for 2, 3, *etc.*, initial clusters and a partition with the best indices is chosen. The following indices were used in this work, calculation details are in [48,51]:

1. Hubert's gamma statistics. The maximum value indicates the correct clustering.

2. Modified Hubert's gamma statistics. In this case, significant change in the value of the index (detection of a 'knee' in a graph) indicates the correct number of clusters.

3. The silhouette coefficient. The maximum value points out the correct number of clusters.

The use of these indices is illustrated in Figure 159.

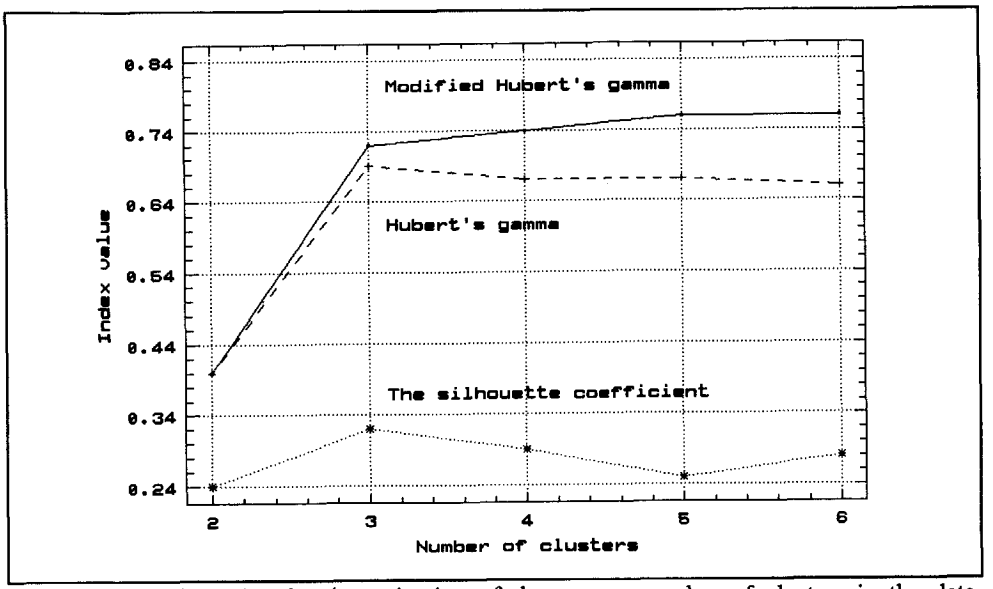

Figure 159. Indices for the determination of the correct number of clusters in the data. Results indicate that the partition to three clusters is correct.

In this example, Forgy's and MacQueen's methods were applied to fingerprints of electrode bounded cavities at the high voltage side aged for 90 minutes (details of the test procedure are given in Chapter 5). Figure 159 shows the indices for MacQueen's method. It can be seen that Hubert's gamma has a maximum for three clusters. The same is valid for the silhouette coefficient. The most significant change in the modified Hubert's statistics is also clearly visible. The partition to three clusters corresponds to the measured data, where three ageing stages have been found: virgin, conditioned and aged.

Similar results have been obtained when using Forgy's method, although partitions for 4, 5 and 6 clusters were not identical to those obtained when using MacQueen's method.

In practice, the indices may not behave in a convenient way. They may show several maxima, or the change for the modified Hubert's statistics may not always be sharp. Also the algorithms have to be run several times to avoid local minima, which is a practical limitation of these methods.

Fuzzy clustering

The methods discussed above assign a fingerprint to one and only one cluster. Fuzzy clustering can assign a fingerprint to two or more clusters. This is a generalization of partitioning. The fuzziness principle is very attractive because it can describe vagueness, uncertainty and ambiguity in the data. It is usually expressed in the form of the fuzzy membership value, which shows the degree of belonginess of a fingerprint to a cluster. It ranges from zero to 100. This can be seen in Figure 160.

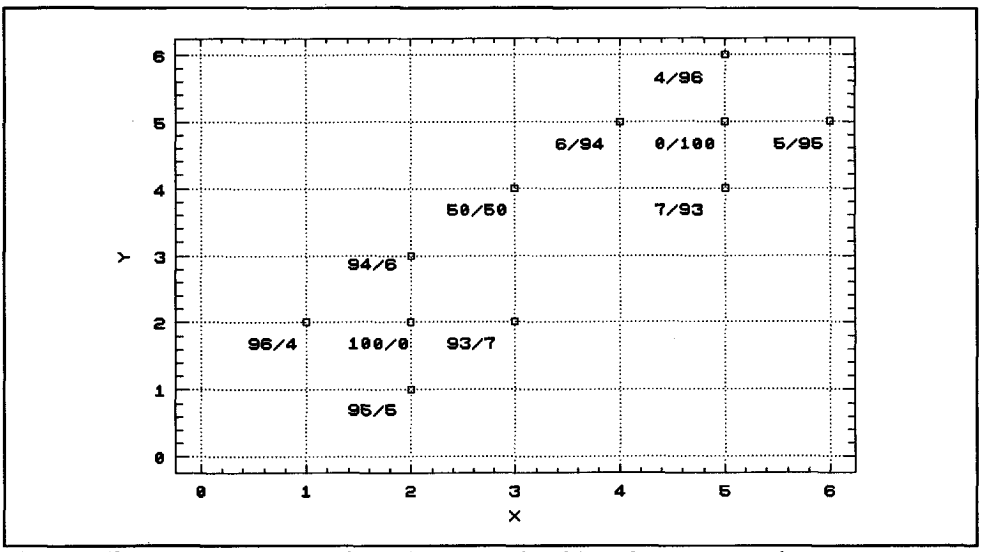

Figure 160. An artificial example of fuzzy membership values for two clusters.

In this hypothetical example, the fuzzy membership values of fingerprints of two clusters are shown. The membership values for a fingerprint between two clusters are remarkable. It belongs to both clusters with a membership of 50%.

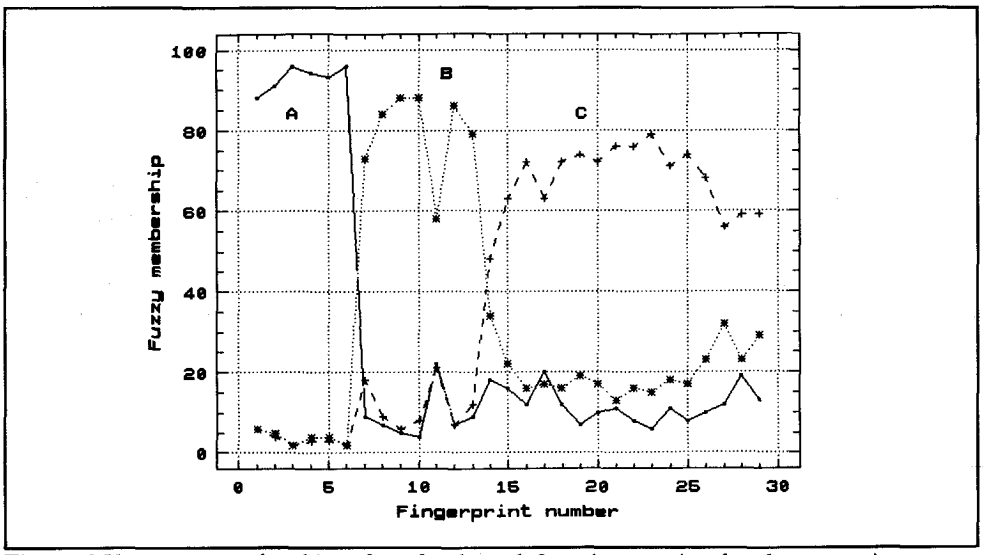

Figure 161. Fuzzy membership values for three defects in a gas-insulated system: A - corona in SF_6, B - cavity discharges in a spacer and C - conducting particle on a spacer applied half-way between the conductor and the ground.

There are various methods for fuzzy clustering. Three of them were used in this study: fuzzy k-means [8], fuzzy clustering with L_1 norm [51,117], and fuzzy clustering with a fuzzy covariance matrix [39]. An example of fuzzy clustering with fuzzy k-means method on actual discharge data is shown in Figure 161, where fuzzy membership values of three defects in gas-insulated switchgear are shown. The existence of three groups in the data was considered to be *a priori* knowledge. The first six fingerprints belong to corona in SF6, fingerprints ranking from 7 to 13 originated from cavity discharges in a spacer, and the other ones from conducting particles on a spacer applied half-way between the conductor and the ground. The difference between the three clusters is clear, although fingerprint No.14 appears to be fuzzy.

The main advantage of fuzzy clustering is that it gives detailed information on the structure of the data. However, as the number of clusters and the number of fingerprints grow, so does the output of the programs. It may then become difficult to digest all the information. Furthermore, due to fuzzy clustering, the representative fingerprints of each cluster may not be available [51]. There is also a considerable lack of indices which indicate the correct number of clusters in the data.

B.2 Classification of discharge patterns

The recognition rate and centour score have been discussed in Chapter 4. In this Appendix, less successful classification procedures investigated in this work are briefly discussed.

Prior probabilities in classification

The term prior probability is used in the sense that such a probability is known before a classification is performed. The prior probabilities are usually based on the relative size of populations involved in the analysis. For example, if there are two populations, say sixty Dutchmen and forty Englishmen, then a randomly selected individual has the prior probability 60% for a Dutchman and 40% for an Englishman. The main purpose of the methods that use prior probabilities is to increase the probability of assigning a fingerprint to a population with a relatively large prior probability and of decreasing the probability of assignment to a population with a relatively small prior probability. In our case, it is inconvenient to set prior probabilities only to the number of available fingerprints of a particular defect. Instead, they are set to $1/G$, where G is the number of populations involved in the analysis. In some cases, by setting prior probabilities for some populations to zero, it is possible to exclude these populations from the analysis. For example, we exclude fingerprints of discharges in oil and discharges in SF_6 when analysing an epoxy insulation transformer, which is equal to setting their prior probabilities to zero.

The decision rule is to assign a fingerprint $x'_i = (x_{i1}, x_{i2}, \ldots, x_{ip})$, which consists of p statistical operators, with the prior probability $P(H_g)$ for gth defect, to gth defect ($g=1,2, \ldots, G$) for which the posterior probability $P'(H_g|x_i)$ or $P(H_g|x_i)$ is the largest. The posterior probabilities are:

$$P'(H_g|x_i) = \frac{P(H_g) \; |V|^{-\frac{1}{2}} \exp(-\frac{1}{2} d^2_{ig,V})}{\sum_{g=1}^{G} P(H_g) \; |V|^{-\frac{1}{2}} \exp(-\frac{1}{2} d^2_{ig,V})}, \quad g = 1, 2, \ldots, G, \qquad (19)$$

and

$$P(H_g|x_i) = \frac{P(H_g) \; |V_g|^{-\frac{1}{2}} \exp(-\frac{1}{2} d^2_{ig,V_g})}{\sum_{g=1}^{G} P(H_g) \; |V_g|^{-\frac{1}{2}} \exp(-\frac{1}{2} d^2_{ig,V_g})}, \quad g = 1, 2, \ldots, G, \qquad (20)$$

which are cases with the equal and unequal covariance matrices.

In the first case, it is supposed that each defect has the same covariance matrix. The elements of the matrix V are then calculated according to:

$$v_{jk} = \frac{\sum_{l=1}^{G} \left(\sum_{i=1}^{n_l} (x_{ijl} - \overline{x_{jl}}) (x_{ikl} - \overline{x_{kl}}) \right)}{n_1 + n_2 + \ldots + n_G - G}, \quad j, k = 1, 2, \ldots, p, \qquad (21)$$

where $\overline{x_{jl}}$ is the mean value for jth statistical operator estimated from n_l fingerprints of lth defect ($l = 1, 2, \ldots, G$) and n_l is the number of available fingerprints x_{ijl} ($i = 1, 2, \ldots, n_l$; $j = 1, 2, \ldots, p$) for lth defect. For the calculation of distances $d^2_{ig,V}$ (see equation 29) the same covariance matrix V is used for each defect. Symbol $|V|$ denotes determinant of the matrix V.

In the second case, the covariance matrix is calculated for each defect according to equation 33 in Appendix B.3. This matrix is then used for the calculation of distances d^2_{ig,V_g} in equation 29, see Appendix B.3.

The main disadvantage of this method is that a fingerprint must belong to one of G reference defects. This may cause troubles when classifying the fingerprints of discharge defects. The test of the method with actual discharge fingerprints is discussed in section "Comparison of classification methods" in this Appendix.

Sample space partition

This linear discriminating rule consists of set of the functions [63]:

$$L_g(\boldsymbol{x}_i) = w_{g1}\, x_{i1} + w_{g2}\, x_{i2} + \cdots + w_{gp}\, x_{ip} + w_{gp+1}\,, \qquad g = 1, 2, \ldots, G, \tag{22}$$

derived from

$$L_g(\boldsymbol{x}_i) = \ln(P(H_g)) + \overline{\boldsymbol{x}'_g}\, \boldsymbol{V}^{-1} \left(\boldsymbol{x}_i - \frac{1}{2}\overline{\boldsymbol{x}_g}\right), \qquad g = 1, 2, \ldots, G. \tag{23}$$

Here, w_{gj} are weights determined from equation 23 ($j = 1, 2, \ldots, p$), p is the number of statistical operators, G is the number of defects involved in the analysis, $P(H_g)$ are prior probabilities (usually set to 1/G),

$$\overline{\boldsymbol{x}'_g} = (\overline{x_{1g}}, \overline{x_{2g}}, \ldots, \overline{x_{pg}})$$

is the vector of the mean estimates for gth defect, $\boldsymbol{x}'_i = (x_{i1}, x_{i2}, \ldots, x_{ip})$ is ith fingerprint to be classified and V is the estimate of the covariance matrix by equation 21. Classification of a fingerprint of unknown origin is made to a defect for which $L_g(\boldsymbol{x}_i)$, ($g = 1, 2, \ldots, G$), is the largest.

The method uses the assumption of the equality of the covariance matrices for all reference defects, which does not necessarily hold in practice. The results of classification with fingerprints of discharge defects are shown in section "Comparison of classification methods" in this Appendix.

The Anderson method

The main purpose of the classification procedure developed by Anderson is to minimize misclassification [2]. A simple example is to assign a fingerprint of unknown origin to two known defects. Two errors may occur. First, a fingerprint can be classified as, *e.g.*, treeing discharges, while actually the fingerprint belongs to, *e.g.*, a dielectric bounded cavity. The second error is a misclassification of the fingerprint to a dielectric bounded cavity, when it actually belongs to treeing discharges.

The classification rule is to assign ith fingerprint $\boldsymbol{x}'_i = (x_{i1}, x_{i2}, \ldots, x_{ip})$ to gth group if:

$$u_{gk}(\boldsymbol{x}_i) > \ln\frac{P(H_k)}{P(H_g)}$$

for all $k = 1, 2, \ldots, G$; $k \neq g$.

The function $u_{gk}(x_i)$ is:

$$u_{gk}(x_i) = [x_i - \frac{1}{2}(\overline{x_g} + \overline{x_k})]' \; V^{-1} (\overline{x_g} - \overline{x_k}) , \tag{25}$$

where

$$\overline{x_g} = (\overline{x_{g1}}, \overline{x_{g2}}, \ldots, \overline{x_{gp}})$$

is the estimate of a mean vector for gth defect, p is the number of statistical operators, V is the estimate of the covariance matrix by equation 21 and $P(H_g)$ is the prior probability for gth defect. If all prior probabilities are equal ($P(H_g) = 1/G$), then the classification rule is to assign ith fingerprint to gth defect if $u_{gk}(x_i) \geq 0$, for all $k = 1, 2, \ldots, G$; $k \neq g$.

The main disadvantages of this method are that a fingerprint must belong to one of G reference defects, and it also uses assumption of the equality of the covariance matrices for all reference defects. This method is tested with actual discharge patterns in section "Comparison of classification methods" in this Appendix.

Geisser classifier

Classification procedures discussed above have been based on a large number of samples. The method derived by Geisser is based on a small-sample theory and involves gamma functions [72]. The statistics used is:

$$P(H_g|x_i) = \frac{P_{ig}}{\sum_{k=1}^{G} P_{ik}} , \tag{26}$$

in which

$$P_{ig} = P(H_g) \left[\frac{n_g}{n_g + 1}\right]^{\frac{p}{2}} \frac{\Gamma\left[\frac{1}{2}(n - G + 1)\right]}{\Gamma\left[\frac{1}{2}(n - p - G + 1)\right]} \times \times \left[1 + \frac{n_g \, d_{ig}^2}{(n_g + 1)(n - G)}\right]^{-\frac{1}{2}(n - G + 1)} \tag{27}$$

The classification rule is to assign a fingerprint of unknown origin to a defect for which the posterior probability $P(H_g|x_i)$ is the largest. Here, $P(H_g|x_i)$ is the probability that a fingerprint x_i belongs to gth defect, $P(H_g)$ is the prior probability for gth defect, n_g is the number of fingerprints for gth defect, n is the total number of fingerprints, G is the number of defects involved in the analysis, p is the number of statistical operators. For the calculation of d^2_{ig}, the equation 29 with the matrix V is used.

The main disadvantages of this method are that a fingerprint must belong to one of G reference defects, and the assumption of the equality of covariance matrices for the all reference defects. The test of the method with actual discharge fingerprints is discussed in the section "Comparison of classification methods" in this Appendix.

Comparison of classification methods

To illustrate the use of the conventional classifiers discussed in this Appendix, a fingerprint of discharges in 3-core belted cable, phase T (see Chapter 3 for details) was classified. The results are given in Table 18.

Table 18. Classification results for a fingerprint of discharges in 3-core belted cable, phase T, obtained by conventional classifiers. Two methods of testing were applied with prior probabilities - with matrices V and V_g, see equations 19 and 20.

CLASSIFICATION METHOD	RESULT
PRIOR PROBABILITIES - V	COR-AIR - 96%
PRIOR PROBABILITIES - Vg	TREE-COND - 100%
SAMPLE SPACE PARTITION	COR-AIR
ANDERSON	COR-AIR
GEISSER	COR-AIR - 77%
RECOGNITION RATE	NONE
CENTOUR SCORE	NONE
EXPECTED DEFECT	NONE

In this case, a classification to none of the standard defects was expected. The standard defects to be compared with the fingerprint of phase T were prepared in a different way and neither they were measured at three-phase voltage. It can be seen that only the recognition rate and centour score gave correct answers. All other methods misclassified the fingerprint of phase T. It follows that methods which use the assumption of equal covariance matrices, or the assumption that a fingerprint of unknown origin must belong to one of the studied defects, are not satisfactory tools for discharge recognition.

B.3 Centour score

The first step in calculating the centour score is made by measuring the distance between the statistical operators of unknown fingerprint and the mean values of the operators of known fingerprints. A simple example is to classify unknown fingerprint to two known defects using one statistical operator. The distance is:

$$d_k^2 = \frac{(u - \mu_k)^2}{\sigma_k^2}, \qquad k = 1, 2, \tag{28}$$

where u is the value of the statistical operator of unknown fingerprint, μ_1 and μ_2 are the means of the same statistical operator for two known defects *1* and 2, σ_1 and σ_2 are standard deviations of the operators for these two defects. Generally, the measure of the distance for jth unknown fingerprint u_j, based on p statistical operators of kth defect ($k = 1, 2, \ldots, G$) is

$$d_{jk}^2 = \boldsymbol{U}_{jk}' \, C_k^{-1} \, \boldsymbol{U}_{jk} \tag{29}$$

where the unknown measurement is

$$\boldsymbol{u}_j = \begin{bmatrix} u_{j1} \\ u_{j2} \\ \cdots \\ u_{jp} \end{bmatrix} \tag{30}$$

$$\boldsymbol{U}_{jk} = \begin{bmatrix} u_{j1} - \mu_{1k} \\ u_{j2} - \mu_{2k} \\ \cdots \\ u_{jp} - \mu_{pk} \end{bmatrix} \tag{31}$$

the covariance matrix is

$$C_k = \begin{bmatrix} \sigma_{1k}^2 & \sigma_{12k} & \cdots & \sigma_{1pk} \\ \sigma_{21k} & \sigma_{2k}^2 & \cdots & \sigma_{2pk} \\ \cdots & \cdots & \cdots & \cdots \\ \sigma_{p1k} & \sigma_{p2k} & \cdots & \sigma_{pk}^2 \end{bmatrix} \tag{32}$$

and $\boldsymbol{U}_{jk}'$ is the transpose of vector $\boldsymbol{U}_{jk}$.

The covariance matrix can be considered to be a multidimensional generalization of the one-dimensional standard deviation.

However, the parameters as the mean of statistical operators, the standard deviation and the covariance matrix are usually unknown in practice. They are estimated from the sampled data. The estimation of elements of the covariance matrix for kth defect in equation 32 can be calculated in the following way [72]:

$$e_{lm} = \frac{\sum_{i=1}^{n_k} (u_{il} - \overline{u_l})(u_{im} - \overline{u_m})}{n_k - 1} \qquad l, m = 1, 2, \ldots, p \tag{33}$$

where $\overline{u_l}$ is the mean value for lth statistical operator estimated from n_k measurements of kth defect.

If the distribution of u is normal with the mean μ and variance σ^2, the equation 28 has a χ^2 distribution with one degree of freedom. This fact was used to create the centour score, a measure of resemblance [72]. The centour score is defined as:

$$cs = 100 - PR_{d^2_{jk,p}} \tag{34}$$

where PR is the percentile rank of d^2_{jk}, see equation 29, in the distribution of χ^2 with p degrees of freedom (if 15 operators are used then $p = 15$). The maximum value for the centour score is 100. The minimum value is 0.

Appendix C

Computation of fractal dimension and lacunarity for surfaces

The fractal dimension and the lacunarity were determined using a box-counting method [52]. The method is as follows.

Let $P(m, L)$ be the probability that there are m points within a box of size L centred around an arbitrary point of the surface. For each value of L it is

$$\sum_{m=1}^{N} P(m,L) = 1, \tag{35}$$

where N is the number of possible points within the box. Let S be the number of image points (i.e. pixels within an image). If one overlays the image with boxes of side L, then the number of boxes with m points inside the box is $(S/m)P(m,L)$. Therefore, the expected total number of boxes needed to cover the whole image is

$$\langle N(L)\rangle = \sum_{m=1}^{N} \frac{S}{m} P(m,L) = S \sum_{m=1}^{N} \frac{1}{m} P(m,L) \tag{36}$$

Hence, if we let

$$N(L) = \sum_{m=1}^{N} \frac{1}{m} P(m,L) \tag{37}$$

this value is proportional to L^{-D} (from $N(L)=(L_{max}/L)^{-D}$) and can be used to estimate fractal dimension D. The $P(m,L)$ and $N(L)$ are obtained for various values of L. For this work the calculations were made for L=3, 5, 7, 9 and 11. Fractal dimension D is then determined by doing the least squares fit on $[\log(L), -\log(N(L))]$.

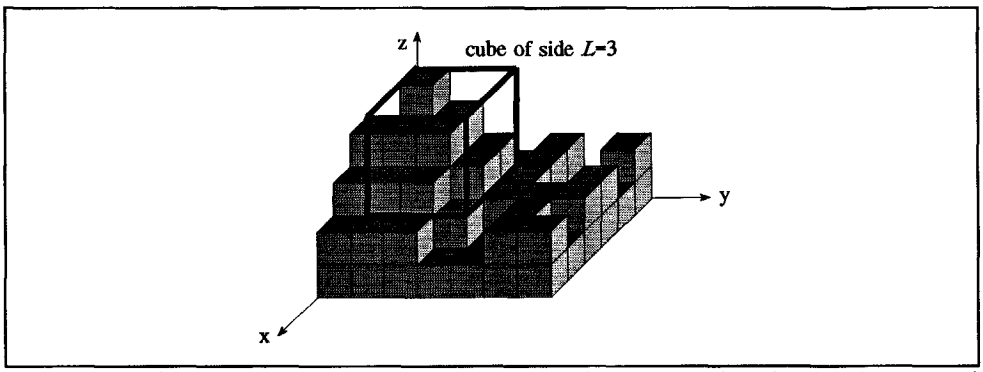

Figure 162. The principle of the box-counting method for a fractal surface (3-dimensional image). A box is centred around each pixel x, y, $f(x,y)$ and points inside the box are counted.

To estimate $P(m,L)$ the cube of size L is centred around each point of the image surface, see Figure 162. The number of neighbouring points m that fall within the cube are counted. Values of L are chosen to be odd to simplify the centring process. The centring and counting process is restricted to a pixel having all their neighbours inside the image. This leaves out image portions of width $(L-1)/2$ on the border area.

The lacunarity Λ is calculated from $P(m,L)$ as well. Letting

$$M(L) = \sum_{m=1}^{N} mP(m,L) \tag{38}$$

and

$$M^2(L) = \sum_{m=1}^{N} m^2 P(m,L) \tag{39}$$

the lacunarity is defined as

$$\Lambda(L) = \frac{M^2(L) - [M(L)]^2}{[M(L)]^2} \tag{40}$$

In this work the lacunarity for box size L=3 is used for discrimination purposes.

List of symbols

cc - a statistical operator: the cross-correlation factor

$H_n(\varphi)$ - the pulse count discharge distribution

$H_{qmax}(\varphi)$ - the maximum pulse height discharge distribution

$H_{qn}(\varphi)$ - the mean pulse height discharge distribution

$H(q)$ - the distribution of the number of discharges n as a function of the discharge magnitude q

$H(p)$ - the distribution of the number of discharges n as a function of the discharge energy p

Ku - a statistical operator: the kurtosis

Pe - a statistical operator: the number of peaks

q - apparent charge

Sk - a statistical operator: the skewness

U_a - ageing voltage

U_t - test voltage

Acknowledgements

During the four years of research many people were of great help to me. I would like to thank in particular:

- my promoter, professor F. H. Kreuger for his leadership during the course of this work,
- my colleagues, E. Gulski and P. Morshuis, for many valuable discussions,
- P. Bauer, U. Fromm, M. Jeroense and T. Jing - brothers in Ph.D - for lifting my spirits during hard days,
- W. A. Sonneveld, G. Ikkink and A. van der Graaf for technical assistance,
- Mrs. J. Zaat-Jones for careful reading and correcting of the English text.

This research would have been impossible without the generous financial support of the KEMA N.V., Arnhem, the Netherlands, the Dutch Institute for the testing of materials.

Samenvatting

Ontladingsdetectie en -herkenning zijn tegenwoordig belangrijke hulpmiddelen om de kwaliteit van hoogspanningsconstructies te beoordelen. Deze dissertatie beoogt enkele technieken uit de patroonherkenning toe te passen om ontladingen te *discrimineren* en te *classificeren.*

Deze dissertatie beschrijft de voortzetting van het eerdere werk van Dr. E. Gulski op het gebied van ontladingsherkenning dat eveneens is uitgevoerd in het Hoogspanningslaboratorium van de Technische Universiteit Delft. Het doel van deze studie was het verbeteren van de bestaande technieken van ontladingsherkenning. Daarbij zijn vele methoden getoetst.

Voor *classificatie* bleek de 'centour score' methode goed te voldoen. Deze methode heeft hier zijn kracht bewezen voor de classificatie van ontladingen in hoogspanningscomponenten en is met succes geimplementeerd in een commercieel ontladingsdetectiesysteem. Neurale netwerken bleken geen goede methode te verschaffen om ontladingen te classificeren.

Voor *discriminatie* van ontladingen bleek de 'group average' methode goed te werken, met name voor de analyse van ontladingspatronen tijdens de veroudering van isolatie. De methode kan worden gebruikt voor data analyse bij het periodiek testen van hoogspannings-componenten. Ook fractal-beschrijvers van ontladingspatronen bleken goede discriminerende eigenschappen te bezitten.

Hoofdstuk 1 geeft een algemene introduktie.

In hoofdstuk 2 worden verschillende ontladingsverdelingen beschreven die zijn gebruikt voor herkenning van ontladingen. De verdelingen worden gekwantificeerd met behulp van statistische parameters, zoals skewness, kurtosis, enz. Een verzameling van 29 statistische parameters word gebruikt als basis voor de herkenning van ontladingen; deze 29 parameters vormen tezamen de vingerafdruk van een ontlading.

Een gedetailleerde beschrijving van de vingerafdrukken van verschillende ontladingsbronnen is in hoofdstuk 3 te vinden.

Hoofdstuk 4 beschrijft de verschillende mathematische methoden die gebruikt zijn om ontladingspatronen te discrimineren en te classificeren.

'Mapping' technieken, cluster-analyse en fractal technieken zijn toegepast om ontladingspatronen te *discrimineren.* Van al de geteste en bestudeerde methoden bleek de 'group average' te prefereren. Fractale technieken bleken ook een waardevolle en geschikte methode ter discriminatie van ontladingspatronen te zijn.

Neurale netwerken en conventionele classificatiemethoden zijn gebruikt om ontladingspatronen te *classificeren*. Uit deze studie volgde dat neurale netwerken geen goede methode opleverden om ontladingen te herkennen. Conventionele classificatiemethoden, in het bijzonder de 'centour score' methode, hebben echter hun waarde bewezen in het herkennen van ontladingen.

Ontladingspatronen, verkregen tijdens het verouderen van eenvoudige modellen en van enkele industriële hoogspanningscomponenten, worden in hoofdstuk 5 gepresenteerd. Met de technieken als hierboven beschreven werden de patronen geanalyseerd. De studie heeft ons geleerd dat enkele technieken, zoals de 'group average' methode en de 'centour score' methode, goede hulpmiddelen voor industrieele toepassing kunnen zijn, zoals het periodiek testen van de electrische isolatie in hoogspanningscomponenten.

In hoofdstuk 6 worden de conclusies van dit onderzoek gepresenteerd en enkele suggesties voor toekomstig onderzoek gedaan.

Curriculum vitae

Andrej Krivda was born in Humenné, Slovakia (Czecho-Slovakia), on June 28, 1967. He graduated from the comprehensive school, Gymnázium Humenné in 1984. From 1984 until 1990 he studied power engineering at Košice University of Technology, Slovakia, where he graduated with distinction. After graduation he worked one year as a research assistant at the same university. In 1991 he joined the High Voltage Laboratory of Delft University of Technology where he performed research on the recognition of discharges, which led to the current thesis.